Electrospun Fiber Cues Influence Differentiation of Oligodendrocyte Progenitor Cells and Neural Stem Cells in 3D Hyaluronic Acid Hydrogels

---

A Dissertation

Presented to the faculty of the School of Engineering and Applied Science

University of Virginia

---

in partial fulfillment

of the requirements for the degree

Doctor of Philosophy

by

Rachel Ann Mazur

August 2024

APPROVAL SHEET

This Dissertation
is submitted in partial fulfillment of the requirements
for the degree of
Doctor of Philosophy

Author Signature: Rachel Mazur

This Dissertation has been read and approved by the examining committee:

Advisor: Kyle Lampe

Committee Member: Rachel Letteri

Committee Member: Steven Caliari

Committee Member: Chris Highley

Committee Member: Sarah Kucenas

Accepted for the School of Engineering and Applied Science:

Jennifer L. West, School of Engineering and Applied Science

August 2024

Electrospun Fiber Cues Influence Differentiation of Oligodendrocyte Progenitor Cells and Neural Stem Cells in 3D Hyaluronic Acid Hydrogels

---

A Dissertation Presented to the Faculty of the School of Engineering and Applied Science at The University of Virginia

---

In partial fulfillment of the requirements for the degree of

Doctor of Philosophy in Chemical Engineering

Rachel A. Mazur

August 2024

Committee Members:

Kyle J. Lampe, PhD Advisor

Rachel A. Letteri, Chair

Steven R. Caliari

Christopher B. Highley

Sarah C. Kucenas

Abstract

Demyelination occurs when the protective myelin sheath surrounding mature neurons is degraded. Neural stem cells (NSC) and oligodendrocyte progenitor cells (OPC) are responsible for replacing damaged myelin by migrating to the injured area, differentiating into mature oligodendrocytes (OLs), and extending processes to re-wrap exposed neurons. Unfortunately, oligodendrocyte differentiation and remyelination are understudied. Most research in this area has been conducted using *in vivo* models, which are complicated by the presence of extraneous cell types and biological processes. Existing *in vitro* studies have been conducted in 2D, which does not appropriately reflect the 3D environment of native tissue. 3D hydrogels are a promising alternative approach to *in vivo* or 2D *in vitro* culture due to their ability to replicate natural tissue characteristics without the presence of confounding variables. Norbornene-functionalized hyaluronic acid (NorHA) is an attractive option since HA is a key component of the extracellular matrix, and NorHA gel stiffness can be easily tuned within the range of native brain tissue. We can also replicate structural cues by incorporating electrospun HA fibers with diameters similar to native axons. Here, we construct a 3D tissue mimetic model system by co-encapsulating cells and electrospun topographical cues within NorHA hydrogels.

In this thesis, we explore the effect of electrospun topography on NSC and OPC growth and differentiation. Chapter 2 discusses the need for an *in vitro* model system to elucidate the molecular-level effects of demyelinating disease and injury cascades. In Chapter 3, our model system investigates the effects of electrospun topographical cues on OPCs. Confocal imaging revealed that the presence of fibers affected OPC morphology, resulting in the extension of numerous cellular processes associated with OPC differentiation. Chapter 4 explores the effects of electrospun topography on NSCs. Unlike the OPCs used, NSCs were not genetically modified and so are more representative of native cells. Additionally, the use of NSCs represents a step back along the differentiation pathway, allowing us to determine whether cells unbiased towards glial fates would still differentiate into OL in the presence of fiber cues. Once again, NSCs in fiber-containing gels displayed more mature morphologies. Lastly, Chapter 5 focuses on practical applications of our model in determining OPC response to traumatic brain injury (TBI). A shockwave generator system was used to simulate the effects of mild TBI on OPCs encapsulated in NorHA gels. Blast overpressure did not have a significant effect on hydrogel material properties,

but inclusion of electrospun fibers did result in an increase in bulk storage modulus. Cell viability and proliferation were not significantly affected by overpressure exposure in either the presence or absence of fibers. As before, inclusion of fiber cues influenced OPC differentiation; however, blast injury on the scale of mild TBI was demonstrated to have minimal impact on cell differentiation.

Acknowledgements

Hey, look Ma, I made it! It's been a long (but enjoyable) 6 years, and I can't believe my time in graduate school has finally come to an end. I'm immensely thankful for the connections I've forged throughout the years, and for the invaluable guidance and support from those who made this dissertation a reality.

First, I would like to thank my thesis advisor, Dr. Kyle Lampe, for accepting me into his lab despite having no background or knowledge of this research area. You took a gamble on me, and hopefully it has paid off! Thank you to my committee: Dr. Rachel Letteri, Dr. Steven Caliari, Dr. Chris Highley and Dr. Sarah Kucenas for your help, feedback, and encouragement over the years. And finally, thank you to my undergraduate research advisor, Dr. Robert Kelly, for introducing me to research and steering me towards UVA.

I owe a lot to the past and present Lampe members. Thank you to James Tang and Nick Murphy, my fellow NCSU alums, for welcoming me into the lab (go Wolfpack!). Thank you to Lauren Russell and Deniz Unal, who previously worked on this project- without you, this dissertation literally would not have been possible. Thank you to Bev Miller, who taught me everything I know about electrospinning. Thank you to Zhiqi Zhang and Jonathan Florian, who kept the lab going through the COVID years, and to Nadeesani Sirinayake, who helped us get going again afterwards. Huge shoutout to JR Eisold for the huge burst of energy and enthusiasm he's brought to the lab, and also for taking over all of my lab chores (sorry!). Finally, thanks to the newest additions, Joseph Maliakkal, Shimanto Roy, and Rumesh Nanayakkara- I know with you around the lab will be in good hands.

This work would have been impossible without the contributions of all my undergraduate students over the years. Thank you to DessaRae Lampkins, Lauran Pearson, Mariano Sieglie Gonzalez, and Leila Ghaffari for all the hard work you put in over the summers. And thank you to Elaina Lee, Ava Bankert, and Will Ferguson for all the effort you put in during the school years. Special thanks to Hannah Hockensmith, my very first UG assistant, who taught me a lot about how to be a good mentor. I wish you all the best of success in everything you end up doing!

A huge thank you to the VandeVord group: Dr. Pam VandeVord, Ryosuke Yokosawa, and Kelsey Wilson for teaching me all about TBI and gene expression analysis! You all were incredible in applying the NorHA + fibers model system to a real-world application, and it was a blast to see the TBI model in action.

Huge thanks to the Squid squad: Stephanie Guthrie, Costanza Perosi, Evan Eckersley, Nate Sallada, Madison Mann, Holly Mayton, Melissa Deschamps, Lia Baldwin, Jenna Sumey, Natalie Smith, Eric Holmgren, Natalia Diaz Montenegro, Tracy Kuper, Kelly Bukovic, and Rhea Braun. Y'all were a lot of fun and made Charlottesville a great place to live.

Thanks to my family for always pushing me to try my best and teaching me the value of education- without you I would never have succeeded in getting an engineering degree. Special shout out to my sister, Dorian, for all the memes and nonsense you've sent me over the years.

Thank you to my cat, Schmutz Mazur-Basri, for sitting on the floor and wailing the whole time I wrote this thesis. I'm not sure why you thought that would help but I appreciate the effort.

Finally, to my husband, Sameh Basri, thanks for sticking with me this whole experience, through good times and bad. We've had so much fun together, whether we were hiking, tubing, swimming, cooking, or even just buying Monster energy drinks at Wawa. I can't think of anyone else I'd rather go to the gym, and then eat too much tikka masala, with. Plus, you're cute too! Here's to many more years together.

Table of Contents

List of Figures

Chapter 2

Chapter 3

Chapter 4

Chapter 5

Appendix A

List of Tables

Chapter 1: Introduction and Background

1.1 Neural Stem Cells, Oligodendrocyte Progenitor Cells, and Oligodendrocytes

In healthy central nervous system (CNS) tissue, axons of mature neurons are coated with a myelin sheath which improves the efficiency of signal transduction. These myelin sheaths are produced by mature oligodendrocytes (OLs). In the aftermath of a demyelinating disease or injury, the myelin sheaths surrounding the neurons are degraded, preventing efficient signal transduction and damaging the oligodendrocytes [1]. Oligodendrocyte progenitor cells (OPCs) can replace damaged myelin by migrating into the area, differentiating into mature OLs and extending processes around the axon to replace the myelin sheath [1].

Myelination occurs primarily after birth in humans and peaks during the first year of life; however, the process of myelination continues into young adulthood [2]. Areas of the brain required for basic homeostasis are the first to be myelinated, while regions of the brain associated with more complex tasks are myelinated later [3]. Myelination is also size-dependent, as larger axons (>1 μm) are fully myelinated earlier in development, while smaller axons (0.2-0.8 μm) are myelinated later and to a lesser extent [4]. Myelination in the peripheral nervous system (PNS) has been well characterized and progresses based on the "carpet crawler" model. During PNS myelination, a thin sheet of myelin is first spread over the surface of the axon, following which the leading edge of the sheet turns under the existing myelin membrane and continues to coil underneath the growing outer sheath [5]. However, the morphology of myelin in the CNS suggests that the "carpet crawler" model does not apply [6]. While various other models for *de novo* CNS myelination have been proposed, the exact mechanisms behind myelin sheath formation and compaction remain unclear.

In addition to performing *de novo* myelination during brain development, populations of OPCs and their parent cells, neural stem cells (NSCs), remain in the adult brain [7, 8]. OPCs are involved with myelin replacement and repair following CNS disease or injury. During early stages of development, NSCs and OPCs can migrate through the CNS until they reach demyelinated areas [9, 10]. These cells then proliferate locally before differentiating into mature myelinating OLs and re-wrapping exposed neurons [1, 11]. Unfortunately, remyelinated sheaths tend to be shorter and thinner than original sheaths [12]. In many clinical manifestations remyelination can fail entirely, resulting in cell death of both the OLs and exposed neurons [13]. Currently, the underlying mechanisms surrounding demyelination and remyelination are not well understood.

1.2 Modeling Demyelinating Disease and Injury

To address existing knowledge gaps, several models of CNS disease and injury have been developed. Most existing models have been carried out *in vivo* and consist of inducing demyelination in an animal subject and subsequently monitoring its recovery. The most commonly used *in vivo* model for demyelinating diseases such as multiple sclerosis (MS) is the experimental autoimmune encephalitis (EAE) model, in which CNS proteins such as myelin

basic protein (MBP) or proteolipid protein (PLP) are injected into an animal to generate an inflammatory response resulting in demyelination [14]. Another common model for MS demyelination is the cuprizone model, in which the toxin cuprizone is fed to mice to induce demyelination [15]. Demyelinating injuries, such as traumatic brain injury (TBI), can also be modeled *in vivo* by exposing a model organism to a mechanical insult such as a blast overpressure [16].

More recently, *in vitro* hydrogel models have been developed which present an exciting alternative to *in vivo* studies. These models allow a greater degree of tunability since researchers can vary individual model parameters, such as stiffness, culture time, topography, and degradation, with greater control than is possible for *in vivo* studies [17-19]. Additionally, *in vitro* models allow study of injury and recovery mechanisms on a cellular and molecular level, without the presence of confounding variables. A variety of different hydrogel types exist; one example is Matrigel, a collection of proteins extracted from mouse sarcoma. Matrigel is advantageous in its ability to replicate the complex composition of extracellular matrix, but its composition is not well-defined and contains high batch-to-batch variability [20]. These inconsistencies result in poor tunability and heterogenous material properties [21]. Fully synthetic polymers, such as polyethylene glycol (PEG), provide a chemically consistent environment with tight control over mechanical properties [22]. Hydrogels derived from natural polymers, such as hyaluronic acid (HA), laminin, or collagen, combine the benefits of both options; they have a consistent composition, tunable mechanical properties, and their biochemically relevant compositions allow for cell-substrate interactions which reflect those in native tissue [23]. HA is of particular interest for CNS applications, due to the unique makeup of its extracellular matrix (ECM). While other common ECM proteins such as laminin, collagen and fibronectin are present in the CNS, they are primarily located in the basement membrane, while HA is the primary component of brain ECM [24]. A semi-synthetic HA-based hydrogel would therefore best reflect the composition of native CNS tissue.

1.3 Tunable Parameters for *In Vitro* Hydrogel Model Systems

In vitro hydrogel models possess many factors which can be tuned independently to assess their impact on cells. Gel physical properties, such as stiffness, are one example. Stiffness cues from the ECM influence the growth and differentiation of various cell types (including OPC/OL), with cells tending to prefer in vitro stiffness cues reflective of those present in their native environment [25]. Native brain tissue stiffness has been reported to have a storage modulus between 200-2000 kPa [26]. OPCs have previously demonstrated increased cell viability and spheroid volume in norbornene-functionalized hyaluronic acid (NorHA) hydrogels of low (G' = 170 Pa) stiffness as compared to intermediate (G' = 800 Pa) and high stiffness (G' = 2200 Pa) gels [17]. Development of a 3D hydrogel model within this stiffness range would help to further elucidate the role of matrix stiffness on OPC/OL development.

Topographical cues are another matrix factor that influences OPC migration, differentiation, and OL myelination. When seeded onto electrospun polystyrene fibers with diameters similar to in vivo myelinated axons (0.3 - 4 μm), some OPCs differentiate and wrap the fibers, particularly for fibers of larger diameters (>0.4 μm) [27, 28]. Polycaprolactone (PCL) fibers coated with graphene oxide and laminin also increased NSC differentiation into oligodendrocytes [29]. Most previous research involving electrospun fiber cues has been conducted in 2D. However, other

topographical cues, such as ablated microchannels or interfaces between gel types in bicontinuous hydrogels, have been demonstrated to influence cell migration in 3D [30, 31]. Combining these two approaches by co-encapsulating electrospun fiber cues alongside NSCs/OPCs could help determine the impact of axon-mimicking fibers in a 3D context which better reflects the dimensionality of native tissue. Electrospun HA fibers are of particular interest for this purpose due to their relatively low stiffness [32]. While materials like PCL and polystyrene typically result in stiff fibers, softer HA fibers would be biomimetic in terms of both their physical and chemical properties [33, 34].

In addition to determining the role of environmental cues in guiding OPC growth and development, it is also vital to determine the role of OPCs in shaping their surrounding environment. Cells influence their local microenvironment in a variety of ways, such as by degrading the surrounding matrix, or by adding to it through the secretion of ECM proteins [18, 35]. Previous studies on the OPC secretome have found that OPCs are capable of ECM protein deposition, primarily composed of laminin and fibronectin [36, 37]. Both laminin and fibronectin have been previously implicated in OPC survival and proliferation, and laminin in particular is known to play a role in signaling pathways related to differentiation and myelination [38, 39]. However, the molecular-level nuances underlying many OPC-ECM interactions are not well understood. *In vitro* hydrogel models could help to shed light on OPC ECM deposition in 3D and determine how the pattern and composition of ECM deposition varies with OPC differentiation.

1.4 Objectives of This Work

The overall objective of this work is to develop a 3D *in vitro* hydrogel system capable of modeling NSC and OPC maturation and differentiation under developmental or injury conditions. Here, we use an HA-based bulk gel due to its tunable mechanical properties and its role as the primary component of native brain ECM. We co-encapsulate NSCs or OPCs alongside electrospun HA microfibers with similar dimensions and mechanical properties to native axons, with the goal of determining the impact of structural cues on cell growth and differentiation. The specific objectives of this work are as follows:

1. Investigate the role of electrospun microfiber structural cues in guiding differentiation of OPCs into mature myelinating oligodendrocytes.
2. Determine the role of axon-mimicking fibers in influencing NSC growth, differentiation, and gene expression.
3. Implement the OPC + fiber model system to determine the effects of simulated mild traumatic brain injury (mTBI) on cell survival, proliferation, and differentiation.

Cells were cultured in hydrogels over a seven-day period. Morphology was assessed using phalloidin staining and confocal microscopy. Cell proliferation was similarly measured through EdU staining. Changes in cell metabolic activity were determined using ATP and DNA plate reader assays. ECM deposition was assessed through immunostaining for laminin and fibronectin. NSC maturation was additionally assessed with quantitative polymerase chain reaction (qPCR) for maturation markers at various stages along the NSC-OPC-OL differentiation pathway, as well as through a NanoString gene profiling panel. These results enhance our understanding on how environmental factors guide NSC and OPC maturation, proliferation, and

differentiation into mature OLs. From this knowledge, the mechanisms underlying OPC development, injury, and recovery can be determined on a molecular level, furthering our understanding of OL biology and ultimately contributing to the development of therapeutic treatments for CNS disease and injury.

1.5 References

[1] H.-f. Wang, X.-k. Liu, R. Li, P. Zhang, Z. Chu, C.-l. Wang, H.-r. Liu, J. Qi, G.-y. Lv, G.-y. Wang, Effect of glial cells on remyelination after spinal cord injury, Neural regeneration research 12(10) (2017) 1724-1732.

[2] R.D. Fields, White matter in learning, cognition and psychiatric disorders, Trends in neurosciences 31(7) (2008) 361-370.

[3] B.A. Brody, H.C. Kinney, A.S. Kloman, F.H. Gilles, Sequence of central nervous system myelination in human infancy. I. An autopsy study of myelination, Journal of Neuropathology & Experimental Neurology 46(3) (1987) 283-301.

[4] M.E. Bechler, M. Swire, C. ffrench-Constant, Intrinsic and adaptive myelination—A sequential mechanism for smart wiring in the brain, Developmental neurobiology 78(2) (2018) 68-79.

[5] R.P. Bunge, M.B. Bunge, M. Bates, Movements of the Schwann cell nucleus implicate progression of the inner (axon-related) Schwann cell process during myelination, The Journal of cell biology 109(1) (1989) 273-284.

[6] R.L. Knobler, J.G. Stempak, M. Laurencin, Nonuniformity of the oligodendroglial ensheathment of axons during myelination in the developing rat central nervous system. A serial section electron microscopical study, Journal of ultrastructure research 55(3) (1976) 417-432.

[7] D.K. Ma, M.A. Bonaguidi, G.-l. Ming, H. Song, Adult neural stem cells in the mammalian central nervous system, Cell research 19(6) (2009) 672-682.

[8] M.R. Dawson, A. Polito, J.M. Levine, R. Reynolds, NG2-expressing glial progenitor cells: an abundant and widespread population of cycling cells in the adult rat CNS, Molecular and Cellular Neuroscience 24(2) (2003) 476-488.

[9] E.G. Hughes, S.H. Kang, M. Fukaya, D.E. Bergles, Oligodendrocyte progenitors balance growth with self-repulsion to achieve homeostasis in the adult brain, Nature neuroscience 16(6) (2013) 668-676.

[10] J. Imitola, K. Raddassi, K.I. Park, F.-J. Mueller, M. Nieto, Y.D. Teng, D. Frenkel, J. Li, R.L. Sidman, C.A. Walsh, Directed migration of neural stem cells to sites of CNS injury by the stromal cell-derived factor 1α/CXC chemokine receptor 4 pathway, Proceedings of the National Academy of Sciences 101(52) (2004) 18117-18122.

[11] X. Wang, P. Seekaew, X. Gao, J. Chen, Traumatic brain injury stimulates neural stem cell proliferation via mammalian target of rapamycin signaling pathway activation, ENeuro 3(5) (2016).

[12] I.D. Duncan, R.L. Marik, A.T. Broman, M. Heidari, Thin myelin sheaths as the hallmark of remyelination persist over time and preserve axon function, Proceedings of the National Academy of Sciences 114(45) (2017) E9685-E9691.

[13] P. Patrikios, C. Stadelmann, A. Kutzelnigg, H. Rauschka, M. Schmidbauer, H. Laursen, P.S. Sorensen, W. Brück, C. Lucchinetti, H. Lassmann, Remyelination is extensive in a subset of multiple sclerosis patients, Brain 129(12) (2006) 3165-3172.

[14] C.S. Constantinescu, N. Farooqi, K. O'Brien, B. Gran, Experimental autoimmune encephalomyelitis (EAE) as a model for multiple sclerosis (MS), British journal of pharmacology 164(4) (2011) 1079-1106.
[15] J. Praet, C. Guglielmetti, Z. Berneman, A. Van der Linden, P. Ponsaerts, Cellular and molecular neuropathology of the cuprizone mouse model: clinical relevance for multiple sclerosis, Neuroscience & Biobehavioral Reviews 47 (2014) 485-505.
[16] H.J. Cho, V.S.S.S. Sajja, P.J. Vandevord, Y.W. Lee, Blast induces oxidative stress, inflammation, neuronal loss and subsequent short-term memory impairment in rats, Neuroscience 253 (2013) 9-20.
[17] D.B. Unal, S.R. Caliari, K.J. Lampe, 3D hyaluronic acid hydrogels for modeling oligodendrocyte progenitor cell behavior as a function of matrix stiffness, Biomacromolecules 21(12) (2020) 4962-4971.
[18] E. Meco, W.S. Zheng, A.H. Sharma, K.J. Lampe, Guiding Oligodendrocyte Precursor Cell Maturation With Urokinase Plasminogen Activator-Degradable Elastin-like Protein Hydrogels, Biomacromolecules 21(12) (2020) 4724-4736.
[19] E. Hui, K.I. Gimeno, G. Guan, S.R. Caliari, Spatiotemporal control of viscoelasticity in phototunable hyaluronic acid hydrogels, Biomacromolecules 20(11) (2019) 4126-4134.
[20] C.S. Hughes, L.M. Postovit, G.A. Lajoie, Matrigel: a complex protein mixture required for optimal growth of cell culture, Proteomics 10(9) (2010) 1886-1890.
[21] L.N. Russell, K.J. Lampe, Oligodendrocyte precursor cell viability, proliferation, and morphology is dependent on mesh size and storage modulus in 3D poly (ethylene glycol)-based hydrogels, ACS Biomaterials Science & Engineering 3(12) (2017) 3459-3468.
[22] C.D. Spicer, Hydrogel scaffolds for tissue engineering: the importance of polymer choice, Polymer Chemistry 11(2) (2020) 184-219.
[23] E.E. Benarroch, Extracellular matrix in the CNS: Dynamic structure and clinical correlations, Neurology 85(16) (2015) 1417-1427.
[24] S.W. Moore, P. Roca-Cusachs, M.P. Sheetz, Stretchy proteins on stretchy substrates: the important elements of integrin-mediated rigidity sensing, Developmental cell 19(2) (2010) 194-206.
[25] X. Li, E. Katsanevakis, X. Liu, N. Zhang, X. Wen, Engineering neural stem cell fates with hydrogel design for central nervous system regeneration, Progress in polymer science 37(8) (2012) 1105-1129.
[26] S. Lee, M.K. Leach, S.A. Redmond, S.C. Chong, S.H. Mellon, S.J. Tuck, Z.-Q. Feng, J.M. Corey, J.R. Chan, A culture system to study oligodendrocyte myelination processes using engineered nanofibers, Nature methods 9(9) (2012) 917-922.
[27] S. Lee, S.C. Chong, S.J. Tuck, J.M. Corey, J.R. Chan, A rapid and reproducible assay for modeling myelination by oligodendrocytes using engineered nanofibers, Nature protocols 8(4) (2013) 771-782.
[28] S. Shah, P.T. Yin, T.M. Uehara, S.T.D. Chueng, L. Yang, K.B. Lee, Guiding stem cell differentiation into oligodendrocytes using graphene-nanofiber hybrid scaffolds, Advanced materials 26(22) (2014) 3673-3680.
[29] O. Ilina, G.-J. Bakker, A. Vasaturo, R.M. Hoffman, P. Friedl, Two-photon laser-generated microtracks in 3D collagen lattices: principles of MMP-dependent and-independent collective cancer cell invasion, Physical biology 8(1) (2011) 015010.

[30] K.L. Xu, N. Di Caprio, H. Fallahi, M. Dehghany, M.D. Davidson, L. Laforest, B.C. Cheung, Y. Zhang, M. Wu, V. Shenoy, Microinterfaces in biopolymer-based bicontinuous hydrogels guide rapid 3D cell migration, Nature Communications 15(1) (2024) 2766.
[31] C. Loebel, R.L. Mauck, J.A. Burdick, Local nascent protein deposition and remodelling guide mesenchymal stromal cell mechanosensing and fate in three-dimensional hydrogels, Nature materials 18(8) (2019) 883-891.
[32] W.K. Kim, D. Kim, J. Cui, H.H. Jang, K.S. Kim, H.J. Lee, S.U. Kim, S.-M. Ahn, Secretome analysis of human oligodendrocytes derived from neural stem cells, PLoS One 9(1) (2014) e84292.
[33] Z. Yang, R. Suzuki, S.B. Daniels, C.B. Brunquell, C.J. Sala, A. Nishiyama, NG2 glial cells provide a favorable substrate for growing axons, Journal of Neuroscience 26(14) (2006) 3829-3839.
[34] M. Kang, Y. Yao, Laminin regulates oligodendrocyte development and myelination, Glia 70(3) (2022) 414-429.
[35] J. Hu, L. Deng, X. Wang, X.M. Xu, Effects of extracellular matrix molecules on the growth properties of oligodendrocyte progenitor cells in vitro, Journal of neuroscience research 87(13) (2009) 2854-2862.

Chapter 2: The Need for Tissue Engineered Models to Facilitate the Study of Oligodendrocyte Progenitor Cells in Traumatic Brain Injury and Repair

Rachel A. Mazur[1], Ryosuke Yokosawa[2], Pamela J. VandeVord[2], Kyle J. Lampe[1]

1 Department of Chemical Engineering, University of Virginia, Charlottesville, VA USA

2 Department of Biomedical Engineering and Mechanics, Virginia Polytechnic Institute and State University, Blacksburg, VA USA

Published as: RA Mazur, R Yokosawa, PJ VandeVord, KJ Lampe, "The need for tissue-engineered models to facilitate the study of oligodendrocyte progenitor cells in traumatic brain injury and repair," Current Opinion in Biomedical Engineering, 22: 100378 (2022).

2.1 Abstract

Traumatic brain injury (TBI) is an important public health issue as these high-rate mechanical insults to brain tissue, even on a mild scale, progress to secondary injury cascades that prolong and augment the injury. More effective models are vital to study the injury mechanism and progression. Although oligodendrocyte progenitor cells (OPCs) and mature oligodendrocytes (OLs) have been shown to play a large role in TBI injury and recovery, research into OPC/OL effects post-injury has previously been ignored in favor of neuronal research. Optimizing a hydrogel-based *in vitro* model system to elucidate the unique contributions of OPC/OL to the injury cascade would elevate molecular knowledge in TBI research. In this manuscript, we identify several key parameters and potential next steps for consideration in the development of such models.

2.2 Introduction

TBI is a mechanical insult to the brain that can be caused by multiple mechanisms, such as rapid head acceleration, head collision with an object, and blast exposure. TBI has been described as a "silent epidemic," with recent estimates suggesting that 64-74 million individuals worldwide suffer a TBI each year [1]. Military service members are particularly at risk of suffering a TBI due to single or repeated blast exposures; within the US military alone, approximately 400,000 personnel have been diagnosed with TBI in the past 20 years [2, 3]. Literature supports that even mild TBIs (mTBI) can lead to long-term (>1 year) sequelae [4, 5]. Additionally, while the behavior and functional outcomes following TBI are well documented, cellular-level injury mechanisms and long-term anatomical effects, such as demyelination, are still poorly understood, leading to a lack of effective treatments for recovery [6]. In particular, the roles of OPCs and OLs in neurodegeneration following injury are understudied.

2.3 Current TBI Models and their Limitations

When reviewing TBI literature, the majority of experimental studies are conducted with *in vivo* models, particularly rodent models. These models have provided valuable insight into the aftermath of TBI, which includes microglia and macrophage recruitment, astrocyte activation, neurodegeneration, oligodendrocyte death and demyelination, and transient proliferation of OPCs [7-9]. While *in vivo* studies provide system level information on the aftereffects of TBI, it can be difficult to determine how individual molecular parameters, such as the extracellular matrix (ECM), influences the pathology due to the presence of multiple confounding variables. As a result, *in vivo* studies often fail to capture the molecular nuances of the cellular response to injury. Additionally, due to the differences between rodents and humans in terms of size, shape and composition, results generated through rodent models do not necessarily reflect the injury and recovery conditions of humans [10-12]. Development of a tunable *in vitro* platform that can accurately represent the human brain environment under varying injury conditions would be optimal for molecular-level discovery.

2.4 OPCs and OLs in Health and Disease

OPCs are present during early development, peaking between 15-20 weeks gestational age (GA) in humans [13]. OPCs are characterized by the expression of platelet-derived growth factor receptor α (PDGFR-α), a cell-surface receptor which plays a role in cell migration and proliferation. OPCs migrate through the developing brain to reach areas of unmyelinated axons. Upon reaching their target, they proliferate locally, followed by differentiation into pre-myelinating oligodendrocytes (pre-OLs) and ultimately into mature myelinating oligodendrocytes (OLs) [13]. Pre-OLs can be distinguished from OPCs as they begin to express oligodendrocyte markers including proteolipid protein (PLP), O1 and O4, while mature OLs express myelination markers such as myelin basic protein (MBP), myelin-associated glycoprotein (MAG) and myelin-oligodendrocyte glycoprotein (MOG) [14]. Myelination in humans begins between 20-30 weeks GA and peaks during the first year of life, but ultimately continues over the next several decades [13].

Although most myelination occurs in early development, OPCs persist in the fully developed adult brain, making up about 3% of the cell population in grey matter and 8% in white matter [15]. *In vivo* studies have shown that when remyelination is required following an injury, OPCs in the adult brain can migrate to the injury site, differentiate into adult OLs and remyelinate damaged axons [16, 17]. OPCs also act as regulators of neuroinflammation and are involved in phagocytosis of myelin debris [18]. Adult OLs adjacent to the injury site may also participate in remyelination to some degree [19]. Remyelinated axons can be identified by the presence of new myelin sheaths, which are shorter and thinner than myelin sheaths produced during early development. Multiple experimental models confirm the presence of thin myelin sheaths is a hallmark sign of remyelination [20].

Currently, the prevailing explanation for *de novo* axon ensheathment is the recapitulation hypothesis, which states that developmental myelination and remyelination should follow similar processes [21]. However, this is difficult to confirm as the details of OPC differentiation and myelination (such as the interplay of environmental cues, etc.) are not well understood. This is partially because OPCs and OLs are under-studied in comparison to their neuronal peers. As

shown in Figure 1, historically, TBI models and pre-clinical intervention studies primarily focused on neuronal effects in grey matter and have not investigated the impact on OLs or the resulting demyelination which ensues in white matter following TBI [22]. The amount of white matter disruption plays a greater role than grey matter in predicting neurological outcomes [22]. A recent study demonstrated that white matter lesions in humans are correlated with cognitive impairment ($\Delta R^2 = 0.044$), while grey matter injury was less consistent ($\Delta R^2 = 0.034$) based on regression modeling [23]. The importance of OLs on neural regeneration and functional recovery has been overshadowed and research into how OLs respond to injury is warranted.

Neuroinflammation is a confirmed response following TBI. Both *in vitro* and *in vivo* models have demonstrated that OPCs and OLs are affected by the inflammatory response [24]. Following TBI, activated astrocytes and microglia initiate the inflammatory cascade through the release of inflammatory molecules, primarily chemokines and cytokines [9]. The resulting inflammation can both stimulate and inhibit OPC proliferation [9, 25-27]. Recent studies have shown that some of the inflammatory molecules such as proinflammatory chemokine CXCL10 and high mobility group box-1 (HMGB1) caused a reduction of OPCs proliferation and loss of OPCs and OLs [25, 27]. By contrast, leukemia inhibitory factor (LIF) and interleukin-1 beta (IL-1β) increase OPC proliferation at the expense of OLs [9, 26]. However, the exact mechanisms that influence the outcomes have not yet been established [9]. Thus, the incorporation of inflammatory molecules within an *in vitro* model, either via culture medium or hydrogel encapsulation, will allow for more relevant investigation into their individual effects on OPCs and OLs.

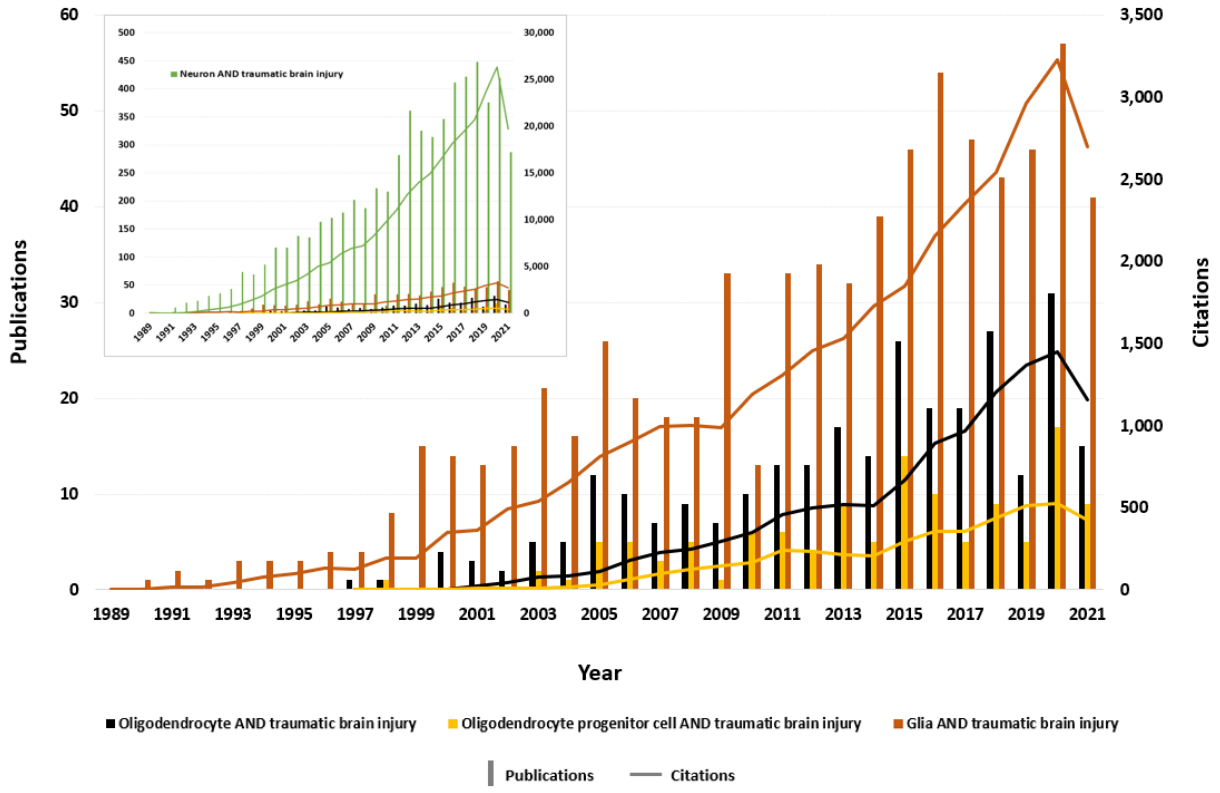

Figure 2.1. Trends comparing the number of neurons, glia and oligo publications and citations over the past two decades.Keywords included "oligodendrocyte AND traumatic brain injury," "oligodendrocyte progenitor cell AND

traumatic brain injury," and "glia AND traumatic brain injury" between 1989 and 2021. Trends were generated using Web of Science's "Citation Report" tool. "Glia" returns the most results in conjunction with TBI, followed by "oligodendrocyte" and "oligodendrocyte progenitor cell." Note that the keyword results for "oligodendrocyte" trends also contain all results for "oligodendrocyte progenitor cell" trends. Inset: a comparison of oligodendrocyte, OPC and glia-TBI trends from the main graph to trends for "neuron AND traumatic brain injury." The results for "neuron" in conjunction with TBI far outnumber OPC, OL and glia-related search results.

2.5 Proposed Hydrogel Research to Address Limitations of Current TBI Models

In vitro platforms offer a promising alternative approach to the challenges of working with *in vivo* models. In contrast to animal models, *in vitro* models require relatively low costs and preparation, while taking shorter periods of time to complete. Hydrogel properties can further enhance the benefits of *in vitro* systems, including the allowance of varying stiffness, topographical cues, and matrix degradation, that all impact cell growth and differentiation [28-30]. The flexibility can provide greater tunability allowing more precise modeling of the diverse range of TBI pathologies. *In vitro* modeling also gives researchers control over the inclusion or exclusion of individual parameters, allowing the elimination of potential confounding variables. Since the overwhelming majority of TBI studies have so far been conducted *in vivo*, there is a knowledge gap that persists at the cellular level.

The complex interactions that occur between glia and neurons has limited the number of research models proposed to study TBI [31]. *In vivo* studies on OPC/OL report white matter injury including axonal damage, demyelination, and oligodendrocyte loss [32]. I*n vitro* model development is an emerging research area that studies the mechanics of white matter injury and mechanical properties of white matter. Studies include cell stretch devices to model axonal damage and demyelination, a 3D printed weight drop system, co-culture of glial cells and 3D cell culture in hydrogels [33-35]. However, few *in vitro* TBI models focus on OPC and OL, with only one study using *in vitro* methodology in the past five years [34]. This study, which used a cell stretching device to assess the impact of mechanical strain on mature OLs, found that mechanical stretch induced a transient loss of myelin protein [34]. Other studies continue to focus on axons, astrocytes, and microglia, but not the oligodendrocyte itself. Additionally, most *in vitro* models have been developed based on animal sources; in particular, 84% are based on rodent models [36]. This introduces a potential translational concern with the rodent *in vitro* models as well due to the differences between rodent and human brain physiology. Therefore, OPC and OL-focused models based on human design parameters are necessary to advance our understanding of OPC/OL injury mechanisms and contributions to functional recovery.

While *in vivo* models have attempted to investigate the cellular response to TBI, the inability to exclude confounding factors causes a lack of precise control over *in vivo* model parameters, making the effects of individual factors difficult to measure. In particular, the effects of TBI on OPC/OL remain under-studied. Creating tunable *in vitro* TBI models could be valuable platforms that would allow fundamental investigation of mechanical insult effects on OPCs, with precise and tunable control over both spatial and temporal parameters, as shown in Figure 2. Using a model system that encapsulates OPCs in a 3D hydrogel would allow the expansion into investigation of how specific hydrogel properties (stiffness, degradability, etc.) affect OPC growth and differentiation while eliminating confounding variables. Further, changes in these properties can be investigated in conjunction with a mechanical insult to simulate the effects of

TBI on encapsulated OPCs leading to a fundamental understanding of the mechanostimulation within OPC.

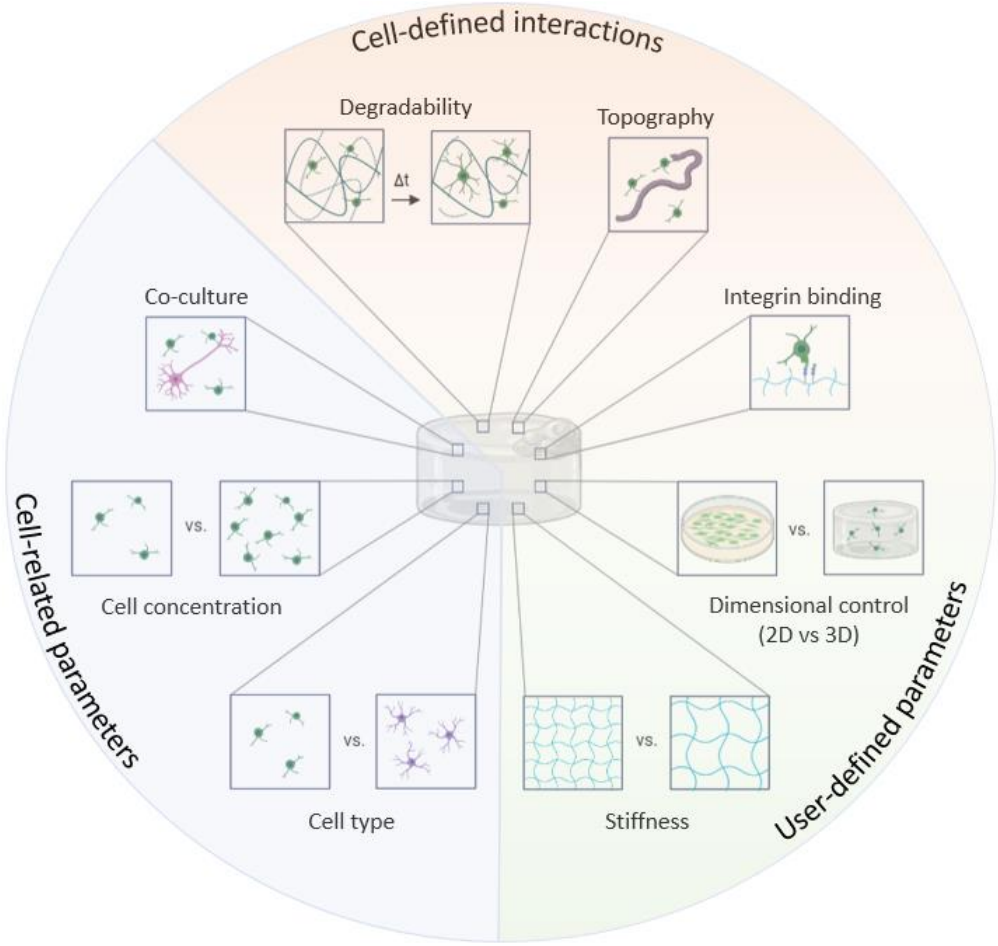

Figure 2.2. Potential injury model parameters for hydrogel biomaterial design. Parameters may be purely cell-based or involve cell-material interactions. Clockwise from top: hydrogels may be engineered for localized degradability by encapsulated cells; may incorporate topographical cues, e.g. electrospun fibers, to provoke cell response; may be designed to incorporate sites for integrin binding; may be designed in either two or three dimensions; may be constructed with specific material properties, e.g. stiffness; may include different cell types; may include different concentrations of cells; may include multiple cell types for co-culture.

Hydrogel properties are an emerging topic of investigation for *in vitro* model advancements with the goal of simulating the natural 3D tissue environment. Examples such as culturing OPCs in 3D gels and inducing TBI of varying mechanisms (stretch, compression) and severities would provide valuable data on the unique OPC responses to mechanical insult [28, 29, 37]. Current knowledge gaps regarding the role of OPCs and OLs in TBI injury response mechanisms can therefore be addressed by collaboration of multiple research groups with experience in hydrogel design, OPC culture, TBI models, and neuropathology to produce a 3D *in vitro* hydrogel model of TBI on encapsulated OPCs. Combination of these expertise would allow the development of a relevant model to examine outcomes such as cell survival, differentiation potential, myelin production, and how injury parameters impact hydrogel properties (see Figure 3). These interdisciplinary discussions can also be used to further optimize pre-existing *in vitro* models which investigate purely axonal effects of TBI, such as axon stretching [38]. Co-culture of both OPC and neurons within the same hydrogel would allow for further investigation into the impact

of TBI on white matter specifically, which is more clinically relevant to neurological outcomes than grey matter [22]. Additionally, this would permit analysis of the interplay between neurons and OPC which cannot be obtained from models containing only one of these cell types individually.

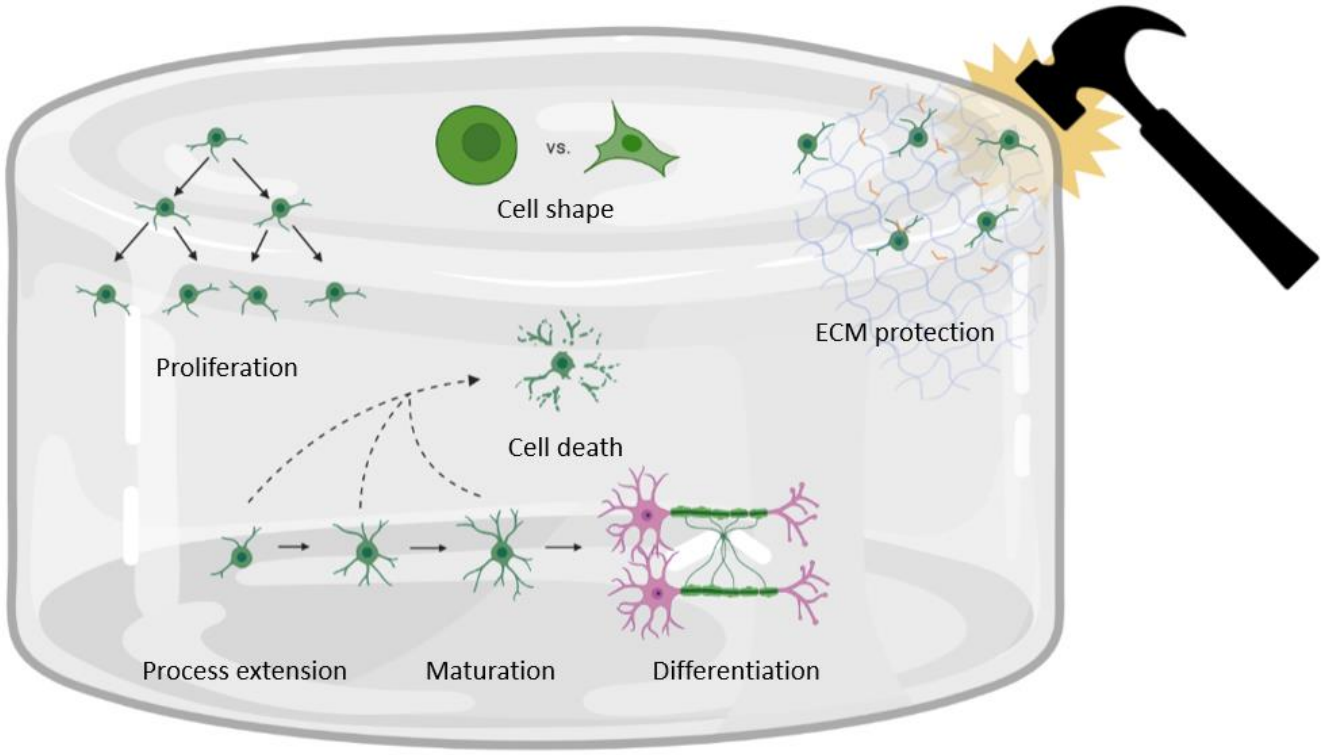

Figure 2.3. Potential impacts of hydrogel culture on encapsulated cells in an injury model. Hydrogel cultures may impact proliferation rates of encapsulated OPCs (top left) as well as cell shape (top center). The hydrogel matrix may also shield encapsulated OPC from mechanical insult (top right) by dissipating transmitted forces. Physical and biochemical cues from the hydrogel culture system may also impact the development of encapsulated OPCs such as the degree of process extension and the extent of maturation and differentiation (bottom). At any point in the maturation and differentiation process, the artificial ECM and developmental cell stage may have combinatorial effects on how mechanical forces transmitted through/by the hydrogel may differentially impact cell survival (center).

Preliminary investigations by our team have shown that OPCs can be cultured in both norbornene-functionalized hyaluronic acid (NorHA) and dimethacrylated polyethylene glycol (PEG-DM) hydrogels of tunable stiffness. Further advancement with the addition of electrospun methacrylated hyaluronic acid (MeHA) fibers that can be co-encapsulated with OPCs in order to provide topographical cues which mimic those of native axons has been conducted (see Figure 2.4). In these original experiments, we encapsulated MADM OPCs in 3D 1.5% (w/v) norbornene-modified hyaluronic acid hydrogels as previously published. However, here, we co-encapsulated OPCs either with, or without, methacrylate-modified hyaluronic acid fibers electrospun with diameters similar to mature axons. As before, cells encapsulated without fibers continued to proliferate and form OPC spheroids. However, in the presence of axon-mimicking fibers, OPCs slowed proliferation and instead developed processes indicating maturation. In future studies, both cell- and fiber-containing gels can be subjected to a mechanical insult,

followed by confocal imaging, immunostaining, ATP/DNA analysis, and rheology to determine the impact of injury on OPCs or OLs in a tissue-like 3D environment. A 3D hydrogel that mimics native ECM mechanics could provide protective, force-dissipating characteristics that reduce damage to cells. Alternatively, an elastic matrix could propagate mechanical forces, transmitting them more directly to cells and thereby intensifying cell damage. We, among a limited number of other research groups, are attempting to elucidate this relationship [39, 40]. Such other groups include the Kaplan lab, which uses an *in vitro* contusion model to track the spread of neural network degeneration in 3D space following a TBI, and the Botvinick lab, which measures the displacement of fibers in a fibrin hydrogel to track the propagation of forces within fibrous ECM [39,40].

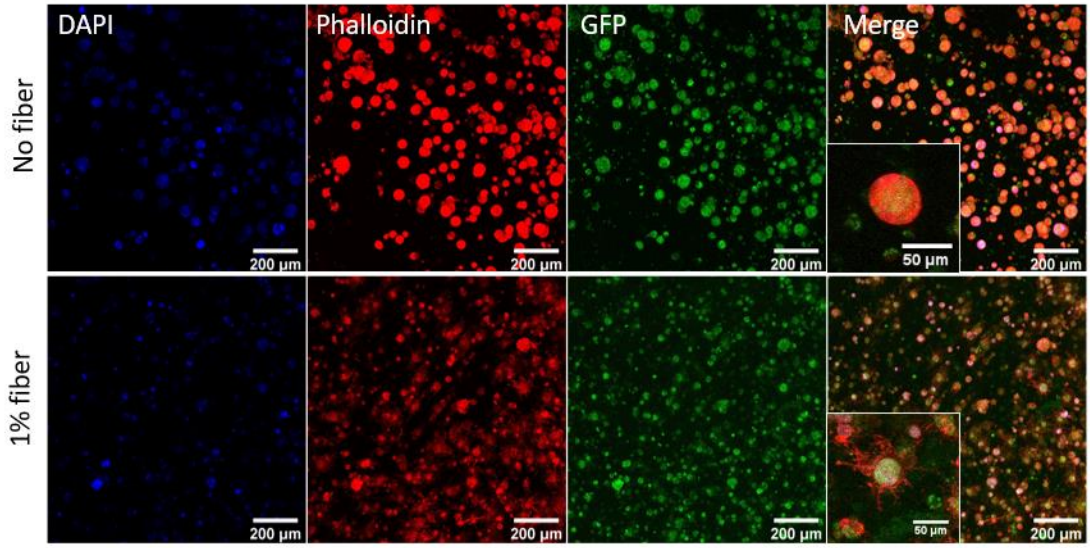

Figure 2.4. Representative Z-stack maximum projections (depth 400 µm) for MADM OPCs encapsulated in 1.5 % (w/v) NorHA gels with or without 1 % (w/v) MeHA fibers. Cell nuclei are stained with DAPI (blue), f-actin is stained with phalloidin (red) and living cells constitutively express GFP (green). Cells are co-encapsulated in the presence of 1% electrospun MeHA fiber (bottom row) or in control gels containing no fiber (top row). Cells encapsulated in the presence of electrospun fibers extend numerous processes, while those encapsulated in control gels retain a smooth, rounded morphology and form large multicellular spheroids.

Construction of a 3D *in vitro* OPC or co-culture model for TBI research is a vital step towards development of clinically relevant tools for identifying and testing therapeutics. Initial *in vitro* work with OPC in hydrogels will address the current knowledge gap by allowing precise, tunable control of hydrogel design parameters while simultaneously eliminating confounding variables. This permits the fundamental analysis of the influence of each parameter (e.g., topography, injury, severity) on the fate of post-TBI OPC as a function of time. Next steps towards more accurately recapitulating the native brain tissue environment may include neuronal co-culture with OPCs to study effects of TBI on white matter; further tuning matrix properties like stiffness, topography and integrin inclusion to better reflect native ECM conditions; and/or incorporation of inflammatory cytokines to determine the effects of inflammation on OPCs/OLs following TBI. Then, once the effects of TBI and ECM parameters on OPC and OL are better understood, the resulting knowledge can be adapted to develop an injectable therapeutic hydrogel for OPC delivery. This adaptation will depend on researchers with experience in hydrogel design, as

injectable therapeutic delivery introduces new potential design considerations such as shear-thinning and self-healing [41-43].

2.6 Conclusions

In summary, OLs are an essential cell type within the CNS which maintains homeostasis of the axons and efficient neurotransmission. TBI results in damage to the tissue as a whole, but little research has been focused on how the OLs' response to injury is associated with clinical outcomes. There is a substantial knowledge gap that exists surrounding the impact of TBI on OPC/OL in white matter specifically. Effective therapeutics cannot be designed for axonal regeneration unless fundamental research on OL is enhanced. Collaboration of researchers from various backgrounds spanning hydrogel design, OPC culture and brain injury models will be vital to comprehensively understand the role of OLs in TBI recovery. By combining these skill sets, *in vitro* platforms can be developed for studying cell development where OPCs grow, differentiate, and produce myelin similarly to *in vivo.* Such a model can then be perturbed by a mechanical insult to model the effects of TBI on growth and development of encapsulated OPCs. Through the development of a hydrogel-based TBI model, it may soon be possible to elucidate the impacts of brain injury on a molecular and cellular level. With some additional design considerations, the future looks bright for the development and screening of hydrogel-based injectable therapeutics that can positively influence the survival of OLs and ultimately enhance the functional recovery of neurons following injury.

2.7 Acknowledgements

This work was supported by the National Science Foundation [grant number 2104723] (KJL, PJV), as well as the University of Virginia Dean's Scholar Fellowship award (RAM). Funding sources were not involved in study design, data collection or analysis, in the writing of the report, or in the decision to submit the article for publication.

2.8 References

[1] M.C. Dewan, A. Rattani, S. Gupta, R.E. Baticulon, Y.-C. Hung, M. Punchak, A. Agrawal, A.O. Adeleye, M.G. Shrime, A.M. Rubiano, Estimating the global incidence of traumatic brain injury, Journal of neurosurgery 130(4) (2018) 1080-1097.
[2] D.V. Bradshaw Jr, Y. Kim, A. Fu, C.M. Marion, K.L. Radomski, J.T. McCabe, R.C. Armstrong, Repetitive Blast Exposure Produces White Matter Axon Damage without Subsequent Myelin Remodeling: In Vivo Analysis of Brain Injury Using Fluorescent Reporter Mice, Neurotrauma Reports 2(1) (2021) 180-192.
[3] D. Freedman, N. Nived, B. Decker, S. Narla, S. Shafik, S. Manohar, R. Salvi, M.K. Stachowiak, E.K. Stachowiak., Neurogenesis and Oligodendrogenesis in a Mouse Model of Blast-Induced Traumatic Brain Injury., NEUROLOGY AND NEUROBIOLOGY, 2020.
[4] A. Chendrasekhar, B. Kuczabski, D. Cohen, M. Grageda, D. Genovese-Scullin, J. Patwari, L. Harris, Delayed sequelae related to mild traumatic brain injury in children, Global pediatric health 7 (2020) 2333794X20947988.

[5] L.D. Nelson, N.R. Temkin, S. Dikmen, J. Barber, J.T. Giacino, E. Yuh, H.S. Levin, M.A. McCrea, M.B. Stein, P. Mukherjee, Recovery after mild traumatic brain injury in patients presenting to US level I trauma centers: a transforming research and clinical knowledge in traumatic brain injury (TRACK-TBI) study, JAMA neurology 76(9) (2019) 1049-1059.
[6] J. Haarbauer-Krupa, M.J. Pugh, E.M. Prager, N. Harmon, J. Wolfe, K.C. Yaffe, Epidemiology of chronic effects of traumatic brain injury, Journal of neurotrauma (ja) (2021).
[7] J. Anderson, M. Patel, D. Forenzo, X. Ai, C. Cai, Q. Wade, R. Risman, L. Cai, A novel mouse model for the study of endogenous neural stem and progenitor cells after traumatic brain injury, Experimental neurology 325 (2020) 113119.
[8] J. Flygt, F. Clausen, N. Marklund, Diffuse traumatic brain injury in the mouse induces a transient proliferation of oligodendrocyte progenitor cells in injured white matter tracts, Restorative neurology and neuroscience 35(2) (2017) 251-263.
[9] J. Flygt, K. Ruscher, A. Norberg, A. Mir, H. Gram, F. Clausen, N. Marklund, Neutralization of interleukin-1β following diffuse traumatic brain injury in the mouse attenuates the loss of mature oligodendrocytes, Journal of neurotrauma 35(23) (2018) 2837-2849.
[10] R. Vink, Large animal models of traumatic brain injury, Journal of neuroscience research 96(4) (2018) 527-535.
[11] L.W. Swanson, Mapping the human brain: past, present, and future, Trends in neurosciences 18(11) (1995) 471-474.
[12] H.A. Kinder, E.W. Baker, F.D. West, The pig as a preclinical traumatic brain injury model: current models, functional outcome measures, and translational detection strategies, Neural regeneration research 14(3) (2019) 413.
[13] E. van Tilborg, C.G. de Theije, M. van Hal, N. Wagenaar, L.S. de Vries, M.J. Benders, D.H. Rowitch, C.H. Nijboer, Origin and dynamics of oligodendrocytes in the developing brain: Implications for perinatal white matter injury, Glia 66(2) (2018) 221-238.
[14] S. Kuhn, L. Gritti, D. Crooks, Y. Dombrowski, Oligodendrocytes in development, myelin generation and beyond, Cells 8(11) (2019) 1424.
[15] A. Fernandez-Castaneda, A. Gaultier, Adult oligodendrocyte progenitor cells–multifaceted regulators of the CNS in health and disease, Brain, behavior, and immunity 57 (2016) 1-7.
[16] P. Assinck, G.J. Duncan, J.R. Plemel, M.J. Lee, J.A. Stratton, S.B. Manesh, J. Liu, L.M. Ramer, S.H. Kang, D.E. Bergles, Myelinogenic plasticity of oligodendrocyte precursor cells following spinal cord contusion injury, Journal of Neuroscience 37(36) (2017) 8635-8654.
[17] N. Nagoshi, M. Khazaei, J.E. Ahlfors, C.S. Ahuja, S. Nori, J. Wang, S. Shibata, M.G. Fehlings, Human spinal oligodendrogenic neural progenitor cells promote functional recovery after spinal cord injury by axonal remyelination and tissue sparing, Stem cells translational medicine 7(11) (2018) 806-818.
[18] A. Fernández-Castañeda, M.S. Chappell, D.A. Rosen, S.M. Seki, R.M. Beiter, D.M. Johanson, D. Liskey, E. Farber, S. Onengut-Gumuscu, C.C. Overall, The active contribution of OPCs to neuroinflammation is mediated by LRP1, Acta neuropathologica 139(2) (2020) 365-382.
[19] I.D. Duncan, A.B. Radcliff, M. Heidari, G. Kidd, B.K. August, L.A. Wierenga, The adult oligodendrocyte can participate in remyelination, Proceedings of the National Academy of Sciences 115(50) (2018) E11807-E11816.
[20] I.D. Duncan, R.L. Marik, A.T. Broman, M. Heidari, Thin myelin sheaths as the hallmark of remyelination persist over time and preserve axon function, Proceedings of the National Academy of Sciences 114(45) (2017) E9685-E9691.

[21] M. Abu-Rub, R.H. Miller, Emerging cellular and molecular strategies for enhancing central nervous system (CNS) remyelination, Brain sciences 8(6) (2018) 111.
[22] H. Pu, X. Zheng, X. Jiang, H. Mu, F. Xu, W. Zhu, Q. Ye, Y. Jizhang, T.K. Hitchens, Y. Shi, Interleukin-4 improves white matter integrity and functional recovery after murine traumatic brain injury via oligodendroglial PPARγ, Journal of Cerebral Blood Flow & Metabolism 41(3) (2021) 511-529.
[23] J. Reber, K. Hwang, M. Bowren, J. Bruss, P. Mukherjee, D. Tranel, A.D. Boes, Cognitive impairment after focal brain lesions is better predicted by damage to structural than functional network hubs, Proceedings of the National Academy of Sciences 118(19) (2021).

** This study assesses the level of general cognitive impairment associated with lesions in highly connected regions, or "hubs", of the human brain. Lesions disrupting white matter hubs are highly associated with cognitive impairment, while lesions disrupting grey matter hubs exhibit a weaker association based on regression modeling.
[24] C.S. Baaklini, K.S. Rawji, G.J. Duncan, M.F. Ho, J.R. Plemel, Central nervous system remyelination: Roles of glia and innate immune cells, Frontiers in molecular neuroscience 12 (2019) 225.
[25] T. Sen, P. Saha, R. Gupta, L.M. Foley, T. Jiang, O.S. Abakumova, T.K. Hitchens, N. Sen, Aberrant ER stress induced neuronal-IFNβ elicits white matter injury due to microglial activation and T-cell infiltration after TBI, Journal of Neuroscience 40(2) (2020) 424-446.
[26] M.J. Frondelli, M.L. Mather, S.W. Levison, Oligodendrocyte progenitor proliferation is disinhibited following traumatic brain injury in leukemia inhibitory factor heterozygous mice, Journal of neuroscience research (2021).
[27] R. Ved, F. Sharouf, B. Harari, M. Muzaffar, S. Manivannan, C. Ormonde, W. Gray, M. Zaben, Disulfide HMGB1 acts via TLR2/4 receptors to reduce the numbers of oligodendrocyte progenitor cells after traumatic injury in vitro, Scientific Reports 11(1) (2021) 1-14.
[28] D.B. Unal, S.R. Caliari, K.J. Lampe, 3D hyaluronic acid hydrogels for modeling oligodendrocyte progenitor cell behavior as a function of matrix stiffness, Biomacromolecules 21(12) (2020) 4962-4971.

**Authors introduce a semi-synthetic 3D NorHA hydrogel with tunable stiffness to model the effects of matrix properties on encapsulated OPCs. OPCs are viable in biomaterial gels with storage modulus from 200-2000 Pa, with higher levels of viability and larger cell spheroid formation in lower stiffness gels.

[29] E. Meco, W.S. Zheng, A.H. Sharma, K.J. Lampe, Guiding oligodendrocyte precursor cell maturation with urokinase plasminogen activator-degradable elastin-like protein hydrogels, Biomacromolecules 21(12) (2020) 4724-4736.
[30] E. Hui, K.I. Gimeno, G. Guan, S.R. Caliari, Spatiotemporal control of viscoelasticity in phototunable hyaluronic acid hydrogels, Biomacromolecules 20(11) (2019) 4126-4134.
[31] M. Braun, K. Vaibhav, N.M. Saad, S. Fatima, J.R. Vender, B. Baban, M.N. Hoda, K.M. Dhandapani, White matter damage after traumatic brain injury: a role for damage associated molecular patterns, Biochimica et Biophysica Acta (BBA)-Molecular Basis of Disease 1863(10) (2017) 2614-2626.
[32] C.M. Marion, K.L. Radomski, N.P. Cramer, Z. Galdzicki, R.C. Armstrong, Experimental traumatic brain injury identifies distinct early and late phase axonal conduction deficits of white

matter pathophysiology, and reveals intervening recovery, Journal of Neuroscience 38(41) (2018) 8723-8736.
[33] W. Shi, P. Dong, M.A. Kuss, L. Gu, F. Kievit, H.J. Kim, B. Duan, Design and evaluation of an in vitro mild traumatic brain injury modeling system using 3D printed mini impact device on the 3D cultured human iPSC derived neural progenitor cells, Advanced Healthcare Materials (2021) 2100180.
[34] J. Kim, A.A. Adams, P. Gokina, B. Zambrano, J. Jayakumaran, R. Dobrowolski, P. Maurel, B.J. Pfister, H.A. Kim, Mechanical stretch induces myelin protein loss in oligodendrocytes by activating Erk1/2 in a calcium-dependent manner, Glia 68(10) (2020) 2070-2085.

*Authors use an *in vitro* cellular stretch device to assess the impact of mechanical strain on mature OLs. Mechanical stretch was found to induce a transient loss of myelin protein in OLs, which was mediated by an Erk1/2-dependent mechanotransduction mechanism.

[35] C.T. Tsui, S.R. MacGillivray, S.M. Weber, L. McAllister, M.A. Churchward, C.R. Dennison, K.G. Todd, Applying a novel 3D hydrogel cell culture to investigate activation of microglia due to rotational kinematics associated with mild traumatic brain injury, Journal of the Mechanical Behavior of Biomedical Materials 114 (2021) 104176.
[36] Y.-H. Wu, S. Rosset, T.-r. Lee, M. Dragunow, T. Park, V. Shim, In Vitro Models of Traumatic Brain Injury: A Systematic Review, Journal of Neurotrauma (2021).
[37] N. Hlavac, F. Guilhaume-Corrêa, P.J. VandeVord, Mechano-stimulation initiated by extracellular adhesion and cationic conductance pathways influence astrocyte activation, Neuroscience Letters 739 (2020) 135405.

*Authors demonstrate astrocyte activation following overpressure stimulation using both 3D hydrogel and 2D monolayer cell culture to model TBI. The results show how focal adhesion and cation channel conductance contribute to early patterns of astrocyte activation.

[38] J.C. Maggiore, J.C. Burrell, K.D. Browne, K.S. Katiyar, F.A. Laimo, Z.S. Ali, H.M. Kaplan, J.M. Rosen, D.K. Cullen, Tissue engineered axon-based "living scaffolds" promote survival of spinal cord motor neurons following peripheral nerve repair, Journal of Tissue Engineering and Regenerative Medicine 14(12) (2020) 1892-1907.
[39] Q. Hu, T.A. Morris, A. Grosberg, A.J. Levine, E.L. Botvinick, Actively driven fluctuations in a fibrin network, Frontiers in Physics 8 (2021) 653.
[40] V. Liaudanskaya, J.Y. Chung, C. Mizzoni, N. Rouleau, A.N. Berk, L. Wu, J.A. Turner, I. Georgakoudi, M.J. Whalen, T.J. Nieland, Modeling Controlled Cortical Impact Injury in 3D Brain-Like Tissue Cultures, Advanced healthcare materials 9(12) (2020) 2000122.
[41] J.D. Tang, C. Mura, K.J. Lampe, Stimuli-responsive, pentapeptide, nanofiber hydrogel for tissue engineering, Journal of the American Chemical Society 141(12) (2019) 4886-4899.
[42] B.A. Aguado, W. Mulyasasmita, J. Su, K.J. Lampe, S.C. Heilshorn, Improving viability of stem cells during syringe needle flow through the design of hydrogel cell carriers, Tissue Engineering Part A 18(7-8) (2012) 806-815.
[43] J.D. Tang, E.B. Roloson, C.D. Amelung, K.J. Lampe, Rapidly Assembling Pentapeptides for Injectable Delivery (RAPID) Hydrogels as Cytoprotective Cell Carriers, ACS Biomaterials Science & Engineering 5(5) (2019) 2117-2121.

*Authors describe the shear-thinning and self-healing properties of a self-assembling peptide hydrogel which exhibits material properties similar to native brain tissue. These properties allow RAPID gels to be syringe injectable and protect cells, including OPCs, from mechanical and shear forces, thus increasing the viability of cells delivered via injection.

Chapter 3: Guiding oligodendrocyte progenitor cell maturation using electrospun fiber cues in a 3D hyaluronic acid hydrogel culture system

Rachel A. Mazur[1], Kyle J. Lampe[1]

1 Department of Chemical Engineering, University of Virginia, Charlottesville, VA USA

3.1 Abstract

The current lack of therapeutic approaches to demyelinating disorders and injuries stems from a lack of knowledge surrounding the underlying mechanisms of myelination. This knowledge gap motivates the development of effective models to study the role of environmental cues in oligodendrocyte progenitor cell (OPC) maturation. Such models should focus on determining which factors influence OPCs to proliferate and differentiate into mature myelinating oligodendrocytes (OLs). Here, we introduce a hyaluronic acid (HA) hydrogel system composed of crosslinked HA containing encapsulated HA fibers with swollen diameters similar to mature axons (2.7 ± 0.2 μm). We tuned hydrogel storage moduli to simulate native brain tissue (200-2000 Pa) and studied the effects of fiber presence on OPC proliferation, metabolic activity, protein deposition, and morphological changes in intermediate stiffness (800 ± 0.3 Pa) gels. OPCs in fiber-containing gels at culture days 4 and 7 exhibited a significantly greater number of process extensions, a morphological change associated with differentiation. By contrast, OPCs in fiber-free control gels maintained more proliferative phenotypes with 2.2-fold higher proliferation at culture day 7, and 1.8-fold higher metabolic activity at culture days 4 and 7. Fibers were also found to influence extracellular matrix (ECM) deposition and distribution, with more, and more distributed, nascent ECM deposition occurring in the fiber-containing gels. Overall, these data indicate that the inclusion of appropriately sized HA fibers provide topographical cues which guide OPCs toward differentiation. This HA hydrogel/fiber system is a promising *in vitro* scheme providing valuable insight into the underlying mechanisms of differentiation and myelination.

3.2 **Introduction and Background**

In healthy central nervous system (CNS) tissue, neuronal axons are protected by a lipid-rich myelin sheath which increases the specificity and efficiency of electrical signal conduction [1]. Demyelination occurs when a CNS injury or disorder causes degradation of the myelin sheath. Therapeutic strategies for minimizing demyelination and promoting remyelination are essential for addressing demyelinating disorders and injuries, which collectively affect over 5 million people throughout the world [2, 3]. Multiple sclerosis (MS), the most common demyelinating disorder, is estimated to affect 2.5 million individuals worldwide [3]. Central nervous system injuries such as brain or spinal cord trauma can also result in demyelination [4]. While some

symptoms of demyelinating disorders and injuries can be managed, there is currently no treatment capable of reversing the underlying damage caused by demyelination [5, 6].

As oligodendrocytes (OLs) mature, they extend multiple processes which wrap around axons and compact to form the final myelin sheath [7]. Demyelination can be initiated through direct physical or chemical insult to the oligodendrocyte (primary demyelination), or as a result of axonal loss (secondary demyelination) [8]. Demyelination leads to many neurological difficulties, including decreased cognitive function and impaired coordination. Remyelination can occur in vivo to some extent, as new oligodendrocyte progenitor cells (OPCs) migrate to the affected area, proliferate locally, and differentiate and mature into myelinating oligodendrocytes. However, the resulting sheaths are typically shorter and thinner than normal [9]. Additionally, this process often fails due to inadequate migration of OPCs to the injury site (recruitment failure) or an inability of recruited OPCs to differentiate and mature into oligodendrocytes (differentiation failure) [9]. In order to engineer potential therapeutics, the underlying factors which govern myelination and remyelination must first be determined. Unfortunately, a knowledge gap persists in this area since the specific factors which influence OPC/OL development are under-studied [10].

To further understand the mechanisms behind myelination, demyelination, and recovery, it is vital to identify specific factors capable of guiding neural stem cells (NSCs) or OPCs into mature myelinating oligodendrocytes. Of the studies which do exist, the vast majority have been conducted *in vivo* [11, 12]. The existing *in vivo* studies provide insight into the roles of OPC/OL in demyelination and recovery, but rarely permit independent examination of key factors of interest. Furthermore, due to the presence of confounding factors in *in vivo* developmental cascades, it is often difficult to determine the precise impact of individual factors on OPC/OL growth and development.

In contrast to *in vivo* animal models, *in vitro* biomaterial systems are an emerging platform for studying responses to individual environmental cues at the cellular level. *In vitro* neural tissue models simulate important properties of the native extracellular matrix (ECM) but allow for precise and tunable control of model parameters not possible in vivo. Some examples of parameters with the potential to impact cell growth and differentiation include matrix stiffness, OPC/neuron co-culture, topographical cues, integrin-ligand interactions, drug or growth factor delivery, and/or matrix degradation [13-20]. As one example, stiffness within the native brain tissue range (G' = 200-2000 Pa) promotes cell viability and differentiation [21, 22]. Tuning these parameters within an engineered *in vitro* model permits investigation into the unique effects of individual factors while simultaneously eliminating potential confounding variables.

Hydrogel platforms are a promising choice for *in vitro* culture since they are biocompatible, tunable, and facilitate cell behaviors such as migration, proliferation, and differentiation. Previous work has demonstrated that OPCs and their parent cells (neural stem cells) can be cultured in 3D hydrogels of various types, including polyethylene glycol (PEG), chitosan, and

collagen [16, 17, 23, 24]. Hyaluronic acid (HA) hydrogels are especially relevant for CNS applications, since HA is a key component of brain extracellular matrix (ECM), particularly within the perineural net [25]. Norbornene-functionalized hyaluronic acid (NorHA) gels can be covalently crosslinked under UV light to reliably form gels within the range of native brain tissue [22]. Our group has previously demonstrated OPC viability and growth in this system [22]. This system also facilities detection of nascent ECM by the encapsulated cells. Encapsulated cells are known to remodel their local microenvironment and deposit ECM proteins within HA and other hydrogel systems [26]. *In vivo,* OPCs have been shown to secrete ECM proteins such as laminin and fibronectin [27, 28]. However, the amount, pattern, and composition of OPC protein deposition remains undetermined. Our hydrogel system can be used to elucidate these factors and to determine how protein deposition by OPCs varies in response to fiber cues.

Topographical cues, such as electrospun fibers, are another matrix factor that influences OPC differentiation and OL myelination. When seeded onto electrospun polystyrene fibers with diameters similar to in vivo myelinated axons (0.3 - 4 μm), some OPCs differentiate and wrap the fibers, particularly for fibers of larger diameters (>0.4 μm) [29, 30]. Fiber systems composed of other polymeric materials, including poly(trimethylene carbonate-co-ε-caprolactone) (P(TMC-CL)) and graphene oxide and laminin-coated polycaprolactone (PCL), also increased NSC differentiation into oligodendrocytes [31, 32]. To the best of our knowledge, the effects of electrospun fiber topography on OPCs have only been conducted in 2D with stiff polymeric materials. Hydrogel-fiber composite materials have been explored for non-neural cell types in various contexts, including guiding angiogenesis or cardiomyocyte alignment [33, 34]. 3D cultures containing other forms of topography, such as ablated microchannels and interfaces between bicontinuous hydrogel systems, have shown that topographical cues guide cell migration in a 3D context [35, 36]. Our novel culture system allows for independent tuning of factors such as bulk gel stiffness, fiber size, and fiber concentration. This independent control over individual parameters allows precise examination of the role of micron-scale hydrogel fiber topography in guiding cell behaviors, such as proliferation and differentiation, in a 3D context.

In this work, we use electrospun methacrylated hyaluronic acid (MeHA) fibers with swollen diameters representative of native axons (2.7 ± 0.2 μm) to simulate the micron-scale structural cues of native axons [37]. Both nanoindentation and rheology were performed to test the effects of fiber inclusion on both the local and bulk gel stiffness, respectively. We directly compared MADM OPC cultures in fiber-containing hydrogels (+ fibers) to fiber-free control gels (- fibers) over a seven-day period via immunostaining and examination of cell morphology. We performed an EdU-based proliferation assay and an ATP/DNA assay to assess how fiber presence impacted cell proliferation and metabolic activity, respectively. Finally, we conducted immunostaining assays to quantify how OPCs deposited laminin and fibronectin to remodel their local environments within the hydrogel.

3.3. Materials and Methods

3.3.1 Flask Preparation and Cell Culture

Sterile T75 (VWR) tissue culture flasks were coated with 5 mL of a 10 µg/mL polyornithine solution and incubated at 37 °C for a minimum of 4 hours and rinsed with Dulbecco's Phosphate-Buffered Saline (DPBS). Green fluorescent protein positive (GFP+) mosaic analysis with double markers (MADM) OPCs were a generous gift from Prof. Hui Zong's lab [38]. All cells were cultured in OPC proliferation media throughout all maintenance and experiments. Proliferation media consisted of Dulbecco's Modified Eagle Medium (DMEM) with 4.5 g/L D-glucose, 4 mM L-glutamine, and 110 mg/L sodium pyruvate (Invitrogen), supplemented with N2 supplement (Invitrogen), B27 supplement (Invitrogen), and 1% penicillin-streptomycin (Invitrogen). Cells were seeded onto flasks at a seeding density of 1 x 10^4 cells/cm^2. Media was changed every two days, and cells were passaged at 80-90% confluence. During cell passaging, cells were detached using a solution of 0.125% (0.5x) trypsin, followed by rinsing the flask with 10 mL DPBS. The resulting cell solution was centrifuged at 1000 rpm for 5 minutes, after which the supernatant was aspirated. Cells were resuspended in 300 µL of PBS plus 4.5 g/L D-glucose (PBSG) for cell counting.

3.3.2 NorHA Synthesis

Method 1: Norbornene-functionalized hyaluronic acid (NorHA) was synthesized similar to previously published work [39, 40]. Briefly, hyaluronic acid tert-butyl ammonium salt (HA-TBA) was synthesized by allowing sodium hyaluronate (Lifecore, 74 kDa) to undergo proton exchange with Dowex 50W resin, filtering, titrating with TBA-OH to pH 7.05, and lyophilizing. HA-TBA was brought to room temperature and added to a round bottomed flask equipped with a stir bar. To achieve a 20-30% functionalization efficiency, 0.3 stoichiometric equivalents of 5-norbornene-2-methylamine were added, and the flask was purged with nitrogen for five minutes to ensure anhydrous reaction conditions. Anhydrous dimethyl sulfoxide (DMSO) was then added by cannulation (0.5 mL DMSO per 0.1 g HA-TBA) and mixed until the HA-TBA was completely dissolved. 0.3 stoichiometric equivalents of benzotriazole-1-yl-oxy-tris-(dimethylamino)-phosphonium hexafluorophosphate (BOP) were added via cannulation and the reaction was allowed to proceed for 2 hours at room temperature. The reaction was then quenched with 10 mL of deionized water and transferred to pre-soaked dialysis tubing with a 6-8 kDa molecular weight cut-off. Dialysis against deionized water was conducted for 5 days, changing the water twice daily. Products were vacuum filtered and dialyzed for an additional 5 days before lyophilizing. Purity and degree of norbornene functionalization were determined with ^{1}H NMR (Varian Inova 500 MHz) using D_2O as a solvent (Figure S3.1). The final NorHA product was stored under nitrogen at 4 °C.

Method 2: Norbornene-functionalized hyaluronic acid (NorHA) was synthesized using previously published methods [41]. Briefly, 4-(4,6-dimethoxy[1,3,5]triazin-2-yl)-4-

methylmorpholinium chloride (DMTMM) as a coupling agent. Hyaluronic acid (60 kDa, LifeCore) was dissolved at 25 mg/mL in 40 mL of 1 mM 2-(N-morpholino)ethanesulfonic acid (MES) buffer and pH was adjusted to 5.5 with 10 M NaOH. DMTMM coupling agent (VWR) was added to a concentration of 31 mg/mL and mixed until the DMTMM was completely dissolved (about 10 minutes). To achieve a 20-30% functionalization efficiency, 0.271 mL of 5-norbornene-2-methylamine (TCI America) was added, and the mixture was stirred overnight at room temperature. The reaction was then precipitated into 250 mL of cold 95% ethanol. Precipitate was collected by vacuum filtration and re-dissolved in 2M brine solution, followed by transferring to pre-soaked dialysis tubing with a 6-8 kDa molecular weight cut-off. Dialysis was conducted against DI water for 24 hours, followed by brine solution for 24 hours, changing the water twice daily. A final round of dialysis was conducted against DI water for 24 hours, followed by lyophilizing. Purity and degree of norbornene functionalization were determined with ^{1}H NMR (Varian Inova 500 MHz) using D_2O as a solvent (Figure S3.2). The final NorHA product was stored under nitrogen at 4 °C.

3.3.3 MeHA synthesis

Methacrylated hyaluronic acid (MeHA) was synthesized according to previously established protocols [42, 43]. Briefly, methacrylic anhydride (MA) was added dropwise to research grade sodium hyaluronate (Lifecore Biomedical, 74 kDa) at 1% w/v and stirred until homogeneous. The solution was kept on ice and the pH was maintained between 8-9 with 5 N NaOH. MA was added in a 1:1 molar ratio to HA with 12.3x molar excess. After all methacrylic anhydride was added, the solution was continually stirred overnight. The solution was then dialyzed (molecular weight cutoff 6-8 kDa) for 5 days against deionized water. Macromer solution was frozen overnight at –80° C and lyophilized for 3 days. Purity and degree of norbornene functionalization were determined with ^{1}H NMR (Varian Inova 500 MHz) using D_2O as a solvent (Figure S3.3). The final MeHA product was stored under nitrogen at 4 °C.

3.3.4 Electrospinning and fiber characterization

Electrospinning parameters were selected based on previously established protocols [44, 45]. Briefly, electrospinning solution was prepared in 2 mL batches containing 2 wt% MeHA, 3 wt% 9 kDa polyethylene oxide (Sigma), 0.05 wt% Irgacure D-2959 photoinitiator (I2959, Sigma) and 0.415 mg/mL methacrylated rhodamine B (Sigma) dissolved in deionized water. Solution was protected from light and allowed to dissolve in a 5 mL Cadence syringe for 24-48 hours with stirring. Fibers were then spun using a Spraybase electrospinning machine at 21% relative humidity with a 21 cm collection distance, 8-11 kV voltage, 20-gauge needle and 0.4 mL/hr flow rate. Dry fibers were collected on a sheet of aluminum foil and stored under nitrogen until crosslinking. Crosslinking was conducted for 15 minutes using an Omnicure UV light (365 nm) set to an intensity of 14 mW/cm^2. Dry electrospun fibers were imaged using SEM with a voltage of 1.0 kV and working distance of 21 cm. 4 images of different sites were sampled at 5,000x and

10,000x magnifications. Fiber diameters were determined using the length measuring tool in FIJI ImageJ (taking scale bar as a reference) [46]. Images of dry fibers are shown in Figure S3.9.

Dry fibers were swollen overnight in deionized water and processed by repeatedly passing through an 18-gauge needle, followed by a 21-gauge needle similar to previously established protocols [45]. This process is illustrated in Figure S3.8. This swollen fiber solution was used for subsequent hydrogel encapsulation. Swollen fiber solution (5 wt% in PBS) was applied to a microscope slide and imaged using a Zeiss inverted fluorescent microscope. Fluorescent signal from the tagged rhodamine B was imaged between 2.5-10x at multiple sites. Fiber diameters were determined using the length measuring tool in FIJI ImageJ, using the scale bar as a reference [46]. Images of swollen fibers encapsulated in NorHA gels are shown in Figure S3.7.

3.3.5 Rheology

NorHA macromer solution was created by dissolving 1 – 2wt% NorHA macromer, 0.0328wt% LAP, and dithiothreitol (DTT, Sigma) at an 0.312 thiol-norbornene ratio in PBS. For fiber-containing conditions, electrospun fibers were also included at 1 wt% (based on dry mass). 75 µL aliquots were pipetted onto a UV-configured plate of an Anton Parr MCR 302 rheometer. A 25 mm diameter smooth cone and plate with a 0.505º angle was used to perform a time sweep. Gels were cured in-situ under conditions previously determined to be within the LVE range (0.1% oscillatory strain and 10 rad/s oscillation frequency), and 4 mW/cm^2 UV light intensity (365 nm). Samples were exposed to oscillatory motion in the absence of UV light for 30s at the start of each test. UV light exposure was introduced underneath the plate for 2 min, after which UV light was turned off and oscillatory motion continued for an additional 60s. Plateau storage modulus was calculated by averaging over the final 30s.

3.3.6 3D Cell Encapsulation and Hydrogel Culture

NorHA macromer solution was created by dissolving 1 – 2wt% NorHA macromer, 0.0328wt% LAP and dithiothreitol (DTT) at an 0.312 thiol-norbornene ratio in PBS. For fiber-containing conditions, gel precursor solution also contained swollen electrospun fiber solution at 1 wt% (based on pre-swollen fiber dry mass). OPCs were combined with precursor solution to a final concentration of 0.5 x 10^7 cells/mL. Cylindrical hydrogel molds were constructed by cutting the Luer-Lock tips off of BD disposable 1 mL syringes. Gel precursor solution was added in 40 µl aliquots to the syringe molds and exposed to UV light at 4 mW/cm^2 (365 nm) for 10 minutes. Gels were transferred to 24 well plates and rinsed three times with 500 µl PBS. 1 mL of OPC media per gel was added and the gels were cultured for up to 7 days, changing media every other day.

3.3.6 Nanoindentation

An Optics11 Chiaro nanoindenter with attached brightfield microscope was used to determine local elastic moduli of 1.5% NorHA hydrogels containing encapsulated cells (0.5 x 10^7cells/mL) and fibers (1 wt%) at culture day 5. Probe stiffness was 0.021 N/m and glass tip

radius was 24.5 um. Measurements were performed when the spherical tip of the probe was located directly above the bulk gel, distant (>10 μm) from cells and fibers (n= 3 measurement replicates for the cell and fiber condition, 6 for cell only); directly above electrospun fibers (n= 4 measurement replicates); or directly above a cluster of encapsulated OPCs (n=3 measurement replicates for both conditions).

3.3.7 Microplate Biomolecular Assays

Hydrogel samples with encapsulated OPCs were collected at days 1, 4 and 7 of culture with six sample replicates per condition. Hydrogels were separated into microtubes (1 gel per tube) containing 300 μl 1x passive lysis buffer (Promega) and frozen at -80℃. Prior to conducting the assays, samples were retrieved from storage in the -80 ℃ freezer and thawed on ice for 1 hour. After thawing, gels were homogenized using a handheld pestle homogenizer followed by sonication for 10 seconds.

ATP concentrations of each sample were measured to assess the metabolic activity of OPCs within the hydrogel microtissues. Homogenized samples were pipetted with three pipetting replicates for each of six sample replicates. In a white 384-well plate, 20 μL of PBS was combined with 5 μL of sample in each sample well. 25 μL of CellTiter-Glo 2.0 reagent (CellTiter-Glo 2.0 Cell Viability Assay, Promega) were then added to each of the standard and sample wells. The plate was incubated at room temperature for 10 minutes, and luminescence was measured using a BMG Clairostar microplate reader.

The concentration of DNA was measured in a similar way to the ATP assay. Homogenized samples were pipetted with three pipetting replicates for each of six sample replicates. For each sample, 5 μL of sample were added to 15 μL 1x TE buffer. The Pico Green reagent (Quant-iT PicoGreen dsDNA Kit, Invitrogen) was prepared by adding 50 μL of Pico Green dye to 10 mL 1x TE Buffer. 20 μL of dye was added to each of the standard and sample wells. The plate was incubated at room temperature for 10 minutes. Samples were excited at 480 nm and fluorescence was measured at 520 nm using a BMG Clariostar microplate reader. ATP values for each sample were normalized to DNA values, since DNA concentration scales with the number of cells. Resulting ATP/DNA ratios were then normalized to the day 1 no-fiber control.

3.3.8 Cell Morphology Staining and Imaging

To assess cell morphology, gels were fixed and stained with DAPI and phalloidin at culture days 1, 4 and 7 to label nuclei and the f-actin cytoskeleton, respectively. Hydrogel microtissues were fixed in 4% paraformaldehyde solution for 1 h at 37 °C. Three 5 min washes with 3% bovine serum albumin (BSA) in PBS were conducted after fixation and between each subsequent step. Fixed hydrogels were permeabilized at room temperature in 0.1% Triton X-100 (Fisher Scientific) for 30 min at 4°C with gentle shaking. Gels were stained overnight at 4°C with 2 U/mL AlexaFluor 647 phalloidin (ThermoFisher) in PBS with 1% BSA. To label cell nuclei, gels

were stained with 300 nM DAPI (Sigma) for 1 h at 4°C with shaking. Following staining, gels were rinsed 4-6 times in 1 hour washes with 3% BSA in PBS. Stained gels were stored in PBS followed by imaging with a Leica SP8 confocal. Z stack images were collected at 20x magnification to a Z depth of 300-500 um.

3.3.9 Cell Morphology Image Quantification

9 z-stack images were taken for each of the + fiber and – fiber conditions (3 images per gel across 3 gel replicates). Multiple maximum intensity projections of Z depth interval 20.56 um were constructed to span the entire Z depth of the hydrogel (300-500 um). Every second interval was quantified to avoid potential double-counting of cells spanning multiple intervals. For each Z interval, DAPI and phalloidin channels were separated and converted to 16-bit images. The brightness of each channel was adjusted using the Auto Brightness function in FIJI ImageJ [46]. Images were processed using the Auto Threshold function. The Despeckle function was then applied to remove background noise. The Analyze Particles function was used to quantify signal area for both the DAPI and phalloidin channels. Signal area from particles less than 20 pixels^2 in size was excluded to avoid counting non-cellular signal. Phalloidin signal area was then normalized to DAPI signal area to determine the average phalloidin signal area per cell.

3.3.10 Cell Proliferation Staining and Imaging

MADM OPC proliferation in 1.5 wt% NorHA gels was measured on days 1, 4 and 7 by staining hydrogels using the Click-iT EdU Imaging kit (Life Technologies). Briefly, cell-laden hydrogels were incubated in EdU solution for 1 h at 37 °C. Microtissues were then fixed in 4% paraformaldehyde solution for 1 h at 37 °C. Two 5 min washes with 3% bovine serum albumin (BSA) in PBS were conducted after fixation and between subsequent steps. Fixed hydrogels were permeabilized at room temperature in 0.1% Triton X-100 for 30 min, then incubated in Click-iT reaction buffer for 30 min. To label cell nuclei, gels were stained with 300 nM DAPI (Sigma) for 1 h at 4°C with shaking. Following staining, gels were stored in PBS followed by imaging with a Leica SP8 confocal. Z stack images were collected at 20x magnification to a Z depth of 300-500 um.

3.3.11 Cell Proliferation Image Quantification

9 z-stack images were taken for each of the + fiber and – fiber conditions (3 images per gel across 3 gel replicates). A maximum intensity projection was made over the entire Z depth (300-500 um). DAPI and EdU channels were separated and converted to 8-bit images. For each channel, brightness was adjusted using the Auto Brightness function in ImageJ. Images were processed using the Auto Threshold function in ImageJ. The ImageJ Watershed function was applied to better distinguish the signal of individual cells within clusters. The Despeckle function was then applied to remove background noise. The Analyze Particles function was used to quantify signal area for both the DAPI and EdU channels. Signal area from particles less than 8 pixels^2 in size was excluded to avoid counting signal area resulting from cell debris. EdU signal

area was then normalized to DAPI signal area to determine the average proliferation signal area per cell.

3.3.12 Extracellular Matrix Deposition

Nonspecific ECM protein labeling was conducted according to previously established protocols [26]. Briefly, cell-containing gels were cultured in a modified media consisting of glutamine-, methionine- and cystine-free high glucose DMEM (Gibco) supplemented with 0.201 mM cystine, 0.151 mM methionine, 100 µg/mL sodium pyruvate, 4 mM glutamine, N2 supplement, B27 supplement, 1% penicillin-streptomycin, and 50 µM azidohomoalanine (AHA, Click Chemistry Tools). Medium was replenished every second day. Gels were cultured for a period of 5 days. To stain for nascent protein deposition, hydrogels were washed twice with 1% BSA in PBS, followed by 30 min staining with 15 µM DBCO-647 (Click Chemistry Tools) at 37°C/5% CO2. After three washes with 1% BSA-PBS, hydrogels were fixed in 4% paraformaldehyde for 1 hour at room temperature (RT) followed by three washes in 1% BSA-PBS. Cell membrane was stained for 40 minutes in CellMask Orange (1:1000, Thermofisher) followed by three washes in 1% BSA-PBS. Samples were stored in 1% BSA-PBS at 4 °C.

3.3.13 Laminin and Fibronectin Immunostaining

Cell-containing gels were cultured in normal growth media, which was replenished every second day. To stain for specific ECM proteins, gels were fixed in paraformaldehyde for 1 hour at 37 °C/5% CO2, followed by 3 washes in 2% BSA-PBS. A blocking step was conducted in 2% BSA-PBS at RT, and gels were incubated with primary antibodies (rabbit anti-laminin α5, 1:100, Thermofisher or rabbit anti-fibronectin, 1:250, Abcam) in 2% BSA-PBS for 12 hours at 4°C. Gels were washed twice, followed by a 6-8 hr rinse in 2% BSA-PBS. Secondary antibody (donkey anti-rabbit 647, 1:200, Abcam) was applied in 2% BSA-PBS at 4°C for 12 hours. Plasma membrane was stained with CellMask Orange (1:1000, Thermofisher) for 35 minutes, followed by 3 rinses with 2% BSA-PBS. Gels were stored in 2% BSA-PBS at 4°C.

3.3.14 ECM Deposition Image Quantification

4-6 z-stack images were taken for each of the + fiber and – fiber conditions (2 images per gel across 2-3 gel replicates). Z stacks were taken at 20x magnification in intervals of 2 µm to a depth of 250-400 µm. For each Z interval, CellMask and protein channels were separated and processed using the Otsu thresholding function in FIJI ImageJ [46]. The Despeckle function was then applied to remove background noise. A dedicated ImageJ macro was used for automated quantification of signal area of both the CellMask and protein channels for each Z interval in the sample [45]. Protein signal area was then divided by CellMask signal area to determine the amount of extracellular matrix deposition normalized to cell surface area.

3.3.15 Statistical Analysis

Error bars for rheological characterization represent standard deviation with error propagation. Morphology and proliferation signal areas, ATP data, and DNA data were analyzed using two-sample t test with a α-value of 0.05. ECM deposition results were analyzed using 3-way ANOVA with a α-value of 0.05. Box plots cover the second and third data quartiles with error bars covering the first and fourth quartiles. Box plots also include marks for mean (x) and median (bar) data values.

3.4 Results

3.4.1 Biomaterial Stiffness Characterization

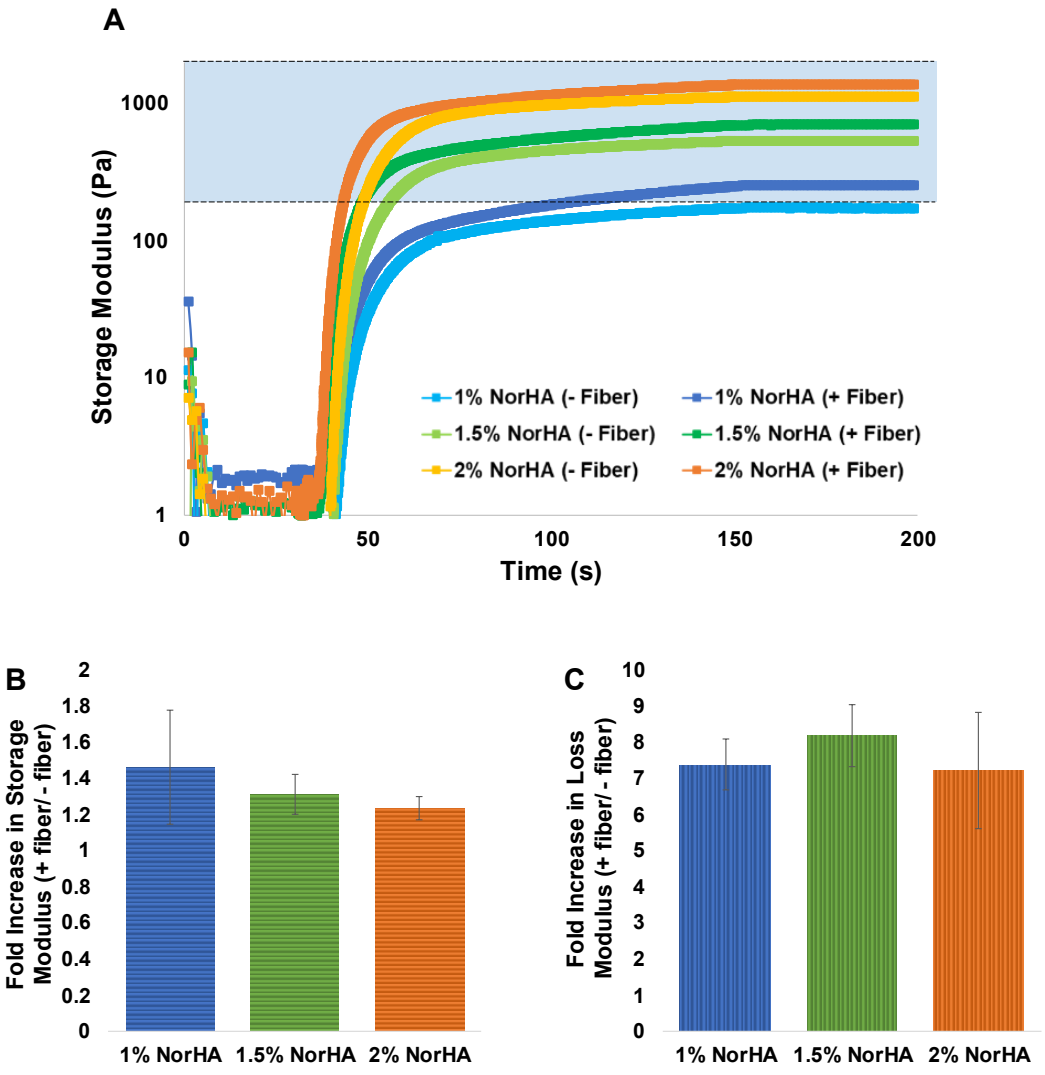

Figure 3.1. Rheological characterization of NorHA gels +/- fibers. A) Time-sweep oscillatory shear rheology measurements for on-stage gelation of 1-2 wt% NorHA gels. Each trace represents the average of multiple trials (n=4). The shaded blue region represents the stiffness range of native brain tissue (G' = 200-2000 Pa). Plateau storage modulus increases with increasing NorHA concentration. Fiber containing gels at each stiffness condition had higher storage moduli than no-fiber controls with equivalent NorHA concentrations. B) Fold increase in final storage moduli of fiber-containing gels (n=4) as compared to control gels (n=4) of equivalent NorHA concentration. The addition of fibers resulted in a 20-40% increase in final storage modulus, with the percent increase being more

pronounced in softer gels. C) Fold increase in final loss modulus of fiber-containing gels (n=4) as compared to control gels (n=4) of equivalent NorHA concentration. Fiber containing gels have a 7-8 fold increase in loss modulus as compared to no fiber controls.

Hydrogels containing between 1-2 wt% NorHA (functionalization 24-30%) accurately reproduced the range of storage moduli present in native brain tissue (200-2000 Pa) (Figure 3.1A) [48]. Although two different methods of NorHA synthesis were used, both methods produced comparable products with equivalent levels of functionalization (Figures S3.1 and S3.2). Inclusion of crosslinked electrospun fibers at a concentration of 1 wt% in the gel precursor solution resulted in a 20-40% increase in plateau storage modulus as compared to hydrogels - fibers, with the effects of fiber addition being most pronounced in the most compliant (1% NorHA) gel condition (Figure 3.1B). Inclusion of fibers was also associated with a several-fold increase in plateau loss modulus as compared to gels without fibers (Figure 3.1C).

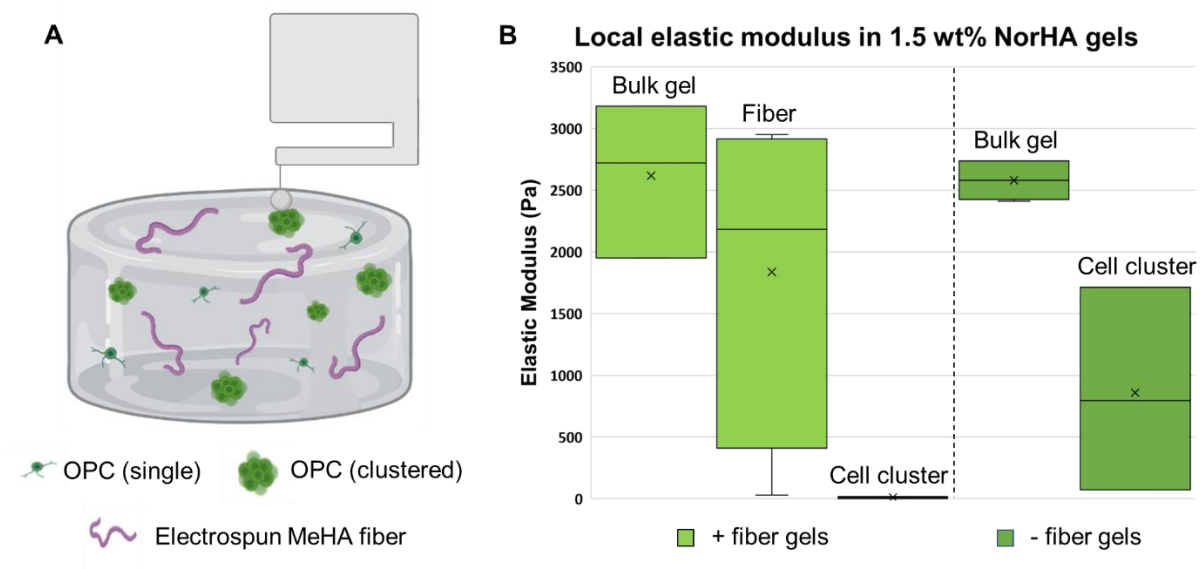

Figure 3.2. Mechanical characterization of local stiffness properties using nanoindentation. A) A nanoindentation probe was used to determine local elastic moduli of 1.5% NorHA hydrogels containing encapsulated cells (0.5 x 10^7cells/mL) and fibers (1 wt%). B) Local elastic modulus readings for 1.5% NorHA hydrogels (n = 3 gel replicates). The midline of the boxes represents the median, while the x in the box represents the mean. The boxes represent the range between the first and fourth quartiles, and the whiskers indicate the minimum and maximum values.

To determine the effects of fibers on local stiffness, single point nanoindentation was also performed on intermediate stiffness (1.5 wt% NorHA) hydrogels containing both cells and fibers. The nanoindentation probe was positioned directly above various features of the hydrogel system (cells, fibers, or bulk gel) to determine local elastic modulus near these features (Figure 3.2A). In both hydrogel types (+ fibers or – fibers) the presence of cell clusters decreases local elastic modulus (Figure 3.2B). Mean stiffness was equivalent in both conditions (Figure 2 B). Elastic modulus of the bulk gel, measured far (>10 µm) from encapsulated fibers, was on par with expectations based on the fiber-free rheology data (Figure 3.1B).

3.4.2 Cell morphology and proliferation assays

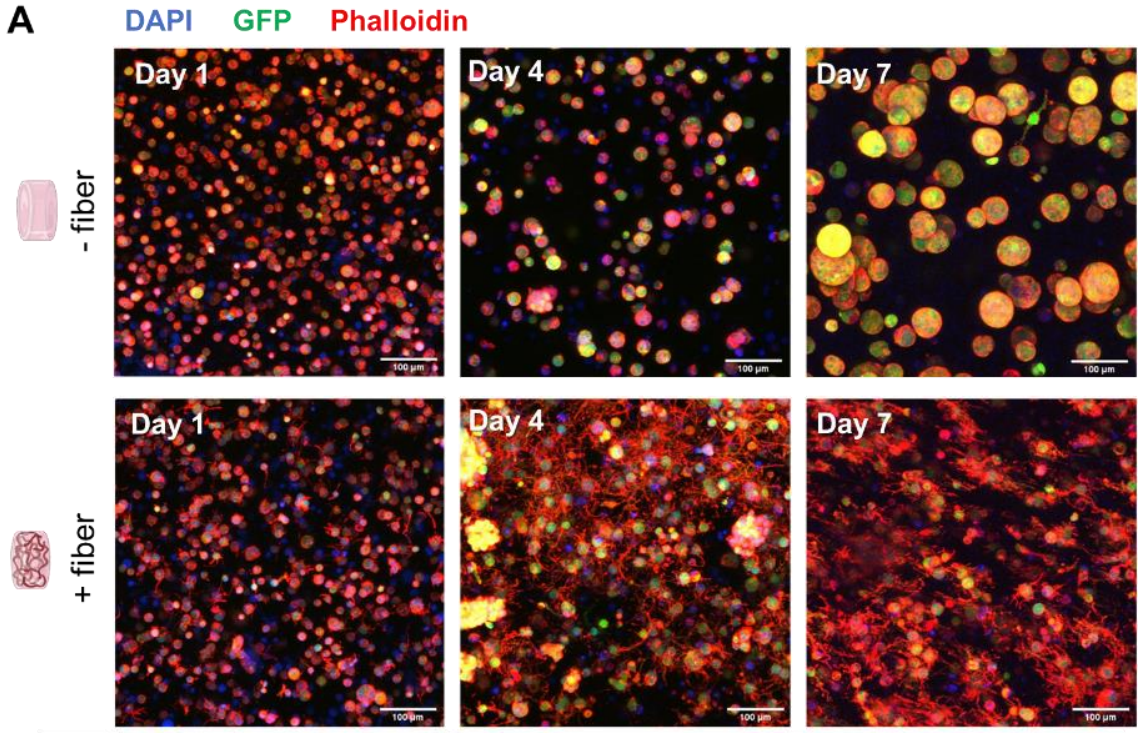

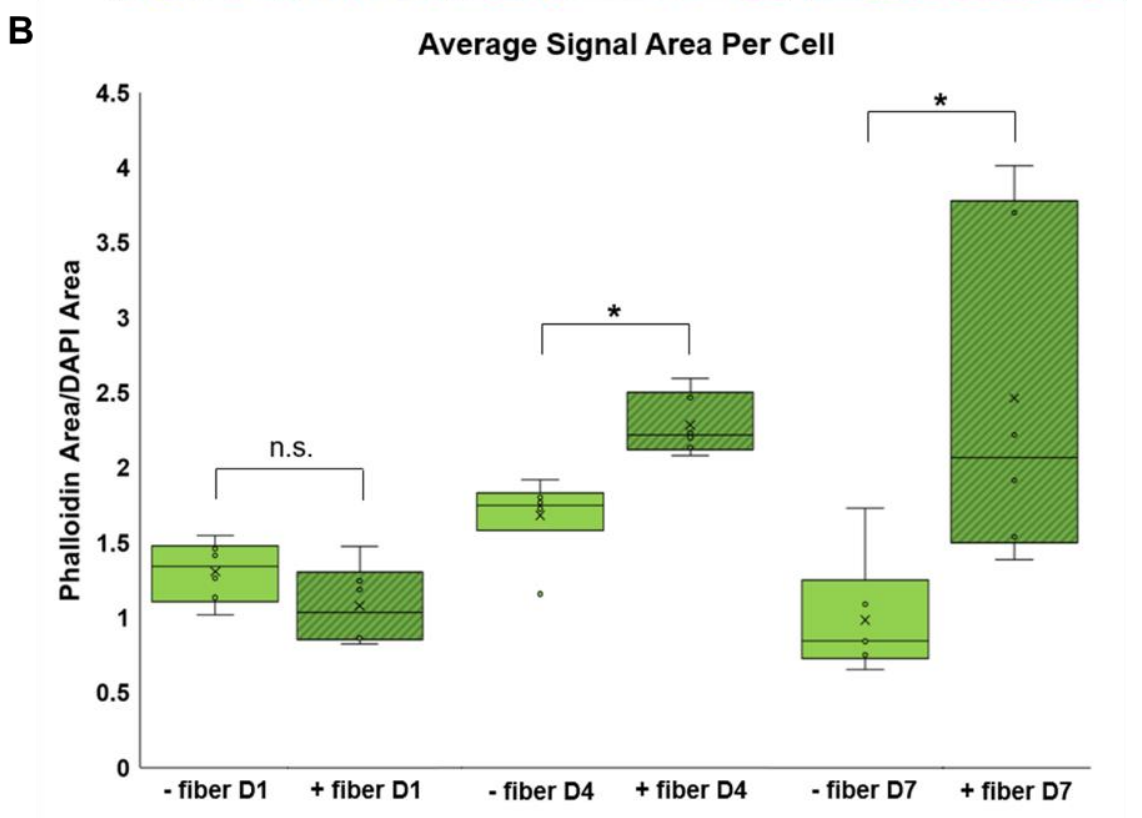

Figure 3.3. OPC morphology in fiber-containing gels and fiber-free controls A) Maximum intensity projection of OPCs encapsulated in – fiber (top row) control gels and + fiber (bottom row) gels after 1, 4, and 7 days of culture: DAPI (blue, nuclei), phalloidin (red, cytoskeleton), green fluorescent protein (green, cytoplasm). In the absence of fibers, cells retained a rounded and immature morphology, and grow mostly as clonal spheroids. B) Average phalloidin signal area per cell was initially similar for both conditions at culture day 1 (D1) but increased significantly for cells in fiber containing gels at D4 and D7 time points. n.s. indicates no significant difference between conditions, while * indicates a significant difference (p=0.05).

.

To evaluate the effect of fiber presence on the morphology of encapsulated OPCs, gels from both the + fiber and - fiber groups were fixed and stained at days 1, 4 and 7 of culture. Maximum intensity projections of phalloidin-labeled cells in the no-fiber control gels show that cells grow and form clusters over a 7-day culture period but maintain a rounded and immature morphology (Figure 3.3A and Figure S3.4). By contrast, cells in fiber-containing gels consistently demonstrate a more mature morphology, indicated by the cells' extension of numerous processes (Figure 3.3B and Figure S3.4).

Encapsulated OPCs initially exhibit similar cytoskeletal volumes, as determined by phalloidin/DAPI ratios, across both conditions at day 1 of culture (with mean signal area ratios of 1.08 and 1.30 for + fiber and - fiber gels, respectively). However, cells in gels + fibers displayed significantly larger cytoskeletal area ratios by day 4 of culture. The difference between conditions continued to increase with time and was most pronounced at Day 7 of culture, where fiber-containing gels had a mean phalloidin/DAPI signal area ratio of 2.47, compared to 0.99 for cells in gels without fibers (Figure 3.3C). Because the size of the main cell body remained the same across conditions, the increase in signal area can be attributed to their increased levels of process extension.

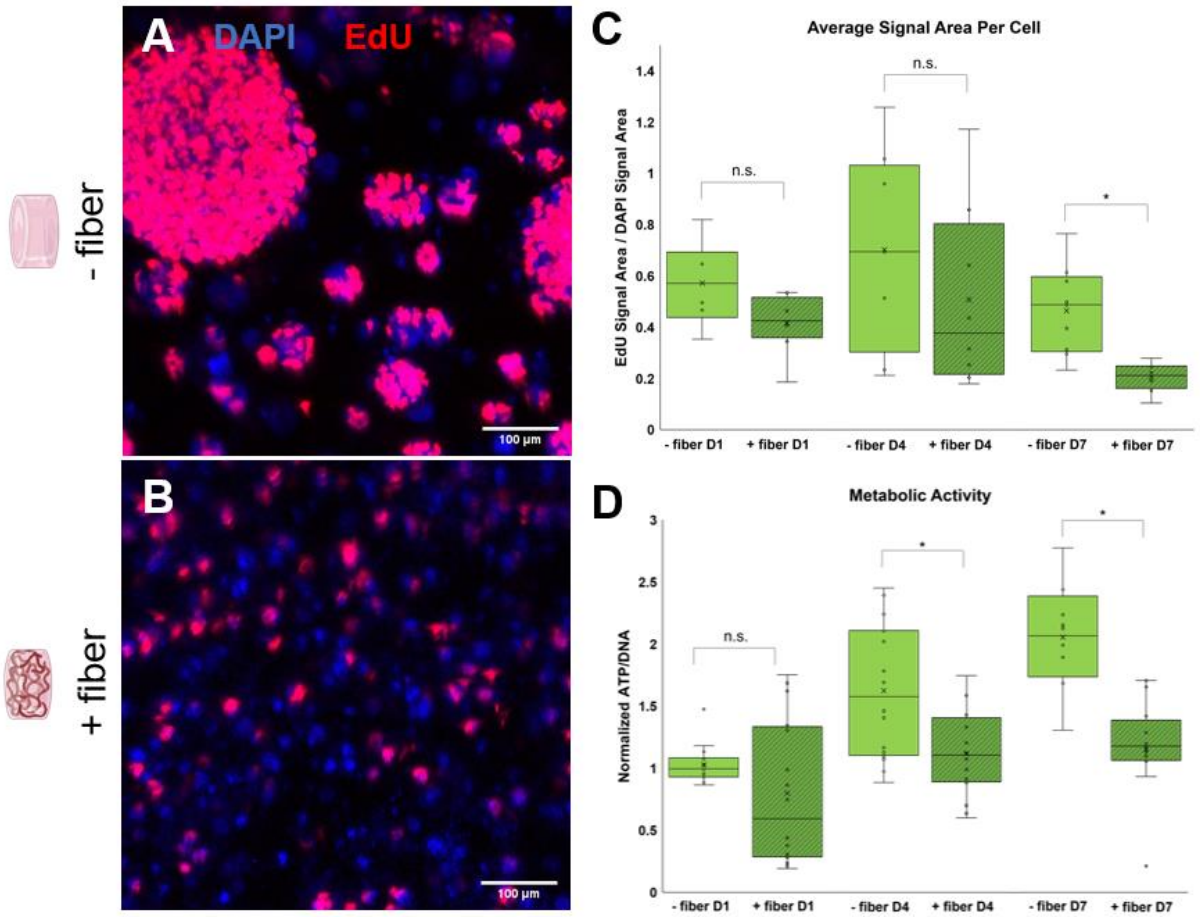

Figure 3.4. OPC proliferation in fiber-containing gels as compared to no-fiber controls. A) OPCs encapsulated in - fiber control gels resulted in a high proportion of proliferating cells at D7, and many large clusters. (B. Cells in fiber-containing gels do not form large clusters and proliferate to a lesser extent as compared to cells in no-fiber controls. C) Fraction of actively proliferating OPCs based on normalized EdU/DAPI signal area. While proliferation was initially similar at D1 and D4, fiber-containing gels trended toward lower proliferation rates throughout the study and exhibited significantly lower proliferation levels at D7. n.s. indicates no significant difference between conditions, while * indicates a significant difference ($p = 0.05$). D) Average metabolic activity (ATP normalized to DNA) was initially similar across both conditions at D1 but was significantly higher for cells in no-fiber controls at D4 and D7 timepoints, consistent with a higher proportion of proliferating progenitor cells ($p = 0.05$).

Similarly, proliferation in both the control and experimental groups was evaluated at days 1, 4 and 7 of culture with DAPI/EdU staining (Figure 3.4A-B and Figure S3.5). OPC proliferation appears similar across both the – fiber control and + fiber conditions at the D1 timepoint (with mean EdU/DAPI ratios of 0.57 and 0.42, respectively), and peak at a similar level on D4 (mean EdU/DAPI ratios of 0.7 and 0.5). However, proliferation for both groups declines after D4, and the proliferation ratio for fiber-containing gels was found to be statistically lower at the D7 timepoint (mean EdU/DAPI = 0.21) as compared to no-fiber controls (mean EdU/DAPI = 0.46) (Figure 3.4C and Figure S3.6). Metabolic activity, as measured by normalized ATP/DNA concentration, was initially similar across conditions at D1, but was significantly lower in + fiber gels at D4 and D7 timepoints (Figure 3.4D).

3.4.3 Extracellular Matrix Deposition

Since our hydrogels do not include specific integrin-binding sequences, we hypothesized that, like other cells, OPCs may be depositing extracellular matrix proteins to remodel their local environment. Nascent ECM deposition occurred in both the – fiber and + fiber conditions. In the – fiber control gels, cells retained a rounded morphology and ECM deposition occurred in a thin spherical shell surrounding the outside of cells and cell clusters (Figure 3.5A). In the + fiber condition, ECM deposition occurred in a similar pattern surrounding the main cell bodies but also occurred in association with cell process extensions (Figure 3.5B).

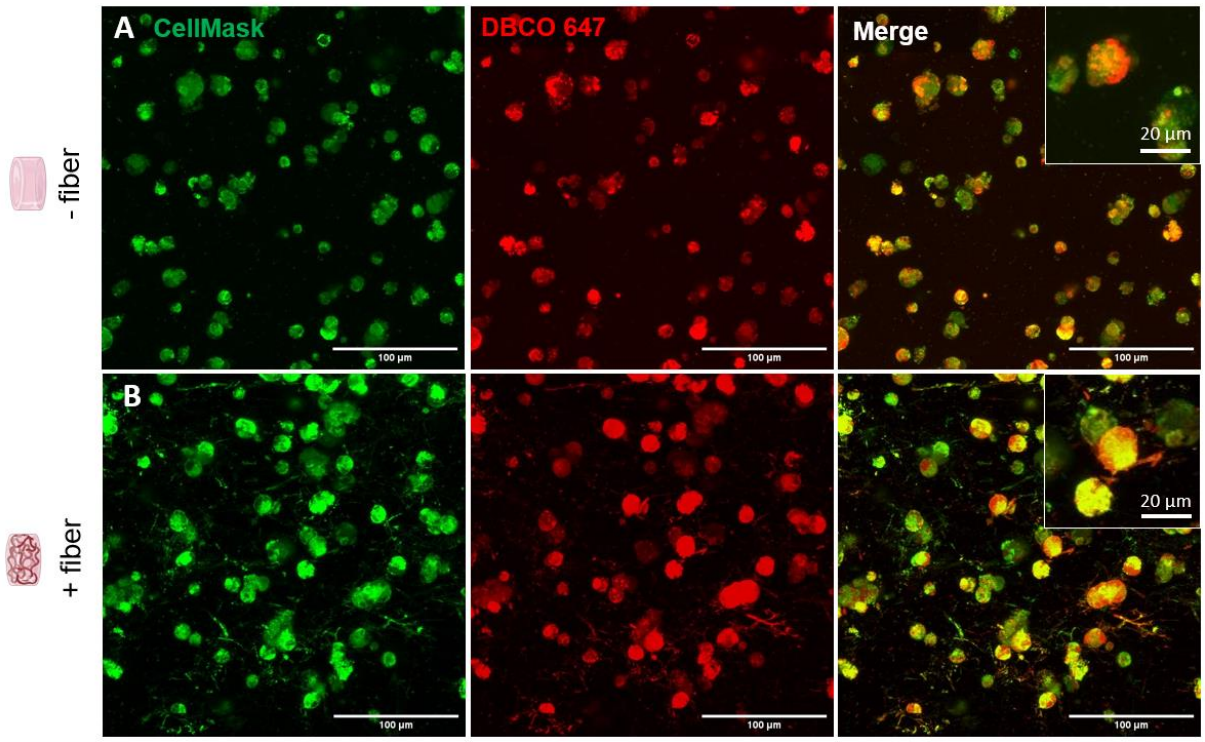

Figure 3.5. Maximum intensity projections of nascent extracellular matrix deposition around OPCs in - fiber (A) and + fiber (B) samples at culture day 5. Merge projections reveal that in the – fiber condition, extracellular matrix proteins were deposited around the outside of cells and cell clusters in a thin spherical shell (A, inset). In the + fiber condition, ECM deposition surrounded the main cell bodies, but was also seen to extend along the lengths of cell process extensions (B, inset).

In order to assess the composition of ECM deposits, immunostaining was performed for two common ECM proteins, laminin and fibronectin. These proteins were chosen due to their previous implication as part of the OPC secretome [27, 28]. Based on signal area in immunostained max projections, OPCs deposited laminin and fibronectin in – fiber and + fiber gels in similar amounts (Figure 3.6).

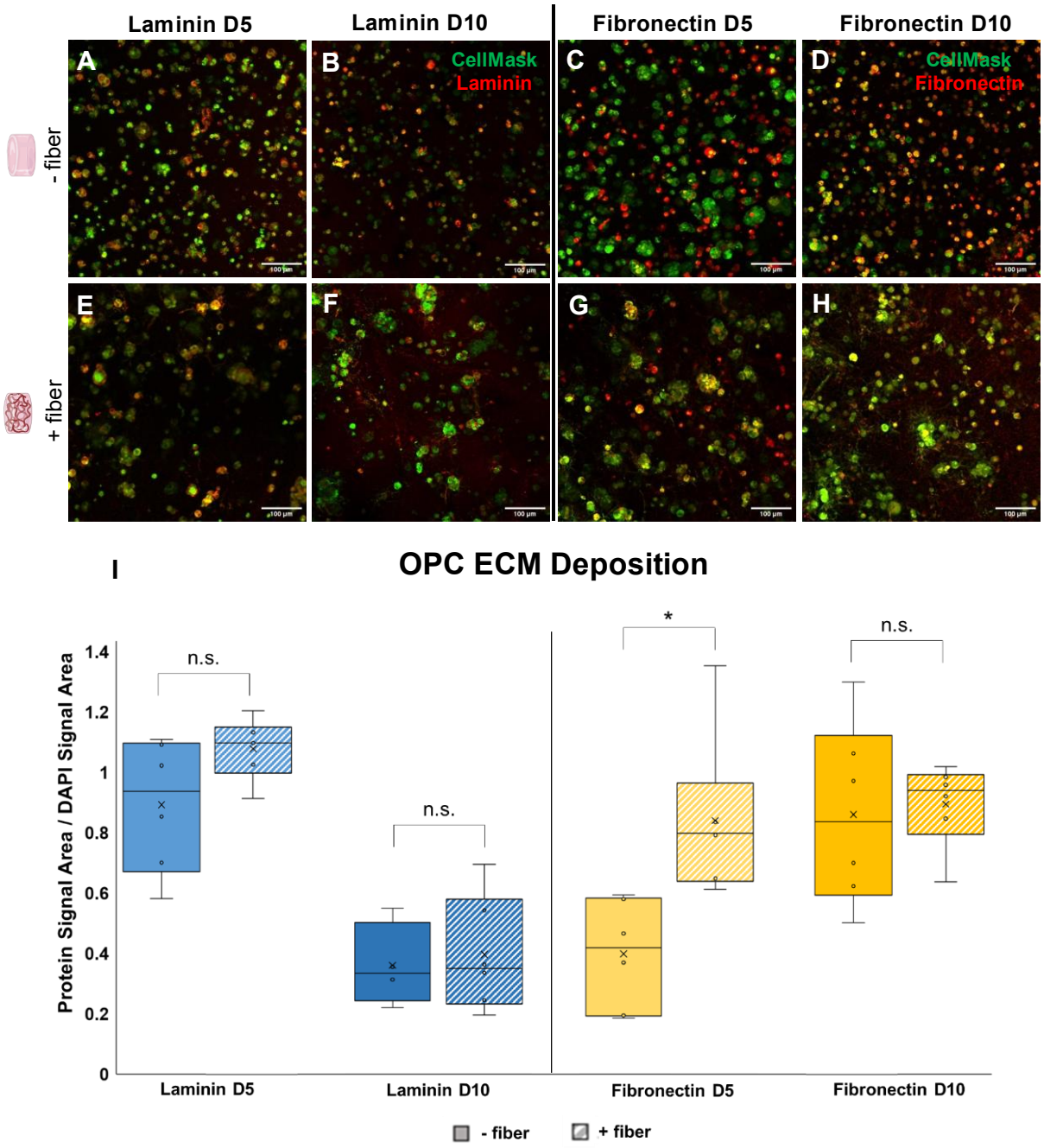

Figure 3.6. Maximum intensity merge projections of laminin (LN) and fibronectin (FN) matrix deposition around OPCs in - fiber (A-D) and + fiber (E-H) samples at culture days 5 and 10. CellMask (green) was used to label cell membranes, while immunostaining (red) was used to assess for the presence of laminin or fibronectin. Staining for specific ECM proteins reveals similar patterns of deposition as were observed in the nonspecific ECM deposition assay. I) Quantification of protein signal area for laminin and fibronectin. Laminin deposition decreases between timepoints for + and – fiber conditions, while fibronectin deposition increases between timepoints for – fiber gels and remains consistent between timepoints for + fiber gels.

3.5 Discussion

3.5.1 Biomaterial Stiffness Characterization

Fiber inclusion was consistently found to increase bulk storage modulus in + fiber gels as compared to – fiber gels (Figure 3.1A and B). Because the fibers are solids with a higher storage modulus than the surrounding hydrogel, inclusion of fibers therefore results in an increase in the overall bulk reading. However, in all conditions, the difference in moduli resulting from fiber inclusion was much smaller than the difference between different polymer weight percent conditions. For example, the most pronounced difference due to fiber inclusion (between 1% NorHA + fiber and 1% NorHA - fiber) was 80 Pa, while the difference between 1% and 1.5% NorHA was an order of magnitude larger, at 365 Pa. We have previously demonstrated the change in stiffness between HA hydrogels of different wt % to impact OPC proliferation, but observed no effect on cell morphology or process extension [22]. The increase in loss modulus (Figure 3.1C) is explainable as fibers dispersed throughout the gel increase its viscous nature.

Nanoindentation measurements taken atop cell clusters have a wide range of stiffnesses, due to variability of cell cluster depth. However, in both hydrogel types (+ fibers or – fibers) the presence of underlying cell clusters decreases local elastic modulus; this is attributed to OPCs' low elastic modulus and their local disruption of the hydrogel mesh (Figure 3.2B) [49]. Similarly, measurements taken atop fibers have a large variance in stiffnesses, due to variation of fiber depth (Figure 3.2B). However, while bulk gel readings in the fiber-containing gels showed a wider range of stiffnesses compared to equivalent measurements in no-fiber gels, the mean stiffness was equivalent in both conditions (Figure 3.2B). This suggests that, although fibers consistently increase bulk stiffness of the gel (Figure 3.1A), local stiffness of the gel is largely unaffected. These materials characterization results suggest that while fiber presence has an impact on material stiffness, this impact is local and limited to a range within 10 μm from the fibers. Overall, material properties remain comparable between + fiber and – fiber conditions.

3.5.2 Cell morphology and proliferation assays

Morphology results for OPCs in – fiber gels are consistent with previous work in both NorHA and polyethylene glycol-based hydrogel systems [22, 23]. Their rounded appearance is consistent with immature OPCs (Figure 3.3A). By contrast, process extensions, a hallmark of cell maturation, appeared uniformly throughout the entirety of + fiber gels. Notably, this result occurred in standard proliferation media; no specific soluble cues were added or subtracted to promote differentiation. Changes in morphology across conditions cannot be attributed to differences in bulk modulus, since previous experiments by our group have shown that OPCs grown in – fiber gels across a wide range of stiffnesses produce no observable process extensions [22]. These results indicate that topographical cues alone are capable of prompting OPC maturation in 3D despite strong mitogenic input. While unexpected, the notable decrease in proliferation in fiber-containing gels (Figure 3.4C) is consistent with our observations of cell morphology over a seven-day culture period; cells in the absence of electrospun fiber cues

retained an immature, proliferative state, while OPCs in the presence of fibers proliferated less and instead matured and differentiated toward post-mitotic phenotypes.

Previous work by other groups has demonstrated that OPCs and oligodendrocytes in 2D culture are able to extend processes and wrap around axon-mimicking fibers to deposit myelin [29, 30]. These studies found that fiber cues with diameters similar to mature axons (2.0-4.0 μm) were preferentially ensheathed by about 60% of OPCs and oligodendrocytes [29]. Our results are consistent with these studies, as only those OPCs grown in the presence of fibers extended substantial processes, and almost all cells extended processes (Figure 3.3A-B). However, our culture system provides the novel advantage of encapsulating both OPCs and fiber cues fully in 3D in an ECM-mimicking hydrogel (as opposed to culturing OPCs atop fibers alone). Our results may therefore more accurately model OPC behavior by better mimicking conditions in native tissue, both in terms of gel stiffness and fiber diameter. Additionally, our system provides the opportunity for substantial scaleup beyond 2D surfaces.

3.5.3 Extracellular Matrix Deposition

While both laminin and fibronectin have been implicated in the OPC secretome, the overall composition and distribution of nascent OPC ECM deposition is understudied [27, 28]. Additionally, the timeline of protein deposition, and how it varies over the course of cell differentiation, remains poorly understood. We confirmed that both laminin and fibronectin deposition occurred in hydrogels across all tested conditions (Figure 3.6). These results prove that not only do OPCs synthesize and locally deposit their own matrix in these hydrogels, but also demonstrates that the presence of fibers directs cell morphology, which in turn influences the pattern of extracellular matrix deposition.

In general, the relative amount of deposition is unaffected by the presence of fibers; although more fibronectin deposition was observed in the + fiber condition at day 5, there was no significant difference in fibronectin deposition at culture day 10 or in laminin deposition at either timepoint. ANOVA did indicate that there was a significant difference between timepoints, with laminin area decreasing and fibronectin area increasing between days 5 and 10. This indicates that the majority of laminin deposition occurs before day 5 of culture, with minimal deposition occurring between days 5 and 10. By contrast, fibronectin deposition continues to occur past day 5 in – fiber gels. Overall, both proteins were deposited in similar amounts, but the timeline of deposition was different. Laminin was deposited earlier and decreased over time, whereas fibronectin levels remained steady or increased.

3.5.4 Limitations

Our model system was constructed to be representative of native tissue, both in terms of stiffness and fiber diameter. However, some limitations do exist. The OPC cell line used in these experiments was a mouse glioma-derived cell line which express many OPC markers but contain gene knockouts which prevent complete differentiation into myelinating OLs. As such, these

cells are not fully representative of endogenous OPC [50]. Additionally, fibers were incorporated at a low concentration (1 wt% based on dry mass), which is not reflective of axonal density in the CNS. Despite these limitations, the system represents a promising first step towards modeling OPC response to axonal topography in the CNS, and it is encouraging to note the dramatic morphological response which occurs even at low fiber concentrations. Furthermore, due to the tunability of our model design, future modifications can easily include an alternative cell line capable of complete differentiation (e.g., primary OPCs, neural stem cells) as well as a higher encapsulation density of electrospun fibers.

3.6 Conclusions

Using NorHA hydrogels between 1 and 2 wt%, we were able to successfully replicate the stiffness range of native CNS tissue (G' ~ 200-2000 Pa). Inclusion of electrospun fibers was found to affect the bulk stiffness of the overall hydrogel, resulting in a small, but significant, increase in storage moduli across all conditions. However, differences resulting from fiber presence were much smaller than differences resulting from different polymer concentrations. Additionally, nanoindentation data indicate that stiffness differences due to fibers were a localized effect and did not affect the stiffness far (>10 μm) away from fibers. Overall, bulk material properties remained comparable between + fiber and - fiber gels.

Despite their similar bulk mechanical properties, + fiber and - fiber gels resulted in strikingly different OPC morphologies. In fiber-free NorHA gels, OPCs primarily expand as multicellular spheroids, without notable morphological features or substantial process extensions. By contrast, the presence of electrospun fibers in the hydrogel dramatically changed OPC morphology, leading to extensive process elongation (an indicator of maturation) from almost all OPCs throughout the microtissue. Notably, this effect occurred even though cells were cultured under standard proliferation media, with no additional soluble factors included (or excluded) to promote differentiation. Due to their abundant process extensions, cells in + fiber conditions displayed correspondingly larger normalized phalloidin/DAPI signal areas as compared to those in fiber-free control gels. OPCs in fiber-free controls demonstrated higher levels of proliferation (as measured by normalized EdU/DAPI signal area) and metabolic activity (as measured by normalized ATP/DNA concentration). Thus, the inclusion of topographical cues in the form of electrospun fibers promotes OPC maturation, directing cell fate away from the OPC proliferation pathway they otherwise experience under these conditions.

While OPCs were known to secrete ECM proteins to remodel their local environment, information regarding the distribution, composition, and timeline of ECM deposition was limited. Using nonspecific ECM staining, we confirmed that OPCs in NorHA gels do deposit nascent ECM proteins, and that ECM secretion occurred in a thin spherical shell surrounding cells or spheroids. ECM deposition also occurred along the lengths of process extensions in the + fiber condition. Immunostaining assays determined that both laminin and fibronectin were secreted by OPCs, and that deposition of both proteins occurred in similar amounts across conditions. However, deposition of laminin occurred primarily before culture day 5 and decreased on a per cell basis between culture days 5 and 10; by contrast, fibronectin deposition increased over this time period. These novel results demonstrate that nascent ECM deposition by

OPCs varies significantly with time, while cell maturity has little effect on the amount or composition of secreted ECM.

3.7 Acknowledgements

This work was supported by the National Science Foundation [grant number 2104723] (KJL), as well as the University of Virginia Dean's Fellowship award (RAM). NMR data were collected on an instrument funded by the NSF-MRI grant CHE-2215062. Funding sources were not involved in study design, data collection or analysis, in the writing of the report, or in the decision to submit the article for publication. We gratefully acknowledge the Cai Lab at UVA for the usage of the Leica SP8 confocal microscope, as well as the UVA Program in Fundamental Neuroscience for usage of its Leica Stellaris 5 confocal system. Finally, we offer thanks to Will Ferguson for his work in developing our fiber characterization method.

3.8 References

[1] K.-A. Nave, H.B. Werner, Myelination of the nervous system: mechanisms and functions, Annual review of cell and developmental biology 30 (2014) 503-533.
[2] M. Mekhail, G. Almazan, M. Tabrizian, Oligodendrocyte-protection and remyelination post-spinal cord injuries: A review, Progress in Neurobiology 96(3) (2012) 322-339.
[3] B.D. Trapp, K.-A. Nave, Multiple sclerosis: an immune or neurodegenerative disorder?, Annu. Rev. Neurosci. 31 (2008) 247-269.
[4] H.M. Bramlett, W.D. Dietrich, Long-term consequences of traumatic brain injury: current status of potential mechanisms of injury and neurological outcomes, Journal of neurotrauma 32(23) (2015) 1834-1848.
[5] M. Mecha, F.J. Carrillo-Salinas, L. Mestre, A. Feliu, C. Guaza, Viral models of multiple sclerosis: neurodegeneration and demyelination in mice infected with Theiler's virus, Progress in neurobiology 101 (2013) 46-64.
[6] L.D. Nelson, N.R. Temkin, S. Dikmen, J. Barber, J.T. Giacino, E. Yuh, H.S. Levin, M.A. McCrea, M.B. Stein, P. Mukherjee, Recovery after mild traumatic brain injury in patients presenting to US level I trauma centers: a transforming research and clinical knowledge in traumatic brain injury (TRACK-TBI) study, JAMA neurology 76(9) (2019) 1049-1059.
[7] T.A. Watkins, B. Emery, S. Mulinyawe, B.A. Barres, Distinct stages of myelination regulated by γ-secretase and astrocytes in a rapidly myelinating CNS coculture system, Neuron 60(4) (2008) 555-569.
[8] A.G. Shivane, A. Chakrabarty, Multiple sclerosis and demyelination, Current Diagnostic Pathology 13(3) (2007) 193-202.
[9] R.J. Franklin, Why does remyelination fail in multiple sclerosis?, Nature Reviews Neuroscience 3(9) (2002) 705-714.
[10] R.A. Mazur, R. Yokosawa, P.J. VandeVord, K.J. Lampe, The Need for Tissue Engineered Models to Facilitate the Study of Oligodendrocyte Progenitor Cells in Traumatic Brain Injury and Repair, Current Opinion in Biomedical Engineering (2022) 100378.
[11] G. Srinivasan, D.A. Brafman, The Emergence of Model Systems to Investigate the Link Between Traumatic Brain Injury and Alzheimer's Disease, Frontiers in aging neuroscience 13 (2021).
[12] J.E. Merrill, In vitro and in vivo pharmacological models to assess demyelination and remyelination, Neuropsychopharmacology 34(1) (2009) 55-73.
[13] S. Hyung, B.Y. Lee, J.C. Park, J. Kim, E.M. Hur, J.K.F. Suh, Coculture of Primary Motor Neurons and Schwann Cells as a Model for In Vitro Myelination, Scientific Reports 5 (2015) 11.
[14] M.E. Bechler, L. Byrne, CNS myelin sheath lengths are an intrinsic property of oligodendrocytes, Current Biology 25(18) (2015) 2411-2416.
[15] H. Wen, W.W. Xiao, S. Biswas, Z.Q. Cong, X.M. Liu, K.S. Lam, Y.H. Liao, W.B. Deng, Alginate Hydrogel Modified with a Ligand Interacting with alpha 3 beta 1 Integrin Receptor Promotes the Differentiation of 3D Neural Spheroids toward Oligodendrocytes in Vitro, Acs Applied Materials & Interfaces 11(6) (2019) 5821-5833.

[16] M.R. Pinezich, L.N. Russell, N.P. Murphy, K.J. Lampe, Encapsulated oligodendrocyte precursor cell fate is dependent on PDGF-AA release kinetics in a 3D microparticle-hydrogel drug delivery system, Journal of Biomedical Materials Research Part A 106(9) (2018) 2402-2411.
[17] N.D. Leipzig, M.S. Shoichet, The effect of substrate stiffness on adult neural stem cell behavior, Biomaterials 30(36) (2009) 6867-6878.
[18] N.D. Leipzig, R.G. Wylie, H. Kim, M.S. Shoichet, Differentiation of neural stem cells in three-dimensional growth factor-immobilized chitosan hydrogel scaffolds, Biomaterials 32(1) (2011) 57-64.
[19] T. Zahir, Y.F. Chen, J.F. MacDonald, N. Leipzig, C.H. Tator, M.S. Shoichet, Neural stem/progenitor cells differentiate in vitro to neurons by the combined action of dibutyryl cAMP and interferon-γ, Stem cells and development 18(10) (2009) 1423-1432.
[20] E. Meco, W.S. Zheng, A.H. Sharma, K.J. Lampe, Guiding Oligodendrocyte Precursor Cell Maturation With Urokinase Plasminogen Activator-Degradable Elastin-like Protein Hydrogels, Biomacromolecules 21(12) (2020) 4724-4736.
[21] S.W. Moore, P. Roca-Cusachs, M.P. Sheetz, Stretchy proteins on stretchy substrates: the important elements of integrin-mediated rigidity sensing, Developmental cell 19(2) (2010) 194-206.
[22] D.B. Unal, S.R. Caliari, K.J. Lampe, 3D hyaluronic acid hydrogels for modeling oligodendrocyte progenitor cell behavior as a function of matrix stiffness, Biomacromolecules 21(12) (2020) 4962-4971.
[23] L.N. Russell, K.J. Lampe, Oligodendrocyte precursor cell viability, proliferation, and morphology is dependent on mesh size and storage modulus in 3D poly (ethylene glycol)-based hydrogels, ACS Biomaterials Science & Engineering 3(12) (2017) 3459-3468.
[24] K. Watanabe, M. Nakamura, H. Okano, Y. Toyama, Establishment of three-dimensional culture of neural stem/progenitor cells in collagen Type-1 Gel, Restorative neurology and neuroscience 25(2) (2007) 109-117.
[25] K. Sugitani, D. Egorova, S. Mizumoto, S. Nishio, S. Yamada, H. Kitagawa, K. Oshima, D. Nadano, T. Matsuda, S. Miyata, Hyaluronan degradation and release of a hyaluronan-aggrecan complex from perineuronal nets in the aged mouse brain, Biochimica et Biophysica Acta (BBA)-General Subjects 1865(2) (2021) 129804.
[26] C. Loebel, R.L. Mauck, J.A. Burdick, Local nascent protein deposition and remodelling guide mesenchymal stromal cell mechanosensing and fate in three-dimensional hydrogels, Nature materials 18(8) (2019) 883-891.
[27] W.K. Kim, D. Kim, J. Cui, H.H. Jang, K.S. Kim, H.J. Lee, S.U. Kim, S.-M. Ahn, Secretome analysis of human oligodendrocytes derived from neural stem cells, PLoS One 9(1) (2014) e84292.
[28] Z. Yang, R. Suzuki, S.B. Daniels, C.B. Brunquell, C.J. Sala, A. Nishiyama, NG2 glial cells provide a favorable substrate for growing axons, Journal of Neuroscience 26(14) (2006) 3829-3839.

[29] S. Lee, M.K. Leach, S.A. Redmond, S.C. Chong, S.H. Mellon, S.J. Tuck, Z.-Q. Feng, J.M. Corey, J.R. Chan, A culture system to study oligodendrocyte myelination processes using engineered nanofibers, Nature methods 9(9) (2012) 917-922.
[30] S. Lee, S.C. Chong, S.J. Tuck, J.M. Corey, J.R. Chan, A rapid and reproducible assay for modeling myelination by oligodendrocytes using engineered nanofibers, Nature protocols 8(4) (2013) 771-782.
[31] S. Shah, P.T. Yin, T.M. Uehara, S.T.D. Chueng, L. Yang, K.B. Lee, Guiding stem cell differentiation into oligodendrocytes using graphene-nanofiber hybrid scaffolds, Advanced materials 26(22) (2014) 3673-3680.
[32] D.N. Rocha, E.D. Carvalho, L.R. Pires, C. Gardin, I. Zanolla, P.K. Szewczyk, C. Machado, R. Fernandes, U. Stachewicz, B. Zavan, It takes two to remyelinate: A bioengineered platform to study astrocyte-oligodendrocyte crosstalk and potential therapeutic targets in remyelination, Biomaterials Advances 151 (2023) 213429.
[33] X. Li, B. Cho, R. Martin, M. Seu, C. Zhang, Z. Zhou, J.S. Choi, X. Jiang, L. Chen, G. Walia, Nanofiber-hydrogel composite–mediated angiogenesis for soft tissue reconstruction, Science translational medicine 11(490) (2019) eaau6210.
[34] S. Choi, K.Y. Lee, S.L. Kim, L.A. MacQueen, H. Chang, J.F. Zimmerman, Q. Jin, M.M. Peters, H.A.M. Ardoña, X. Liu, Fibre-infused gel scaffolds guide cardiomyocyte alignment in 3D-printed ventricles, Nature materials 22(8) (2023) 1039-1046.
[35] O. Ilina, G.-J. Bakker, A. Vasaturo, R.M. Hoffman, P. Friedl, Two-photon laser-generated microtracks in 3D collagen lattices: principles of MMP-dependent and-independent collective cancer cell invasion, Physical biology 8(1) (2011) 015010.
[36] K.L. Xu, N. Di Caprio, H. Fallahi, M. Dehghany, M.D. Davidson, L. Laforest, B.C. Cheung, Y. Zhang, M. Wu, V. Shenoy, Microinterfaces in biopolymer-based bicontinuous hydrogels guide rapid 3D cell migration, Nature Communications 15(1) (2024) 2766.
[37] I.L. Kim, S. Khetan, B.M. Baker, C.S. Chen, J.A. Burdick, Fibrous hyaluronic acid hydrogels that direct MSC chondrogenesis through mechanical and adhesive cues, Biomaterials 34(22) (2013) 5571-5580.
[38] C. Liu, J.C. Sage, M.R. Miller, R.G. Verhaak, S. Hippenmeyer, H. Vogel, O. Foreman, R.T. Bronson, A. Nishiyama, L. Luo, Mosaic analysis with double markers reveals tumor cell of origin in glioma, Cell 146(2) (2011) 209-221.
[39] E. Hui, K.I. Gimeno, G. Guan, S.R. Caliari, Spatiotemporal control of viscoelasticity in phototunable hyaluronic acid hydrogels, Biomacromolecules 20(11) (2019) 4126-4134.
[40] W.M. Gramlich, I.L. Kim, J.A. Burdick, Synthesis and orthogonal photopatterning of hyaluronic acid hydrogels with thiol-norbornene chemistry, Biomaterials 34(38) (2013) 9803-9811.
[41] N.J. Darling, W. Xi, E. Sideris, A.R. Anderson, C. Pong, S.T. Carmichael, T. Segura, Click by click microporous annealed particle (MAP) scaffolds, Advanced healthcare materials 9(10) (2020) 1901391.

[42] C. Chung, J.A. Burdick, Influence of three-dimensional hyaluronic acid microenvironments on mesenchymal stem cell chondrogenesis, Tissue Engineering Part A 15(2) (2009) 243-254.
[43] K.A. Smeds, M.W. Grinstaff, Photocrosslinkable polysaccharides for in situ hydrogel formation, Journal of Biomedical Materials Research: An Official Journal of The Society for Biomaterials and The Japanese Society for Biomaterials 54(1) (2001) 115-121.
[44] H.G. Sundararaghavan, J.A. Burdick, Gradients with depth in electrospun fibrous scaffolds for directed cell behavior, Biomacromolecules 12(6) (2011) 2344-2350.
[45] M.E. Prendergast, M.D. Davidson, J.A. Burdick, A biofabrication method to align cells within bioprinted photocrosslinkable and cell-degradable hydrogel constructs via embedded fibers, Biofabrication 13(4) (2021) 044108.
[46] J. Schindelin, I. Arganda-Carreras, E. Frise, V. Kaynig, M. Longair, T. Pietzsch, S. Preibisch, C. Rueden, S. Saalfeld, B. Schmid, Fiji: an open-source platform for biological-image analysis, Nature methods 9(7) (2012) 676-682.
[47] T. Villani, Loading and Measurement of Volumes in 3D Confocal Image Stacks with ImageJ, Visikol, 2024.
[48] X. Li, E. Katsanevakis, X. Liu, N. Zhang, X. Wen, Engineering neural stem cell fates with hydrogel design for central nervous system regeneration, Progress in polymer science 37(8) (2012) 1105-1129.
[49] A. Jagielska, A.L. Norman, G. Whyte, K.J.V. Vliet, J. Guck, R.J. Franklin, Mechanical environment modulates biological properties of oligodendrocyte progenitor cells, Stem cells and development 21(16) (2012) 2905-2914.
[50] P.P. Gonzalez, J. Kim, R.P. Galvao, N. Cruickshanks, R. Abounader, H. Zong, p53 and NF 1 loss plays distinct but complementary roles in glioma initiation and progression, Glia 66(5) (2018) 999-1015.

3.9 Supplemental Figures

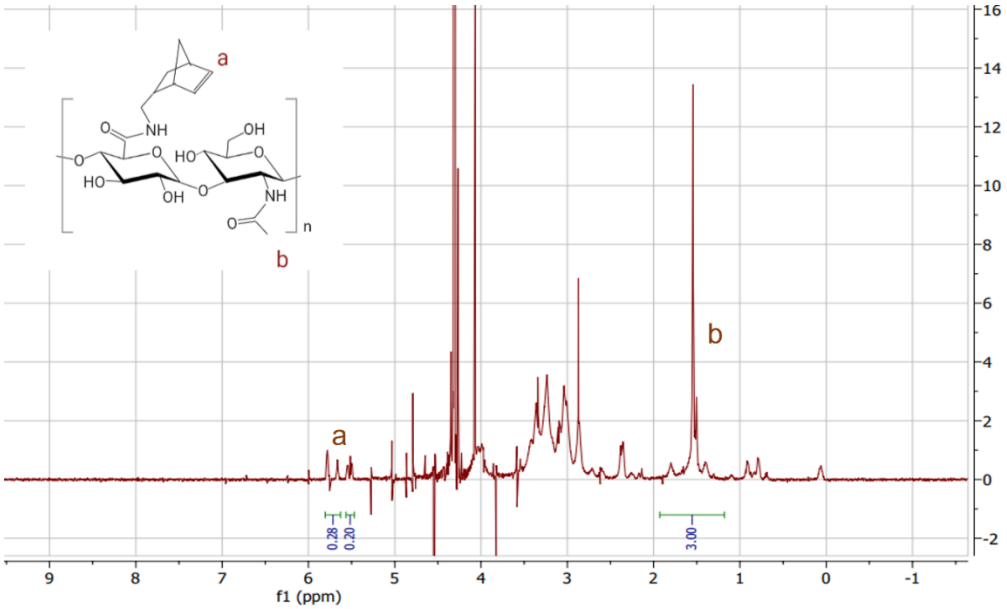

Figure S3.1. NMR spectra of 24% functionalized NorHA. Functionalization efficiency is calculated by normalizing the methyl peak area (b) to a value of 3. The average area of the two norbornene peaks (a) is then taken to determine the functionalization efficiency. Macromer product was generated using the BOP reaction scheme (Synthesis Method 1).

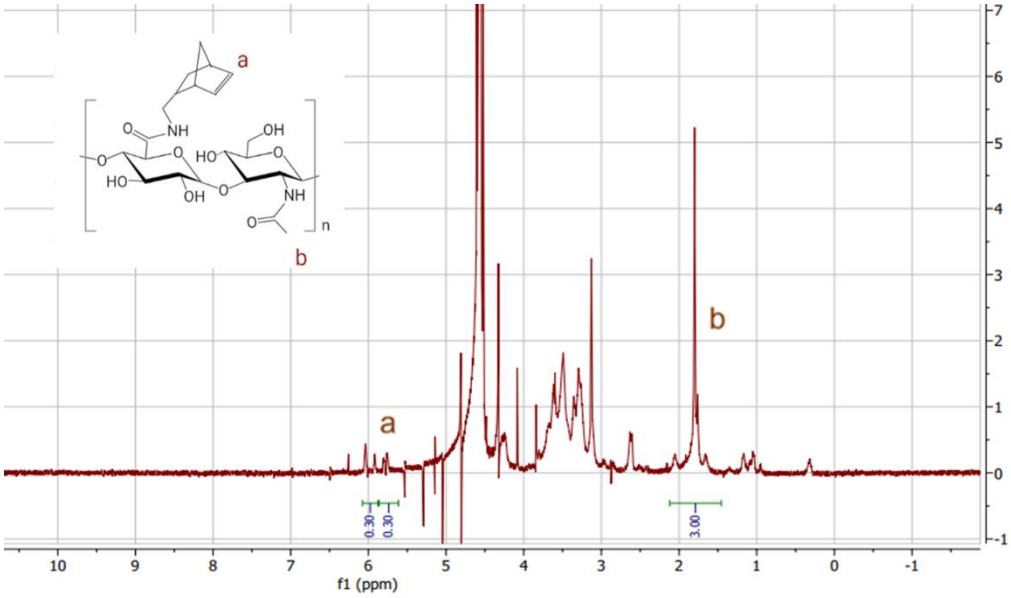

Figure S3.2. NMR spectra of 30% functionalized NorHA. Functionalization efficiency is calculated by normalizing the methyl peak area (b) to a value of 3. The average area of the two norbornene peaks (a) is then taken to determine the functionalization efficiency. NorHA macromer was synthesized using the DMTMM protocol (synthesis method 2). Despite the difference in synthesis methods, both BOP and DMTMM synthesis mechanisms produced equivalent products with comparable levels of norbornene functionalization.

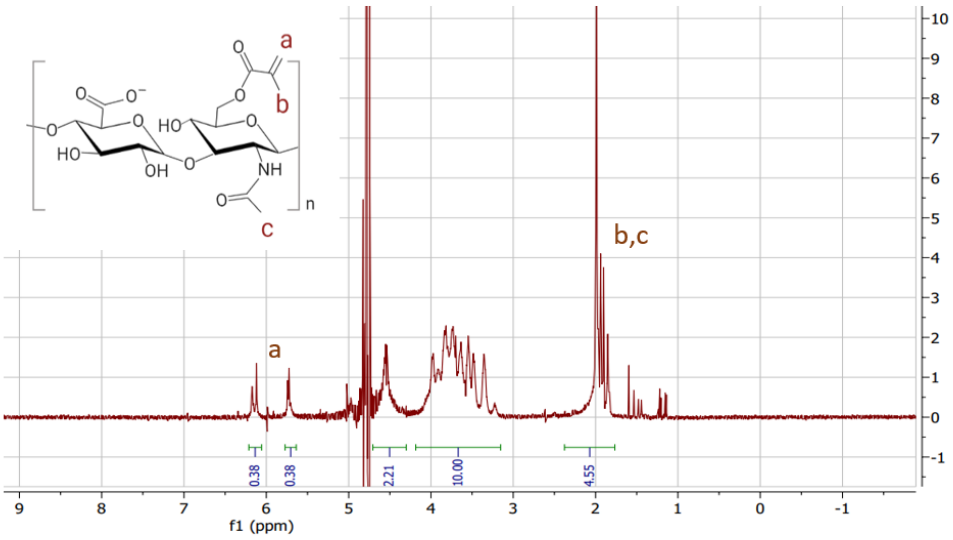

Figure S3.3. NMR spectra of 38% functionalized MeHA. Functionalization efficiency is calculated by normalizing the backbone peak area to a value of 10. The methacrylate peak areas (a) are then averaged to determine the functionalization efficiency.

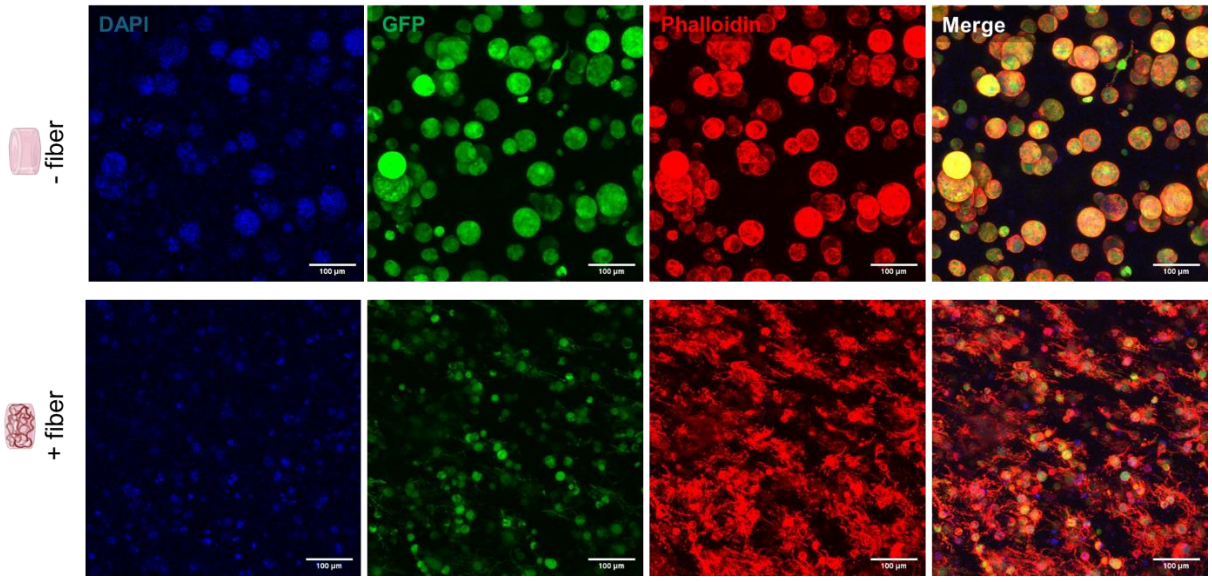

Figure S3.4. OPCs in – fiber (top row) and + fiber (bottom row) NorHA gels at culture day 7. Individual images are shown for each of the DAPI (blue), GFP (green) and phalloidin (red) channels. DAPI was used to stain cell nuclei, while phalloidin stains for f-actin in the cytoskeleton. The OPC cell line used (GFP+ MADM OPCs) constitutively express GFP in the cytoplasm. Overall, cells in – fiber gels display rounded immature morphologies, while OPCs in + fiber gels extend numerous processes throughout the microtissue.

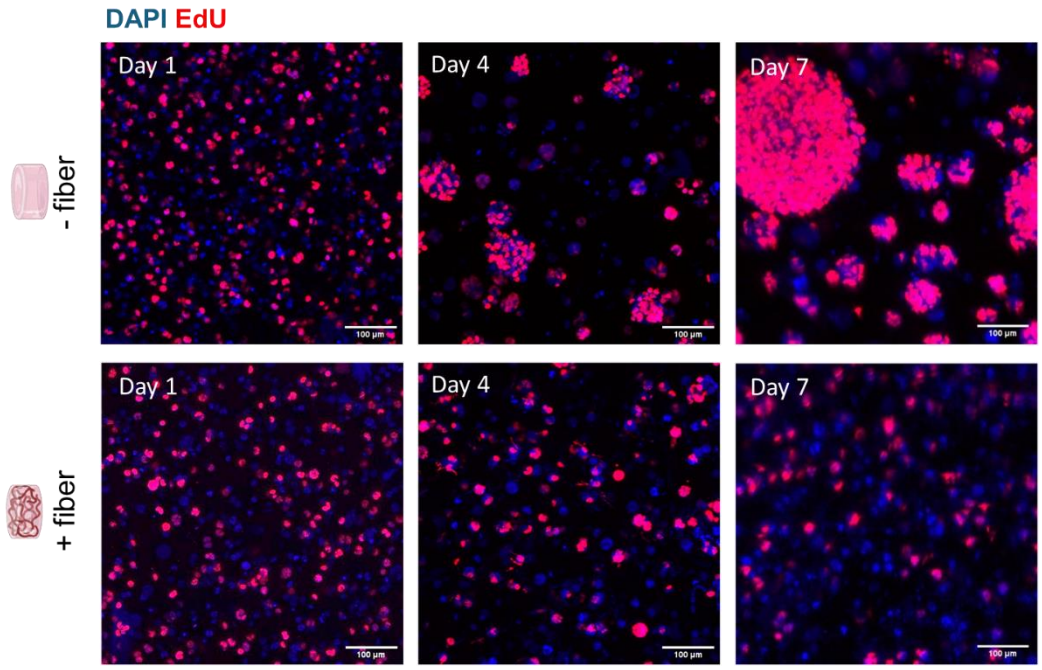

Figure S3.5. OPCs in – fiber (top row) and + fiber (bottom row) NorHA gels at culture days 1, 4 and 7. DAPI (cell nuclei stain) is labeled in blue while EdU (cell proliferation stain) is labeled in red. Proliferation rate appears similar across both – fiber and + fiber conditions at Day 1. Clusters of highly proliferative cells can be seen in – fiber gels at day 4, with large clusters in evidence by day 7. By contrast, no evident clusters are present in + fiber gels, and proliferation remains consistent between days 1 and 4, with a slight decline by day 7.

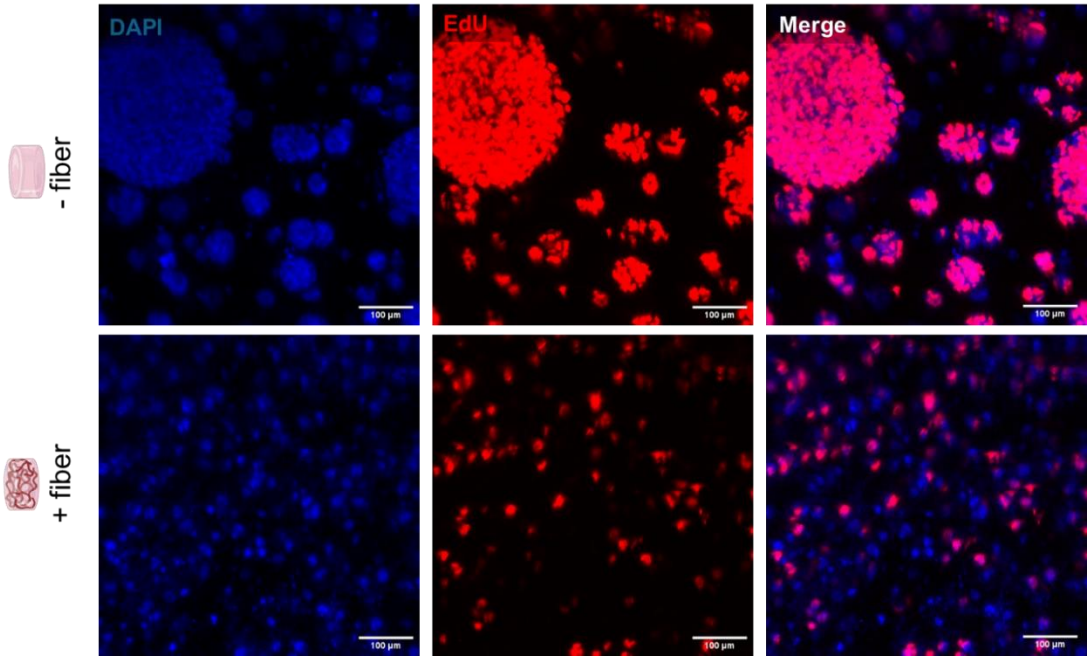

Figure S3.6. OPCs in – fiber (top row) and + fiber (bottom row) NorHA gels at culture day 7. Individual images are shown for each of the DAPI (blue) and EdU (red) channels. DAPI was used to stain cell nuclei, while EdU labels

cells which are actively proliferating. OPCs in the – fiber condition show higher rates of proliferation, particularly within large cell clusters. Proliferation continues to occur in + fiber gels, but to a lesser extent.

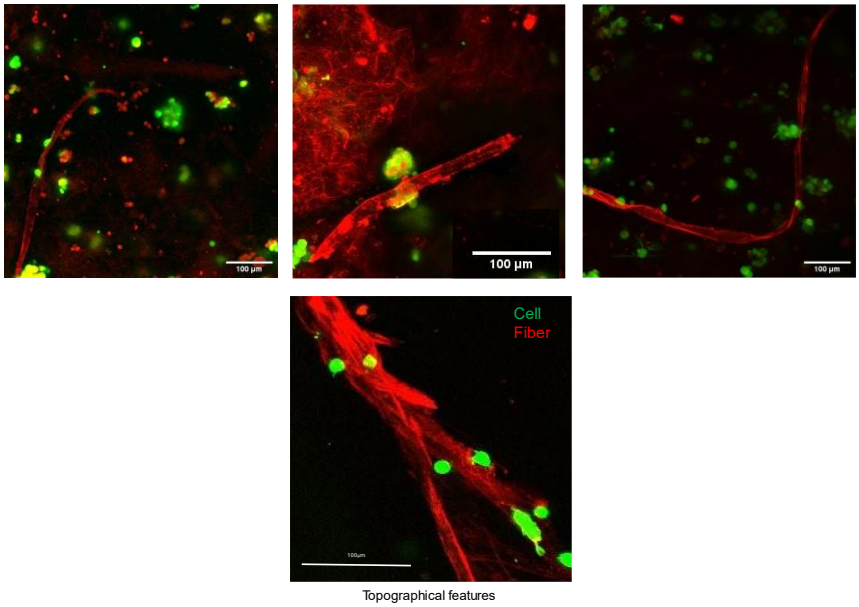

Figure S3.7. Maximum intensity projections of OPCs (green) grown in proximity to swollen electrospun MeHA fibers (red) in 3D NorHA gels. OPCs are shown to be viable when co-encapsulated with fibers, and in some instances appear to associate with fibers and elongate with fiber direction.

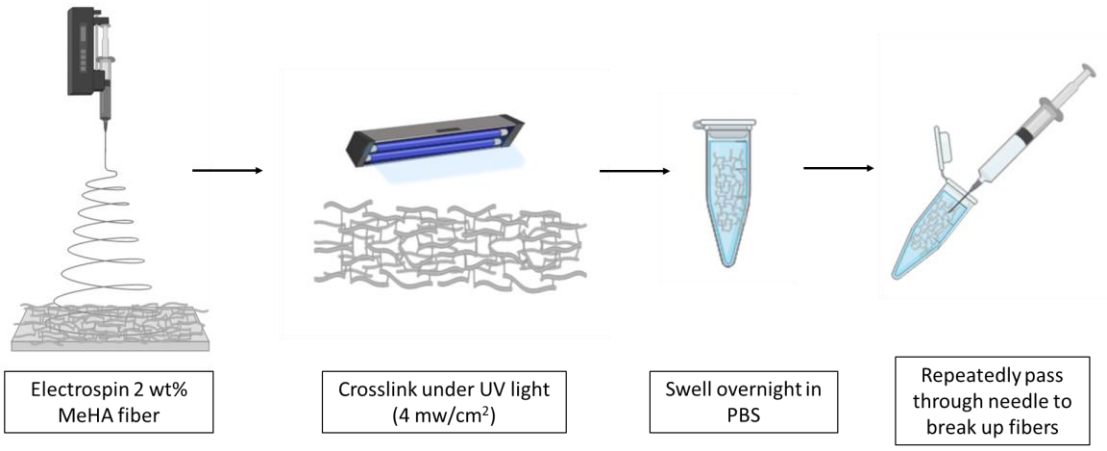

Figure S3.8. Schematic of fiber processing. Fibers were electrospun followed by crosslinking under UV light. Swelling was conducted in PBS for 24-48 hours until equilibrium was reached. Fiber mats were broken up by repeatedly (20-30x) pushing fiber solution through first an 18G, then a 21G needle.

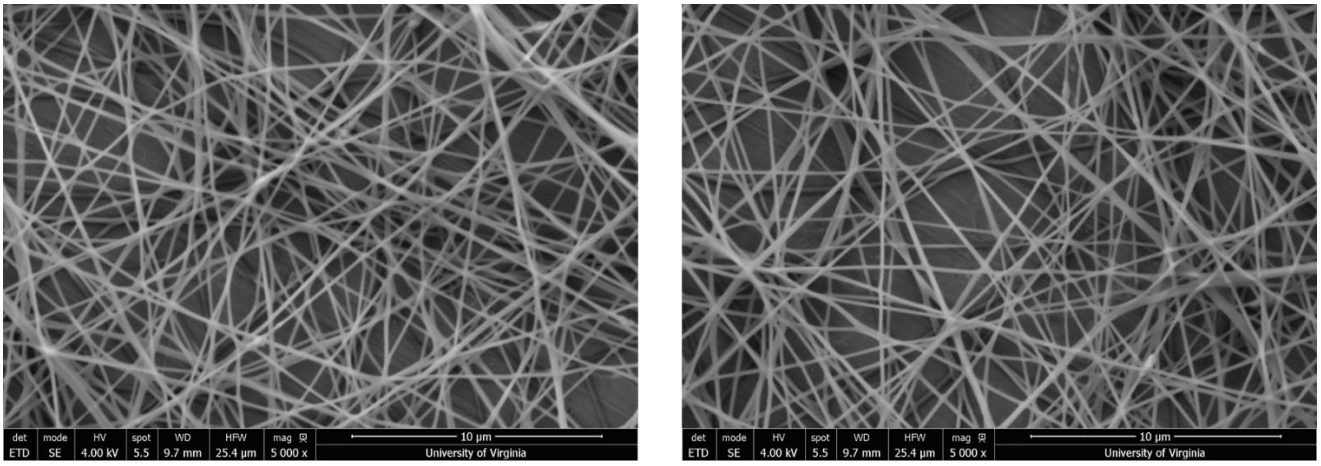

Figure S3.9. Representative SEM micrographs of dry electrospun MeHA fibers. Fibers exhibit smooth even morphologies with consistent diameters.

Chapter 4: Electrospun microfiber cues drive neural stem cell differentiation and extracellular matrix deposition in 3D hydrogels

Rachel A. Mazur[1], Kelsey Wilson[2], Mariano J. Seiglie Gonzalez[3], Pamela J. VandeVord[2], Kyle J. Lampe[1]

1 Department of Chemical Engineering, University of Virginia, Charlottesville, VA USA

2 Department of Biomedical Engineering and Mechanics, Virginia Polytechnic Institute and State University, Blacksburg, VA USA

3 Department of Biological Sciences, Florida International University, Miami, FL, USA

4.1 Abstract

Neural stem cells (NSCs) transplanted into the injured or diseased central nervous system (CNS) can differentiate into new neurons and glia to repair damaged tissue. However, the role of environmental cues in guiding differentiation towards specific cell fates remains poorly understood, particularly toward oligodendroglial cell fates. Here, we introduce a 3D hydrogel system which simulates the properties of native CNS tissue to drive glial development. The system is composed of crosslinked amorphous hyaluronic acid (HA) containing encapsulated HA fibers with swollen diameters designed to mimic mature axons (2.7 ± 0.2 μm). We tuned hydrogel storage moduli to approximate that of native brain tissue (200-2000 Pa) and studied the effects of fiber presence on NSC proliferation, gene expression, metabolic activity, and morphological changes in intermediate stiffness (800 Pa) gels. NSCs in fiber-containing gels at culture days 4-7 exhibited significantly more process extension and morphological changes associated with differentiation. NSCs in fiber-containing gels also exhibited 2-fold higher proliferation rates at day 7. By contrast, metabolic activity was slightly lower in fiber-containing gels. qPCR analysis shows elevated levels of nestin (NSC marker) and O1 (early oligodendrocyte differentiation marker) in fiber-containing gels at days 4 and 7. Gene profiling indicates that NSCs upregulate neural and oligodendroglial differentiation with modified cell signaling and mechanotransduction pathways. Cells remodeled their local microenvironment by depositing both laminin and fibronectin extracellular matrix proteins with ECM distribution impacted by fiber presence. These data indicate that the inclusion of electrospun fibers provides topographical cues which increase proliferation and dramatically direct differentiation even in the presence of typical stem cell proliferation cues.

4.2 Introduction and Background

During development, neural stem cells (NSCs) have the capacity to differentiate into neurons, astrocytes, or oligodendrocytes (OLs) [1]. Central nervous system (CNS) myelination occurs when NSCs differentiate down an OL pathway, becoming first oligodendrocyte progenitor cells (OPCs), then immature OLs, and finally mature, myelinating oligodendrocytes. Both NSCs and OPCs retain a proliferative nature and can migrate throughout the developing brain [2, 3]. Upon reaching a site for myelination, OPCs extend processes which wrap around and ensheath neuronal axons. This myelin sheath enhances the speed and efficiency of signal transduction and provides trophic support to the myelinated neuron [4].

Unfortunately, many aspects of the *de novo* myelination process remain unknown. In particular, a knowledge gap exists regarding NSC differentiation toward OL fates. The use of soluble factors has been demonstrated to drive NSC differentiation into each of the neuronal, astrocytic, and OL lineages [5]. However, the bulk of research focuses on differentiation into neuronal cell fates; the differentiation of NSCs in a glial context remains under-studied by comparison [6]. The mechanisms by which OPCs select which axons to myelinate also remain unclear. Neuronal activity has been demonstrated to enhance remyelination, as stimulating axons increases proliferation and differentiation of OPCs as well as myelin deposition [7]. However, myelination has been shown to occur successfully even in the absence of such activity [8, 9]. One potential explanation is that two modes of *de novo* myelination exist, one which is activity-dependent and one which is activity-independent. Currently, the literature is overwhelmingly focused on activity-dependent myelination, while activity-independent myelination remains under-studied, particularly in a 3D context [10].

Here we propose a novel 3D, *in vitro* model for *de novo* activity-independent CNS myelination. We have developed a hydrogel system consisting of norbornene-functionalized hyaluronic acid (NorHA). Hyaluronic acid is a key component of the extracellular matrix (ECM), making it highly biologically relevant [11]. In addition, the thiol-ene mechanism of crosslinking NorHA gels is easily tunable and can reliably form gels within the range of native brain tissue (G' = 200-2000 Pa) [12, 13]. Our group has previously demonstrated excellent OPC viability and proliferation in this system [12]. Within our hydrogel system, we have sparsely incorporated electrospun methacrylated hyaluronic acid (MeHA) hydrogel fibers with micron-scale diameters. These fibers were designed to provide structural cues similar to those of native axons. Fiber systems composed of other polymeric materials, including polystyrene, poly(trimethylene carbonate-co-ε-caprolactone) (P(TMCCL)), and both uncoated and graphene oxide and laminin-coated polycaprolactone (PCL), have been shown to prompt activity-independent differentiation of NSCs into myelinating OLs [8, 9, 14-16]. 3D cultures containing other forms of topography, such as ablated microchannels, magnetic microparticle templating, and interfaces between bicontinuous hydrogel systems, also provide topographical cues that guide cell migration and remodeling in a 3D context [17-20]. Hydrogel-fiber composite materials have been explored for other cell types and applications, such as guiding angiogenesis or cardiomyocyte alignment [21,

22]. However, to the best of our knowledge, the effects of electrospun fiber topography on oligodendroglial lineages have only been conducted in 2D with stiff polymeric materials. Our model therefore provides a new opportunity for probing cell response to 3D topography, with independently and tunable control over hydrogel stiffness, fiber size, and fiber density.

We encapsulated NSCs in HA hydrogels both with and without HA fibers and cultured them in proliferation media over a seven-day period. We conducted staining to assess cell morphology and determine whether cells grown in the presence of fibers extended more elongated processes (a hallmark of maturation) compared to those in fiber-free control gels. Additionally, we performed an EdU-based proliferation assay and an ATP/DNA assay to quantify how the presence of fibers impacted cell proliferation and metabolic activity, respectively. Both qPCR and NanoString gene profiling were used to determine the impact of fiber presence on gene expression levels. Gene ontology analysis was conducted to assess which biological processes were most likely implicated based on dysregulated genes, and centrality analysis was used to determine which of the dysregulated genes were most important within the overall network. Finally, laminin and fibronectin ECM deposition were probed to assess remodeling of the local cellular microenvironment, and how this process was affected by the presence of electrospun microfibers.

4.3 Materials and Methods

4.3.1 Flask Preparation and Cell Culture

Sterile T75 tissue culture flasks (VWR) were coated with 5 mL of a 20 µg/mL polyornithine solution and incubated at 37 ℃ for one hour. Subsequently, the flasks were rinsed with Dulbecco's Phosphate-Buffered Saline (DPBS) and incubated in 5 mL of a 5 µg/mL laminin (Sigma; from Engelbreth-Holm-Swarm murine sarcoma basement membrane) solution for one hour. Flasks were rinsed and stored at -20 ℃ until use.

Adult rat hippocampal neural stem cells were sourced from Sigma Aldrich (catalog no. SCR022). Throughout all maintenance and experiments, cells were cultured in NSC proliferation media, comprising Dulbecco's Modified Eagle Medium/Nutrient Mixture F-12 (DMEM/F12 1:1) with 17.5 mM D-glucose and 55 mg/L sodium pyruvate (Gibco). The media were supplemented with 2 mM L-glutamine (Gibco), B27 supplement (Invitrogen), 1% penicillin-streptomycin (Invitrogen), and 20 ng/mL FGF-2. Cells were seeded onto flasks at a density of 1 x 10^4 cells/cm^2. Media were refreshed every two days, and cells were passaged when reaching 80-90% confluence. During cell passaging, detachment was achieved using Accutase (Sigma), followed by rinsing the flask with DPBS. The resulting cell solution underwent centrifugation at 200g for 5 minutes, and the supernatant was aspirated. Cells were then resuspended in 300 µL of media for cell counting. Cells between passage 2-10 were used for all experiments.

4.3.2 NorHA Synthesis

Norbornene-functionalized hyaluronic acid (NorHA) was synthesized following previously established protocols [23]. Briefly, hyaluronic acid (74 kDa, LifeCore) was dissolved at a concentration of 25 mg/mL in 40 mL of 1 mM 2-(N-morpholino)ethanesulfonic acid (MES) buffer, then pH adjusted to 5.5 using 10 M NaOH. 31 mg/mL 4-(4,6-dimethoxy[1,3,5]triazin-2-yl)-4-methylmorpholinium chloride (DMTMM) was added as a coupling agent and thoroughly mixed until DMTMM completely dissolved (approximately 10 minutes). To achieve a 20-30% functionalization efficiency, 0.271 mL of 5-norbornene-2-methylamine (TCI America) was introduced, and the mixture was stirred overnight at room temperature. The reaction product was precipitated in 250 mL of cold 95% ethanol, collected via vacuum filtration, and re-dissolved in a 2M brine solution. The precipitate was transferred to pre-soaked dialysis tubing with a molecular weight cut-off of 6-8 kDa. Dialysis was carried out against DI water for 24 hours, followed by brine solution for another 24 hours, with water changes twice daily. A final dialysis round against DI water was performed for 24 hours before lyophilization. Purity and the extent of norbornene functionalization were assessed using 1H NMR (Varian Inova 500 MHz) with D2O as the solvent. (NMR spectrum for NorHA in Supplementary Figure S4.1.) The resulting NorHA product was stored under nitrogen at 4 °C.

4.3.3 MeHA synthesis

Methacrylated hyaluronic acid (MeHA) was synthesized according to previously established protocols [24]. Briefly, methacrylic anhydride (MA) was gradually added dropwise to research-grade sodium hyaluronate (LifeCore, 74 kDa) at a concentration of 1% w/v and stirred until homogenous. The solution was kept on ice, and the pH was carefully regulated between 8-9 using 5 N NaOH. MA was added to HA with a 20x molar excess. Once all methacrylic anhydride was introduced, the solution was continuously stirred overnight. Subsequently, the solution underwent a five-day dialysis against deionized water using a molecular weight cutoff of 6-8 kDa. The resulting macromer solution was frozen overnight at –80°C, followed by a 3-day lyophilization period. (NMR spectrum for MeHA in Supplementary Figure S4.2.) The resulting MeHA product was stored under nitrogen at 4°C.

4.3.4 Electrospinning

Electrospinning solution was prepared in 2 mL batches, comprising 2 wt% MeHA, 3 wt% polyethylene oxide (PEO, 900 kDa), 0.05 wt% Irgacure D-2959 photoinitiator (I2959), and 0.415 mg/mL methacrylated rhodamine B dissolved in deionized water. The solution was shielded from light and allowed to dissolve in a 5 mL Cadence syringe for 24-48 hours with continuous stirring. Subsequently, fibers were spun using a Spraybase electrospinning machine under conditions of 21% relative humidity, a 21 cm collection distance, 8-11 kV voltage, 20-gauge needle, and 0.4 mL/hr flow rate. Dry fibers were collected on aluminum foil sheets and stored under nitrogen until crosslinking. Fibers were crosslinked for 15 minutes using an Omnicure UV light at an intensity of 14 mW/cm^2 and wavelength of 365 nm. The fibers were then swollen overnight in

deionized water at a stock concentration of 5 wt% and treated by passing through an 18-gauge needle repeatedly, followed by a 21-gauge needle, in accordance with established protocols [25].

4.3.5 Fiber characterization

SEM imaging of dry electrospun fibers was conducted at a voltage of 1.0 kV, with a working distance ranging between 5-6 mm. Four images from distinct sites were captured at magnifications of 5,000x and 10,000x. Fiber diameters were quantified using the length measuring tool in FIJI ImageJ [26].

For swollen fiber solutions (5 wt% in PBS), a Zeiss inverted fluorescent microscope was employed. The solution was applied to a microscope slide, and fluorescent signals from the rhodamine B tag were captured at magnifications between 2.5-10x at various locations. Fiber diameters were again determined using the length measuring tool in FIJI ImageJ [26].

4.3.6 Rheology

NorHA macromer solution was prepared by dissolving 1–2 wt% NorHA macromer, 0.0328 wt% LAP, and dithiothreitol (DTT) at a 0.312 thiol-norbornene ratio in PBS. For conditions involving fibers, swollen electrospun fibers were also included at 1 wt%. Using a pipette, 75 µL aliquots were dispensed onto a UV-configured plate of an Anton Parr MCR 302 rheometer. A 25 mm diameter smooth cone and plate with a 0.505º angle was employed to perform a time sweep. The samples underwent 30 seconds of oscillatory motion without UV light exposure. Gels were then cured for 120 seconds at 0.1% oscillatory strain, 10 rad/s oscillation frequency, and 4 mW/cm2 UV light intensity (365 nm) followed by an additional 60 seconds of oscillatory motion. The plateau storage modulus was calculated by averaging over the final 30 seconds.

4.3.7 3D Cell Encapsulation and Hydrogel Culture

NorHA macromer solution was created by dissolving 1 – 2wt% NorHA macromer, 0.0328wt% LAP and dithiothreitol (DTT) at an 0.312 thiol-norbornene ratio in PBS. For fiber-containing conditions, gel precursor solution also contained sparse fibers by diluting the 5% fiber stock solution with PBS to a final concentration of 1 wt%. Rat NSCs were incorporated at a final concentration of 0.5 x 10^7 cells/mL. Gel precursor solution was pipetted in 40 µl aliquots to sterile, trimmed 1 mL syringes (Cadence) and exposed to UV light at 4 mW/cm^2 (365 nm) for 10 minutes. Gels were transferred to 24 well plates and rinsed three times with 500 µl PBS. 1 mL of NSC media per gel was added and the gels were cultured for up to 7 days, changing media every other day.

4.3.8 Microplate Biomolecular Assays

Hydrogel samples containing encapsulated NSCs were collected on days 1, 4, and 7 of culture, with three sample replicates per condition. The hydrogels were divided into microtubes (1 gel per tube) containing 300 µl of 1x passive lysis buffer (Promega) and frozen at -80°C. Before conducting the assays, the samples were retrieved from the -80°C freezer and thawed on ice for 1 hour. Following thawing, the gels were homogenized using a handheld pestle homogenizer, followed by probe sonication for 10 seconds.

ATP and DNA concentrations of each sample were measured to evaluate the metabolic activity and cell number, respectively, within the hydrogel microtissues. Homogenized samples were pipetted in triplicate (n=3) for each of three sample replicates. CellTiter-Glo 2.0 reagent (Promega) for ATP or PicoGreen dye (Promega) for DNA was added to each of the standard and sample wells. The plate was incubated at room temperature for 10 minutes. Luminescence (ATP) or fluorescence (DNA) was measured using a BMG Clairostar microplate reader. ATP or DNA concentrations in sample wells were determined based on an ATP or DNA standard curve. ATP values for each sample were normalized to DNA values, as DNA concentration is known to scale with the number of cells.

4.3.9 Cell Morphology Staining, Imaging, and Quantification

To evaluate cell morphology, hydrogels were fixed and stained with DAPI and phalloidin on culture days 1, 4, and 7 to label nuclei and f-actin, respectively. The hydrogels were fixed with a 4% paraformaldehyde solution for 1 hour at 37 °C. Subsequent to fixation, three 5-minute washes with 3% bovine serum albumin (BSA) in PBS were performed between each of the following steps: The fixed hydrogels underwent permeabilization at room temperature in 0.1% Triton X-100 for 30 minutes at 4°C with gentle shaking. Subsequently, the gels were stained overnight at 4°C with AlexaFluor 647 phalloidin (ThermoFisher) at a concentration of 2 U/mL in PBS with 1% BSA. To label cell nuclei, the gels were stained with 300 nM DAPI (Sigma) for 1 hour at 4°C with shaking. After staining, the gels were rinsed 4-6 times in 1-hour washes with 3% BSA in PBS. The stained gels were stored in PBS before imaging with a Leica Stellaris 5 confocal microscope. Z-stack images were captured at 20x magnification to a Z depth of 300-500 μm.

For each of the + fiber and – fiber conditions, between 6-9 z-stack images were captured for each time point (3 images per gel across 2-3 gel replicates). Z stacks were taken in intervals of 2 μm to a depth of 200-400 μm. For each Z interval, the DAPI and phalloidin channels were separated and processed using the Otsu threshold function in FIJI ImageJ [26]. The Despeckle function was applied to each channel to eliminate background noise. A dedicated ImageJ macro was used for automated quantification of signal area of both the DAPI and phalloidin channels for each Z interval in the sample [27]. Using the macro, signal areas for both the DAPI and phalloidin channels were quantified for each Z slice and summed together to find total signal area in each channel. Phalloidin signal area was normalized to the DAPI signal area to determine the average phalloidin signal area per cell.

4.3.10 Cell Proliferation Staining, Imaging and Quantification

To quantify NSC proliferation within 1.5 wt% NorHA gels, hydrogels were stained using the Click-iT EdU Imaging kit (Life Technologies) on days 1, 4, and 7. Cell-laden hydrogels were incubated in EdU solution for 1 hour at 37 °C. Subsequently, gels were fixed in a 4% paraformaldehyde solution for 1 hour at 37 °C. Following fixation, two 5-minute washes with 3% bovine serum albumin (BSA) in PBS were performed, both after fixation and between subsequent steps: The fixed hydrogels were permeabilized at room temperature in 0.1% Triton

X-100 for 30 minutes, followed by incubation in Click-iT reaction buffer for another 30 minutes. For nuclear labeling, gels were stained with 300 nM DAPI (Sigma) for 1 hour at 4°C with shaking. After staining, the gels were stored in PBS prior to imaging with a Leica Stellaris 5 confocal microscope. Z-stack images were captured at 20x magnification to a Z depth of 300-500 µm.

For each of the + fiber and – fiber conditions, 9 z-stack images were captured (3 images per gel across 3 gel replicates). Z stacks were taken in intervals of 2 µm to a depth of 200-400 µm. For each Z interval, the DAPI and EdU channels were separated and processed using the Otsu threshold function in FIJI ImageJ [26]. The Despeckle function was applied to each channel to eliminate background noise. As before, the dedicated ImageJ macro was used to quantify signal areas for each Z slice in both the DAPI and EdU channels [27]. Signal areas were added together to find total signal area in each channel. EdU signal area was then normalized to the DAPI signal area to determine the average EdU signal area per cell.

4.3.11 Gene expression

To assess changes in gene expression for cells in both fiber-containing gels and no-fiber controls, qPCR was performed at days 0, 2, 4 and 7. Each hydrogel was allocated into individual microtubes, with one gel per tube, and stored in 300µL of RNA lysis buffer at -80°C prior to downstream analysis. Prior to performing qPCR, samples were thawed, mechanically homogenized, and RNA was extracted using the Zymo Research Quick-RNA Miniprep Kit. RNA concentration was normalized to 30 µg/ml for all samples and subsequently converted into cDNA using the iScript™ cDNA Synthesis Kit (Bio-Rad) and combined with Sso Advanced Universal SYBR Green Supermix (Bio-Rad). 2µL cDNA was loaded into each well of a 96-well plate. The plate was then loaded into the CFX Connect Real-Time PCR Detection System (Bio-Rad) and run under optimized conditions and cycling parameters. Primers for NSC maturation markers and reference genes were selected as follows:

Gene	Forward	Reverse
GAPDH	5’- ACT CCC ATT CTT CCA CCT TTG -3’	5’- CCC TGT TGC TGT AGC CAT ATT -3’
Nestin	5’- CAA GGT CTG GTC TGG TGT ATG -3’	5’- GGC TTT ATT CAG GGA GGA AGA G -3’
PDGFRα	5’- CAC ACG CCA GAC TGT GTA TAA -3’	5’- CAT GGT GAT GCC TTT GTT TCT C -3’
O1	5’- CCC ACT CCC TGG CAA TTA AA -3’	5’- GAC TTC TGG CTC TAA ACT GGT G -3’
MBP	5’- AAC TGG CAG AAA GGA AGG AG -3’	5’- CCA TCA CCA CTG TCC AAT CA -3’

Fold change (FC) of each target was calculated using the Livak Method (2 -ΔΔCt) normalized to GAPDH and no-fiber day 0 gels to identify differentially expressed genes (DEGs).

4.3.12 NanoString Glial Profiling Panel

Hydrogel samples containing encapsulated NSCs were collected on day 7 of culture and stored following the procedure above. Before profiling, the samples were thawed, mechanically homogenized, and sonicated for 10 seconds. RNA was extracted by the UVA Spatial Biology Core and gene expression was analyzed using the NanoString Glial Profiling Panel. Raw data was analyzed using the nCounter ROSALIND platform to identify DEGs (FC > 1.3, p-value <0.05) in + fiber gels at the D7 timepoint. To define the properties and putative biological relevance of the significantly dysregulated genes, DEGs were input into the STRING database where functional enrichment analysis using gene ontology (GO) and Kyoto Encyclopedia of Genes and Genomes (KEGG) tools was performed. Additionally, a protein-protein interaction network (PPIN) was generated with a minimum interaction score set to 0.7 to ensure high confidence and imported into Cytoscape to visualize and assess the network's topological properties with the query proteins of the DEGs represented as the nodes. The following centrality parameters were calculated using the Cytoscape software to determine the biologically significant nodes in our network. Degree centrality refers to the number of links connected to a given node. In PPINs, nodes with higher degrees are considered hubs and are typically located at the network's center. Betweenness centrality measures the number of shortest paths that pass through a node. Nodes with high betweenness, known as bottlenecks, monitor the flow of information within the network. Closeness centrality calculates the average distance of all shortest paths between a node and every other node in the network. A high closeness value indicates that a node is in close proximity to all other nodes. Stress centrality measures the number of shortest paths passing through a node, similar to betweenness centrality, but counts all paths rather than the minimal ones. Eccentricity centrality measures the greatest distance between a node and any other node in the network, indicating how far a node is from the node that is furthest from it. Centrality values of the nodes were imported into Python (3.12) and manually ranked based on metric importance, with stress and betweenness holding the highest weights, followed by degree, closeness, and eccentricity. This was followed by a separate weighting method using the PageRank algorithm. Nodes were then ordered by their ranks in descending order. The top 10 nodes identified by each weighting method were considered as the most important to the overall network.

4.3.13 Laminin and Fibronectin Immunostaining and Image Quantification

Cell-containing gels were cultured in standard growth media, replenished every other day. To visualize specific extracellular matrix (ECM) proteins, gels were fixed in paraformaldehyde for 1 hour at 37 °C/5% CO2, followed by three washes in 2% BSA-PBS. A blocking step was performed in 2% BSA-PBS at room temperature, and gels were incubated with primary antibodies (rabbit anti-laminin α5, 1:100, Thermofisher, or rabbit anti-fibronectin, 1:250, Abcam) in 2% BSA-PBS for 12 hours at 4°C. After two washes, gels underwent a 6-8 hour incubation in 2% BSA-PBS. The secondary antibody (donkey anti-rabbit 647, 1:200, Abcam) was applied in 2% BSA-PBS at 4°C for 12 hours. Plasma membrane was stained with CellMask Orange (1:1000, Thermofisher) for 35 minutes, followed by three rinses with 2% BSA-PBS. Gels were stored in 2% BSA-PBS at 4°C.

3 z-stack images were taken for each of the + fiber and – fiber conditions (1 image for each of 3 gel replicates). Z stacks were taken in intervals of 2 µm to a depth of 200-400 µm. For each Z interval, CellMask and protein channels were separated and processed using the Otsu

thresholding function in FIJI ImageJ [26]. The Despeckle function was then applied to remove background noise. Using the macro, signal area for both the CellMask and protein channels were quantified for each Z interval in the sample [27]. Protein signal area was then divided by CellMask signal area to determine the amount of extracellular matrix deposition normalized to cell surface area.

4.3.14 Statistical Analysis

Morphology and proliferation signal areas, ATP data, and DNA data were analyzed using two-sample t test with a α-value of 0.05. ECM deposition results were analyzed using 3-way ANOVA with a α-value of 0.05. Box plots cover the second and third data quartiles with error bars covering the first and fourth quartiles. Box plots also include marks for mean (x) and median (bar) data values, as well as separate dots for outlier data points.

4.4 Results and Discussion

4.4.1 Fiber size characterization

Electrospun fibers were imaged using SEM to assess morphology and dry fiber diameter (Figure 4.1 A). Fiber diameters remained consistent along the lengths of fibers and between different fibers. Dry fiber diameter was quantified at 181 ± 4 nm, consistent with MeHA fibers generated by other groups using similar electrospinning parameters [28].

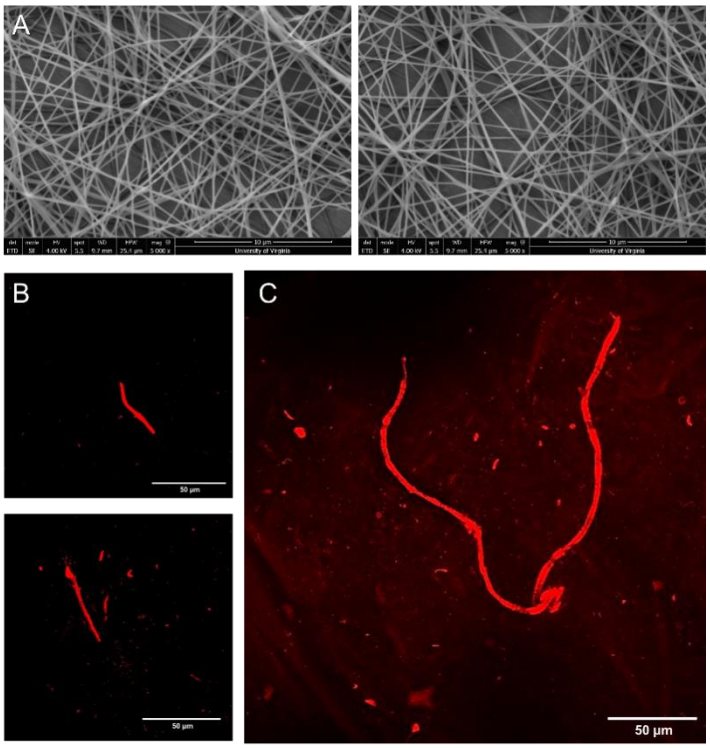

Figure 4.1. Fiber size characterization. A) SEM images taken of dry electrospun fiber mats. Dry fiber diameter was determined to be 181 ± 4 nm. B) Fluorescent images of swollen hydrated fibers (2D). Swollen fiber diameter was quantified as 2680 ± 170 nm. C) Confocal image of long swollen fiber encapsulated in 3D hydrogel (acellular).

Following fiber swelling and breakup, fiber stock solution was imaged in 2D using fluorescent microscopy to determine the swollen fiber diameter (Figure 4.1 B). Swollen fiber diameter was quantified to be 2670 ± 170 nm. Most myelinated axons in the central nervous system are known to have diameters between 0.3 µm to 2 µm [8]. Previous 2D *in vitro* studies with OPCs have found that fibers with diameter above 0.4 µm were preferentially myelinated, with OPCs displaying a preference for large diameter (2-4 um) fibers [8]. Our fiber size therefore represents ideal diameters for neural cell engagement, and accurately reflects mature CNS axon size.

4.4.2 Biomaterial stiffness characterization

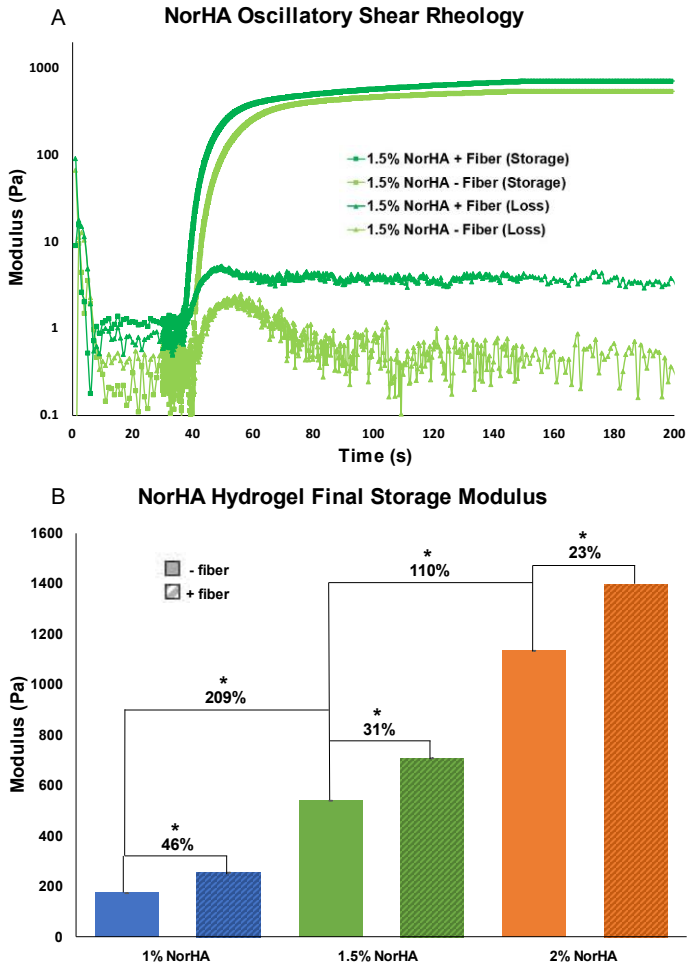

Figure 4.2. Rheological characterization of NorHA gels with and without fibers (n=4). A) Representative time-sweep oscillatory shear rheology measurements for on-stage gelation of 1.5 wt% NorHA gels. Blue region represents stiffness range of native brain tissue. B) Final storage moduli for 1-2 wt% NorHA gels with and without fibers. Plateau storage modulus increases with increasing NorHA concentration. Fiber containing gels at each stiffness condition had higher storage moduli than no-fiber controls with equivalent NorHA concentrations. All conditions were found to be significantly different from one another ($p<0.05$). Percentages indicate the percent increase between adjacent bars.

Hydrogels containing between 1-2 wt% NorHA were able to accurately reproduce the range of storage moduli present in native brain tissue (200-2000 Pa), with 1.5 wt% NorHA falling into the intermediate range (Figure 4.2A) [29]. Inclusion of crosslinked electrospun fibers at a concentration of 1 wt% in the gel precursor solution results in stiffer gels, with a 20-50% increase in plateau storage modulus as compared to hydrogels containing no fibers (Figure 4.2 B). However, the effect of polymer concentration on final stiffness was more pronounced than effects due to fibers, with a 100-210% increase in stiffness between different polymer concentrations in no fiber gels. In general, percent increases between conditions were more pronounced at lower stiffnesses. Overall, changes in both polymer concentration and fiber presence were found to have a significant effect on final storage modulus.

4.4.3 Cell morphology and proliferation assays

Samples from both control and experimental groups were fixed and stained on days 1, 4, and 7 of culture to assess the impact of fiber presence on the morphology of encapsulated NSCs. Maximum intensity projections of phalloidin-labeled cells in – fiber control gels revealed that, over the 7-day culture period, cells grew and formed clusters but maintained a rounded and immature morphology (Figure 4.3A and Supplementary Figure S4.3). These findings are consistent with literature, as NSCs/NPCs have been observed to grow in large clusters with relatively few process extensions in 3D PEG, collagen and hyaluronic acid hydrogels of comparable stiffnesses [30-33]. By contrast, cells in gels + fibers consistently exhibited a more mature morphology, as indicated by the extension of numerous processes throughout the gel

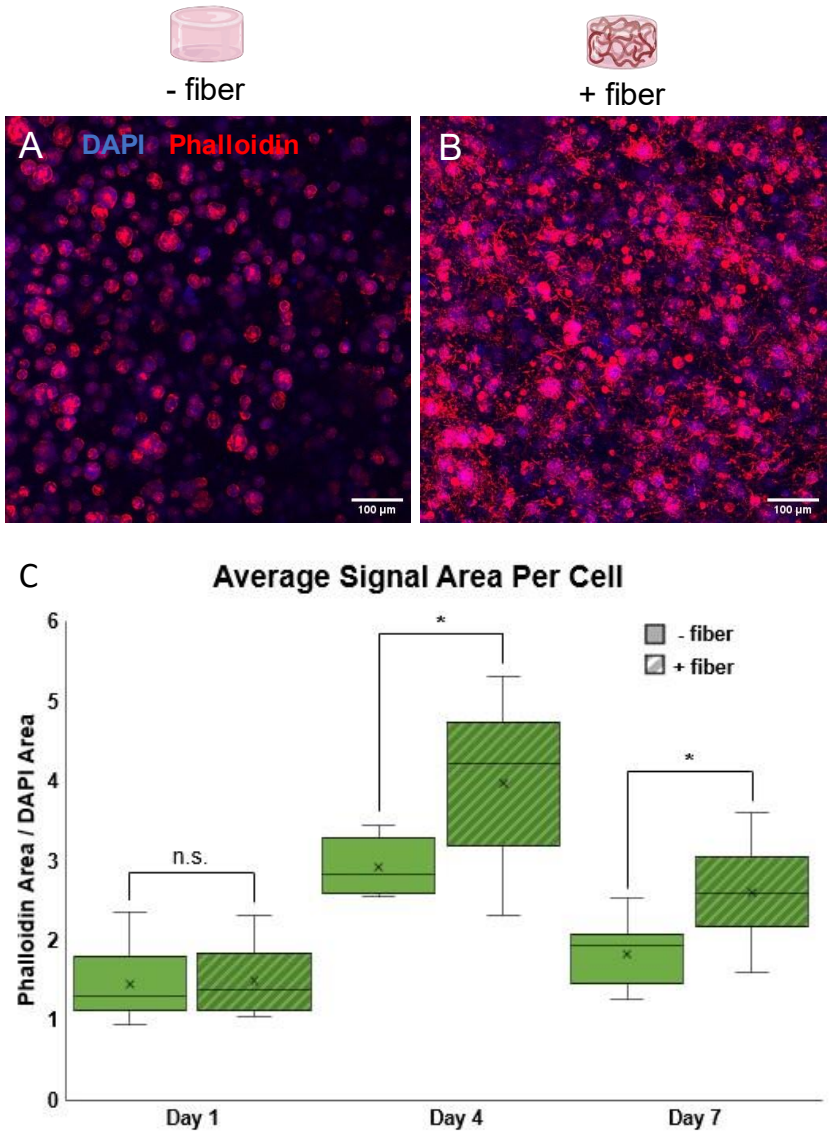

Figure 4.3. Assessment of cell morphology for NSCs in fiber-containing gels as compared to no-fiber controls. NSCs were fixed and stained with DAPI (blue) and phalloidin (red). A) Maximum intensity projection of DAPI and phalloidin signal for cells encapsulated in no-fiber control gels after 7 days of culture (D7). In the absence of fibers, cells retained a rounded and immature morphology. B) Maximum intensity projection of DAPI and phalloidin signal for cells co-encapsulated alongside electrospun MeHA fibers at D7. Cells in fiber-containing gels extended numerous processes, an indicator of differentiation. C) Area of phalloidin signal was collected and normalized to DAPI signal area to calculate average signal area per cell. n.s. indicates no significant difference between conditions, while * indicates a significant difference ($p<0.05$). A significant difference in per-cell signal area was observed at both D4 and D7.

(Figure 4.3B). In published literature, fiber cues promote differentiation and process extension [34-36]. However, previous fiber-based experiments used NSC seeded atop electrospun nanofiber scaffolds designed to mimic fibrous ECM cues, whereas our co-encapsulation method more accurately reflects the 3D nature and compliant physical properties of native tissue as well as axon dimensions.

Phalloidin signal area was quantified for each condition and normalized to the DAPI area as an indicator of average cell size. Initially, both conditions showed similar phalloidin/DAPI ratios on day 1 (D1) of culture, with mean signal area ratios of 1.49 and 1.44 for + fiber and - fiber gels, respectively. However, cells in fiber-containing gels displayed significantly larger signal area ratios over time, a difference which was most pronounced by D4 where fiber-containing gels had a mean phalloidin/DAPI signal area ratio of 3.97, compared to 2.92 for cells in gels without fibers (Figure 4.3C). By D7, the DAPI-phalloidin ratios for both conditions had decreased somewhat, but fiber-containing gels continued to exhibit significantly larger ratios (2.60 for + fiber, 1.82 for

– fiber). The decrease from D4 to D7 is unexpected, but indicative of the possibility of process selection as cells retract or prune small processes and enhance major processes. The consistent size of the main cell body across conditions indicated that the increase in signal area could be attributed to greater amount of process extension associated with cell maturation. Notably, the maturation effect occurred even in the presence of FGF2, a mitogen which would be expected to maintain NSC stemness and prevent differentiation. No soluble factors were added (or removed) to induce differentiation. This indicated the potential for physical cues to overpower or suppress the effects of known soluble cues like mitogens.

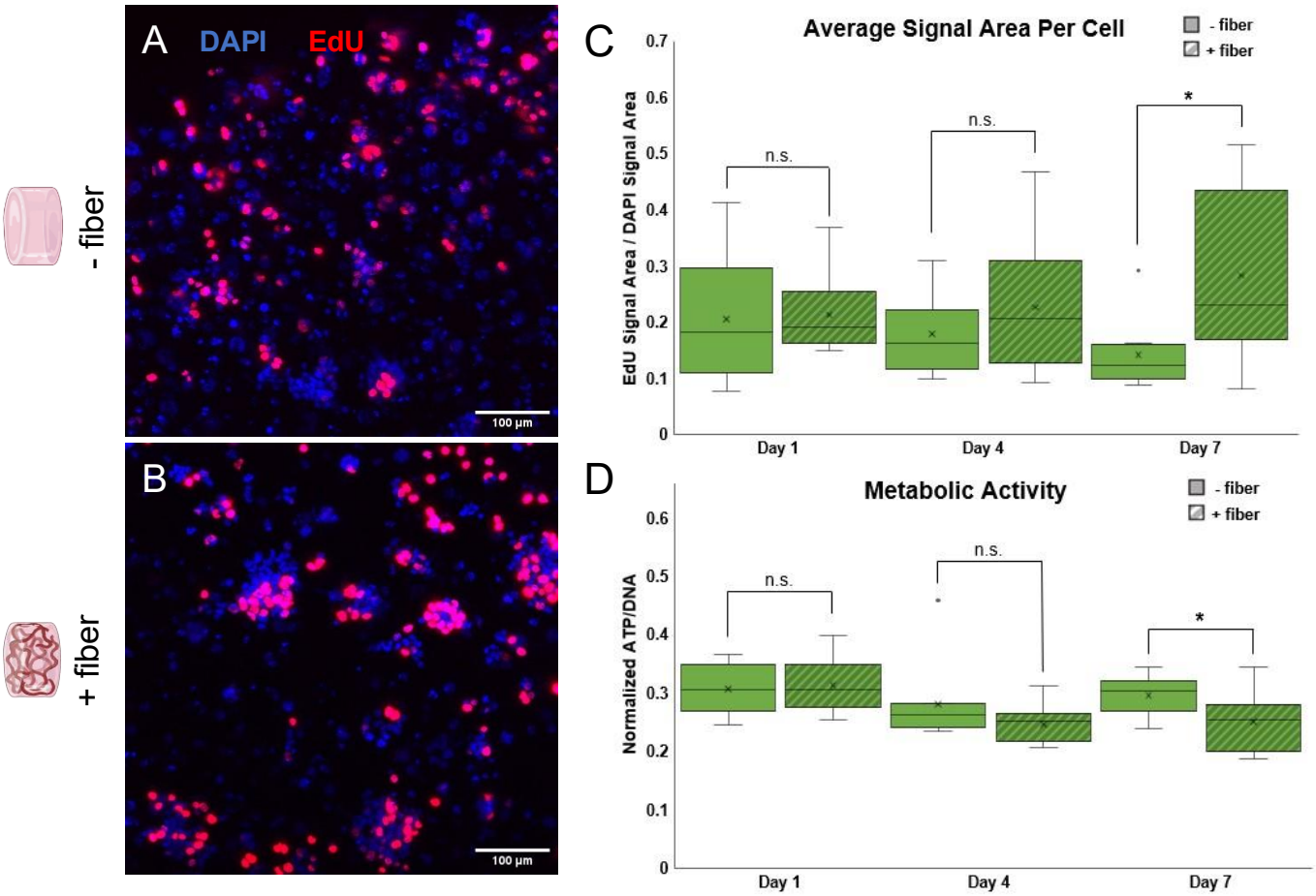

Figure 4.4. Assessment of cell proliferation for NSCs in fiber-containing gels as compared to no-fiber controls. A) Maximum intensity projection of DAPI (blue) and EdU signal (red) for cells encapsulated in no-fiber control gels at D7. B) Maximum intensity projection of DAPI and EdU signal for cells co-encapsulated alongside electrospun MeHA fibers at D7. C) Area of EdU signal was collected and normalized to DAPI signal area to calculate the fraction of actively proliferating NSCs. n.s. indicates no significant difference between conditions, while * indicates a significant difference ($p<0.05$). Proliferation was found to be significantly higher within the fiber-containing gels at D7. D) ATP concentration was normalized to DNA concentrations to determine average metabolic activity per cell ($p < 0.05$). Metabolic activity of cells in – fiber gels was significantly higher than cells in + fiber gels at D7.

Proliferation assays were also conducted for + fiber and – fiber groups on days 1, 4, and 7 of culture. Nuclei were stained with DAPI, and EdU labeling was used to stain for actively proliferating cells (Figure 4.4 A-B and Supplementary Figure S4.4). NSC proliferation appeared similar between conditions at Days 1 and 4, with mean EdU/DAPI ratios between 0.18-0.23 for both groups at both timepoints. Proliferation remained at a similar level for – fiber gels at D7, with a mean EdU/DAPI ratio of 0.14. However, proliferation was elevated in the + fiber condition at D7, with fiber-containing gels exhibiting a statistically higher proliferation ratio of 0.28 (Figure 4.4C).

While the EdU assay fluorescently labels actively dividing cells, it does not provide insights into the metabolic activity associated with that cell division. Therefore, ATP/DNA assays were utilized to specifically examine bulk changes in metabolic activity due to the presence of fibers. Relative ATP concentration (ATP/DNA) indicates that cells at the D1 and D4 timepoints exhibited similar levels of per-cell metabolic activity across both conditions (Figure 4.4D). However, cells in – fiber gels at D7 demonstrated significantly higher levels of metabolic activity (ATP/DNA of 0.3) compared to + fiber gels, which had an ATP/DNA ratio of 0.25. In general, per-cell metabolic activity remained consistent across all timepoints, with ATP/DNA ratios consistently between 0.25-0.31 for both conditions. (ATP levels in both + fiber and – fiber hydrogels trend upwards across time, with significantly higher ATP concentrations present in the – fiber compared to the + fiber conditions at D4 and D7 [Supplementary Figure S4.5]. DNA concentrations display a similar trend [Supplementary Figure S4.5].) Both the proliferation and metabolic activity assay results support the idea that unlike OPCs, which slow proliferation as they undergo differentiation (as seen in Chapter 3), a population of NSCs continues to proliferate in the presence of fibers. This may be due to the mixed population of cells present after NSCs have been cultured in the presence of fibers for several days.

Literature which investigates NSC culture alongside fibers primarily involves seeding NSC atop electrospun nanofiber scaffolds [35-37], rather than culturing cells in 3D alongside axon-sized fibers. However, Hsieh et al. observed similar increases in NSC DNA between D0 and D4 in a composite hydrogel system with 2μm electrospun poly(3-caprolactone-co-D,L-lactide) (PCL:DLLA) fibers [38]. Our results therefore align with NSC behavior in literature.

4.4.4 PCR

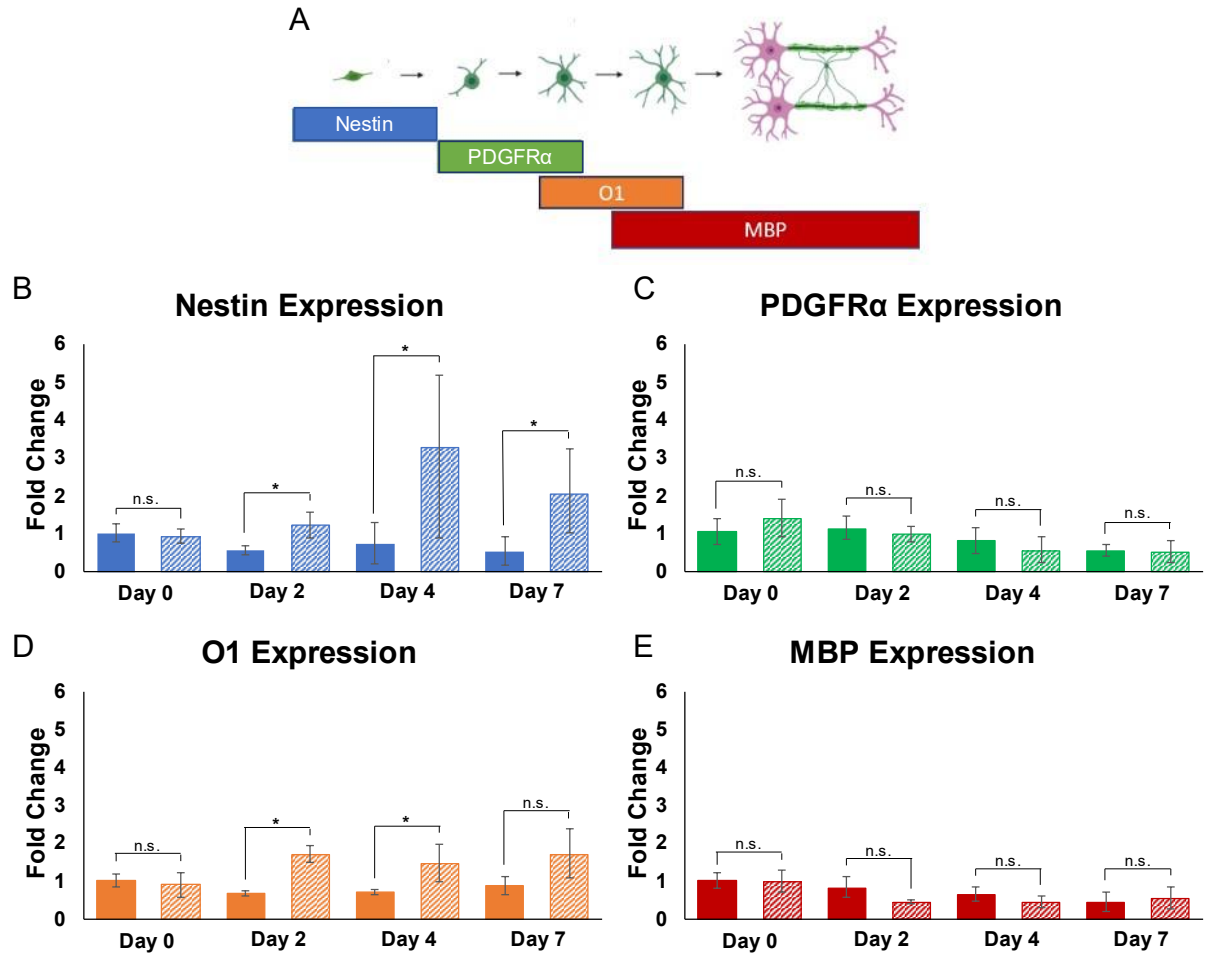

Figure 4.5. Encapsulated NSC gene expression over 7 days. A) Neural stem cell differentiation into oligodendrocytes, with associated gene expression markers at each stage. Nestin is a marker for NSCs, PDGFRα for oligodendrocyte progenitor cells, O1 for immature oligodendrocytes and MBP for mature myelinating oligodendrocytes. B-E) Expression levels of nestin (B), PDGFRα (C), O1 (D), and MBP (E) over a 7-day culture period. Both nestin and O1 were found to be upregulated in the + fiber condition at D2, D4 and D7 as compared to – fiber controls, while PDGFRα and MBP expression levels declined over time for both conditions. n.s. indicates no significant difference between conditions, while * indicates a significant difference ($p<0.05$). Error bars represent standard deviation.

When assessing the fold changes of OPC/OL maturation markers through qPCR, *nestin* (NSC+), was found to be upregulated in the fiber condition at D2 (FC = 1.2), D4 (FC = 3.3), and D7 (FC = 2.1) when compared to – fiber controls (Figure 4.5B). To a lesser extent, *O1*, an immature oligodendrocyte marker, was found to be upregulated in fiber-containing gels at the same timepoints, with a fold change ranging between 1.4-1.7 (Figure 4.5D). For both *nestin* and *O1*, gene expression in no-fiber gels remained consistent across all timepoints. Additionally, *PDGFRα* (OPC marker) and *MBP* (mature myelinating OL marker) levels remained consistent across both conditions over the 7-day period (Figure 4.5C and E). The upregulation of *O1* indicates that the presence of fibers may prompt some cells to begin differentiating towards OL

cell fates; however, they do not complete differentiation into mature myelinating OLs as evidenced by the low expression of *MBP*. The primary impact of the fibers can be seen in the *nestin* results, which indicate the fibers prompt a burst of NSC activity. This result is consistent with our observations from the proliferation and ATP-DNA assays. Hsieh et al. also found that *nestin* expression was elevated in proliferation media in both – fiber and + PCL:DLLA fiber conditions at D7. However, they observed similar *nestin* expression levels across conditions [38], whereas our results show that *nestin* is elevated more for the + fiber condition. This discrepancy may be explained by differences in fiber properties; MeHA fibers have been measured to be softer and more representative of native tissue properties than PCL fibers of comparable size, a distinction which may promote NSC proliferation [28, 39]. Hsieh et al., also showed that *CNPase* (mature OL marker) expression was very low for – fiber and + fiber conditions at D7, which is consistent with our results for *MBP* expression for this relatively early time point in OL maturation [38].

4.4.5 NanoString Glial Profiling Panel

Through gene profiling of D7 samples, we identified 39 genes significantly dysregulated in + fiber gels when compared to the – fiber control condition, with 21 showing upregulation and 18 displaying downregulation (Figure 4.6A). When performing GO enrichment analysis of the upregulated DEGs, 12 were related to neuronal differentiation with a smaller fraction found to relate to other cell fates including oligodendrocyte (3) and astrocyte differentiation (2) (Figure 5B). Excitingly, genes relating to focal adhesion and mechanotransduction, such as *Kit* ligand, *Flt1*, and *Ccl2*, were also upregulated in the + fiber condition (Figure 4.6B) [40, 41]. Consequently, 8 downregulated genes were related to neuronal lineage while two were related to oligodendrocyte cell fate. Notably, *PDGFRα* was downregulated in the + fiber condition aligning with our qPCR results. Collectively, the findings suggest that the introduction of fiber cues significantly influences NSC differentiation towards a predominantly neuronal lineage.

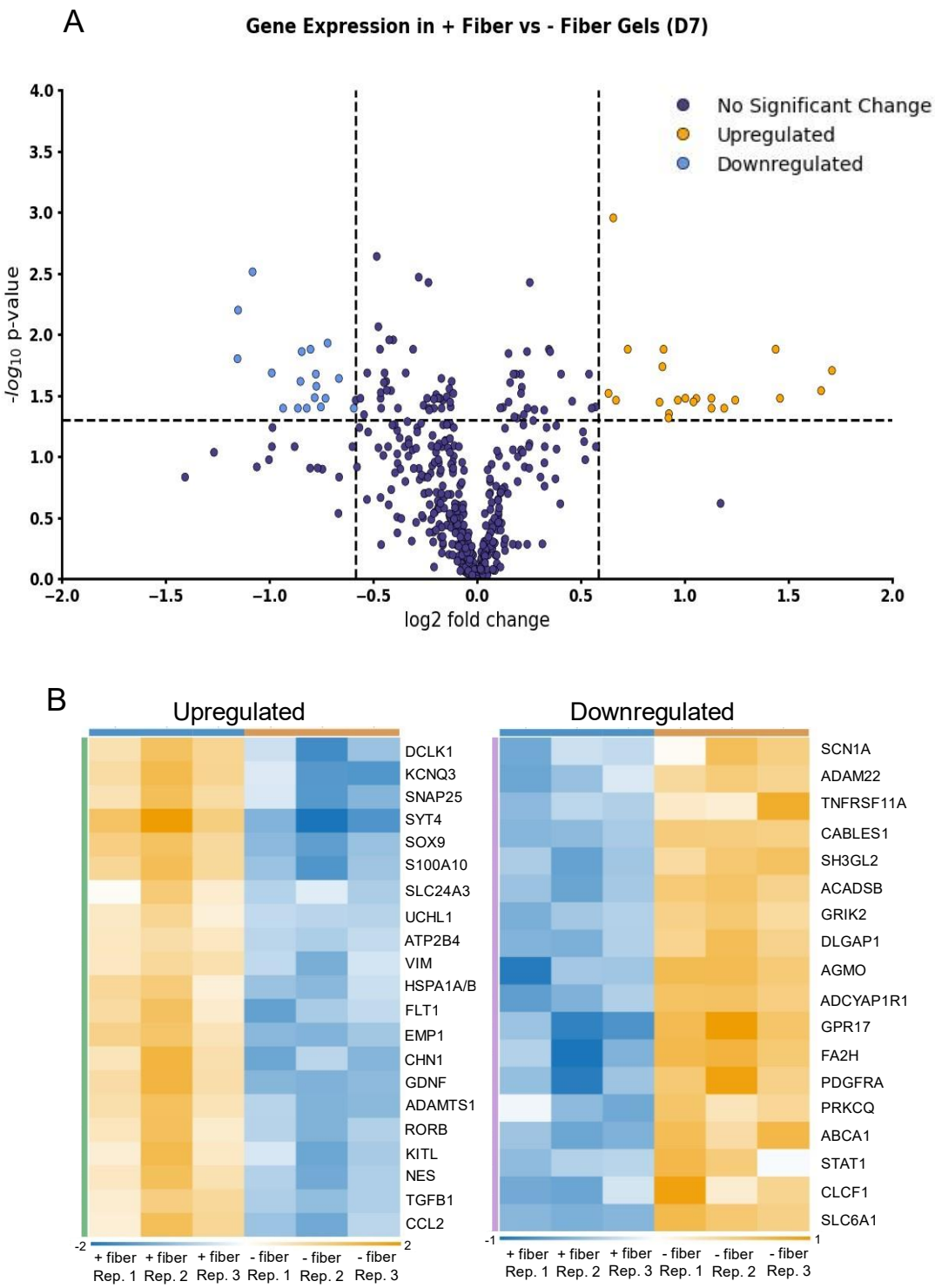

Figure 4.6. Summary of gene expression profiling results. A) Volcano plot of gene expression at D7. 21 genes were significantly upregulated and 18 downregulated in + fiber gels compared to controls. B) Heat maps for the upregulated and downregulated genes. Orange is used to indicate upregulation while blue indicates downregulation.

When performing KEGG pathway enrichment analysis, upregulated DEGs showed significant participation in the Ras/Raf/Mitogen activated protein kinase (MAPK) signaling pathway, as well as the phosphoinositide-3-kinase (PI3K-Akt) signaling pathway (Figure 4.7A and B). The Ras/Raf/MAPK pathway governs signal transduction from the extracellular environment to the cell nucleus and is involved in cell growth, proliferation and differentiation [42]. Similarly, the PI3K-Akt pathway also plays a role in cell metabolism, proliferation and focal adhesion [43]. Upregulation of genes associated with these pathways is consistent with our EdU assay results, which found increased proliferation in the + fiber condition at D7. Interestingly, focal adhesion genes are also upregulated in the + fiber condition, which may indicate that NSC cultured alongside fibers are more likely to adhere to and interact with their local hydrogel environment. Differences in focal adhesion and mechanosensing in + fiber gels could explain changes in cell surface area through increased process extension, as well as impact distribution of cell-secreted ECM. Similarly, downregulated DEGs were related to the Janus kinase/signal transducer (Jak-Stat) and ErbB pathways, which are also involved in mechanotransduction, cell proliferation, differentiation and stem cell maintenance [44, 45]. Overall, these results align with previous literature findings which suggest that NSC mechanosensing in response to matrix topography involves upregulation of MAPK and PI3K pathways [46].

The KEGG database was additionally used to identify which cell fate specifications each DEG was likely to be associated with (Figure 4.8). A total of 25 genes were identified as relating to cell fate specification, with a majority (17) relating to neurogenesis. An additional 7 genes related to gliogenesis, with 5 DEGs relating to OL fates in particular. These results indicate that while fibers do have an effect on cell differentiation, this effect is primarily guiding cells towards neuronal differentiation, with OL differentiation occurring to a lesser extent.

A

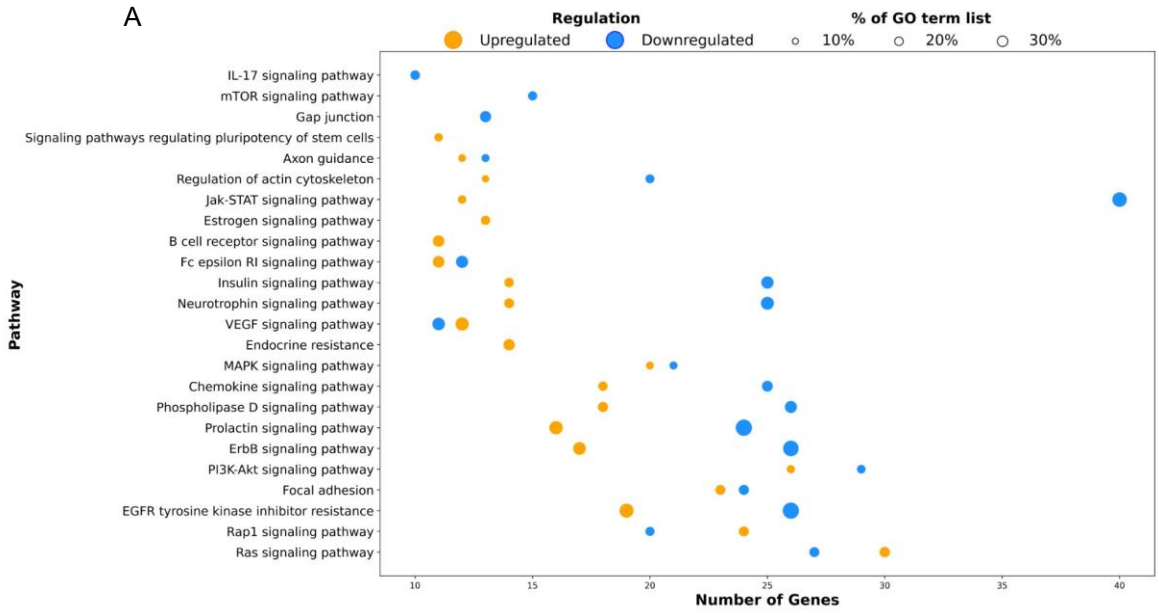
Regulation
Upregulated
Downregulated
% of GO term list
10%
20%
30%
IL-17 signaling pathway
mTOR signaling pathway
Gap junction
Signaling pathways regulating pluripotency of stem cells
Axon guidance
Regulation of actin cytoskeleton
Jak-STAT signaling pathway
Estrogen signaling pathway
B cell receptor signaling pathway
Fc epsilon RI signaling pathway
Insulin signaling pathway
Neurotrophin signaling pathway
VEGF signaling pathway
Endocrine resistance
MAPK signaling pathway
Chemokine signaling pathway
Phospholipase D signaling pathway
Prolactin signaling pathway
ErbB signaling pathway
PI3K-Akt signaling pathway
Focal adhesion
EGFR tyrosine kinase inhibitor resistance
Rap1 signaling pathway
Ras signaling pathway
Pathway
10
15
20
25
30
35
40
Number of Genes

B

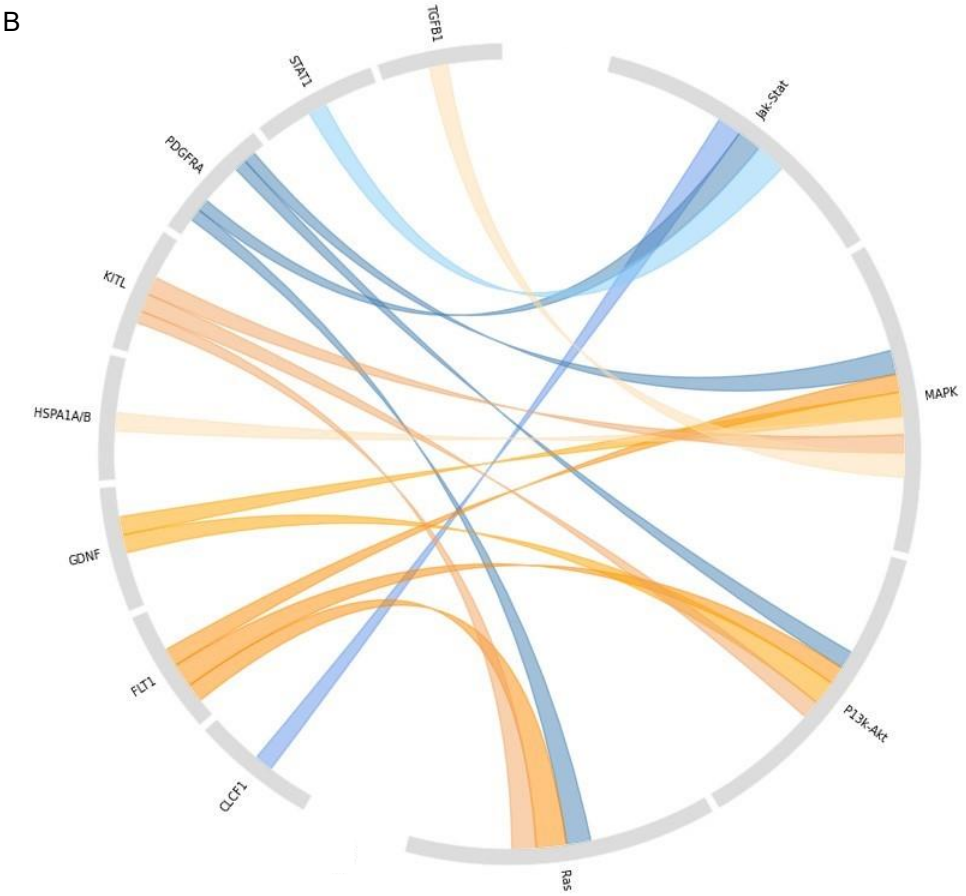
TGFB1
STAT1
Jak-Stat
PDGFRA
KITL
MAPK
HSPA1A/B
GDNF
FLT1
PI3k-Akt
CLCF1
Ras

Figure 4.7. Summary of gene expression pathway analysis. A) Pathway enrichment analysis summaries for each of the upregulated and downregulated gene sets. Biological processes most likely to be involved were typically related to cell signaling pathways, particularly those related to cell proliferation, differentiation, focal adhesion, and mechanotransduction. B) Circos plot of genes implicated in cell signaling pathways. Orange connections indicate upregulated genes while blue indicates downregulated genes. The KEGG database was used to identify which dysregulated genes were associated with 4 signaling pathways (Jak-Stat, MAPK, P13k-Akt, and Ras) previously indicated to be relevant based on gene ontology (GO) data. Overall, 8 genes (5 upregulated and 3 downregulated) were determined to be related to cell signaling. Of these, MAPK and P13k-Akt were found to have the most associated genes (6 and 5 respectively), while a smaller number of genes (3 each) were implicated in the Jak-Stat and Ras pathways. Notably, PDGFRA was implicated in all 4 of the selected cell signaling pathways.

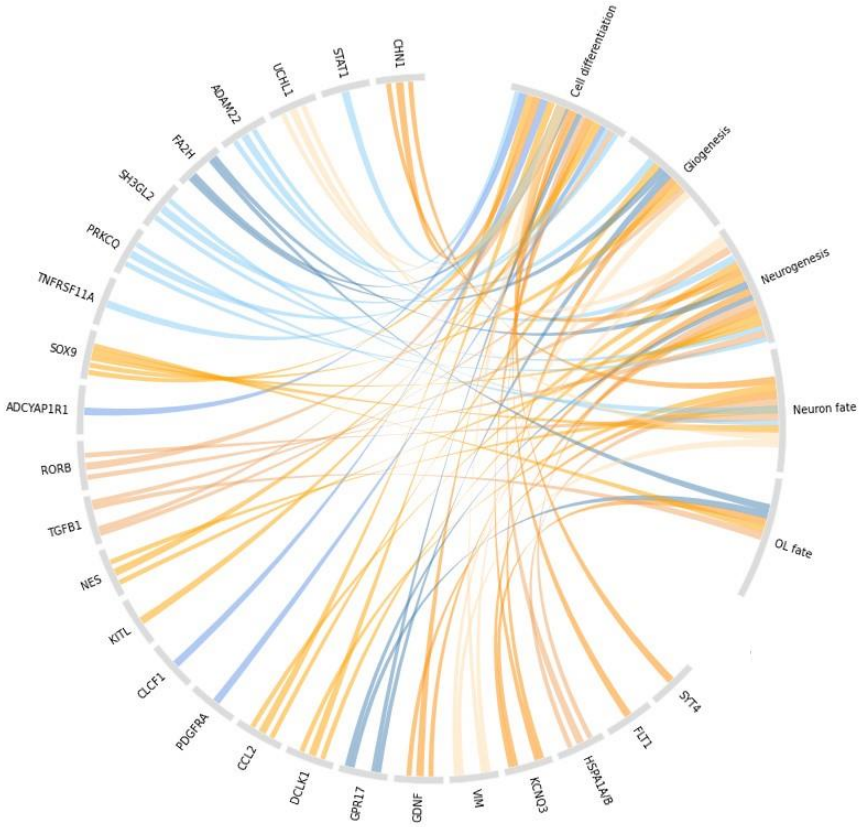

Figure 4.8. Circos plot of genes implicated in cell differentiation pathways. Orange connections indicate upregulated genes while blue indicates downregulated genes. The KEGG database was used to identify which dysregulated genes were associated with cell differentiation. Overall, 25 genes (15 upregulated and 10 downregulated) were determined to be related to cell differentiation. Of these, a majority were found to be related to neurogenesis and neuron fate. A smaller fraction of dysregulated genes were also found to be related to gliogenesis, and ultimately to OL differentiation.

To examine the DEGs identified in a network context as well as identify potential interactions between DEGs and their predicted proteins, we generated a PPIN and performed network analysis using Cytoscape. The top 10 proteins and their associated centrality measurements and

PageRank scores are listed in Table 4.1. PDGFRα, Ccl2, Stat1, Kit, Scn1a, Syt4, Flt1, and Tgfb1 were identified as central nodes by both weighting methods, all playing significant roles in cell signaling, communication, and response to external stimuli. PDGFRα, Flt1, and Kit are membrane receptors that not only trigger the MAPK signaling cascade for proliferation and differentiation but also play crucial roles in Rap1, Ras, and PI3K-Akt signaling. Similarly, Stat1 is a key regulatory protein that functions as a transcription activator for genes involved in cell migration, growth, survival, and differentiation. Ccl2 and Tgfb1, by contrast, are cytokines involved in the remodeling and homeostasis of the extracellular matrix. Interestingly, Scn1a is essential in detecting mechanical stimuli and enabling voltage-gated sodium channel activity and Syt4 serves as a calcium sensor in the process of vesicular trafficking and exocytosis.

Table 4.1. Protein network centrality analysis for NSC encapsulated in + fiber vs – fiber gels.

Gene Symbol	Degree	Betweenness Centrality	Closeness Centrality	Stress Centrality	Eccentricity	Pvalue of Expression	Expression
Pdgfra	4	0.524	0.636	22	3	0.02	↓
Ccl2	3	0.310	0.538	16	3	0.03	↑
Stat1	3	0.333	0.636	16	2	0.04	↓
Kit	3	0.167	0.583	8	3	0.04	↑
Flt1	2	0.048	0.500	4	3	0.03	↑
Nes	1	0	0.412	0	4	0.05	↑
Sox9	1	0	0.412	0	4	0.04	↑
Tgfb1	1	0	0.368	0	4	0.01	↑
Scn1a	1	0	1	0	1	0.03	↓
Syt4	1	0	1	0	1	0.03	↑

Top 10 Nodes Weighted Through PageRank
Pdgfra
Ccl2
Stat1
Kit
Grik2
Scn1a
Snap25
Syt4
Flt1
Tgfb1

PDGFRα is known to be an OPC marker, with the gene being upregulated in OPCs differentiated from NSC, followed by downregulation at the immature OL stage [47]. Its downregulation in this context is therefore not surprising, given that our PCR and NanoString results indicate that differentiation occurs primarily towards a neuronal cell fate, and cells which are maturing towards OL fates primarily express O1 (immature OL marker) by culture day 7. NSCs have previously been shown to upregulate CCL2 and downregulate Stat1 during neuronal differentiation, which also aligns with our results [48, 49].

4.4.6 Laminin and Fibronectin Immunostaining

To assess the composition of ECM deposits, immunostaining was performed for two common ECM proteins, laminin and fibronectin. Laminin and fibronectin proteins are major components of the stem cell niche and are known to encourage and influence various aspects of NSC development, such as adhesion, migration, and differentiation [50]. Engineered materials sometimes incorporate laminin and/or fibronectin proteins or binding motifs to encourage NSC differentiation [51-53]. Additionally, both neural stem/progenitor cells (NSPCs) and NSC-containing neurospheres secrete these ECM proteins [54, 55]. However, limited knowledge exists regarding the capacity of individual NSCs to secrete their own ECM under 3D conditions. In particular, the pattern and composition of NSC ECM deposition is not well understood.

Immunostaining for the presence of laminin and fibronectin at culture days 5 and 10 revealed that both proteins were deposited in each of the control and experimental conditions (Figure 9). In the – fiber control gels, cells retained a rounded morphology and laminin deposition occurred in a thin spherical shell surrounding the outside of cells and cell clusters. In the + fiber condition, laminin deposition occurred in a similar pattern surrounding the main cell bodies but was also found to occur surrounding cell process extensions resulting in an overall more distributed finding (Figure 4.9A). Fibronectin deposition occurred in a similar pattern (Figure 4.9B). The ECM distribution in fiber-free gels aligns with expectations, as nascent deposition of extracellular matrix proteins has been demonstrated to occur in spherical shells around clusters of various cell types, including mesenchymal stromal cells and chondrocytes [56, 57]. Although previous work has not attempted to quantify the relative amounts of protein distribution, immunostaining of ECM protein secretions from mouse embryonic NSPCs has shown similar patterns of deposition, with secreted laminin and fibronectin surrounding the main cell bodies as well as along cellular process extensions [55]. These results indicate that the presence of fibers influences cell morphology, which in turn influences the pattern of extracellular matrix deposition.

Both laminin and fibronectin signal area were quantified and normalized to the size of the cell membrane. Based on 3-way ANOVA, the relative amounts of deposition were significantly different; laminin deposition occurred to a significantly greater extent than fibronectin deposition (Figure 4.9C). In general, the relative amount of deposition is unaffected by the presence of fibers; although more fibronectin deposition was observed in the - fiber condition at day 10, there was no significant difference in fibronectin deposition at culture day 5 or in laminin deposition at either timepoint. ANOVA did indicate that there was a significant difference between timepoints, and deposition levels of both proteins were seen to decrease between days 5 and 10. This indicates that the majority of ECM deposition by NSCs occurs before day 5 of culture. NSCs are commonly cultured on laminin in 2D formats. However, the NSC secretome is not well studied, particularly for ECM proteins. Our results further confirm the ability of NSCs to deposit these specific ECM proteins and provide greater context for deposition of ECM proteins by neural cells in 3D environments.

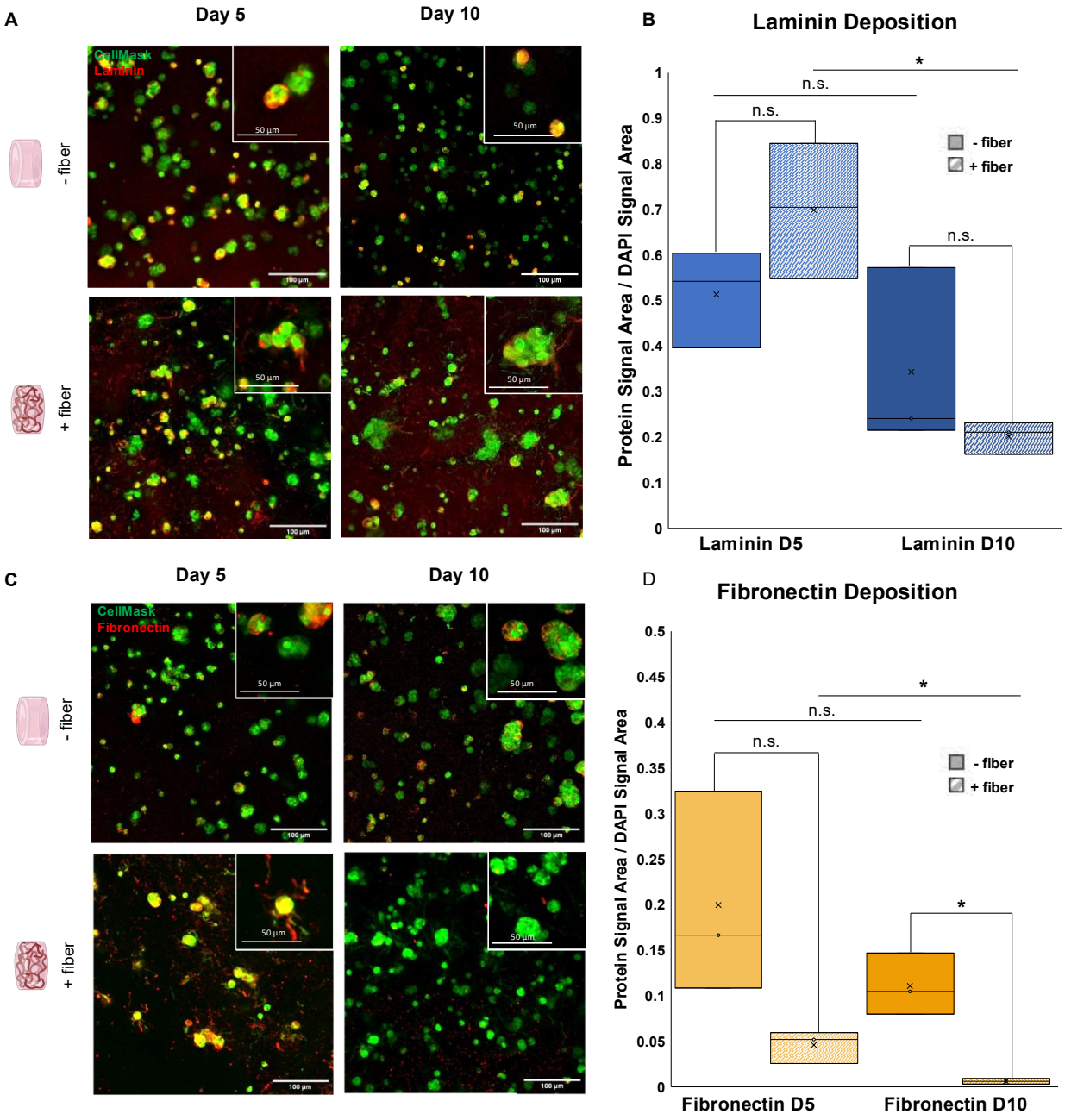

Figure 4.9. NSC deposition of extracellular matrix proteins over a 10-day period. A) Distribution of laminin deposition in – fiber and + fiber gels at D5 and D10. Laminin deposition occurs around cells and clusters, as well as along process extensions in the + fiber condition. B) Quantification of laminin deposition. . n.s. indicates no significant difference between conditions, while * indicates a significant difference ($p<0.05$). ECM deposition of laminin decreased over time, but the decrease between timepoints was statistically significant only in the fiber condition. C) Distribution of fibronectin deposition at D5 and D10. Fibronectin deposition occurs in a similar distribution to laminin. D) Quantification of fibronectin deposition. Fibronectin was deposited to a lesser extent than laminin across all conditions and timepoints. Deposition of fibronectin also decreased over time, with a statistically significant decrease only in the fiber condition. Fibronectin deposition was significantly higher in the – fiber gels compared to the + fiber gels at culture day 10.

4.5 Conclusions

In this study, we demonstrated that NSCs encapsulated in 3D NorHA hydrogels remain viable over a 7-day period, and that the inclusion of electrospun fibers supports high NSC viability and proliferation. Fiber inclusion strongly influence NSC differentiation, with cells in fiber-containing cells displaying mature morphologies and increased expression of genes associated with neuronal and OL differentiation. NSCs secreted laminin and fibronectin ECM proteins to remodel their local microenvironment. Through an integrative systems biology approach, we provide evidence that the transcriptional environment of NSCs is drastically altered by fiber inclusion. We identify key proteins and signaling pathways related to proliferation, differentiation, and mechanotransduction driving their cellular response.

Moving forward, this 3D platform is a valuable tool for modeling the CNS during development and injury conditions. In particular, the tunable nature of this platform could be of interest to unravel molecular-level mechanisms implicated in CNS myelination. Myelination in the PNS is well understood to proceed by Schwann cells via the "carpet crawler" model, wherein the leading edge of the myelin turns and grows underneath the outer layers of the myelin sheath to generate a multi-layered membrane parallel to the axon [58]. However, the morphology of myelin wrappings in the CNS indicates the myelination process differs from the PNS model [59]. While many different models have been proposed, the mechanism of myelin formation in the CNS is still undetermined [60-62]. Culturing cells in this system with OL differentiation media could allow for observation of *de novo* ensheathment in a representative 3D context. Additionally, the impact of cell remodeling through matrix degradation presents another avenue for future investigation. While our current hydrogel system is non-degradable, previous work has demonstrated that degradation of the surrounding matrix plays a role in neural progenitor cell differentiation [63]. Future work incorporating MMP-degradable sites into HA gels could further explore this avenue of cell-matrix remodeling.

4.6 Acknowledgements

This work was supported by the National Science Foundation [grant number 2104723] (KJL), as well as the University of Virginia Dean's Fellowship award (RAM). We gratefully acknowledge the UVA Keck Center for use of their Zeiss 780 microscope, and the UVA Program in Fundamental Neuroscience for usage of its Leica Stellaris 5 confocal system. Further acknowledgement goes to the UVA Spatial Biology core for their role in RNA extraction and Nanostring gene profiling. We acknowledge undergraduate research assistants Elaina Lee and Ava Bankert for their contributions in ECM staining and image analysis quantification. Funding sources were not involved in study design, data collection or analysis, in the writing of the report, or in the decision to submit the article for publication.

4.7 References

[1] H. Okano, S. Temple, Cell types to order: temporal specification of CNS stem cells, Current opinion in neurobiology 19(2) (2009) 112-119.
[2] J. Imitola, K. Raddassi, K.I. Park, F.-J. Mueller, M. Nieto, Y.D. Teng, D. Frenkel, J. Li, R.L. Sidman, C.A. Walsh, E.Y. Snyder, S.J. Khoury, Directed migration of neural stem cells to sites of CNS injury by the stromal cell-derived factor 1α/CXC chemokine receptor 4 pathway, Proceedings of the National Academy of Sciences 101(52) (2004) 18117-18122.
[3] W. Huang, A. Bhaduri, D. Velmeshev, S. Wang, L. Wang, C.A. Rottkamp, A. Alvarez-Buylla, D.H. Rowitch, A.R. Kriegstein, Origins and proliferative states of human oligodendrocyte precursor cells, Cell 182(3) (2020) 594-608. e11.
[4] X. Dai, L.D. Lercher, P.M. Clinton, Y. Du, D.L. Livingston, C. Vieira, L. Yang, M.M. Shen, C.F. Dreyfus, The trophic role of oligodendrocytes in the basal forebrain, Journal of Neuroscience 23(13) (2003) 5846-5853.
[5] S. Shin, M. Vemuri, Culture and differentiation of human neural stem cells, Protocols for Neural Cell Culture: Fourth Edition (2010) 51-73.
[6] R.A. Mazur, R. Yokosawa, P.J. VandeVord, K.J. Lampe, The Need for Tissue Engineered Models to Facilitate the Study of Oligodendrocyte Progenitor Cells in Traumatic Brain Injury and Repair, Current Opinion in Biomedical Engineering (2022) 100378.
[7] S. Mitew, I. Gobius, L.R. Fenlon, S.J. McDougall, D. Hawkes, Y.L. Xing, H. Bujalka, A.L. Gundlach, L.J. Richards, T.J. Kilpatrick, T.D. Merson, B. Emery, Pharmacogenetic stimulation of neuronal activity increases myelination in an axon-specific manner, Nature communications 9(1) (2018) 306.
[8] S. Lee, M.K. Leach, S.A. Redmond, S.C. Chong, S.H. Mellon, S.J. Tuck, Z.-Q. Feng, J.M. Corey, J.R. Chan, A culture system to study oligodendrocyte myelination processes using engineered nanofibers, Nature methods 9(9) (2012) 917-922.
[9] S. Lee, S.C. Chong, S.J. Tuck, J.M. Corey, J.R. Chan, A rapid and reproducible assay for modeling myelination by oligodendrocytes using engineered nanofibers, Nature protocols 8(4) (2013) 771-782.
[10] O. de Faria Jr, D.G. Gonsalvez, M. Nicholson, J. Xiao, Activity-dependent central nervous system myelination throughout life, Journal of Neurochemistry 148(4) (2019) 447-461.
[11] K. Sugitani, D. Egorova, S. Mizumoto, S. Nishio, S. Yamada, H. Kitagawa, K. Oshima, D. Nadano, T. Matsuda, S. Miyata, Hyaluronan degradation and release of a hyaluronan-aggrecan complex from perineuronal nets in the aged mouse brain, Biochimica et Biophysica Acta (BBA)-General Subjects 1865(2) (2021) 129804.
[12] D.B. Unal, S.R. Caliari, K.J. Lampe, 3D hyaluronic acid hydrogels for modeling oligodendrocyte progenitor cell behavior as a function of matrix stiffness, Biomacromolecules 21(12) (2020) 4962-4971.
[13] J.H. Galarraga, A.P. Dhand, B.P. Enzmann III, J.A. Burdick, Synthesis, characterization, and digital light processing of a hydrolytically degradable hyaluronic acid hydrogel, Biomacromolecules 24(1) (2022) 413-425.
[14] S. Shah, P.T. Yin, T.M. Uehara, S.T.D. Chueng, L. Yang, K.B. Lee, Guiding stem cell differentiation into oligodendrocytes using graphene-nanofiber hybrid scaffolds, Advanced materials 26(22) (2014) 3673-3680.
[15] D.N. Rocha, E.D. Carvalho, L.R. Pires, C. Gardin, I. Zanolla, P.K. Szewczyk, C. Machado, R. Fernandes, U. Stachewicz, B. Zavan, J.B. Relvas, A.P. Pêgo, It takes two to remyelinate: A

bioengineered platform to study astrocyte-oligodendrocyte crosstalk and potential therapeutic targets in remyelination, Biomaterials Advances 151 (2023) 213429.
[16] J. Xie, S.M. Willerth, X. Li, M.R. Macewan, A. Rader, S.E. Sakiyama-Elbert, Y. Xia, The differentiation of embryonic stem cells seeded on electrospun nanofibers into neural lineages, Biomaterials 30(3) (2009) 354-362.
[17] O. Ilina, G.-J. Bakker, A. Vasaturo, R.M. Hoffman, P. Friedl, Two-photon laser-generated microtracks in 3D collagen lattices: principles of MMP-dependent and-independent collective cancer cell invasion, Physical biology 8(1) (2011) 015010.
[18] K.L. Xu, N. Di Caprio, H. Fallahi, M. Dehghany, M.D. Davidson, L. Laforest, B.C. Cheung, Y. Zhang, M. Wu, V. Shenoy, L. Han, R.L. Mauck, J.A. Burdick, Microinterfaces in biopolymer-based bicontinuous hydrogels guide rapid 3D cell migration, Nature Communications 15(1) (2024) 2766.
[19] O. Sarig-Nadir, N. Livnat, R. Zajdman, S. Shoham, D. Seliktar, Laser photoablation of guidance microchannels into hydrogels directs cell growth in three dimensions, Biophysical journal 96(11) (2009) 4743-4752.
[20] C.S. Lacko, I. Singh, M.A. Wall, A.R. Garcia, S.L. Porvasnik, C. Rinaldi, C.E. Schmidt, Magnetic particle templating of hydrogels: engineering naturally derived hydrogel scaffolds with 3D aligned microarchitecture for nerve repair, Journal of neural engineering 17(1) (2020) 016057.
[21] X. Li, B. Cho, R. Martin, M. Seu, C. Zhang, Z. Zhou, J.S. Choi, X. Jiang, L. Chen, G. Walia, J. Yan, M. Callanan, H. Liu, K. Colbert, J. Morrissette-McAlmon, W. Grayson, S. Reddy, J.M. Sacks, H.Q. Mao, Nanofiber-hydrogel composite–mediated angiogenesis for soft tissue reconstruction, Science translational medicine 11(490) (2019) eaau6210.
[22] S. Choi, K.Y. Lee, S.L. Kim, L.A. MacQueen, H. Chang, J.F. Zimmerman, Q. Jin, M.M. Peters, H.A.M. Ardoña, X. Liu, A.C. Heiler, R. Gabardi, C. Richardson, W.T. Pu, A.R. Bausch, K.K. Parker, Fibre-infused gel scaffolds guide cardiomyocyte alignment in 3D-printed ventricles, Nature materials 22(8) (2023) 1039-1046.
[23] N.J. Darling, W. Xi, E. Sideris, A.R. Anderson, C. Pong, S.T. Carmichael, T. Segura, Click by click microporous annealed particle (MAP) scaffolds, Advanced healthcare materials 9(10) (2020) 1901391.
[24] C. Chung, J.A. Burdick, Influence of three-dimensional hyaluronic acid microenvironments on mesenchymal stem cell chondrogenesis, Tissue Engineering Part A 15(2) (2009) 243-254.
[25] M.E. Prendergast, M.D. Davidson, J.A. Burdick, A biofabrication method to align cells within bioprinted photocrosslinkable and cell-degradable hydrogel constructs via embedded fibers, Biofabrication 13(4) (2021) 044108.
[26] J. Schindelin, I. Arganda-Carreras, E. Frise, V. Kaynig, M. Longair, T. Pietzsch, S. Preibisch, C. Rueden, S. Saalfeld, B. Schmid, J. Tinevez, D. White, V. Hartenstein, K. Eliceiri, P. Tomancak, A. Cardona, Fiji: an open-source platform for biological-image analysis, Nature methods 9(7) (2012) 676-682.
[27] T. Villani, Loading and Measurement of Volumes in 3D Confocal Image Stacks with ImageJ, Visikol, 2024.
[28] I.L. Kim, S. Khetan, B.M. Baker, C.S. Chen, J.A. Burdick, Fibrous hyaluronic acid hydrogels that direct MSC chondrogenesis through mechanical and adhesive cues, Biomaterials 34(22) (2013) 5571-5580.

[29] X. Li, E. Katsanevakis, X. Liu, N. Zhang, X. Wen, Engineering neural stem cell fates with hydrogel design for central nervous system regeneration, Progress in polymer science 37(8) (2012) 1105-1129.
[30] S.K. Seidlits, J. Liang, R.D. Bierman, A. Sohrabi, J. Karam, S.M. Holley, C. Cepeda, C.M. Walthers, Peptide-modified, hyaluronic acid-based hydrogels as a 3D culture platform for neural stem/progenitor cell engineering, Journal of Biomedical Materials Research Part A 107(4) (2019) 704-718.
[31] E. Mauri, A. Sacchetti, N. Vicario, L. Peruzzotti-Jametti, F. Rossi, S. Pluchino, Evaluation of RGD functionalization in hybrid hydrogels as 3D neural stem cell culture systems, Biomaterials science 6(3) (2018) 501-510.
[32] A.M.C. Gaitán, N.M. Torres-Ruíz, N.G. Carri, Embryonic neural stem cells in a 3D bioassay for trophic stimulation studies, Brain research bulletin 115 (2015) 37-44.
[33] P. Naghdi, T. Tiraihi, F. Ganji, S. Darabi, T. Taheri, H. Kazemi, Survival, proliferation and differentiation enhancement of neural stem cells cultured in three-dimensional polyethylene glycol–RGD hydrogel with tenascin, Journal of tissue engineering and regenerative medicine 10(3) (2016) 199-208.
[34] X.-Y. Xu, X.-T. Li, S.-W. Peng, J.-F. Xiao, C. Liu, G. Fang, K.C. Chen, G.-Q. Chen, The behaviour of neural stem cells on polyhydroxyalkanoate nanofiber scaffolds, Biomaterials 31(14) (2010) 3967-3975.
[35] F. Yang, R. Murugan, S. Ramakrishna, X. Wang, Y.-X. Ma, S. Wang, Fabrication of nano-structured porous PLLA scaffold intended for nerve tissue engineering, Biomaterials 25(10) (2004) 1891-1900.
[36] F. Yang, C. Xu, M. Kotaki, S. Wang, S. Ramakrishna, Characterization of neural stem cells on electrospun poly (L-lactic acid) nanofibrous scaffold, Journal of Biomaterials Science, Polymer Edition 15(12) (2004) 1483-1497.
[37] M.K. Horne, D.R. Nisbet, J.S. Forsythe, C.L. Parish, Three-dimensional nanofibrous scaffolds incorporating immobilized BDNF promote proliferation and differentiation of cortical neural stem cells, Stem cells and development 19(6) (2010) 843-852.
[38] A. Hsieh, T. Zahir, Y. Lapitsky, B. Amsden, W. Wan, M.S. Shoichet, Hydrogel/electrospun fiber composites influence neural stem/progenitor cell fate, Soft Matter 6(10) (2010) 2227-2237.
[39] S.R. Baker, S. Banerjee, K. Bonin, M. Guthold, Determining the mechanical properties of electrospun poly-ε-caprolactone (PCL) nanofibers using AFM and a novel fiber anchoring technique, Materials Science and Engineering: C 59 (2016) 203-212.
[40] T.K. Roberts, E.A. Eugenin, L. Lopez, I.A. Romero, B.B. Weksler, P.-O. Couraud, J.W. Berman, CCL2 disrupts the adherens junction: implications for neuroinflammation, Laboratory investigation 92(8) (2012) 1213-1233.
[41] Z. Gan, K. Hanspers, E. Willighagen, J. Mélius, M. Summer-Kutmon, D. Slenter, M. Martens, E. Weitz, Focal adhesion: PI3K-Akt-mTOR signaling pathway, (2024).
[42] Y.J. Guo, W.W. Pan, S.B. Liu, Z.F. Shen, Y. Xu, L.L. Hu, ERK/MAPK signalling pathway and tumorigenesis, Experimental and therapeutic medicine 19(3) (2020) 1997-2007.
[43] B.A. Hemmings, D.F. Restuccia, Pi3k-pkb/akt pathway, Cold Spring Harbor perspectives in biology 4(9) (2012) a011189.
[44] D.A. Harrison, The jak/stat pathway, Cold Spring Harbor perspectives in biology 4(3) (2012) a011205.

[45] W.W. Chen, B. Schoeberl, P.J. Jasper, M. Niepel, U.B. Nielsen, D.A. Lauffenburger, P.K. Sorger, Input–output behavior of ErbB signaling pathways as revealed by a mass action model trained against dynamic data, Molecular systems biology 5(1) (2009) 239.
[46] J.M. Stukel, R.K. Willits, Mechanotransduction of neural cells through cell–substrate interactions, Tissue Engineering Part B: Reviews 22(3) (2016) 173-182.
[47] D. Ye, Q. Wang, Y. Yang, B. Chen, F. Zhang, Z. Wang, Z. Luan, Identifying genes that affect differentiation of human neural stem cells and myelination of mature oligodendrocytes, Cellular and Molecular Neurobiology 43(5) (2023) 2337-2358.
[48] Y. Liu, M. Yu, D. Jiang, Downregulation of STAT1 induces the differentiation of neural stem cells through JNK pathway, Tissue and Cell 61 (2019) 61-66.
[49] L. Colucci-D'Amato, A.E. Cicatiello, M.G. Reccia, F. Volpicelli, V. Severino, R. Russo, A. Sandomenico, N. Doti, V. D'Esposito, P. Formisano, A. Chambery, A targeted secretome profiling by multiplexed immunoassay revealed that secreted chemokine ligand 2 (MCP-1/CCL2) affects neural differentiation in mesencephalic neural progenitor cells, Proteomics 15(4) (2015) 714-724.
[50] T. Wilems, S. Vardhan, S. Wu, S. Sakiyama-Elbert, The influence of microenvironment and extracellular matrix molecules in driving neural stem cell fate within biomaterials, Brain research bulletin 148 (2019) 25-33.
[51] A.E. Wilkinson, L.J. Kobelt, N.D. Leipzig, Immobilized ECM molecules and the effects of concentration and surface type on the control of NSC differentiation, Journal of Biomedical Materials Research Part A 102(10) (2014) 3419-3428.
[52] M. Cooke, T. Zahir, S. Phillips, D. Shah, D. Athey, J. Lakey, M. Shoichet, S. Przyborski, Neural differentiation regulated by biomimetic surfaces presenting motifs of extracellular matrix proteins, Journal of Biomedical Materials Research Part A: An Official Journal of The Society for Biomaterials, The Japanese Society for Biomaterials, and The Australian Society for Biomaterials and the Korean Society for Biomaterials 93(3) (2010) 824-832.
[53] J. Sypecka, P. Dragun-Szymczak, T. Zalewska, K. Domańska-Janik, Laminin promotes oligogliogenesis and increases MMPs activity in human neural stem cells of HUCB-NSC line, Acta neurobiologiae experimentalis 69(1) (2009) 37-45.
[54] L.S. Campos, Neurospheres: insights into neural stem cell biology, Journal of neuroscience research 78(6) (2004) 761-769.
[55] A.R. Bento, P. Quelhas, M.J. Oliveira, A.P. Pêgo, I.F. Amaral, Three-dimensional culture of single embryonic stem-derived neural/stem progenitor cells in fibrin hydrogels: neuronal network formation and matrix remodelling, Journal of Tissue Engineering and Regenerative Medicine 11(12) (2017) 3494-3507.
[56] C. Loebel, R.L. Mauck, J.A. Burdick, Local nascent protein deposition and remodelling guide mesenchymal stromal cell mechanosensing and fate in three-dimensional hydrogels, Nature materials 18(8) (2019) 883-891.
[57] C. Loebel, M.Y. Kwon, C. Wang, L. Han, R.L. Mauck, J.A. Burdick, Metabolic labeling to probe the spatiotemporal accumulation of matrix at the chondrocyte–hydrogel interface, Advanced functional materials 30(44) (2020) 1909802.
[58] R.P. Bunge, M.B. Bunge, M. Bates, Movements of the Schwann cell nucleus implicate progression of the inner (axon-related) Schwann cell process during myelination, The Journal of cell biology 109(1) (1989) 273-284.

[59] R.L. Knobler, J.G. Stempak, M. Laurencin, Nonuniformity of the oligodendroglial ensheathment of axons during myelination in the developing rat central nervous system. A serial section electron microscopical study, Journal of ultrastructure research 55(3) (1976) 417-432.
[60] S. Szuchet, L.L. Nielsen, M.S. Domowicz, J.R. Austin II, D.L. Arvanitis, CNS myelin sheath is stochastically built by homotypic fusion of myelin membranes within the bounds of an oligodendrocyte process, Journal of structural biology 190(1) (2015) 56-72.
[61] L. Pedraza, J.K. Huang, D. Colman, Disposition of axonal caspr with respect to glial cell membranes: Implications for the process of myelination, Journal of neuroscience research 87(15) (2009) 3480-3491.
[62] B. Sobottka, U. Ziegler, A. Kaech, B. Becher, N. Goebels, CNS live imaging reveals a new mechanism of myelination: the liquid croissant model, Glia 59(12) (2011) 1841-1849.
[63] C.M. Madl, B.L. LeSavage, R.E. Dewi, K.J. Lampe, S.C. Heilshorn, Matrix remodeling enhances the differentiation capacity of neural progenitor cells in 3D hydrogels, Advanced Science 6(4) (2019) 1801716.

4.8 Supplementary Figures

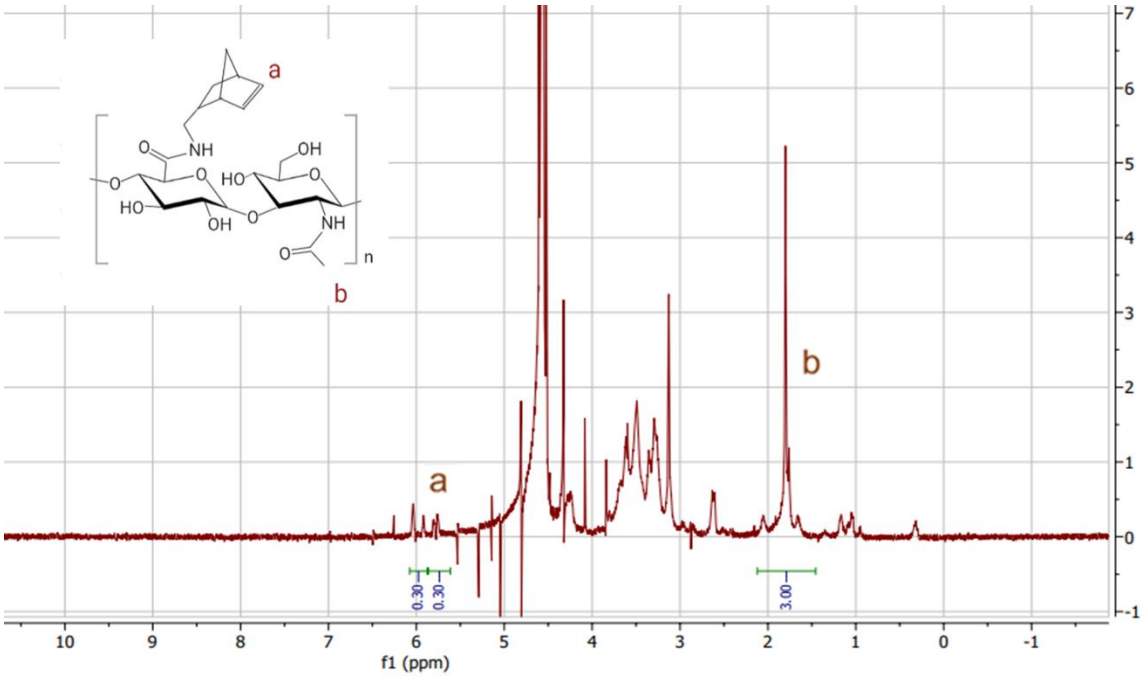

Figure S4.1. NMR spectra of 30% functionalized NorHA. Functionalization efficiency is calculated by normalizing the methyl peak area (b) to a value of 3. The average area of the two norbornene peaks (a) is then taken to determine the functionalization efficiency.

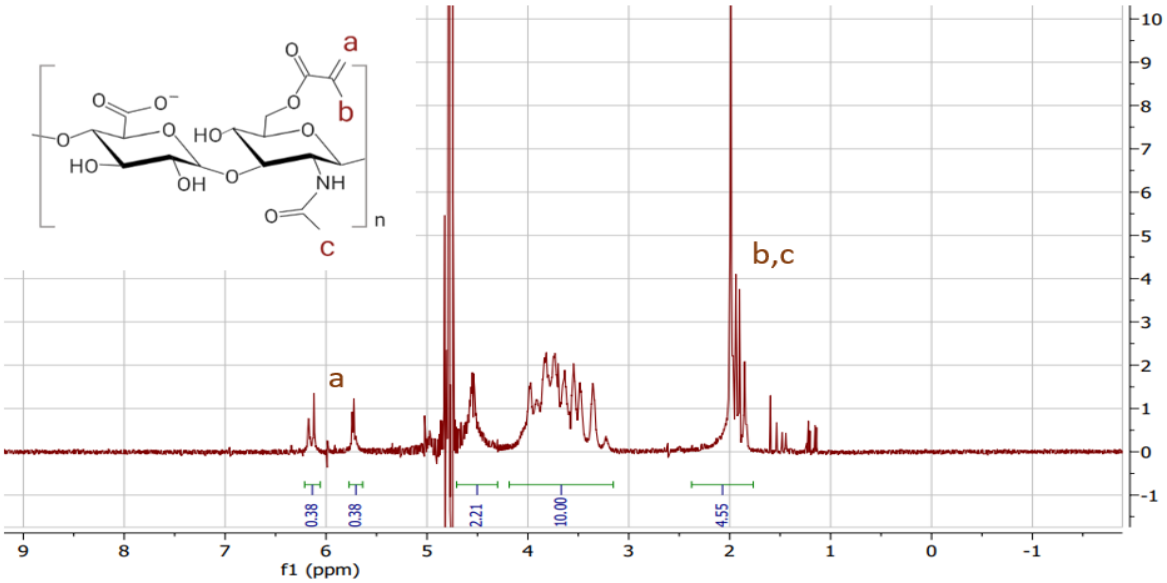

Figure S4.2. NMR spectra of 38% functionalized MeHA. Functionalization efficiency is calculated by normalizing the backbone peak area to a value of 10. The methacrylate peak areas (a) are then averaged to determine the functionalization efficiency.

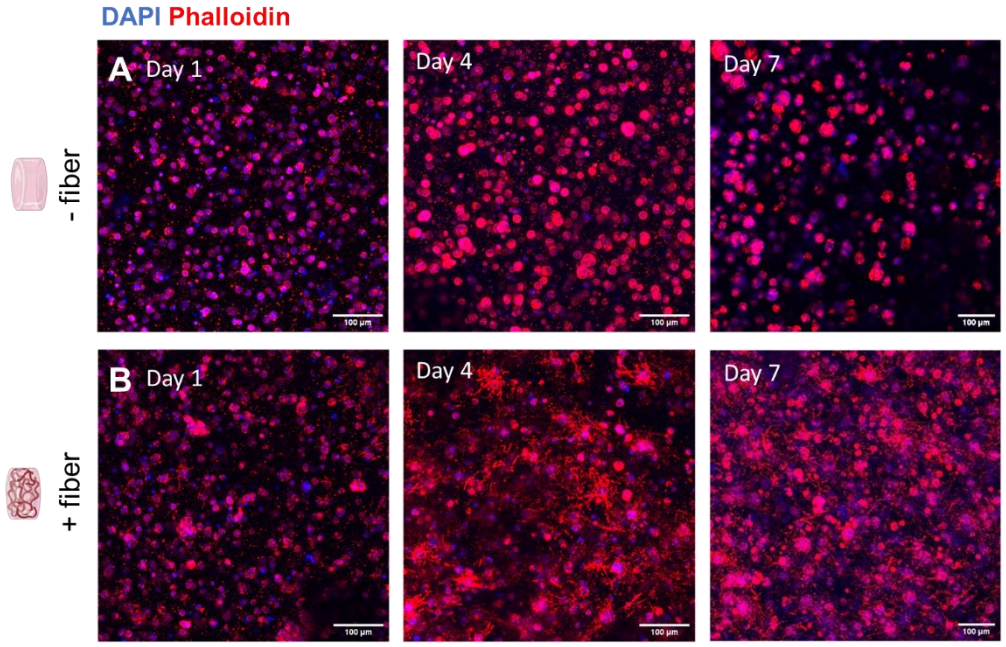

Figure S4.3. Morphology of NSCs in – fiber (top row) and + fiber (bottom row) NorHA gels at culture days 1, 4 and 7. DAPI (blue) was used to stain cell nuclei, while phalloidin (red) stains for f-actin in the cytoskeleton. While cells initially looked similar at Day 1, process extensions were observable in the + fiber condition at Day 4 and were present throughout the microtissue by Day 7. Cells in – fiber gels display rounded immature morphologies throughout the entire culture period.

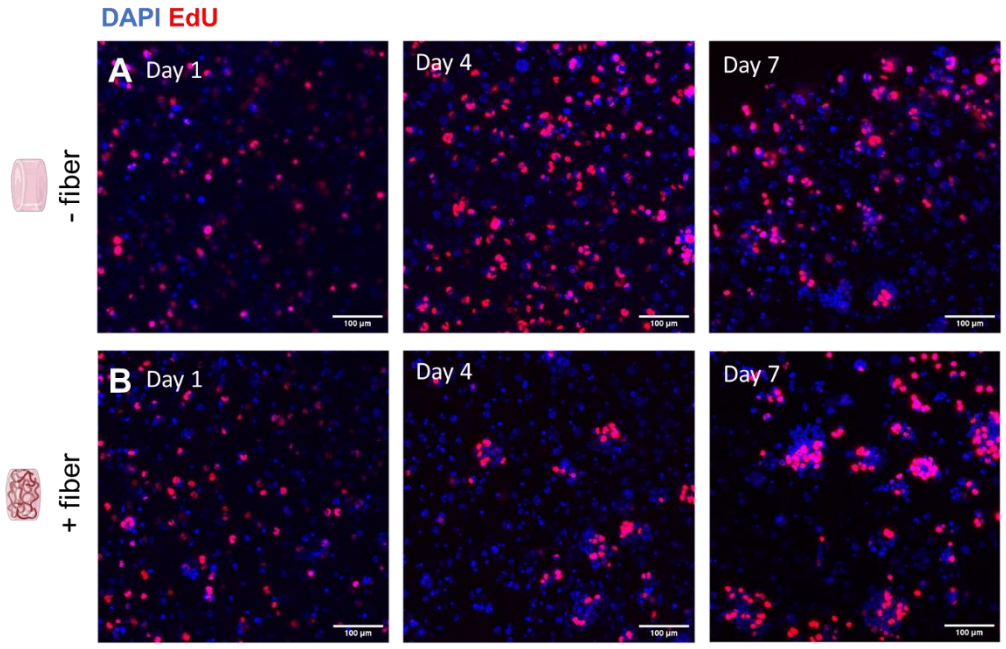

Figure S4.4. Proliferation of NSCs in – fiber (top row) and + fiber (bottom row) NorHA gels at culture days 1, 4 and 7. DAPI (cell nuclei stain) is labeled in blue while EdU (cell proliferation stain) is labeled in red. Proliferation rate appears similar across both – fiber and + fiber conditions at Day 1. Clusters of highly proliferative cells can be seen in + fiber gels at Day 4, with large clusters in evidence by ay 7. By contrast, no evident clusters are present in - fiber gels, and proliferation appears to peak by Day 4, with a slight decline by Day 7.

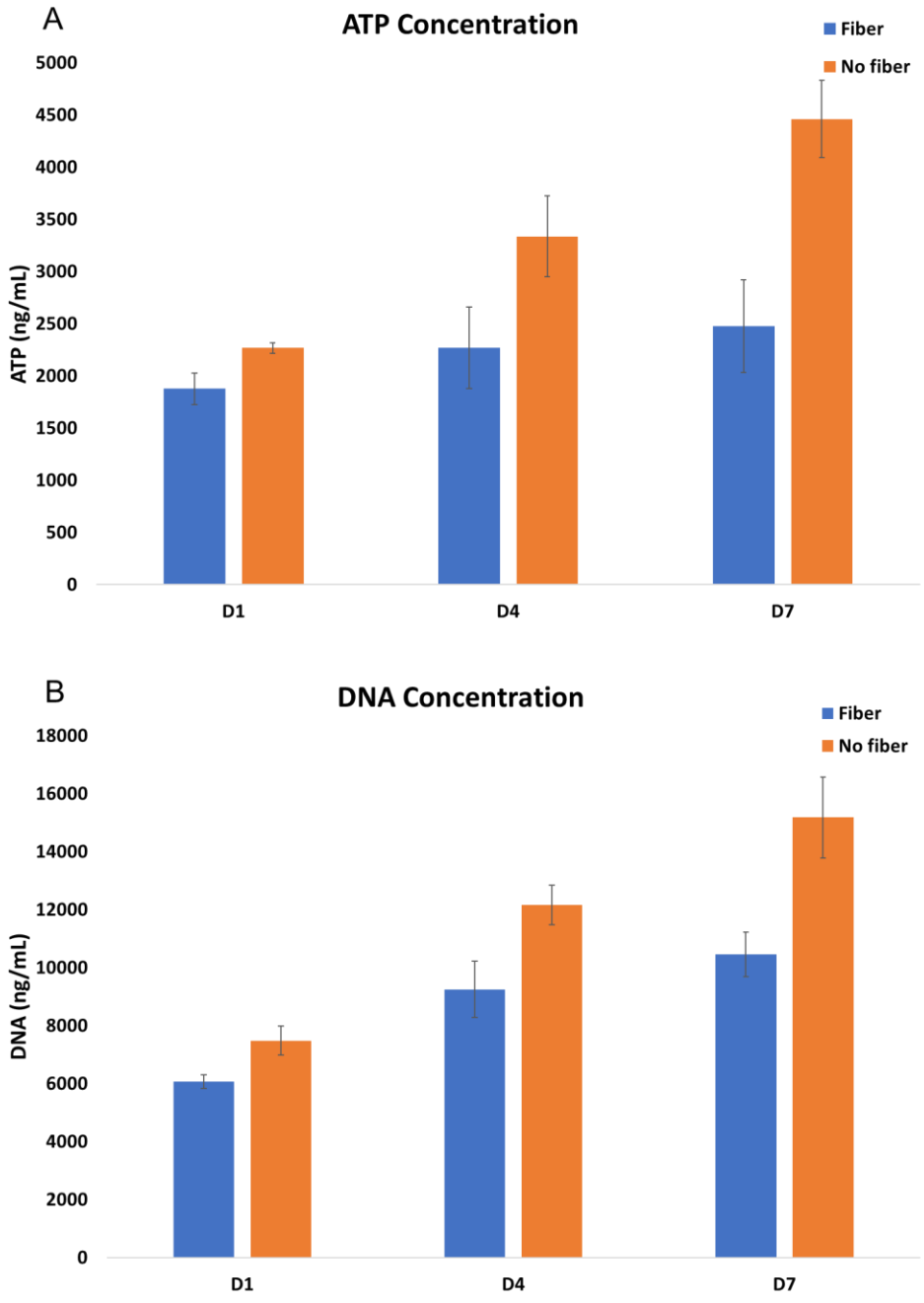

Figure S4.5. ATP and DNA concentrations of NSCs in 1.5% NorHA hydrogels at culture days 1, 4 and 7. A) ATP concentrations of NSCs in fiber (blue) and no-fiber (orange) gels over time. ATP concentrations were initially similar at Day 1 and increased over time for both + fiber and – fiber gels; however, ATP concentration was higher in – fiber gels by Day 4 and substantially higher by Day 7. B) DNA concentrations of NSCs in fiber (blue) and no-fiber (orange) gels over time. DNA concentrations were initially similar at Day 1 and increased over time for both + fiber and – fiber gels with similar trends as the ATP data.

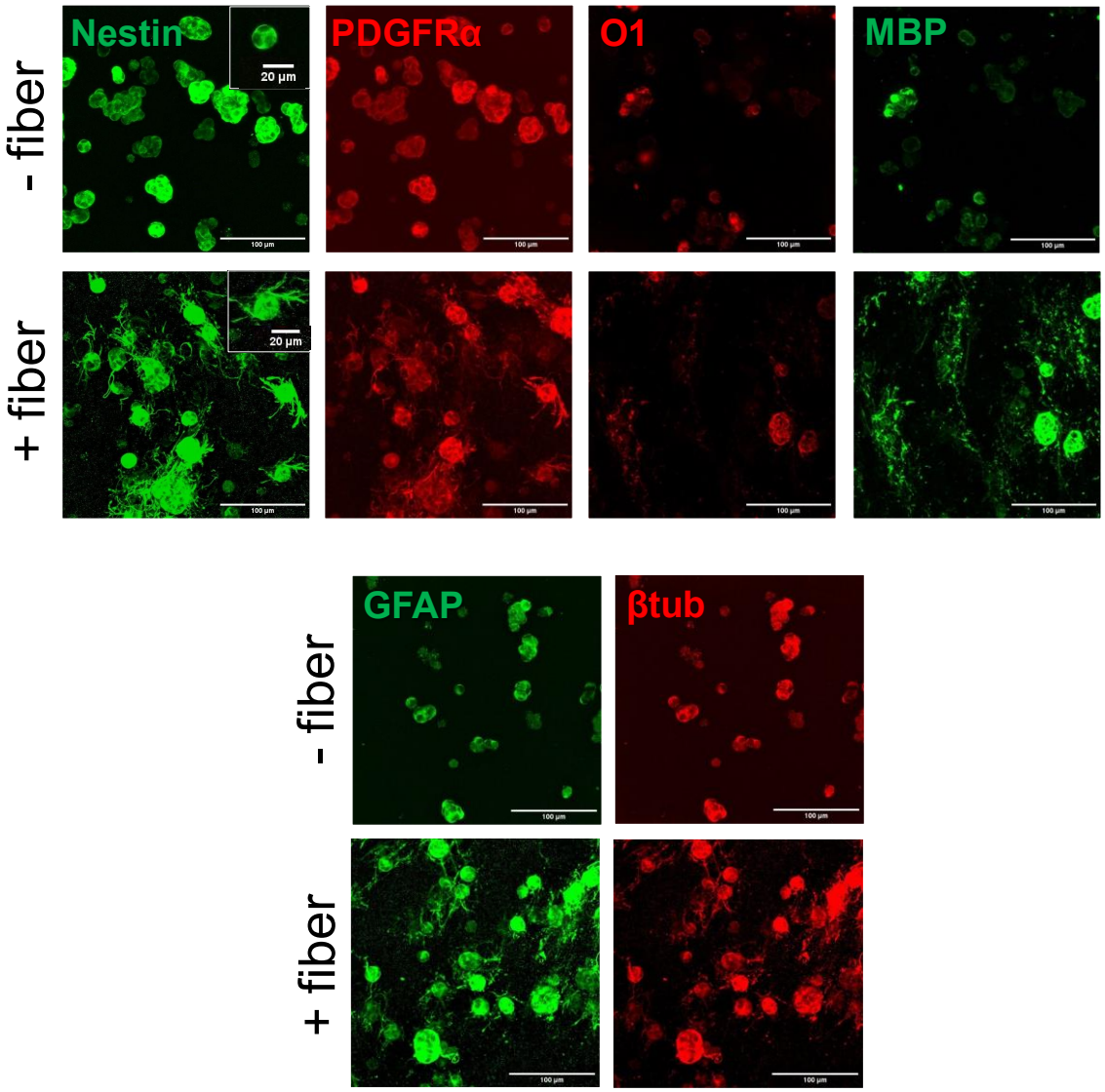

Figure S4.6. Immunostaining for various NSC maturation markers. Nestin is a marker for NSC, PDGFRα for OPC, O1 for immature OL and MBP for mature myelinating OLs. Markers for other cell fates, such as neurons (βtub) and astrocytes (GFP) were also investigated. Overall, NSC and OPC markers (nestin, PDGFRα) were expressed similarly with or without fibers, while mature markers (MBP) and markers for other cell fates (GFAP, βtub) were found to be differentially expressed in + fiber gels.

Chapter 5: Assessing OPC response to simulated mTBI in a 3D *in vitro* hydrogel model with electrospun microfiber cues

Rachel A. Mazur[1], Ryosuke Yokosawa[2], Pamela J. VandeVord[2], Kyle J. Lampe[1]

1 Department of Chemical Engineering, University of Virginia, Charlottesville, VA USA

2 Department of Biomedical Engineering and Mechanics, Virginia Polytechnic Institute and State University, Blacksburg, VA USA

5.1 Abstract

Damage resulting from traumatic brain injury (TBI) prompts oligodendrocyte precursor cells (OPC) to migrate, proliferate, and differentiate into oligodendrocytes (OL) capable of repairing the damaged tissue. However, the response of OPCs to mechanical trauma remains poorly understood. This study employs a 3D *in vitro* hydrogel platform to investigate changes in OPC proliferation and differentiation resulting from brain injury. Electrospun fibers were included in hydrogels to mimic structural cues of native axons in mature brain tissue. Hydrogels without fibers were also created as a negative control. To simulate mild TBI, a shock wave generator delivers a mechanical insult to OPC-containing hydrogels. Material analysis reveals that blast exposure within the range of mild TBI has minimal effect on hydrogel storage moduli, while fiber inclusion increased bulk stiffness. Cell viability remains high across experimental conditions. Cell morphology appeared more mature in fiber-containing gels, and morphology was unchanged between blast and sham conditions. Cell proliferation appeared unaffected by mechanical insult but was decreased in the presence of fibers at later timepoints. Gene expression analysis reveals upregulation of OPC maturation markers in the presence of electrospun fibers, indicating the presence of structural cues prompts OPC differentiation. By contrast, changes in OPC gene expression were not observed following mechanical trauma. Overall, these results suggest that overpressure insult in the range of mild TBI has little effect on OPC proliferation and differentiation.

5.2 Introduction

Traumatic brain injury (TBI) is damage to the brain that can be caused by multiple events such as rapid head movement, head collision with an object, and blast overpressure. US military members are particularly at risk of TBI from explosion-related overpressure, and approximately 400,000 military personnel have been diagnosed with TBI in the past 20 years [1, 2]. While both white matter and grey matter injuries are affected by TBI associated injuries, the amount of white matter disruption plays a significant role in predicting neurological outcomes [3]. The main components of white matter injury are axonal injury and demyelination; therefore, myelin repair may have profound implications for recovery of axon function [4]. Myelin loss and

remyelination following injury have been observed in animal models, as oligodendrocyte progenitor cells (OPCs) migrate to the affected area, differentiate into mature oligodendrocytes (OLs) and extend cellular processes to rewrap exposed axons [5]. Prevention and recovery of these cells are key to reversing myelin damage. However, the factors which influence OPC-related TBI are not well understood on a molecular level.

Animal models are the current gold standard for TBI investigation. However, while these models give insight into the pathophysiology of TBI, they cannot elucidate the fundamental signaling mechanisms of injury and recovery on a molecular level. Since living organisms are complex, animal models vary between individuals and contain numerous confounding variables [6]. *In vitro* brain tissue mimetic hydrogels are a promising alternative, allowing for precise tuning of individual variables to determine which specific factors are involved in injury and recovery cascades. By exposing the hydrogels to blast overpressure, we can determine the effects of mechanical stimulation on encapsulated OPCs in 3D.

Our proposed system consists of norbornene-functionalized hyaluronic acid (NorHA) as the bulk hydrogel. Hyaluronic acid-based gel systems are highly representative of native brain tissue since hyaluronic acid is a key component of the extracellular matrix and particularly the perineural net [7, 8]. Our group has previously demonstrated that OPCs are able to grow and proliferate in NorHA gels, and 1.5% NorHA were demonstrated to reflect the material properties of intermediate stiffness brain tissue [9]. We also included electrospun methacrylated hyaluronic acid (MeHA) fibers within our hydrogel to approximate the structural cues of native axons. Previous work has shown that axon-mimicking fiber cues are able to prompt OPC differentiation into OLs [10-12]. By co-encapsulating OPCs alongside fibers and exposing them to blast overpressure, we can simulate the effects of TBI on OPCs and OLs in the developed brain.

In this manuscript, we investigate the impact of blast overpressure injury within the range of mild TBI on OPC encapsulated in 3D 1.5% NorHA hydrogels. Gels without fibers were included to represent immature OPC in developing tissues, while gels containing axon-mimicking fibers represented more mature tissue. Our results illustrate the impacts of mild TBI on OPC proliferation and differentiation.

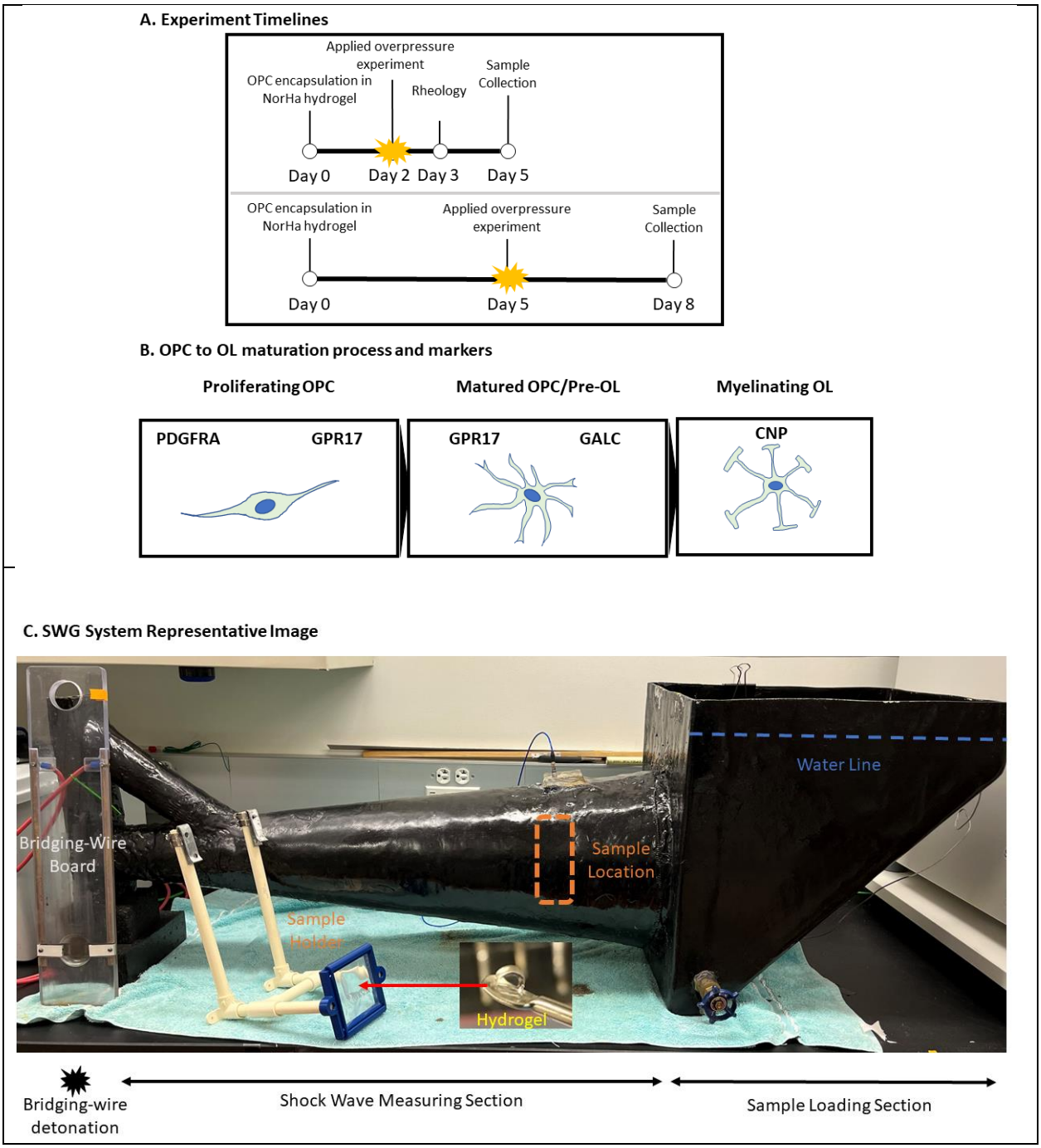

Figure 5.1. Experimental workflow for simulated mild TBI on OPC in 1.5% NorHA gels. A) OPC-containing gels were cultured to a timepoint of either 2 days or 5 days prior to blast (or sham) exposure. All samples were then cultured an additional 2 days before harvesting. Both + fiber and – fiber gels were included for each timeline. Rheology was conducted at experimental day 3 on acellular samples (n=2 for each of + fiber and – fiber gels). At each sample collection timepoint, gel samples (n=3 for each of blast + fiber, blast – fiber, sham + fiber, and sham - fiber) were collected for live-dead imaging. Consistent with previous experiments, OPCs grown in + fiber gels extended processes while OPCs in -fiber gels retained rounded morphologies. Samples were collected and DNA extracted for cell population analysis (n=3) at each timepoint. RNA extraction for PCR was performed on a separate set of samples (n=3) at the same timepoints. PCR was performed to determine the extent of OPC differentiation into

mature myelinating OLs. PDGFRA (OPC marker), GPR17 (late OPC/immature OL marker), GALC (mature OL marker) and CNP (myelination marker) were used as differentiation markers. C) SWG system was used to generate the shock wave due to an evaporation of thin metal wire on the bridging-wire board. OPC samples were placed in a sterile bag and fixed on the sample holder. Sample was submerged in the warm water-filled chamber and exposed to a high-rate overpressure propagation. Magnitude of the overpressure was measured by a sensor mounted on the wall of the chamber right above the sample location.

5.3 Materials and Methods

5.3.1 Flask Preparation and Cell Culture

GFP+ MADM OPCs were cultured in accordance with previously established protocols [Zong 2005, Muzumdar 2007, Liu 2011]. Briefly, a T75 tissue culture flask (Falcon) was coated with 10 µg/mL polyornithine (Sigma) and incubated at 37 °C for 4 hours. Flasks were rinsed prior to use with Dulbecco's phosphate-buffered saline (DPBS) and filled with 5 mL of proliferation media. OPC proliferation media consisted of Dulbecco's modified Eagle's medium (DMEM) containing 4.5 mg/L D-Glucose and 110 mg/L sodium pyruvate (Life Technologies), supplemented with 1% N2 supplement (Life), 2% B27 supplement (ThermoFisher), and 1% penicillin-streptomycin (ThermoFisher). Cells were seeded at a density of 1 x 10^4 cells/cm^2 per flask. The media was refreshed every two days until cells reached 80% confluency.

During cell passaging, cells were detached with a solution of 0.125% (0.5x) trypsin. Flasks were subsequently rinsed with 10 mL of DPBS to ensure optimal cell yield. The resultant cell suspension was centrifuged at 1000 rpm for 5 minutes, following which the supernatant was removed by aspiration. Cells were resuspended in 300 µL of PBS supplemented with 4.5 g/L D-glucose (PBSG) for the purpose of cell counting. Cells with passage number 20-30 were used for this study.

5.3.2 NorHA Synthesis

Norbornene-modified hyaluronic acid (NorHA) was synthesized based on previously established protocols [13]. Briefly, hyaluronic acid (60 kDa, LifeCore) was dissolved at a concentration of 25 mg/mL in 40 mL of 1 mM 2-(N-morpholino)ethanesulfonic acid (MES) buffer, with pH adjusted to 5.5 using 10 M NaOH. 4-(4,6-dimethoxy[1,3,5]triazin-2-yl)-4-methylmorpholinium chloride (DMTMM) coupling agent (VWR) was added to a concentration of 31 mg/mL and mixed until completely dissolved. To attain a functionalization efficiency of 20-30%, 0.271 mL of 5-norbornene-2-methylamine (TCI America) was added, and the mixture was stirred overnight at room temperature. The reaction mixture was then precipitated into 250 mL of cold 95% ethanol. The resulting precipitate was collected via vacuum filtration, re-dissolved in 2M brine solution, and transferred to pre-soaked dialysis tubing with a molecular weight cut-off of 6-8 kDa. Dialysis was performed against deionized (DI) water for 24 hours, followed by brine solution for an additional 24 hours, with water changes twice daily. This process was repeated three times, following which a final dialysis step was carried out against DI water for 24 hours. The product was lyophilized and the extent of norbornene functionalization was assessed using

1H NMR (Varian Inova 500 MHz) with D2O as a solvent. The final NorHA product was stored under nitrogen at 4°C.

5.3.3 MeHA Synthesis

Methacrylated hyaluronic acid (MeHA) was created followed established procedures [14, 15]. Briefly, methacrylic anhydride (MA) was gradually added to research-grade sodium hyaluronate (Lifecore Biomedical, 74 kDa) at a concentration of 1% w/v and stirred until fully blended. The resulting solution was kept on ice and a pH range of 8-9 was maintained with 5 N NaOH. MA was introduced in a 1:1 molar ratio to HA, with a 12.3x molar excess. Once all the methacrylic anhydride was added, the solution was stirred continuously overnight. Subsequently, the solution underwent dialysis (molecular weight cutoff 6-8 kDa) for 5 days against deionized water. The macromer solution was frozen overnight at –80° C and lyophilized for 3 days. The resulting MeHA product was stored under nitrogen at 4 °C.

5.3.4 Electrospinning

Electrospinning solution was prepared in 2 mL batches, consisting of 2 wt% MeHA, 3 wt% polyethylene oxide (PEO), and 0.05 wt% Irgacure D-2959 photoinitiator (I2959) dissolved in deionized water. This solution was shielded from light and allowed to dissolve in a 5 mL Cadence syringe for 24-48 hours with stirring. Fibers were spun using a Spraybase electrospinning machine at 21% relative humidity, with a 21 cm collection distance, 8-11 kV voltage, 20-gauge needle, and 0.4 mL/hr flow rate. The dry fibers were collected on aluminum foil and stored under inert gas until crosslinking. Crosslinking was achieved by exposing fibers to an Omnicure UV light set to an intensity of 14 mW/cm2 for 15 minutes. Subsequently, the fibers were swollen overnight in deionized water and processed by repeatedly passing through an 18-gauge needle, followed by a 21-gauge needle, as per established protocols [16].

5.3.5 3D Cell Encapsulation and Hydrogel Culture

To replicate the stiffness of native brain tissue, a concentration of 1.5% NorHA was chosen based on previously determined storage moduli [9]. NorHA macromer solution was created by combining 1.5 wt% NorHA macromer, 0.0328wt% LAP and dithiothreitol (DTT) at an 0.312 thiol-norbornene ratio. For fiber-containing conditions, gel precursor solution also contained electrospun fiber solution at 1 wt%. The cell suspension was mixed with the pre-prepared solution to achieve a final concentration of 5x10^6 cells/mL. The hydrogel solution (200,000 cells per gel, 40 µL) was loaded into 1 mL BD Disposable Syringes with Luer-Lok™ Tips (BD). The syringes were vertically positioned under a UV lamp and polymerized by exposure to 365 nm UV light at 4 mW/cm^2 for 2 minutes. Hydrogels were retrieved from the syringes and rinsed thrice in DPBS. Subsequently, the hydrogels were incubated in OPC growth media with media replacement every other day.

5.3.6 Mechanical Insult Testing

The shock wave generator (SWG) was used for the overpressure experiment (Figure 5.1). The SWG device has been shown to mimic intracranial pressure found within the rodent brain exposed to an overpressure wave [17, 18]. The SWG was filled with warm distilled water at 37 °C during the time of testing. The SWG uses a bridging-wire detonation system that generates a single shock wave by applying a high voltage through a thin metal wire. (Figure 5.1A) For this study, nichrome wire (0.003 in diameter, Part# 40BNC, Consolidated Electronic Wire & Cable) was used for shock wave generation. The applied overpressure was measured by a piezoelectric pressure sensor (PCB Piezotronics Inc., Model 113B21, Depew, NY, United States) located within the chamber (Figure 5.1B).

OPC- containing hydrogels were exposed to the overpressure insult on days 2 and 5 of cell culture after encapsulation. Gels were blasted 2 at a time in PBS for material characterization, or in batches of 9 in DMEM for cellular and molecular analyses. Individual batches were sealed in 2 oz SureSeal™ Sterile Sampling Bag (MTC Bio) using a bag heat sealer (Sigma). The test bag was tightly attached to the bag holder (Figure 5.1B) and submerged in the SWG chamber (Figure 5.1C). Blast gel samples were exposed to a single insult and then retrieved from the bag and transferred to a 24-well plate (ThermoFisher) with 1 mL of DMEM with supplements per well. Sham samples were prepared by following the same steps without the overpressure exposure. Gels were incubated 3 days or 5 days after overpressure exposure. The media was replaced every day until the day of sample collection.

Overpressure data were collected at 0.5MHz on a SIRIUSi DAQ module (DEWESoft) with a 4-channel signal conditioner (DSI-ACC, DEWESoft) and analyzed using DewesoftX Software (DEWESoft). Acquired data were analyzed and visualized in MATLAB (R2021b, The MathWorks Inc., Natick, MA, United States) where average peak pressure, rise time, positive duration, and positive impulse were reported.

5.3.7 Oscillatory Shear Rheology

1.5wt% NorHA hydrogels with and without 1% fiber were made 1 day prior to the applied overpressure experiment. Samples were exposed to sham and overpressure conditions (n=2 each, with and without fiber). Bulk storage moduli of the hydrogels were then assessed via shear rheology. Premade gels were placed onto the Discover HR-30 rheometer, and an 8 mm diameter parallel plate insert was used to conduct oscillatory frequency sweeps with gap height 1.6 mm, oscillatory strain 0.1%, and angular frequency ranging from 0.1-10 rad/s. Final storage moduli were calculated as the average of data points in the linear region of the graph (angular frequency between 0.63-3.98 rad/s).

5.3.8 Cell Viability Assay

OPC viability within hydrogels was quantified using the LIVE/DEAD™ Viability/Cytotoxicity Kit (ThermoFisher). On day 5 or day 8 of incubation, three gels from each of the overpressure and sham samples were collected and stained with ethidium homodimer and Hoechst33342 (n = 3 per condition per experiment). No live stain was used since the OPC line constitutively

expresses GFP in the cytoplasm of living cells. Dead stain was conducted by incubating samples in 4 µM ethidium homodimer 1 (EthD1) at 37 °C for 30 min. Nuclear staining was conducted by incubating cells with 100 nM Hoechst for 1 hour followed by rinsing twice with DPBS. Live/Dead images were captured using a Zeiss LSM800 MA-Pmt2 confocal microscope with 300-400 µm z-stacks at 5 µm slices using the 10x objectives. Three regions of interest (ROIs) were selected for each gel in between the center and edge of the hydrogel. Images were processed with Max Projection of z-stack image slices. The Max Projection images were analyzed using the ImageJ measurement analysis for intensity density [19].

5.3.9 Morphology Image Quantification

9 z-stack images were taken for each of the + fiber and – fiber conditions (3 images per gel across 3 gel replicates). Z stacks were taken at 20x magnification in intervals of 5 µm to a depth of 200-300 µm. For each Z interval, Hoechst and GFP channels were separated and processed using the Otsu thresholding function in FIJI ImageJ [19]. The Despeckle function was then applied to remove background noise. A dedicated ImageJ macro was used for automated quantification of signal area of both the CellMask and protein channels for each Z interval in the sample [20]. Protein signal area was then divided by CellMask signal area to determine the amount of extracellular matrix deposition normalized to cell surface area.

5.3.10 DNA Quantification

Double stranded DNA (dsDNA) concentration was measured by fluorescent nucleic acid stain using Quant-iT™ PicoGreen™ dsDNA Assay Kits (ThermoFisher Scientific Inc., Waltham, MA, United States) that includes Quant-iT™ PicoGreen™ dsDNA Reagent (fluorescent dye), 20X TE (200 mM Tris-HCl, 20 mM EDTA, pH 7.5), and Lambda DNA standard. 20X TE buffer was diluted to 1X TE buffer in UltraPure™ DNase/RNase-Free Distilled Water. Samples were homogenized using the Disposable Pellet Mixer (VWR) and sonicated three times at 40 J for 10 seconds. DNA standard dilution was prepared from 0 to 1000 ng/µL concentrations in 1X TE buffer. A black 384-well plate (ThermoFisher) was used for the assay. 20 µL of standard dilutions were added to each well. 5 µL samples were added to each well then diluted with 15 µL 1X TE buffer. All samples and standards were prepared in triplicates. Once all samples and standards were in place, 20 µL Quant-iT PicoGreen™ dsDNA Reagent was added to the wells to initiate a reaction. The well-plate was incubated for 10 min at room temperature in dark. Samples were excited at wavelength at 480 nm, and then the fluorescence emission intensity at 525 nm was measured in a SpectraMax M2e microplate reader. A standard curve was determined, and fluorescence OD values were converted to DNA concentrations [ng/mL].

5.3.11 RNA Extraction

Samples were collected on day 5 and day 8 of incubation stored in 600 µL Trizol reagent (ThermoFisher) at -80 °C until sample processing. Samples were homogenized as described in a previous section. RNA was separated from the sample by adding 120 µL chloroform to the 600

μL lysate. The sample was vigorously shaken by hand then incubated at room temperature for 2 min. RNA was isolated from the homogenized cell lysates and purified using the PureLink™ RNA Mini Kit (ThermoFisher) following the manufacturer's instruction. Purified RNA was extracted and measured with the NanoDrop™ One/OneC Microvolume UV-Vis Spectrophotometer (ThermoFisher) to achieve a purity ratio (A260/A280 nm) between 1.8 and 2.0.

5.3.12 Reverse transcription real-time PCR (qPCR)

Changes in gene expression of OPC maturation markers following overpressure were analyzed using qPCR on day 5 and day 8 post overpressure. 100 ng RNA was converted to cDNA using the iScript™ cDNA Synthesis Kit (BIO-RAD, Hercules, CA, United States) following the manufacturer's protocol. A 60 ng cDNA sample was used for qPCR analysis. The samples were mixed in the TaqMan™ Fast Advanced Master Mix (ThermoFisher) that was added to a 96-well plate with 0.2 mL format (ThermoFisher) using QuantStudio™ 3 Real-Time PCR System (ThermoFisher). Taqman primers for OPC maturation marker and reference gene were selected as follows: *GAPDH* (Mm99999915_g1), *PDGFRA* (Mm00440701_m1), *GPR17* (Mm02619401_s1), *GALC* (Mm00484646_m1), and *CNP* (Mm01306641_m1). All samples were analyzed in triplicate. The PCR mixture was denatured at 95°C for 1 second each cycle of 40 cycles of amplification. The delta-delta Ct method ($2^{-\Delta\Delta CT}$) was used to analyze the data, normalizing to *GAPDH* to estimate the relative fold gene expression change.

5.3.13 Statistical Analysis

Statistical comparisons were conducted to compare each experimental condition to control using GraphPad Prism 9 (GraphPad Software, San Diego, CA, United States). The Shapiro-Wilk test was used to verify assumptions of normality. A Student's t-test was used for the PCR (*PDGFRA, GALC, CNP*) results. When the dataset is a non-Gaussian distribution, Mann-Whitney test was used for PCR (*GALC* day 8 sample)results. Data point indicates average of 3 regions of interest per hydrogel and the error bar indicates standard error of the mean. Differences were considered significant when $p < 0.05$.

5.4 Results and Discussion

5.4.1 Mechanical Insult Characterization

A representative blast wave produced by the SWG is shown in Figure 5.2A. Overpressure parameters are summarized in Figure 5.2B. All samples were exposed to a positive impulse of 7.00 ± 2.75 psi, within the range of mild TBI [21]. These wave characteristics align with literature for rat blast-induced neurotrauma modeling, demonstrating translational *in vivo* biomechanics [17, 22].

A

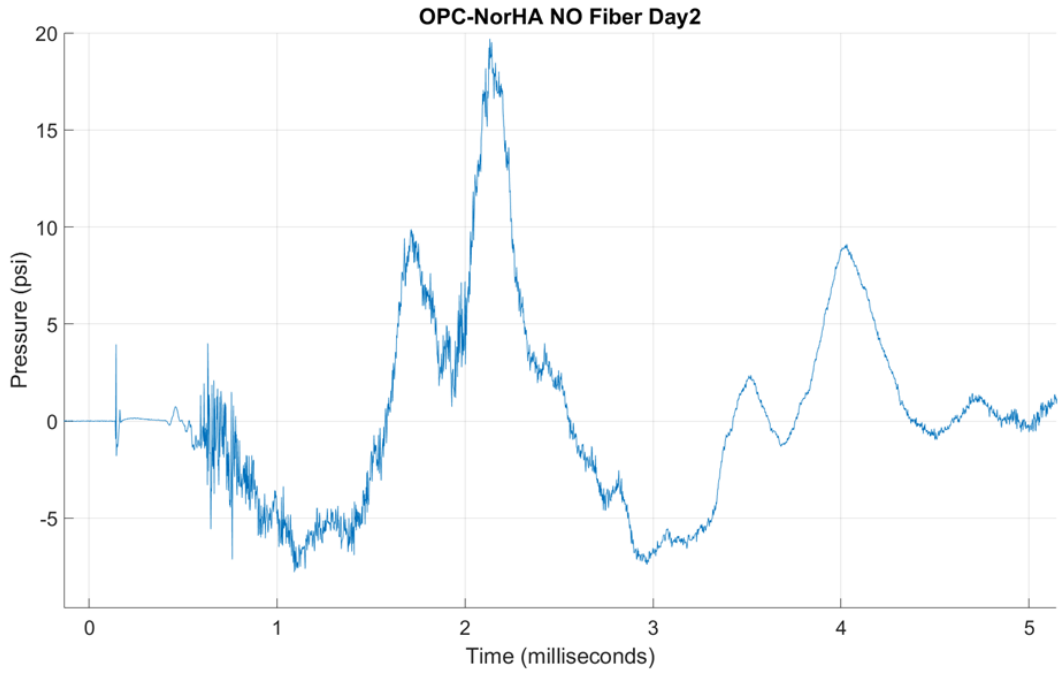

B

Sample	Peak Pressure (psi)	Rise time (ms)	Positive duration (ms)	Positive impulse (psi*ms)
OPC (- fiber)	18.59 ± 0.91	0.53 ± 0.02	0.96 ± 0.02	6.68 ± 0.01
OPC (+ fiber)	37.52 ± 7.60	0.27 ± 0.12	0.48 ± 0.17	7.00 ± 2.75

Figure 5.2. Blast curve data for simulated TBI on OPCs in 1.5% NorHA gels. A) Representative blast curve for OPC – fiber gels blasted on Culture day 2. Area beneath the overpressure curve (overall positive impulse) was consistently between 6-7 psi*ms, consistent with a mild TBI (~6.5 psi*ms). B) Table of peak pressure, rise time, positive duration, and positive impulse for all samples. Data represented with mean ± standard deviation.

5.4.2 Hydrogel Materials Characterization

Oscillatory shear rheology was performed on 1.5 wt% NorHA gels to determine the impact of applied overpressure on gel mechanical properties (Figure 5.3). Frequency sweeps were conducted on both overpressure and sham samples for + fiber and – fiber conditions. Overall storage moduli for all conditions approximated the range of native brain tissue stiffness (G' = 200-2000 Pa) [23]. In the absence of fibers, bulk storage modulus was between 308-468 Pa; however, fiber-containing gels demonstrated slightly elevated moduli, between 309-655 Pa. While storage moduli were generally higher for fiber-containing gels, the difference was not statistically significant. These results are consistent with previous work from our group (outlined in Chapter 3), which indicated that the inclusion of fibers increased bulk gel stiffness by 30% in 1.5% NorHA gels. However, based on nanoindentation measurements, we previously determined that this was a local effect limited to within 10 μm from electrospun fibers. Measurements taken from + fiber gels >10 μm away from fibers had equivalent stiffness with – fiber cues of equivalent polymer concentration (see figure 3.2). Overall, despite the increase in overall bulk

stiffness, material properties are expected to be comparable between + fiber and – fiber NorHA gels. No significant difference occurred as a result of overpressure for either + fiber or – fiber gels, indicating that overpressure within the range of mild TBI does not have an effect on hydrogel structure.

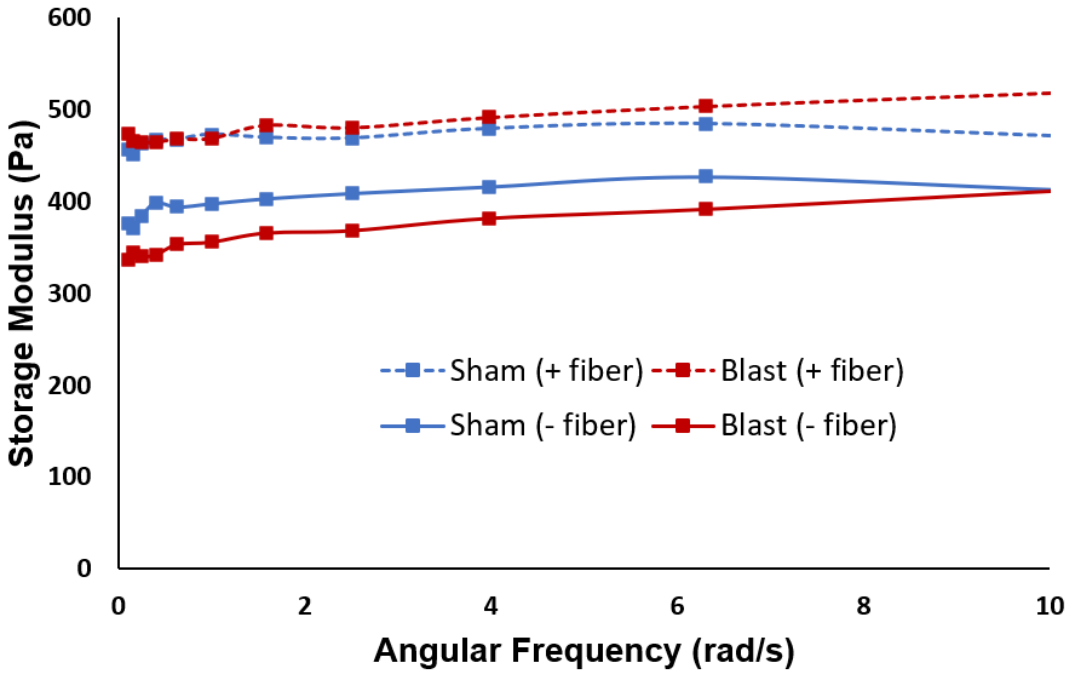

Figure 5.3. Frequency sweep data for + fiber and – fiber gels under blast and sham conditions. Frequency sweeps were performed with angular frequency between 0.1-10 rad/s (n=2 for sham – fiber, n=4 for others). The presence of fibers significantly increased storage modulus, while exposure to blast injury did not have a significant effect on bulk gel stiffness.

5.4.3 Cell Viability Analysis

Live/Dead staining were conducted to determine whether an applied overpressure propagation triggered apoptosis within samples, and how the effects of overpressure propagation differed between – fiber and + fiber conditions (Figure 5.4). Gels were imaged at culture day 5 (Figure 5.4A-D) and day 8 (Figure 5.4E-H). At both timepoints, cells in – fiber gels formed large clusters and retained a rounded, immature morphology. By contrast, cells in + fiber gels extended processes, a hallmark of cell differentiation, at both the day 5 and day 8 timepoints. Once again, these morphology results are consistent with previous work by our group involving OPCs in NorHA gels (Chapter 3). 2D studies by other groups have also yielded similar results using polystyrene and polycaprolactone fibers [10, 24].

The average viability of cells in - fiber gels at day 5 was between 79-98%, with a small (though statistically significant) decrease in viability due to overpressure (Figure 5.4I). The presence of fibers also lowered viability to 78% in + fiber sham gels, and the lowest viability was observed in + fiber blast gels, which had an average viability of 50%. By culture day 8, viability in – fiber gels was between 85-96%, with no significant difference between blast and sham conditions (Figure 5.4 J). While viability in + fiber sham gels remained the same (78%) across both timepoints, viability in + fiber blast gels was higher at day 8 (63%) and was no longer significantly different from the sham value. Overall, both fibers and overpressure exposure were found to significantly decrease viability in day 5 samples. Fibers had a greater and more prolonged effect on viability than overpressure exposure, with decreased viability in + fiber gels persisting at day 8. By contrast, differences in viability due to overpressure were less pronounced and were not significantly present at culture day 8.

Live stain signal area was normalized to nuclear stain signal area to determine the average surface area per cell (Figure 5.4K). In general, + fiber samples demonstrated decreased signal area compared to - fiber samples, although differences between + fiber and – fiber gels were not significantly different under similar conditions/timepoints. While the magnitude of normalized signal area is comparable to previous experiments (Figure 3.3), this trend is not; previous experiments have shown that cells in + fiber gels tend to have significantly higher normalized signal area, due to the increased surface area from process extensions. Additionally, there was no significant difference in normalized signal area between timepoints, indicating that there was little change in cell surface area between days 5 and 8 of culture. Overall, none of the factors tested (time, blast exposure, fiber inclusion) were found to significantly affect cell size.

Based on previous work with OPCs and fibers, we determined that the presence of fibers increased cell differentiation at the expense of proliferation. This resulted in lower rates of proliferation for + fiber gels as compared to – fiber gels (Figure 3.4). However, the overall cell area in + fiber gels was found to be significantly higher because of the high number of cell process extensions in this condition. [how our results are similar/different to this]. Although previous mTBI studies tended to focus on neurons rather than OPCs/OLs, *in vivo* studies found that mild TBI does not produce significant levels of cell apoptosis [25, 26]. The comparable viability between sham and overpressure conditions is therefore consistent with literature. However, the combination of overpressure exposure and fiber presence resulted in a noticeable (though not statistically significant) decrease in viability for + fiber blast gels as compared to other conditions. While perhaps unsurprising, this result is novel and suggests an interaction effect between blast and fibers.

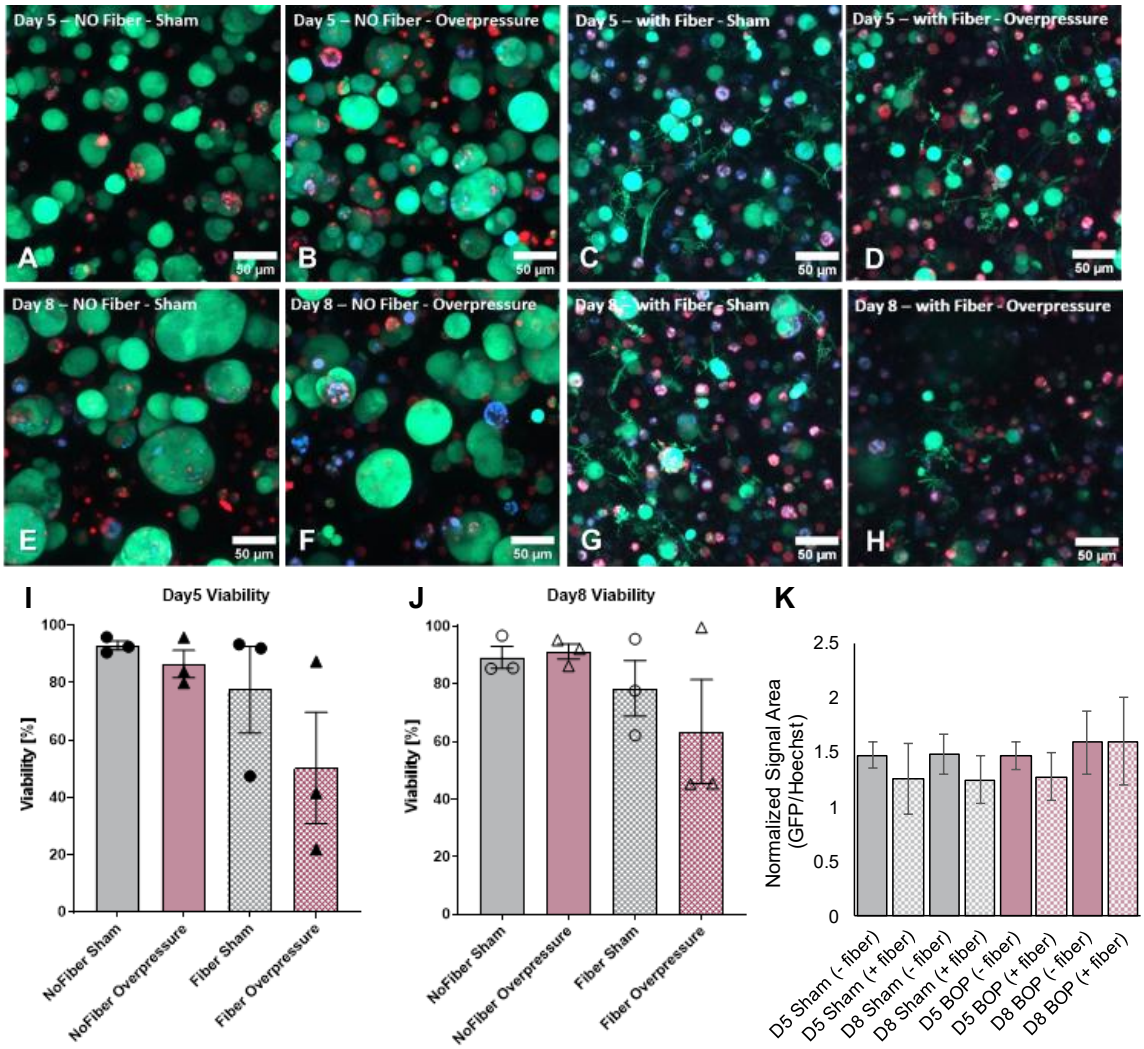

Figure 5.4. Live-dead image analysis of OPC in + fiber and – fiber blast and sham gels. A-D) Images of OPCs in 1.5% NorHA hydrogels at culture day 5. Green signal indicates living cells while red signal indicates dead cells. Hoechst dye (blue) was used to indicate cell nuclei. Cells in – fiber gels form large spherical clusters, while those in + fiber gels extend processes. E-H) Images of OPCs in 1.5% NorHA hydrogels at culture day 8. Trends are consistent with those at culture day 5. I-J) Percent viability of OPCs in each condition at culture days 5 (I) and 8 (J). Overpressure caused a slight (but statistically significant) decrease in viability for both + fiber and – fiber conditions at day 5, though these effects are less pronounced at day 8. Viability in + fiber gels was consistently lower than in – fiber gels. K) GFP signal area was divided by Hoechst signal area to determine average area on a per-cell basis. Cells had consistent per-cell surface areas across all tested conditions.

5.4.4 Cell Population Measurement

Because DNA concentration is expected to increase proportionally to cell population, DNA concentration was quantified to determine the relative cell population of each sample. At culture day 5, the DNA concentration for all samples was between 1090-1295 ng/mL and was not significantly different between + fiber and – fiber gels, or as a result of overpressure exposure

(Figure 5.5A). At culture day 8, DNA concentration for – fiber gels had increased to 2000 ng/mL for – fiber gels, indicating that the cell population had increased between days 5 and 8 due to cell proliferation (Figure 5.5B). This increase in DNA concentration occurred in both sham and blast conditions, indicating that overpressure exposure in the range of mild TBI had limited effect on cell population. Similarly, there was no significant difference in DNA concentration between + fiber blast and sham gels at day 8. However, there was also no increase in cell population for + fiber gels between days 5 and 8, indicating that proliferation was limited in + fiber gels.

Previous work with OPCs in 1.5% NorHA gels (- fiber) of equivalent cell density found DNA concentrations of 3500 ng/mL at culture day 3, and 4500 ng/mL at culture day 7 [9]. A recent study from our group similarly found a DNA concentration of 3000 ng/mL for – fiber sham gels at culture day 5 (see Appendix A, Figure 7.6B). The values for our sham gels at culture days 5 and 8, while lower than those in previous studies, are nevertheless within the appropriate order of magnitude, suggesting cell viability and proliferation rates analogous to previous studies. While few studies have focused on mild TBI specifically, proliferation of OPC has been shown to increase following moderate to severe TBI [27, 28]. These data seem to suggest that, unlike more severe injuries, overpressure within the range of mild TBI does not significantly affect OPC proliferation. Fiber presence appears to decrease proliferation; this is consistent with our results from Chapter 3, where we concluded that fiber cues caused OPC to differentiate at the expense of proliferation.

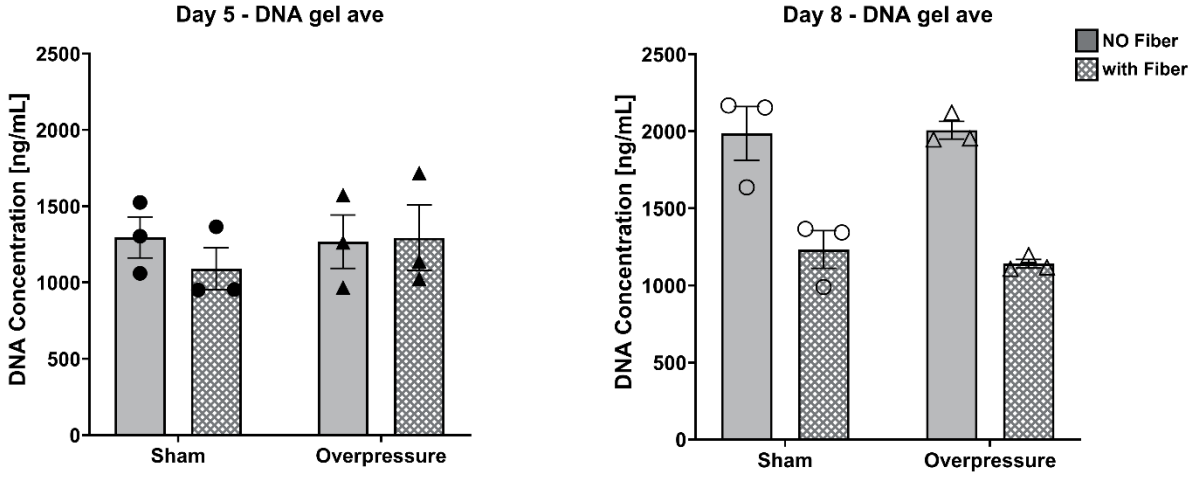

Figure 5.5. DNA concentration for OPCs in + fiber and – fiber blast and sham gels. A) DNA concentration for OPCs in 1.5% NorHA hydrogels at culture day 5. Both + fiber and – fiber gels show consistent DNA concentrations, and there is no significant difference between sham and overpressure conditions. B) DNA concentration for OPCs in 1.5% NorHA hydrogels at culture day 8. No significant difference exists between blast and sham gels at this timepoint. DNA concentrations for – fiber gels are elevated at day 8 as compared to day 5, indicating continued cell proliferation. By contrast, DNA concentration in + fiber gels is consistent with day 5 levels, indicating limited proliferation.

5.4.5 Gene Expression Evaluation

Gene expression for all samples was evaluated through qPCR. Four marker genes were selected for OPCs at different points along the differentiation pathway: *PDGFRA* (OPC marker), *GPR17* (mature OPC-immature OL marker), *GALC* (mature OL marker), and *CNP* (myelination marker).

Data for + fiber gels was normalized to corresponding – fiber gels to determine the effects of fiber presence on OPC differentiation. Expression of *PDGFRA* was initially elevated (between 1.5-1.8x higher) for + fiber gels in both sham and blast conditions at day 5 but drops lower than - fiber condition at day 8 (Figure 5.6A). This indicates a large initial population of OPC at day 5 which is no longer present at culture day 8. *GPR17* is also elevated in + fiber conditions at day 5, to a greater extent than *PDGFRA* (between 3-3.5x higher). This effect is decreased at day 8 but still around 1.5x higher than in the corresponding – fiber conditions, indicating differentiation from OPC to immature OL across both timepoints (Figure 5.6B). Both *GALC* and *CNP* expression are elevated in the + fiber condition at day 5, with *GALC* 3.4-3.5x higher and *CNP* 2.2-2.4x higher in + fiber gels compared to – fiber gels (Figure 5.6C-D). *GALC* remains slightly elevated (1.9x higher) in the + fiber condition at day 8, but expression declines in + fiber sham gels at the same timepoint This may indicate that overpressure injury within the range of mild TBI influences cell differentiation towards mature OLs. *CNP* expression remains close to 1 at day 8, indicating minimal differences between + fiber and – fiber conditions at this timepoint.

When the data for overpressure gels is normalized to corresponding sham gels (Figure 5.6E-H), values remain largely consistent across conditions regardless of the presence of fibers. This indicates that there are limited interactions effects between fiber presence and overpressure exposure. Additionally, most values are near 1, indicating that in general, gene expression is neither up nor downregulated as a result of overpressure exposure. The only exceptions occur for *GPR17* and *GALC* at culture day 8. *GPR17* appears to be slightly downregulated in the + fiber overpressure condition at this timepoint, although – fiber gels show consistent *GPR17* expression regardless of overpressure. Conversely, - fiber gels show a decrease in *GALC* expression for overpressure gels at day 8, while *GALC* expression in + fiber gels remains unaffected by blast exposure. These results may indicate that overpressure injury has a slight effect on differentiation between the immature and mature OL stages.

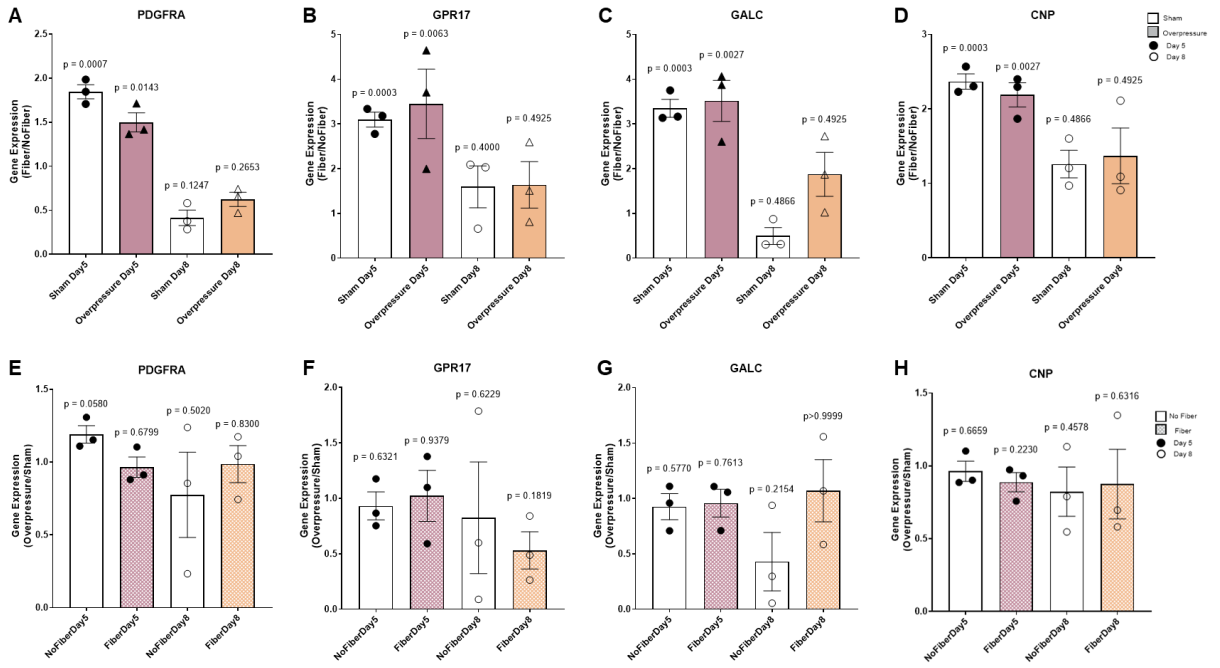

Figure 5.6. Expression of oligodendrocyte differentiation- related genes *PDGFRA* (OPC marker), *GPR17* (OPC-early OL marker), *GALC* (mature OL marker) and *CNP* (myelination marker). A-D) Gene expression in + fiber gels normalized to – fiber gels for *PDGFRA*, *GPR17*, *GALC*, and *CNP*, respectively. Markers for all stages of maturation are elevated in + fiber gels as compared to – fiber gels at day 5. While the magnitude of upregulation is decreased for all conditions at day 8, later maturation markers continue to be upregulated in + fiber gels. E-H) Gene expression in blast overpressure gels normalized to sham gels for *PDGFRA*, *GPR17*, *GALC* and *CNP*, respectively. Exposure to overpressure injury had little to no impact on gene expression at any timepoint.

Table 5.1. qPCR results of maturation markers. OPC with fiber data were normalized to OPC without fiber data for sham and overpressure conditions at each time point. Average and SEM of each condition was represented in the table. Green highlighted value represents upregulation and blue highlighted value represents downregulation due to the fiber contained hydrogel cell culture system.

	Day 5 - Sham		Day 5 – Overpressure		Day 8 - Sham		Day 8 – Overpressure	
Marker	Average	SEM	Average	SEM	Average	SEM	Average	SEM
PDGFRA	1.846	0.080	1.498	0.108	0.414	0.087	0.623	0.080
GPR17	3.099	0.167	3.451	0.776	1.594	0.467	1.639	0.519
GALC	3.351	0.200	3.516	0.458	0.496	0.189	1.874	0.492
CNP	2.367	0.103	2.188	0.163	1.259	0.184	1.370	0.374

Table 5.2. qPCR results of maturation markers. Overpressure OPC data were normalized to sham OPC data for with fiber and without fiber conditions at each time point. Average and SEM of each condition was represented in the table. Green highlighted value represents upregulation

and blue highlighted value represents downregulation due to the fiber contained hydrogel cell culture system.

	Day 5 - Fiber		Day 5 – Overpressure		Day 8 - Sham		Day 8 – Overpressure	
Marker	Average	SEM	Average	SEM	Average	SEM	Average	SEM
PDGFRA	1.190	0.060	0.965	0.070	0.775	0.293	0.986	0.127
GPR17	0.932	0.126	1.023	0.230	0.825	0.503	0.531	0.168
GALC	0.926	0.117	0.958	0.125	0.430	0.264	1.070	0.281
CNP	0.963	0.070	0.888	0.066	0.823	0.170	0.875	0.239

5.5 Conclusions

In this study, we demonstrated that OPCs encapsulated in 3D NorHA hydrogels remain viable over an 8-day culture period, and that the SWG was able to inflict an overpressure injury consistent with mild TBI. Blast overpressure did not have a significant effect on hydrogel material properties, but inclusion of electrospun fibers did result in an increase in bulk storage modulus. Fiber inclusion decreased cell viability and proliferation as compared to – fiber gels, but overall OPCs remained viable in all conditions over an 8-day culture period. Cell viability and proliferation were not significantly affected by overpressure exposure. Fiber cues influenced OPC differentiation, with cells in fiber-containing cells displaying mature morphologies and increased expression of genes associated with OL differentiation. Blast injury on the scale of mild TBI was demonstrated to have minimal impact on OPC differentiation. Moving forward, this 3D platform is expected to constitute a valuable tool for modeling the CNS under a variety of injury conditions. In particular, the tunable nature of this platform could be of interest to unravel molecular-level mechanisms implicated in OL differentiation and to identify potential therapeutic targets capable of guiding cell differentiation and tissue repair.

5.6 Acknowledgements

This work was supported by NSF grant 2104723, as well as the University of Virginia Dean's Fellowship award. We gratefully acknowledge the Virginia Tech Imaging Center for the use of the Zeiss LSM800 confocal microscope, and the VT Materials Characterization Lab for use of the rheometer.

5.7 References

[1] D. Freedman, N. Nived, B. Decker, S. Narla, S. Shafik, S. Manohar, R. Salvi Michal, K. Stachowiak, E.K. Stachowia, Neurogenesis and Oligodendrogenesis in a Mouse Model of Blast-Induced Traumatic Brain Injury., Neurology and Neurobiology, 2020.
[2] D.V. Bradshaw Jr, Y. Kim, A. Fu, C.M. Marion, K.L. Radomski, J.T. McCabe, R.C. Armstrong, Repetitive Blast Exposure Produces White Matter Axon Damage without Subsequent Myelin Remodeling: In Vivo Analysis of Brain Injury Using Fluorescent Reporter Mice, Neurotrauma Reports 2(1) (2021) 180-192.

[3] H. Pu, X. Zheng, X. Jiang, H. Mu, F. Xu, W. Zhu, Q. Ye, Y. Jizhang, T.K. Hitchens, Y. Shi, Interleukin-4 improves white matter integrity and functional recovery after murine traumatic brain injury via oligodendroglial PPARγ, Journal of Cerebral Blood Flow & Metabolism 41(3) (2021) 511-529.
[4] R.C. Armstrong, A.J. Mierzwa, C.M. Marion, G.M. Sullivan, White matter involvement after TBI: Clues to axon and myelin repair capacity, Experimental neurology 275 (2016) 328-333.
[5] R.C. Armstrong, A.J. Mierzwa, G.M. Sullivan, M.A. Sanchez, Myelin and oligodendrocyte lineage cells in white matter pathology and plasticity after traumatic brain injury, Neuropharmacology 110 (2016) 654-659.
[6] R.A. Mazur, R. Yokosawa, P.J. VandeVord, K.J. Lampe, The Need for Tissue Engineered Models to Facilitate the Study of Oligodendrocyte Progenitor Cells in Traumatic Brain Injury and Repair, Current Opinion in Biomedical Engineering (2022) 100378.
[7] Z.Z. Khaing, S.K. Seidlits, Hyaluronic acid and neural stem cells: implications for biomaterial design, Journal of Materials Chemistry B 3(40) (2015) 7850-7866.
[8] G. Brückner, K. Brauer, W. Härtig, J.R. Wolff, M.J. Rickmann, A. Derouiche, B. Delpech, N. Girard, W.H. Oertel, A. Reichenbach, Perineuronal nets provide a polyanionic, glia-associated form of microenvironment around certain neurons in many parts of the rat brain, Glia 8(3) (1993) 183-200.
[9] D.B. Unal, S.R. Caliari, K.J. Lampe, 3D hyaluronic acid hydrogels for modeling oligodendrocyte progenitor cell behavior as a function of matrix stiffness, Biomacromolecules 21(12) (2020) 4962-4971.
[10] S. Lee, M.K. Leach, S.A. Redmond, S.C. Chong, S.H. Mellon, S.J. Tuck, Z.-Q. Feng, J.M. Corey, J.R. Chan, A culture system to study oligodendrocyte myelination processes using engineered nanofibers, Nature methods 9(9) (2012) 917-922.
[11] S. Lee, S.C. Chong, S.J. Tuck, J.M. Corey, J.R. Chan, A rapid and reproducible assay for modeling myelination by oligodendrocytes using engineered nanofibers, Nature protocols 8(4) (2013) 771-782.
[12] Y. Li, M. Ceylan, B. Shrestha, H. Wang, Q.R. Lu, R. Asmatulu, L. Yao, Nanofibers support oligodendrocyte precursor cell growth and function as a neuron-free model for myelination study, Biomacromolecules 15(1) (2014) 319-326.
[13] N.J. Darling, W. Xi, E. Sideris, A.R. Anderson, C. Pong, S.T. Carmichael, T. Segura, Click by click microporous annealed particle (MAP) scaffolds, Advanced healthcare materials 9(10) (2020) 1901391.
[14] C. Chung, J.A. Burdick, Influence of three-dimensional hyaluronic acid microenvironments on mesenchymal stem cell chondrogenesis, Tissue Engineering Part A 15(2) (2009) 243-254.
[15] K.A. Smeds, M.W. Grinstaff, Photocrosslinkable polysaccharides for in situ hydrogel formation, Journal of Biomedical Materials Research: An Official Journal of The Society for Biomaterials and The Japanese Society for Biomaterials 54(1) (2001) 115-121.
[16] M.E. Prendergast, M.D. Davidson, J.A. Burdick, A biofabrication method to align cells within bioprinted photocrosslinkable and cell-degradable hydrogel constructs via embedded fibers, Biofabrication 13(4) (2021) 044108.
[17] A.D.C. Leonardi, C.A. Bir, D.V. Ritzel, P.J. VandeVord, Intracranial pressure increases during exposure to a shock wave, Journal of neurotrauma 28(1) (2011) 85-94.
[18] C.E. Hampton, P.J. Vandevord, Vibrational frequency response to impact loading of skull models, Biomedical Sciences Instrumentation 48 (2012) 157-164.

[19] J. Schindelin, I. Arganda-Carreras, E. Frise, V. Kaynig, M. Longair, T. Pietzsch, S. Preibisch, C. Rueden, S. Saalfeld, B. Schmid, Fiji: an open-source platform for biological-image analysis, Nature methods 9(7) (2012) 676-682.
[20] T. Villani, Loading and Measurement of Volumes in 3D Confocal Image Stacks with ImageJ, Visikol, 2024.
[21] B.D. Stemper, A.S. Shah, M.D. Budde, C.M. Olsen, A. Glavaski-Joksimovic, S.N. Kurpad, M. McCrea, F.A. Pintar, Behavioral outcomes differ between rotational acceleration and blast mechanisms of mild traumatic brain injury, Frontiers in neurology 7 (2016) 31.
[22] R. Bolander, B. Mathie, C. Bir, D. Ritzel, P. VandeVord, Skull flexure as a contributing factor in the mechanism of injury in the rat when exposed to a shock wave, Annals of biomedical engineering 39 (2011) 2550-2559.
[23] X. Li, E. Katsanevakis, X. Liu, N. Zhang, X. Wen, Engineering neural stem cell fates with hydrogel design for central nervous system regeneration, Progress in polymer science 37(8) (2012) 1105-1129.
[24] S. Shah, P.T. Yin, T.M. Uehara, S.T.D. Chueng, L. Yang, K.B. Lee, Guiding stem cell differentiation into oligodendrocytes using graphene-nanofiber hybrid scaffolds, Advanced materials 26(22) (2014) 3673-3680.
[25] S.M. Moochhala, S. Md, J. Lu, C.-H. Teng, C. Greengrass, Neuroprotective role of aminoguanidine in behavioral changes after blast injury, Journal of Trauma and Acute Care Surgery 56(2) (2004) 393-403.
[26] K. Kato, M. Fujimura, A. Nakagawa, A. Saito, T. Ohki, K. Takayama, T. Tominaga, Pressure-dependent effect of shock waves on rat brain: induction of neuronal apoptosis mediated by a caspase-dependent pathway, Journal of neurosurgery 106(4) (2007) 667-676.
[27] J. Flygt, K. Ruscher, A. Norberg, A. Mir, H. Gram, F. Clausen, N. Marklund, Neutralization of interleukin-1β following diffuse traumatic brain injury in the mouse attenuates the loss of mature oligodendrocytes, Journal of neurotrauma 35(23) (2018) 2837-2849.
[28] J. Flygt, A. Gumucio, M. Ingelsson, K. Skoglund, J. Holm, I. Alafuzoff, N. Marklund, Human traumatic brain injury results in oligodendrocyte death and increases the number of oligodendrocyte progenitor cells, Journal of Neuropathology & Experimental Neurology 75(6) (2016) 503-515.

Chapter 6: Outlook and Next Steps

6.1 Introduction

Previous chapters have demonstrated a variety of novel results. In Chapter 3, we discovered that inclusion of electrospun fiber cues prompts glioma-derived OPCs to undergo morphological changes associated with cell maturation, and that these changes occurred at the expense of differentiation. Chapter 4 demonstrated that NSCs in the presence of fibers undergo similar morphological changes, with differentiation occurring primarily towards a neuronal cell fate. Unlike with OPCs, NSC proliferation continued in + fiber gels, suggesting some fraction of the NSC population remains proliferative in the presence of fibers. Both NSCs and OPCs were found to secrete ECM proteins laminin and fibronectin, with minimal differences between the + fiber and – fiber conditions. Chapter 5 demonstrated that exposure to mechanical insult in the range of mild TBI had minimal impact on OPC viability, proliferation or differentiation.

While these results have expanded our understanding of neural cell behavior within our hydrogel system, these findings have also raised a number of questions, prompting several opportunities for future work. Areas of further investigation fall into three general categories: material characterization, cell-related experiments, and assessment of cell-material interactions.

6.2 Material characterization

Many design aspects of our hydrogel system, such as material stiffness and fiber diameter, were tuned to accurately reflect the characteristics of native brain tissue. However, our model system deviates from in vivo conditions in terms of fiber density. The human brain is estimated to have around 85 billion neurons in total, with an estimated 16 billion located in the cerebral cortex and 69 billion in the cerebellum [1, 2]. Given that brain volume in humans tends to be around 1,130 cm3 in females and 1,260 cm3 in males, this leads to an average density of between 6.7-7.5 x 107 axons/cm3, with the cerebellum being more dense (5.5-6.1 x 108 axons/cm3) and the cerebral cortex being less dense (1.6-1.7 axons/cm3) [2, 3]. By contrast, fibers in our system are included at a markedly lower density. While it is exciting to observe that cells respond to fiber presence even at such low fiber concentrations, future experiments could test the effects of incorporating fibers at a higher concentration more representative of axon density in native tissue. Alternatively, a related experiment could be conducted by lowering the fiber density to determine the cutoff below which cells no longer exhibit morphological changes.

Rheological characterization has previously demonstrated that the inclusion of fibers consistently increases storage modulus (Chapters 3-5). However, it remains unknown whether MeHA fibers are crosslinking to the surrounding hydrogel mesh. In theory, UV crosslinking could be occurring between the thiol crosslinkers in the NorHA system and the methacrylate groups on the MeHA fibers. One possible way to investigate the extent of gel-fiber crosslinking would be to cap the methacrylate groups on the MeHA fibers with a small molecule following electrospinning. Previous studies have used Michael addition to react methacrylate groups with cysteines [4, 5]. Similar methods could be used to prevent thiol methacrylate interactions within our system. Modifying the electrospinning solution to spin NorHA fibers instead of MeHA would provide an alternate fiber type known to crosslink with the surrounding hydrogel through thiol-ene reactions. Comparing rheological properties of hydrogels containing encapsulated MeHA,

MeHA-cysteine, and NorHA fibers could illuminate whether the uncapped MeHA fibers used previously have crosslinked to the surrounding gel.

Finally, with regard to Chapter 5, we observed that blast overpressure in the range of mild TBI did not have a significant impact on mechanical properties of the overall hydrogel system. However, it is plausible that more severe blast impacts could cause fragmentation of the fibers. Future experiments could use brightfield or fluorescent confocal microscopy to observe fiber morphology pre- vs post-blast and determine whether fiber structure changes as a result of overpressure exposure.

6.3 Cell-related experiments

In Chapters 3 and 4, we observed an increase in normalized phalloidin signal area for cells grown in + fiber gels. This increase in signal area was attributed to cell process extensions in fiber-containing gels; however, cell spreading and loss of proliferation ability can also be a hallmark of cell senescence [6]. Our results are not likely to be due to senescence, as we have seen no other hallmarks of senescence (e.g. no formation of large vacuoles, no proliferation losses for NSC). Additionally, our OPC cell line contains gene knockouts known to impar cell senescence [7]. However, conducting a beta-galactosidase activity assay would be a straightforward way to prove senescence is not occurring within our cultures [8].

Both NSCs and OPCs are known to migrate in vivo; however, the movement of OPCs within our in vitro cultures has not yet been investigated. Previous work with 1.5% NorHA gels has indicated that mesh sizes are large in comparison with other hydrogel types, potentially allowing for OPC migration through the gel [9]. The Kucenas lab at UVA has previously used spinning disk confocal microscopy to conduct time-lapse imaging of OPC migration in zebrafish [10]. Applying a similar protocol to NSCs in our hydrogel system could be used to track cell movement and determine if migration is occurring within our cultures.

One particularly exciting prospect for our material system is to monitor myelination of our fibers by fully differentiated OLs. Previous work in Chapters 3 and 4 has shown that fiber cues prompt NSC and OPC maturation. However, we have not achieved full differentiation of cells into mature myelinating oligodendrocytes. Previous literature has used differentiation media to generate OPCs from neural stem cells within 4-6 days, and myelinating OLs from OPCs within 18 days [11, 12]. Taking inspiration from these protocols, culture media could be used to guide our NSCs to fully differentiate into myelinating OLs. Electron microscopy could then be used to determine the extent of myelination in our system [13] .

Another easy and straightforward next step would be to repeat the NanoString experiments from Chapter 4 using our OPC cells. Such an experiment could be used to determine the effects of fiber cues on OPC maturation and cell fate. Upon generating a PPI, PageRank or manual weighting methods could be used to determine which genes are most strongly involved in the OPC interaction network, and what biological processes are most likely to be implicated. Finally, this new OPC data could be compared with our NSC data from chapter 4 to determine similarities and differences between the two cell types. A similar experiment (potentially utilizing the NanoString neuroinflammation panel) could be used to determine the impacts of blast on OPCs.

6.4 Cell-material interactions

Immunostaining experiments in Chapters 3 and 4 demonstrated that both NSCs and OPCs secreted laminin and fibronectin to remodel their local microenvironments. Having determined that cells are depositing ECM proteins, a pertinent next step would be to probe how cell-ECM interactions affect cell behavior within the hydrogels. Future experiments in this area could include an extension of the immunostaining assay with additional timepoints. Since both processes and ECM deposition were present at culture day 5, our previous data did not show which came first. The addition of earlier timepoints to our immunostaining experiment could help determine whether process extensions occurred before ECM deposition, or vice versa. To investigate cell-ECM interactions, we could use function-perturbing antibodies to block interactions with secreted proteins as in Loebel et al [14]. By comparing the behavior of antibody-blocked cells to that of cells allowed to interact with ECM, we could determine the impact of cell-ECM interactions on cell behavior. Additionally, while we were able to label nonspecific deposition of ECM in OPCs, NSCs did not label well using this assay. An alternative approach for labeling has been conducted using sugar analogues which may provide an alternative means of nonspecifically labeling secreted ECM by NSCs [15].

The interaction between cells and fibers is also worthy of further investigation. Previous research in 2D has shown that in the absence of neuronal activity, OPCs will preferentially myelinate based on fiber diameter [16]. By varying our electrospinning parameters, we could produce MeHA fibers of different diameters to determine the effects of fiber diameter on cell behavior in 3D. Additionally, we could begin to perturb neuronal activity-dependent maturation, differentiation and myelination by constructing a co-culture system containing both NSCs/OPCs and neurons. Similar 2D coculture studies have been conducted previously, as in Chen et al; we could potentially use a similar approach to compare cell response to electrospun fibers vs. neurons under 3D conditions [17]. Finally, since our fibers have been shown to prompt morphological changes in neural cells, encapsulation of fibers alongside another cell type (e.g. fibroblast) could be a quick way to determine whether fiber presence impacts the morphology of non-neural cells. One previous 2D study found that fibroblasts seeded atop electrospun fibers showed increased cell area with increased fiber diameter [18]. We could apply our materials system to recreate this experiment in a 3D context.

Viscoelasticity is another factor with the potential to affect cell behavior. Native ECM is known to be viscoelastic, while our covalently crosslinked NorHA system is more elastic. Previous work by the Caliari group has utilized NorHA gels containing a secondary physical crosslinking system composed of adamantane and β-cyclodextrin in addition to the primary thiol-ene crosslinking system [19, 20]. The reversible nature of the physical crosslinking network allows the NorHA system to better reflect viscoelastic properties of native ECM. Modifying our hydrogel system in such a way would allow us to probe the role of viscoelasticity on NSC and OPC viability and differentiation.

Lastly, while we did not engineer any additional cell adhesion motifs (e.g. RGD) into our hydrogel system, cells could potentially be interacting with HA in the system through CD44 interactions. CD44, a cell surface receptor for hyaluronic acid, is known to be expressed by both NSCs and OPCs, and is involved in various cell behaviors such as adhesion and migration [21, 22]. However, as yet the role of CD44 interactions in our materials system remains unexplored. Methods such as antibody blocking or CD44 gene knockout have previously been used in

literature to prevent CD44 interactions [22, 23]. By comparing antibody-blocked or CD44 knockout cells to control cells capable of interacting with CD44, we can determine the effects of CD44 interactions on NSC and OPC behavior in our hydrogel system.

Overall, the work performed in this thesis represents an exciting step forward in developing a tunable 3D in vitro system for determining the role of environmental factors on NSC/OPC growth, viability and differentiation. It also lays the groundwork for a wide variety of future investigations and applications, spanning de novo myelination modeling, TBI simulation, and cell-ECM interactions. Moving forward, this model has the potential to enhance our understanding of fundamental NSC and OPC biology or pave the way for advanced therapies targeting CNS diseases or injuries.

6.5 References

[1] C.S. Von Bartheld, J. Bahney, S. Herculano-Houzel, The search for true numbers of neurons and glial cells in the human brain: A review of 150 years of cell counting, Journal of Comparative Neurology 524(18) (2016) 3865-3895.
[2] S. Herculano-Houzel, The human brain in numbers: a linearly scaled-up primate brain, Frontiers in human neuroscience 3 (2009) 857.
[3] K.P. Cosgrove, C.M. Mazure, J.K. Staley, Evolving knowledge of sex differences in brain structure, function, and chemistry, Biological psychiatry 62(8) (2007) 847-855.
[4] Y.G. Kareem, S. Rachid, O. Al-Jaf, Synthesis and characterization of novel poly cysteine methacrylate nanoparticles and their morphology and size studies, RSC advances 14(19) (2024) 13474-13481.
[5] A.M. Alswieleh, N. Cheng, I. Canton, B. Ustbas, X. Xue, V. Ladmiral, S. Xia, R.E. Ducker, O. El Zubir, M.L. Cartron, Zwitterionic Poly (amino acid methacrylate) Brushes, Journal of the American Chemical Society 136(26) (2014) 9404-9413.
[6] A. Biran, L. Zada, P. Abou Karam, E. Vadai, L. Roitman, Y. Ovadya, Z. Porat, V. Krizhanovsky, Quantitative identification of senescent cells in aging and disease, Aging cell 16(4) (2017) 661-671.
[7] P.P. Gonzalez, J. Kim, R.P. Galvao, N. Cruickshanks, R. Abounader, H. Zong, p53 and NF 1 loss plays distinct but complementary roles in glioma initiation and progression, Glia 66(5) (2018) 999-1015.
[8] F. Debacq-Chainiaux, J.D. Erusalimsky, J. Campisi, O. Toussaint, Protocols to detect senescence-associated beta-galactosidase (SA-βgal) activity, a biomarker of senescent cells in culture and in vivo, Nature protocols 4(12) (2009) 1798-1806.
[9] D.B. Unal, S.R. Caliari, K.J. Lampe, 3D hyaluronic acid hydrogels for modeling oligodendrocyte progenitor cell behavior as a function of matrix stiffness, Biomacromolecules 21(12) (2020) 4962-4971.
[10] M.F. Ali, A.J. Latimer, Y. Wang, L. Hogenmiller, L. Fontenas, A.J. Isabella, C.B. Moens, G. Yu, S. Kucenas, Met is required for oligodendrocyte progenitor cell migration in Danio rerio, G3 11(10) (2021) jkab265.
[11] S. Li, J. Zheng, L. Chai, M. Lin, R. Zeng, J. Lu, J. Bian, Rapid and efficient differentiation of rodent neural stem cells into oligodendrocyte progenitor cells, Developmental Neuroscience 41(1-2) (2019) 79-93.
[12] A. Barateiro, A. Fernandes, Temporal oligodendrocyte lineage progression: in vitro models of proliferation, differentiation and myelination, Biochimica et Biophysica Acta (BBA)-Molecular Cell Research 1843(9) (2014) 1917-1929.

[13] M.-T. Weil, T. Ruhwedel, M. Meschkat, B. Sadowski, W. Möbius, Transmission electron microscopy of oligodendrocytes and myelin, Oligodendrocytes: Methods and protocols (2019) 343-375.
[14] C. Loebel, R.L. Mauck, J.A. Burdick, Local nascent protein deposition and remodelling guide mesenchymal stromal cell mechanosensing and fate in three-dimensional hydrogels, Nature materials 18(8) (2019) 883-891.
[15] C. Loebel, M.Y. Kwon, C. Wang, L. Han, R.L. Mauck, J.A. Burdick, Metabolic labeling to probe the spatiotemporal accumulation of matrix at the chondrocyte–hydrogel interface, Advanced functional materials 30(44) (2020) 1909802.
[16] S. Lee, M.K. Leach, S.A. Redmond, S.C. Chong, S.H. Mellon, S.J. Tuck, Z.-Q. Feng, J.M. Corey, J.R. Chan, A culture system to study oligodendrocyte myelination processes using engineered nanofibers, Nature methods 9(9) (2012) 917-922.
[17] Z. Chen, Z. Ma, Y. Wang, Y. Li, H. Lü, S. Fu, Q. Hang, P.-H. Lu, Oligodendrocyte–spinal cord explant co-culture: An in vitro model for the study of myelination, Brain research 1309 (2010) 9-18.
[18] C.A. Bashur, L.A. Dahlgren, A.S. Goldstein, Effect of fiber diameter and orientation on fibroblast morphology and proliferation on electrospun poly (D, L-lactic-co-glycolic acid) meshes, Biomaterials 27(33) (2006) 5681-5688.
[19] E. Hui, K.I. Gimeno, G. Guan, S.R. Caliari, Spatiotemporal control of viscoelasticity in phototunable hyaluronic acid hydrogels, Biomacromolecules 20(11) (2019) 4126-4134.
[20] E. Hui, L. Moretti, T.H. Barker, S.R. Caliari, The combined influence of viscoelastic and adhesive cues on fibroblast spreading and focal adhesion organization, Cellular and molecular bioengineering 14(5) (2021) 427-440.
[21] M. Naruse, K. Shibasaki, S. Yokoyama, M. Kurachi, Y. Ishizaki, Dynamic changes of CD44 expression from progenitors to subpopulations of astrocytes and neurons in developing cerebellum, PLoS one 8(1) (2013) e53109.
[22] W. Su, S.C. Foster, R. Xing, K. Feistel, R.H. Olsen, S.F. Acevedo, J. Raber, L.S. Sherman, CD44 transmembrane receptor and hyaluronan regulate adult hippocampal neural stem cell quiescence and differentiation, Journal of biological chemistry 292(11) (2017) 4434-4445.
[23] L. Bian, M. Guvendiren, R.L. Mauck, J.A. Burdick, Hydrogels that mimic developmentally relevant matrix and N-cadherin interactions enhance MSC chondrogenesis, Proceedings of the National Academy of Sciences 110(25) (2013) 10117-10122.

Appendix A: High-rate mechano-stimulation alters maturation signaling of oligodendrocyte precursor cell in 3D platform

Ryosuke Yokosawa[1], Rachel A. Mazur[2], Kelsey Wilson[1], Jake Lee[1], Noah Showalter[1], Kyle J. Lampe[2], Pamela VandeVord[1]

1 Department of Biomedical Engineering and Mechanics, Virginia Polytechnic Institute and State University, Blacksburg, VA USA

2 Department of Chemical Engineering, University of Virginia, Charlottesville, VA USA

7.1 Abstract

Traumatic brain injury (TBI) causes glial reactivity leading to neuroinflammation, a potential trigger of neurodegeneration. *In vitro* platforms are key for the study of fundamental mechanisms of cell responses to mechanical insults. Tissue damage is known to activate oligodendrocyte precursor cells (OPCs) to migrate, proliferate, and differentiate into oligodendrocytes (OL) to support the function of neuronal activities and brain recovery. OPCs are a potential therapeutic target as their functions of proliferation, and differentiation can help regenerate OL loss after TBI. However, how OPC responds to the mechanical insult is poorly understood. This study utilizes an *in vitro* 3D platform to probe the changes in metabolic- and maturation-related molecules of OPCs. The 3D platform is built by encapsulating OPCs in a hydrogel consisting of norbornene-modified hyaluronic acid (NorHA), creating a brain-like microenvironment. To simulate brain injury, a shock wave generator was used to generate the mechanical insult exposing 3D OPC microtissues to a high-rate overpressure (19.08 ± 6.53 psi for 1.092 ± 0.351 msec). Material characterization of NorHA hydrogel quantified that the storage moduli of OPC-containing gels were lower at all concentrations compared to no cell condition. Overpressure had little effect on OPC-containing gels, and storage moduli increased on the hydrogel without cells for lower NorHA concentrations (1% and 1.5%). Cell viability averaged 91.67±6.14% across all experimental conditions and the overpressure insult did not affect acute cell death. We quantified spheroid volume as a proxy for cell proliferation using an image analysis of OPC fluorescence. Total spheroid volume and average spheroid volume did not significantly change due to overpressure insult. Relative OPC metabolic activity, as measured via ATP normalized to DNA, indicated a significant increase for mechanostimulated samples on day 9. Gene expressions of OPC maturation markers (PDGFRA, GPR17, GALC, and CNP) for mechanostimulated microtissues showed a trend of upregulations (7.7%-61.0%) for all markers on day 1, and PDGFRA increased significantly on day 1 after overpressure insult. Protein expression of GPR17 was significantly downregulated on day 9 of both sham and post-overpressure samples compared to the day 1 sham and post-overpressure samples. GALC protein expression significantly increased on day 9 of both sham and post-overpressure samples when compared to day 1 of both sham and post-overpressure samples. Overall, this study successfully

demonstrated the molecular (ATP, DNA, maturation markers) changes of OPC after overpressure insult. These findings opened up potential future research directions of OPC response after mechanical insult including inflammatory response from neuronal- and non-neuronal cells, and mechanotransduction signaling molecules. Further investigation of OPC response after mechanical insult is necessary to advance the use of OPC as a therapeutic application for patients with neurodegenerative diseases.

7.2 Introduction

In vitro models of traumatic brain injury (TBI) aid in investigating injury mechanisms by studying specific cellular responses to a high-rate overpressure mechanical insult. Neurons are known to be particularly susceptible to mechanical insults [Kermer 1999, Slemmer 2008]. However, the study of glial cell response following mechanical insults without interaction of inflammatory molecules is limited [Clark 2021, Hernandez 2018, Dickerson 2020]. Neurodegeneration following TBI has been correlated to a loss of myelin and oligodendrocytes (OL) likely caused by neuroinflammation [Wolswijk 2000, Mahoney 2022]. Recent research suggests that proliferation and differentiation of oligodendrocyte progenitor cells (OPC) can be a potential therapeutic target to promote remyelination [Flygt et al 2016, 2013, Li et al 2018]. However, the fundamental cell responses of OPC after mechanical insult are understudied [Mahoney 2022, Dent 2015, Huntemer-Silveira 2020]. To further elucidate the underlying cellular response to an applied mechanical insult, OPC response needs an investigation.

Differentiation of OPC after migration and proliferation to the injured brain region is a key process of tissue recovery. The OPC differentiation into OL has been investigated and reviewed based on protein and gene expressions such as platelet-derived growth factor receptor alpha (PDGFRA), G-protein-coupled receptor 17 (GPR17), galactosylceramidase (GALC), and 2', 3'-cyclic nucleotide 3'-phosphodiesterase (CNPase) [Takase 2018, Dent 2015, Kuhn 2019, Fumagalli 2011] (Figure 7.1). PDGFRA, expressed on the cell membrane, is an early marker of OPC to indicate the ongoing proliferation process [Marques 2016, Li 2017, Zhang 2014, Sy 2020, Falcao 2018, Zhang 2021]. GPR17 is a membrane protein that its expression increases to inhibit the maturation process of OPC as the cell entering a maturation phase [Marques 2016, Zhang 2014, Fumagalli 2011, Ceruti 2011, Satoh 2017, Boda 2011]. GALC is a glycolipid protein that is observed in myelinating OL [Casamassa 2016, Sy 2020, Marei 2018, Wang 2019, Pennati 2020, Ehrlich 2017, Narine 2022]. CNP is an enzyme that is fundamental to constructing myelin sheath, which is observed along with myelin basic protein (MBP) [Zhang 2021, Wang 2018, Zou 2014, Hou 2018, Egawa 2022, Casamassa 2016, Snaidero 2016]. Previous *in vitro* study demonstrated that a sudden chemical stimulation of the exogenous PDGF-AA promotes the OPC differentiation [Pinezich 2018]. These molecules are feasible molecular targets to investigate the maturation process of OPC.

Innovation into 3D *in vitro* models is an important step to investigate OPC-focused cell response to mechanical insult by excluding other biological and chemical factors involved in a brain

tissue. The use of a hydrogel system provides a more physiologically relevant environment for cell response as compared to the traditional 2D cultures. This advancement is necessary to replicate the in vivo response more accurately [Solbu 2022, Mazur 2022, Zhao 2020, Cho 2018]. One of the advantages using the hydrogel is to mimic the storage modulus of a native brain tissue with the extracellular matrix (ECM) between 0.2 and 2 kPa [Unal 2020]. This is vital as cell responses and reactivities are significantly affected by their environmental cues [Mazur 2022].

Nor-amine added hyaluronic acid (NorHA) hydrogels are of particular interest for neurological tissue engineering applications, since HA is a key component of brain extracellular matrix (ECM), particularly within the perineural net [Sugitani 2021]. NorHA hydrogels have mechanical properties which can be easily tuned through thiol-norbornene chemistry and are able to replicate stiffnesses equivalent to that of native brain tissue [Gramlich 2013, Unal 2020]. Previous studies have introduced the benefits of a NorHA hydrogel system for OPC culture that is capable of minimizing the hydrogel volume expansion and maintained a high viability of OPCs cultured up to 7 days. Cells activity was reflected by measuring the cell population growth and the cell metabolic activity. Assessment of cell population growth after mechanical insult is fundament of this study to quantify how mechanical insult affects the proliferation of OPCs. As demonstrated by Unal et al, the proliferation of cells is quantified by total cell volume and DNA concentration within a hydrogel [Unal 2020]. Metabolic aberration is one of the indicators for a cell response after mechanical insult. In previous *in vitro* TBI studies using astrocytes demonstrated the aberration in ATP concentration after insult [Hlavac 2019, Hlavac 2021]. Therefore, implementing the NorHA hydrogel OPC culture system has the potential to be a valuable platform for translational studies of OPC response to a mechanical insult.

In this study, we investigated cell responses of OPC encapsulated in NorHA system after applied high-rate mechanical insult for potential metabolic changes and corresponding cell differentiation. Our results will address the OPC responses after mechanical insult and help future studies to identify potential molecular targets that promote OPC proliferation and maturation following TBI.

7.3 Materials and methods

7.3.1 OPC culture

The MADM OPC line utilized for these experiments was developed by Zong et al [Zong 2005, Muzumdar 2007, Liu 2011]. A T75 tissue culture flask surface (Falcon) was treated with 10 µg/mL polyornithine (Sigma) then rinsed three times with Dulbecco's phosphate buffered saline (DPBS). OPC were cultured in Dulbecco's modified Eagle's medium (DMEM) with 4.5 mg/L D-Glucose and 110 mg/L sodium pyruvate (Life Technologies) supplemented with N2 supplement (Life), B27 supplement (Thermo), and 1% penicillin-streptomycin (Thermo). Frozen OPC vial ($1x10^6$ cells per vial) was thawed in a water bath at 37 °C. $0.5x10^6$ cells were plated

per flask with 5 mL of growth media. Media was changed every two days until the confluency reached 80 %. Cell passage number between 20 and 30 was used for this study.

7.3.2 OPC encapsulated hydrogels

NorHA hydrogel material was synthesized and characterized by following the previously reported protocol by Unal et al [Unal 2020]. To mimic the brain tissue stiffness, 1.5 % NorHA concentration was selected based on the previously characterized storage modulus (793.9 ± 203.3 Pa) [Unal 2020]. The hydrogel precursor solution was prepared to a final concentration of 1.5 % NorHA by combining 9 mg/mL NorHA, 6 mg/mL of dithiothreitol (DTT, Sigma), and 23 mM lithium phenyl-2,4,6-trimethylbenzoylphosphonate photoinitiator (LAP, sigma). Lyophilized Nora was sterilized with UV irradiation for 20 min in a biosafety cabinet before use. All materials were solubilized and diluted in DPBS as a stock solution prior to formulation of the hydrogel. The cell suspension was combined with the premixed solution at a final concentration of $5x10^6$ cells/mL, then LAP was added at the end to initiate the polymerization. The 1 mL BD Disposable Syringes with Luer-Lok™ Tips (BD) was used as a hydrogel mold. 40 µL of the hydrogel solution (200,000 cells per gel) was added to the syringe. The syringe was vertically placed under the UV chamber and then polymerized by exposing it to 365 nm UV light at 4 mW/cm^2 for 2 min. OPC encapsulated hydrogels were collected from the syringes and then rinsed three times in DPBS. Hydrogels were incubated in the OPC growth media for 5 days with replacing the media every other day until the day of the experiment.

7.3.3 Mechanical insult testing

A shock wave generator (SWG) was used for the high rate overpressure experiment (Figure 7.2). The SWG device has been shown to mimic intracranial pressure found within the rodent brain exposed to an overpressure wave [Hampton 2012; Leonardi 2011]. The SWG was filled with warm distilled water at 37 ℃ during the time of testing. The SWG uses a bridging-wire detonation system that generates a single shock wave by applying a high voltage through a thin metal wire. (Figure 7.2A) For this study, two wire materials, nichrome wire (0.003 in diameter, Part# 40BNC, Consolidated Electronic Wire & Cable) and silver wire (0.005 in diameter, Cat#: 000303-G5, ThermoFisher). These wires evaporated following the applied high voltage which created a single shock wave with a peak pressure range of 19.08 ± 6.53 psi for the whole experiment. The range of peak pressure was previously reported to mimic mild TBI pathophysiology [Logsdon 2020, Dickerson 2020, Norris 2023]. The applied overpressure was measured by a piezoelectric pressure sensor (PCB Piezotronics Inc., Model 113B21, Depew, NY, United States) mounted above where the sample is located in the chamber (Figure 7.2B).

OPC encapsulated hydrogels were exposed to the applied overpressure on day 5 of cell culture after encapsulation. Two gels were placed in each well of a 6-well cell culture plate (Thermo), a total of 12 gels per plate. DMEM without supplements was added to fill the plate and parafilm was tightly sealed over the plate to exclude bubbles to allow overpressure propagation. The test plate was tightly attached to the plate holder (Figure 7.2C) and submerged

in the SWG chamber. OPC encapsulated hydrogels were exposed to a single insult and then retrieved from each well and transferred to a 24-well plate (Thermo) with 1 mL of DMEM with supplements per well. Sham samples were prepared by following the same steps without the overpressure exposure. Gels were incubated for 1 or 9 days after the exposure. The media was replaced every day until the day of sample collection.

Overpressure data were collected at 1MHz on a Dash 8HF-HS system (Astro-Med, Inc., West Warwick, RI United States) with a 4-channel signal conditioner (PCB Piezotronics Inc., Model 482C05, Depew, NY, United States). Acquired data were analyzed and visualized in MATLAB (R2021b, The MathWorks Inc., Natick, MA, United States) where average peak pressure, rise time, positive duration, and positive impulse were reported.

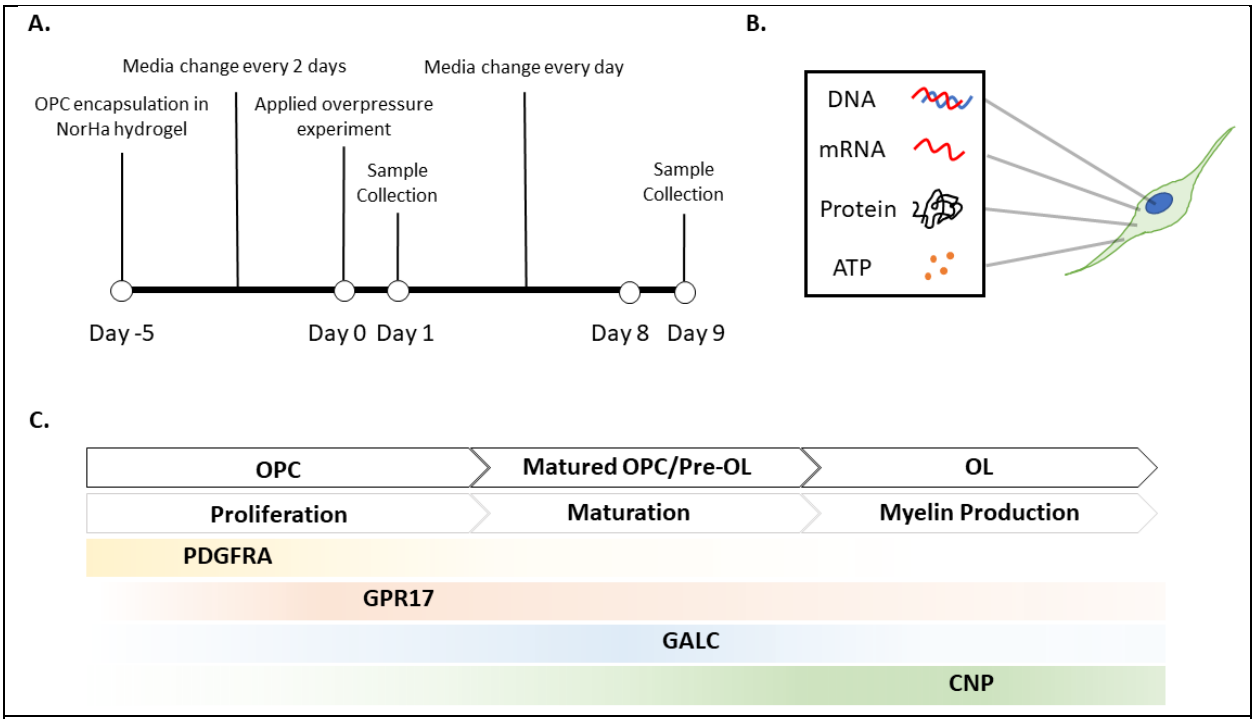

Figure 7.1. Experiment timeline, collected molecules, and OPC to OL maturation process with targeted molecules. **(A)** Day -5: OPC encapsulation in NorHA hydrogel; Day -4 to -1: Cell culture in OPC growth media and the media was replaced every two days; Day 0: Applied overpressure cell injury experiment; Day 1: Sample collection; Day 2 to 8: Continued cell culture in OPC growth media and the media was replaced daily; Day 9: Sample collection. **(B)** Molecular targets to investigate OPC responses after mechanical insult. **(C)** Potential cell maturation process, cell responses at each cell type, and potential maturation markers expressed at each cell type.

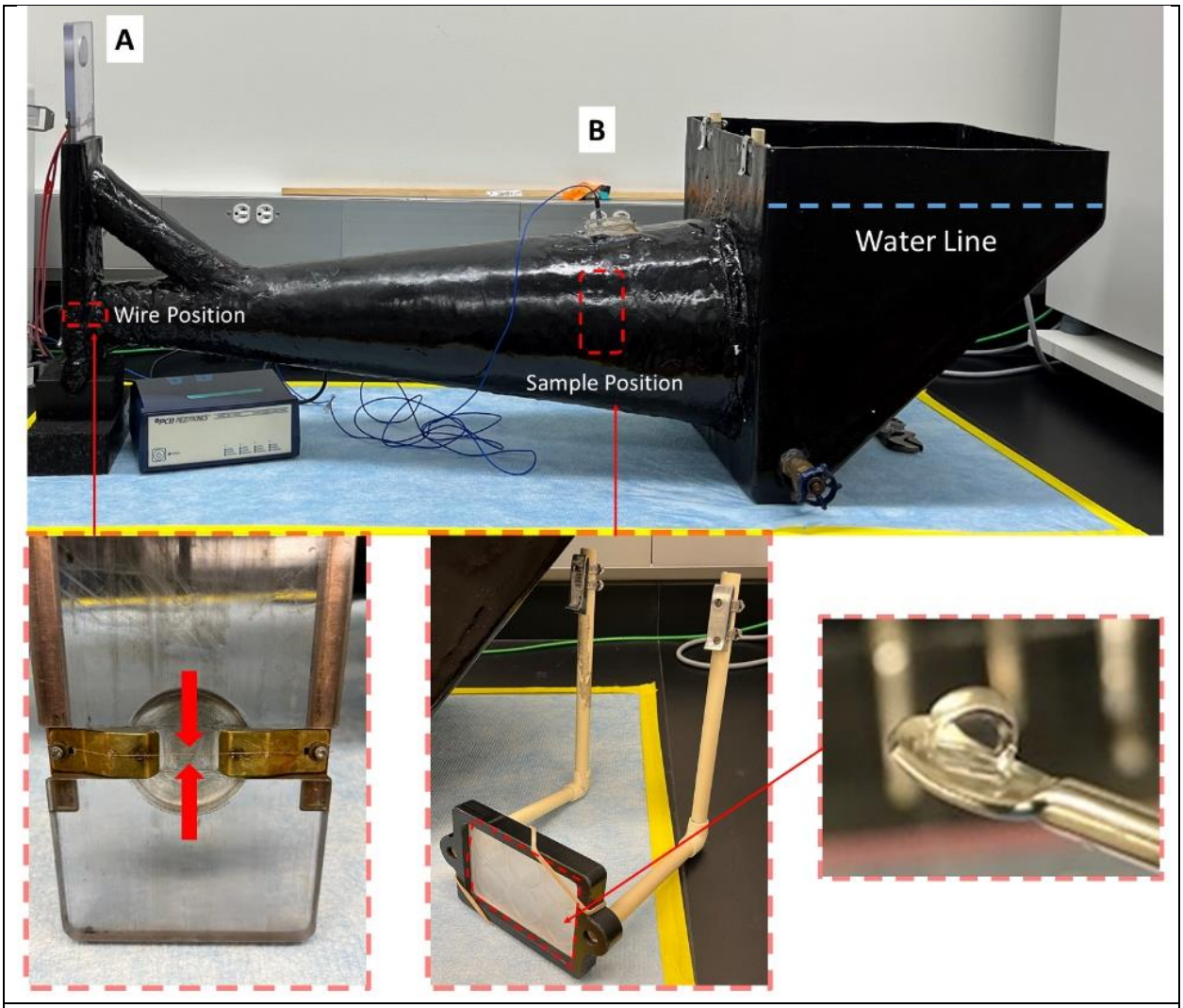

Figure 7.2. Shock Wave Generator (SWG) system for an *in vitro* applied overpressure injury experiment. **(A)** Bridging-wire detonation board with loaded thin metal wire. Thin metal wire was fixed on the board. **(B)** A pressure sensor was mounted above where the samples were located (red dashed line square). Sensor was placed with flush mounting protocol, which the sensor surface is placed exactly on the inner surface of the SWG chamber, orthogonally to the well plate. Water line was annotated with the blue dashed line. Cell culture plate was sealed with a parafilm and then tightly fixed to the plate holder with a rubber band on the corner to ensure the plate stays after applied overpressure. OPC encapsulated hydrogel was placed in each well of the 6-well plate.

7.3.4 NorHA Hydrogel Characterization: Oscillatory Shear Rheology

OPC encapsulated hydrogels at 1, 1.5 and 2wt% NorHA were grown in culture for 5 days, following which they were exposed to either mechanically tested or sham conditions. Material properties of the hydrogel were then assessed via shear rheology. Premade gels were placed onto an Anton Paar MCR 302 rheometer, and an 8 mm diameter parallel plate insert was

used to conduct oscillatory frequency sweeps with gap height 1.6 mm, oscillatory strain 0.1%, and angular frequency ranging from 0.1-10 rad/s.

7.3.5 Cell Viability Assay

The viability of OPC in the NorHA hydrogel was quantified using the LIVE/DEAD™ Viability/Cytotoxicity Kit (Thermo). On day 1 or day 9 post-overpressure, three gels from each of the overpressure and sham samples were collected and a Live/Dead staining was performed (n = 3 per condition per experiment). Briefly, the hydrogels were rinsed in the DPBS, then placed in 1 mL of DMEM without phenol red (Thermo). Live cells were imaged for the GFP expression on the MADM OPCs, and dead cells were stained with a 4 µM ethidium homodimer 1 (EthD1) with incubation at 37 °C for 30 min followed by rinsing twice with DPBS. Live/Dead images were captured using a Zeiss LSM800 MA-Pmt2 confocal microscope with 300-600 µm z-stacks at 5 µm slices using the 10x objectives. Three regions of interests (ROIs) were selected for each gel in between the center and edge of the hydrogel. Images were analyzed in ImageJ using the 3D Object Counter plugin.

7.3.6 Metabolic Activity Assay

OPC cytosolic adenosine triphosphate (ATP) activity was quantified using the CellTiter-Glo® 2.0 Cell Viability Assay (Promega Corporation, Madison, WI, United States). Hydrogel samples were collected in 400 µL of Passive Lysis 1X Buffer (Promega Corporation, Madison, WI, United States) diluted in DPBS. Samples were homogenized using the Disposable Pellet Mixer (VWR) and sonicated three times at 40 J for 10 seconds. The ATP standard was prepared by diluting Adenosine 5'-triphosphate (ATP) disodium salt hydrate (MilliporeSigma, Rockville, MD, United States) from 0 to 9000 ng/µL. A white 384-well plate (Thermo) was used for the assay. Each standard (20 µL/well) and sample (5 µL/well) was tested in triplicate wells. Once all standards and samples were placed in the well plate, 20 µL of the CellTiter-Glo® 2.0 reagent was added to initiate a reaction. The 384-well plate was incubated at room temperature for 10 min in the dark, and luminescence was measured using a SpectraMax M2e microplate reader (Molecular Devices, LLC., San Jose, CA, United States). A standard curve was obtained then the luminescent optical density (OD) value was converted to ATP concentrations [ng/µL].

7.3.7 Double stranded DNA quantification

Double stranded DNA (dsDNA) concentration was measured by fluorescent nucleic acid stain using Quant-iT™ PicoGreen™ dsDNA Assay Kits (Thermo Fisher Scientific Inc., Waltham, MA, United States) that includes Quant-iT™ PicoGreen™ dsDNA Reagent (fluorescent dye), 20X TE (200 mM Tris-HCl, 20 mM EDTA, pH 7.5), and Lambda DNA standard. 20X TE buffer was diluted to 1X TE buffer in UltraPure™ DNase/RNase-Free Distilled Water. Hydrogel samples were homogenized as previously described. DNA standard dilution was prepared from 0 to 1000 ng/µL concentrations in 1X TE buffer. A black 384-well plate (Thermo) was used for the assay. 20 µL of standard dilutions were added to each well. 5 µL

samples were added to each well then diluted with 15 µL 1X TE buffer. All samples and standards were prepared in triplicates. Once all samples and standards were in place, 20 µL Quant-iT PicoGreen™ dsDNA Reagent was added to the wells to initiate a reaction. The well-plate was incubated for 10 min at room temperature in dark. Samples were excited at wavelength at 480 nm, and then the fluorescence emission intensity at 525 nm was measured in a SpectraMax M2e microplate reader. A standard curve was determined, and fluorescence OD values were converted to DNA concentrations [ng/µL].

7.3.8 Spheroid analysis

Spheroid volumes of OPC in hydrogel were quantified using Live/Dead confocal images in the 3D Object Counter plugin in ImageJ. Live (GFP) and Dead (EthD1) cell images were separately analyzed. The 3D Object Counter computed each spheroid volume by connecting the voxels (64.5 nm X 64.5 nm X 200 nm per voxel) within one spheroid, and the number of spheroids in a hydrogel on each ROI was counted. Total spheroid volume was calculated by adding the volume of all spheroids per ROI then three ROI data were averaged to estimate the total volume per ROI in each hydrogel. Mean spheroid volume was calculated by averaging the volume of all spheroids in each ROI, then averaging for three ROIs per hydrogel. The total and mean spheroid volumes of each ROI were calculated for overpressure and sham conditions at each time point. In addition, the occupation ratio of the spheroid within each ROI of the hydrogel was analyzed by normalizing the total spheroid volume to the hydrogel volume at each ROI (638.9 µm x 638.9 µm x z stack slices x 5 µm). The minimum number of voxels was limited to 20 to exclude detected fragments below the single cell volume for all analyses. Three confocal image stacks were taken per sample. Three samples for each overpressure and sham conditions were analyzed from each time point. Four overpressure experiments were conducted, including 12 samples per condition per time point.

7.3.9 RNA and total protein extraction

Samples were collected on days 1 and 9 post overpressure stored in 600 µL Trizol reagent (Thermo) at -80 ℃ until sample processing. Samples were homogenized as described in a previous section. RNA was separated from the sample by adding 120 µL chloroform to the 600 µL lysate, the sample was then vigorously shaken by hand then incubated at room temperature for 2 min. RNA was isolated from the homogenized cell lysates, then RNA was purified using the PureLink™ RNA Mini Kit (Thermo) following the manufacturer's instruction. Purified RNA was extracted and measured with the NanoDrop™ One/OneC Microvolume UV-Vis Spectrophotometer (Thermo Fisher Scientific) to achieve the purity ratio (A260/A280 nm) between 1.8 and 2.0. To process the OPC samples for a protein assay, we used the Mem-PER™ Plus Membrane Protein Extraction Kit (Thermo Fisher) following the manufacturer's protocol. Since a single hydrogel with OPC sample did not provide required protein concentration for this assay, 5 hydrogels from the same experimental condition were combined when preparing the protein sample. Collected samples were stored in -80℃ until the bicinchoninic acid (BCA)

analysis was conducted. Total protein concentration was analyzed with Pierce™ BCA Protein Assay Kit (Thermo Fisher) following the manufacturer's protocol. Protein standards (Pierce™ Bovine Serum Albumin Standard Ampules, Thermo Fisher) were diluted in UltraPure™ DNase/RNase-Free Distilled Water (Thermo Fisher) to give a range from 0 to 2000 µg/mL. The absorbance at 562 nm was measured on SpectraMax M2e microplate reader.

7.3.10 Reverse transcription real-time PCR (qPCR)

Changes in gene expression of OPC maturation markers following overpressure were analyzed using qPCR on days 1 and 9 post overpressure. 100ng RNA was converted to cDNA using the iScript™ cDNA Synthesis Kit (BIO-RAD, Hercules, CA, United States) following the manufacturer's protocol. A 60ng cDNA sample was used for qPCR analysis. The samples were mixed in the TaqMan™ Fast Advanced Master Mix (Thermo Fisher) that was added to a 96-well plate with 0.2 mL format (Thermo) using QuantStudio™ 3 Real-Time PCR System (Thermo Fisher). Taqman primers for OPC maturation marker and reference gene were selected as follows: GAPDH (Mm99999915_g1), PDGFRA (Mm00440701_m1), GPR17 (Mm02619401_s1), GALC (Mm00484646_m1), and CNP (Mm01306641_m1). All samples were analyzed in triplicate. The PCR mixture was denatured at 95°C for 2 min, followed by 40 cycles of amplification. We used the delta-delta Ct method ($2^{-\Delta\Delta CT}$) to analyze the data, normalizing to GAPDH to estimate the relative fold gene expression change. All the calculated $2^{-\Delta\Delta CT}$ values (per target gene expression) were normalized to sham on day 1 post overpressure.

7.3.11 Immunocytochemistry and analysis

Immunocytochemistry was conducted to depict the protein expression on spheroids for every experimental condition. On days 1 and 9 after overpressure exposure, hydrogels were rinsed with DPBS three times then fixed with 4% paraformaldehyde (PFA) and incubated for 30 min at 37 C. Hydrogels were permeabilized with 0.1% Triton-X for 15 min at room temperature and then rinsed three times with DPBS. Samples were blocked by a 1% BSA incubated for 1 hour at room temperature. Gels were stained overnight at 4°C with primary antibodies diluted in 1% BSA: rabbit anti-PDGFRA (1:500, Thermo), rabbit anti-GPR17 (1:500, Thermo), rabbit anti-GALC (1:500, Thermo), and rabbit anti-CNPase (1:500, Thermo). Gels were rinsed 3 times with DPBS, then stained with Donkey anti-Rabbit IgG (H+L) Highly Cross-Adsorbed Secondary Antibody, Alexa Fluor™ 555 (1:500, Thermo) diluted in 1% BSA incubated for 2 hours at room temperature. DAPI (1:10,000, Thermo) was added to the secondary staining at 1-hour incubation time point. Hydrogel samples were rinsed three times with DPBS for 5 min each, then rinsed once with the UltraPure™ DNase/RNase-Free Distilled Water. Hydrogels were placed onto cover glasses (Fisherbrand™ Rectangular) with a rubber sheet (Grainger) with 6 mm hole with a biopsy punch (Miltex-Integra) with a thickness of 1.5 mm. The hydrogels were mounted with the ProLong™ Diamond Antifade Mountant (Thermo).

Samples were imaged z-stack from 100-200 µm with the 2 µm slices using the Axio Observer.Z1/7 confocal microscope with objective of Plan-Apochromat 20x/0.8 M27 with three

channels: AF555, EGFP, DAPI. Scaling setup was 0.312 um x 0.312 um x 2 um. Image size was 1024 x 1024 pixels. Images were projected using the max projection setting by combining all z-stack images per imaged section. Max projection image was quantified using ImageJ to measure raw intensity density of DAPI (blue) and maturation marker (red). Relative expression of each maturation marker was computed by taking ratio from the raw intensity density of maturation marker to DAPI.

7.3.12 Western blot analysis

Alterations in protein expressions of OPC maturation markers was analyzed on days 1 and 9 post overpressure. A capillary-based automated total protein chemiluminescence western analysis was conducted using the Jess™ (ProteinSimple) with a 12-230 kDa Separation Module (ProteinSimple). A 25-well plate with a size range of 25-230 kDa was prepared and filled with samples, reagents, and secondary antibodies according to the manufacturer's protocol. All samples were diluted to 0.26 mg/mL of protein per sample. Antibodies of maturation markers were diluted as follows: rabbit anti-PDGFRA (1:250), rabbit anti-GPR17 (1:250), rabbit anti-GALC (1:250), and rabbit anti-CNPase (1:250). Immunoblots were imaged by the Jess™ system and expression level of each marker was analyzed within the Compass for SW software (ProteinSimple) as the area under the electropherogram for the respective proteins of interest.

Statistical analysis

Statistical comparisons were conducted to compare each experimental condition to control using GraphPad Prism 9 (GraphPad Software, San Diego, CA, United States). Outliers were determined and excluded before proceeding to any statistical analysis. The F-test was used to verify assumptions of homoscedasticity, and then Shapiro-Wilk test was used to verify assumptions of normality. A two-way ANOVA with a multiple comparison was used for ATP, Viability, Spheroid to Hydrogel Ratio, PCR (PDGFRA, GALC, CNP), Western blot (GPR17, GALC), ICC (PDGFRA, GPR17, GALC) results. When there is a not normally distributed dataset, Mann-Whitney test was used for DNA, ATP/DNA, Total Spheroid Volume, Mean Spheroid Volume, PCR (GPR17), Western blot (PDGFRA), ICC (CNP) results. Differences were considered significant when $p < 0.05$.

7.4 Results

7.4.1 Characterization of applied mechanical insult

Overpressure parameters generated by the SWG are summarized in Table 1 which characterized the peak pressure, rise time, positive duration, and positive impulse (Figure 7.3). All samples were exposed to average peak pressures of 19.080 ± 6.530 psi. Further, these wave characteristics are similar to what been previous reported for intracranial pressures measurements collected using a rat blast-induced neurotrauma model therefore, demonstrating translational *in vivo* biomechanics [Bolander 2012, Leonardi 2011].

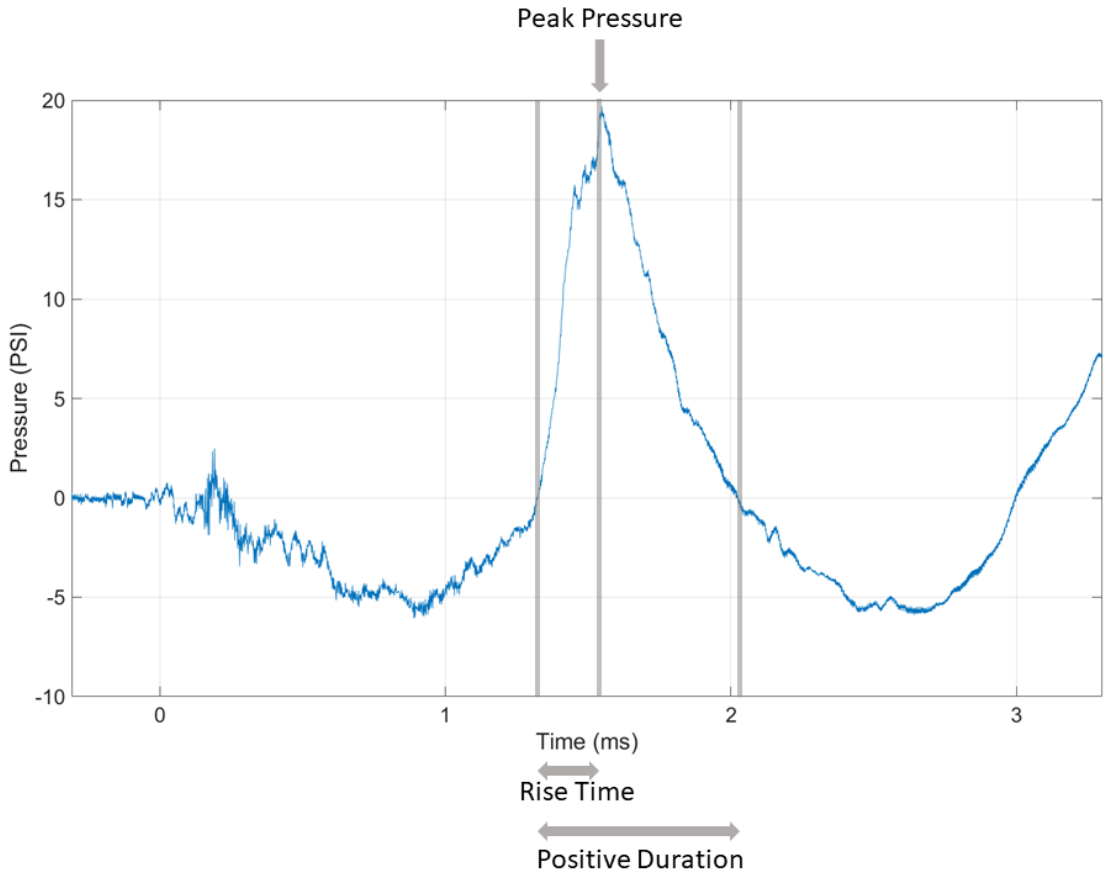

Figure 7.3. Representative data of an overpressure profile for a simulated blast. SWG generated overpressure profile as depicted and annotations for characterized parameters are shown. Grey vertical lines indicate the analyzed range of the overpressure curve. Peak pressure was determined as the first peak of the curve within the range followed by a drastic pressure rise. Pressure is in pound per square inch [psi], and time is in milli second [ms].

Table 7.1. High-rate overpressure parameters.

Parameter	Average	Standard Deviation
Peak Pressure [psi]	19.080	6.530
Rising Time [ms]	0.537	0.470
Positive Duration [ms]	1.092	0.351
Positive Impulse [psi*ms]	5.112	2.059

7.4.2 Characterization of NorHA Hydrogel

Oscillatory shear rheology was performed on 1-2 wt% NorHA gels to determine the impact of applied overpressure on gel mechanical properties (Figure 7.4A-B). Frequency sweeps were conducted on both overpressure and sham samples at each of three NorHA concentrations. Gel stiffness was found to increase as NorHA concentration increased (Figure 7.4A). Analogous experiments were conducted on 1-2 wt% NorHA gels containing encapsulated OPC (Figure 7.4B

and D). Gels without cells at all NorHA concentrations were found to have higher storage moduli than the corresponding cell-containing gels (Figure 7.7A and C).

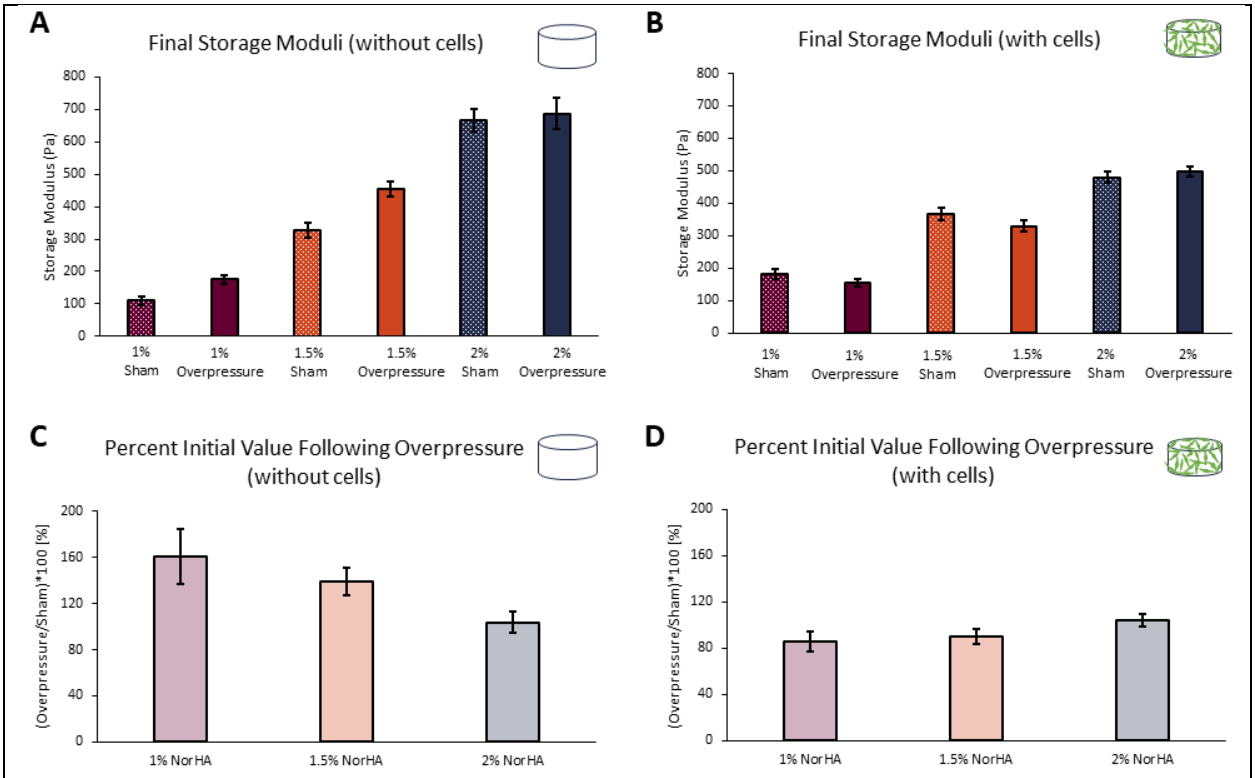

Figure 7.4. Mechanical characterization of sham and overpressure-exposed NorHA hydrogels. **(A)** Final storage moduli readings for 1-2 wt% NorHA gels. (B) Final storage moduli readings for OPC-containing (200,000 cells per gel), 1-2 wt% NorHA gels. (C) Comparison of NorHA gel stiffness between overpressure and sham conditions. **(D)** Comparison of OPC-containing NorHA gel stiffness between overpressure and sham conditions. Cell-containing gels were cultured to a timepoint of 5 days and exposed to either overpressure or sham injury conditions. Frequency sweeps were performed with angular frequency between 0.1-10 rad/s (n=2). Final storage modulus for each gel was averaged across both gel replicates, and percent initial value was then calculated using the formula (overpressure / Sham) * 100.

7.4.3 Live/Dead Spheroid Analysis

Live/Dead viability assays were conducted to determine if the apoptosis was initiated by the applied mechanical insult (Figure 7.5). Between 72-449 spheroids were measured at each ROI for overpressure and sham conditions at each time point (Figure 7.5A). The viability of spheroids for all experimental conditions remained in the range of 91.67±6.14% (Figure 7.5B). Spheroid total volume was not significantly altered between overpressure and sham experimental groups or between time points (Figure 7.5C). For every condition, the total spheroid volume of OPC were in the range between 5.12×10^6 and 5.84×10^6 um^3 except the day 9 post-overpressure samples which showed higher deviation ($5.16 \times 10^6 \pm 2.46 \times 10^6$ um^3) as compared to other three conditions. On day 1 post-overpressure, between sham and overpressure samples, the total

volume result showed a 12% decrease in overpressure compared to sham (Figure 7.5C). The mean volume of a single spheroid within a hydrogel was measured to quantify the size of each spheroid in a hydrogel. Mean volume showed no significant difference between experimental conditions. However, the mean volume on day 9 post- overpressure showed a 16% decrease compared to the sham (Figure 7.5D). In addition, the occupation ratio of spheroids to hydrogel showed between 2.87 % and 3.30 % of the hydrogel was occupied by spheroids in all experimental conditions (Figure 7.5E).

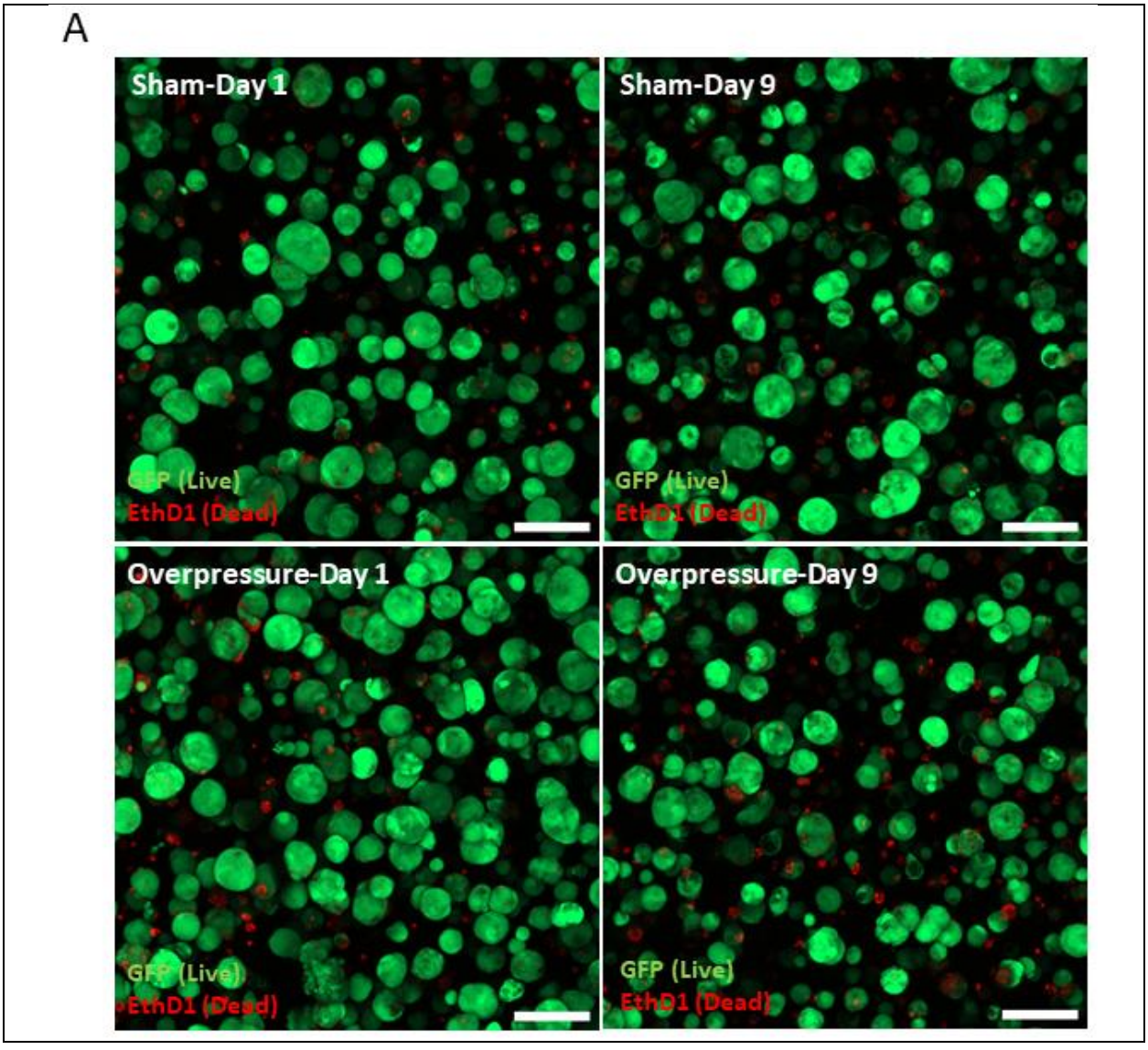

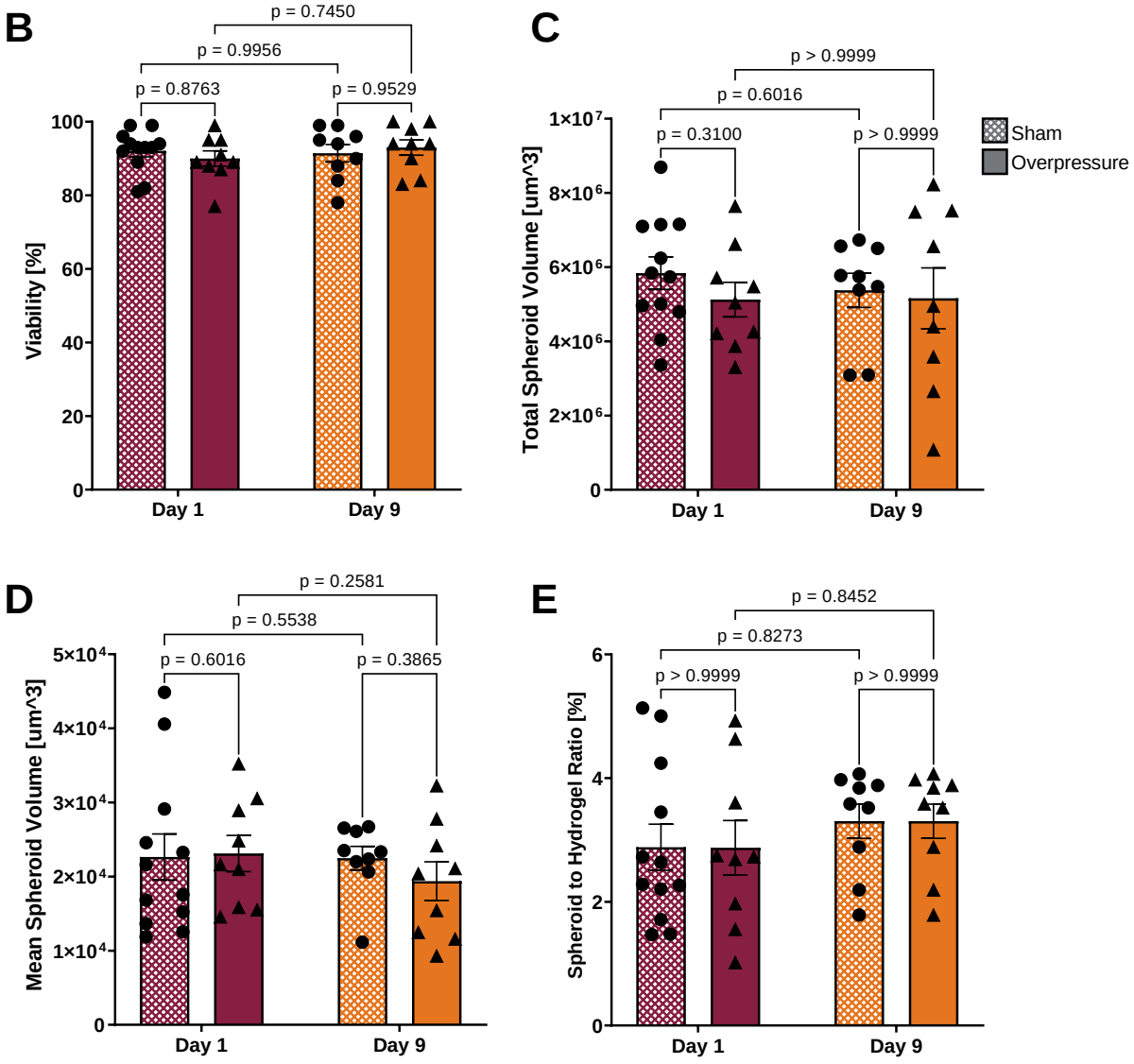

Figure 7.5. Spheroid analysis was conducted to compare all experimental conditions. (A) Representative confocal images of Live/Dead stained spheroids. Live cells are green and dead cells are red fluorescents. Scale bar = 100 µm. (B) Viability of spheroids per hydrogel, which representsa ratio of the live (green) spheroid total volume to spheroid total volume of live (green) and dead (red) spheroids. (C) Mean spheroid voulme per hydrogel. (D) Total spheroid volume per hydrogel. (E) Spheroids to hydrogel occupation ratio. n = 12 for Sham Day 1 and n = 9 for other conditions. Data represented as Mean ± SEM.

7.4.4 ATP/DNA measurement

ATP and DNA concentrations of cell lysate were quantified as well as the ratio between them (Figure 7.6). ATP concentration results showed a 69.97 % increase in concentration on day 9 post-overpressure samples compared to the day 9 sham (Figure 7.6A). DNA concentration

increased overtime for both sham (26.1%) and overpressure (20.4%) in the day 9 samples when compared to the sham at day 1 after an overpressure exposure. The increase of DNA concentration of sham samples between day 1 and day 9 showed a significant increase (p=0.0332). (Figure 7.6B). The ATP to DNA ratio showed a 72.26% increase on day 9 post-overpressure sample, however, the statistical difference did not show significant change (p=0.0753) (Figure 7.6C).

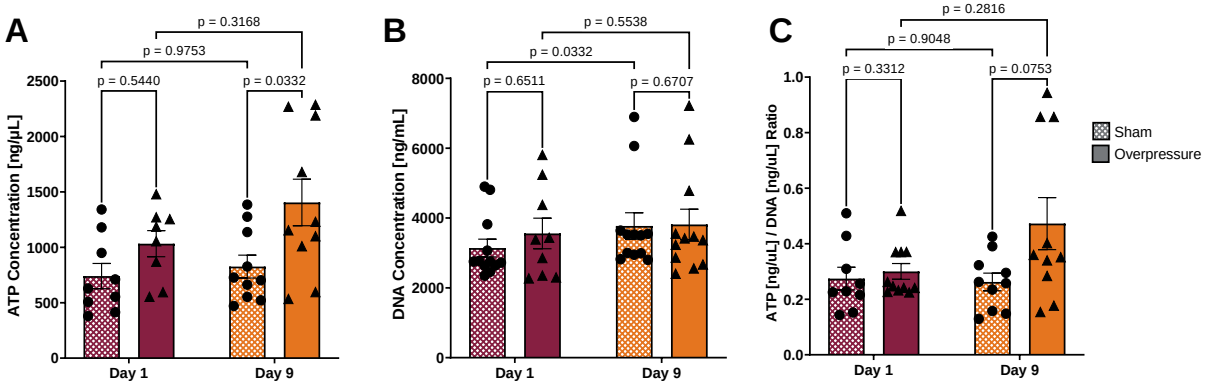

Figure 7.6. ATP/DNA analysis results. (A) ATP concentration of at day 9 following overpressure exposure resulted in a significant increase in ATP levels as compared to sham. (B) DNA concentration of samples for all experimental conditions did not have a significant change over time. (C) The ratio of ATP to DNA concentrations were found to be significantly elevated at day 9 post overpressure exposure as compared to all other test groups. Data represented as Mean±SEM.

7.4.5 Gene expression quantification

OPC has been investigated for its abilities of proliferation and differentiation after TBI, we quantified changes in gene expressions of OPC maturation markers after applied overpressure. Gene expressions of OPC to OL maturation markers were quantified using qPCR. OPC marker PDGFRA expression showed a 31.7% increase on day 1 post-overpressure (p=0.0140, Figure 7.7A). On day 9, the expression level of PDGFRA in both sham and overpressure samples decreased by 18.6 % and 19.4% respectively (Figure 7.7A). GPR17 expressions showed a 61.0 % increase on day 1 post-overpressure. On day 9, both sham and overpressure samples showed downregulation of 47.8% and 55.3% respectively (Figure 7.7B). GALC expressions showed 22% upregulation on day 1 post-overpressure. On day 9 after the injury, the expression returned to the same level as the day 1 sham. (Figure 7.7C) CNP gene expression showed 7.7% upregulation for the overpressure sample, and 20.8% and 26.0% downregulations for sham and overpressure at day 9 (Figure 7.7D).

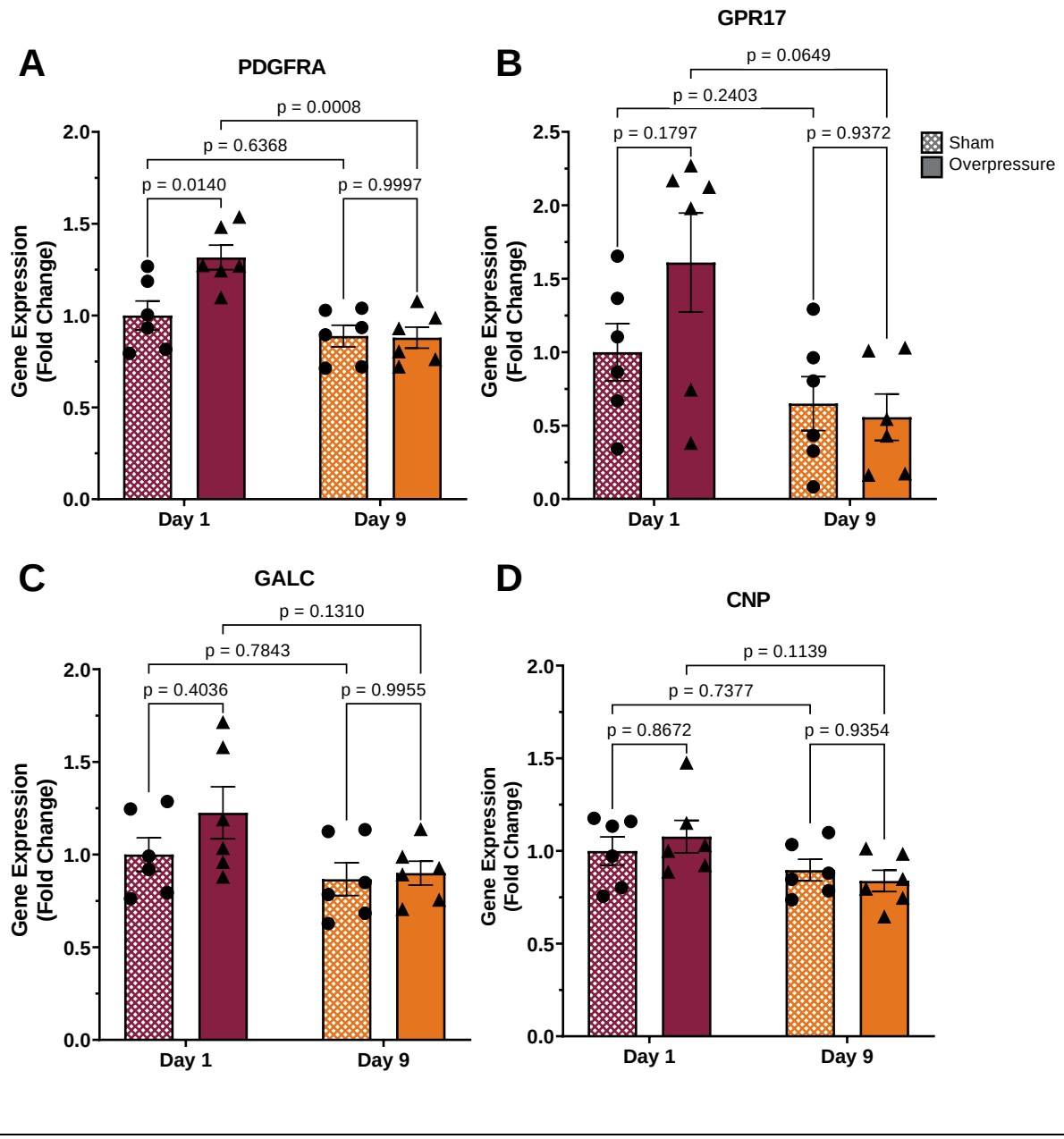

Figure 7.7. OPC maturation gene expression was quantified at day 1 and 9 following mechanical insult. All data were normalized to day 1 sham data of each marker expression. (A) PDGFRA expression indicated that the overpressure exposure significantly increased (1.3 times) as compared to sham on day 1 post-overpressure. (B) GPR17 expression showed trending increases on day 1 post-overpressure with large variability of SEM = 0.337. The expression of GPR17 decreased 50% over time on day 9 sham and post-overpressure. (C) GALC expression demonstrated a non-significant increase on day 1 post-overpressure sample, and GALC expression did not show significant changes over time on day 9 sham and post-overpressure compared to day 1 sham and post-overpressure, respectively. (D) CNP expression showed a non-significant decrease over time on day 1 and day 9 post-overpressure samples. CNP expression

did not show significant changes between sham and post-overpressure at every time point. Data represented as Mean±SEM.

7.4.6 Immunocytochemistry

Protein expression of maturation markers was visualized with ICC imaging (Figure 7.8A-D). Represented spheroid of each marker and experimental condition was indicated by a white arrow on Figure 8A-D, and magnified images were shown on Figure 8A'-D'. Image analysis of all data (DAPI, maturation marker: PDGFRA, GPR17, GALC, CNP, and the ratio between maturation marker and DAPI) showed no significant difference except the DAPI expression on PDGFRA samples showed significantly higher on day 9 post-overpressure compared to day 1 post-overpressure ($p=0.0246$) (Figure 7.8E). Ratio from maturation marker to DAPI expression was computed to show the relative expression of each marker (Figure 7.8M-P). The relative expression of PDGFRA showed a 444% increase on day 1 post-overpressure when compared to day 1 sham, and a 71.8% decrease in day 9 post-overpressure when compared to day 9 sham. The relative expression of PDGFRA over time showed 98.2% decrease on day 9 post-overpressure compared to day 1 post-overpressure, and day 9 sham showed 64.9% decrease compared to day 1 sham (Figure 7.8M). The relative expression of GPR17 showed a 50.5% decrease on day 1 post-overpressure when compared to day 1 sham, and a 777% increase on day 9 post-overpressure when compared to day 9 sham. The relative expression of GPR17 over time showed a 41.9% increase on day 9 post-overpressure compared to day 1 post-overpressure, and day 9 sham showed a 92.0% decrease compared to day 1 sham (Figure 7.8N). The relative expression of GALC showed a 61.8% decrease on day 1 post-overpressure when compared to day 1 sham and a 277.3% increase on day 9 post-overpressure when compared to day 9 sham. The relative expression of GALC over time showed a 321.0% increase on day 9 post-overpressure compared to day 1 post-overpressure, and day 9 sham showed a 57.3% decrease compared to day 1 sham. (Figure 7.8O). The relative expression of CNP showed a 45.4% increase on day 1 post-overpressure compared to day 1 sham, and a 190.1% increase on day 9 post-overpressure compared to day 1 post-overpressure. The relative expression of CNP over time showed a 44.37% increase on day 9 post-overpressure compared to day 1 post-overpressure, and day 9 sham showed a 27.6% decrease compared to day 1 sham.

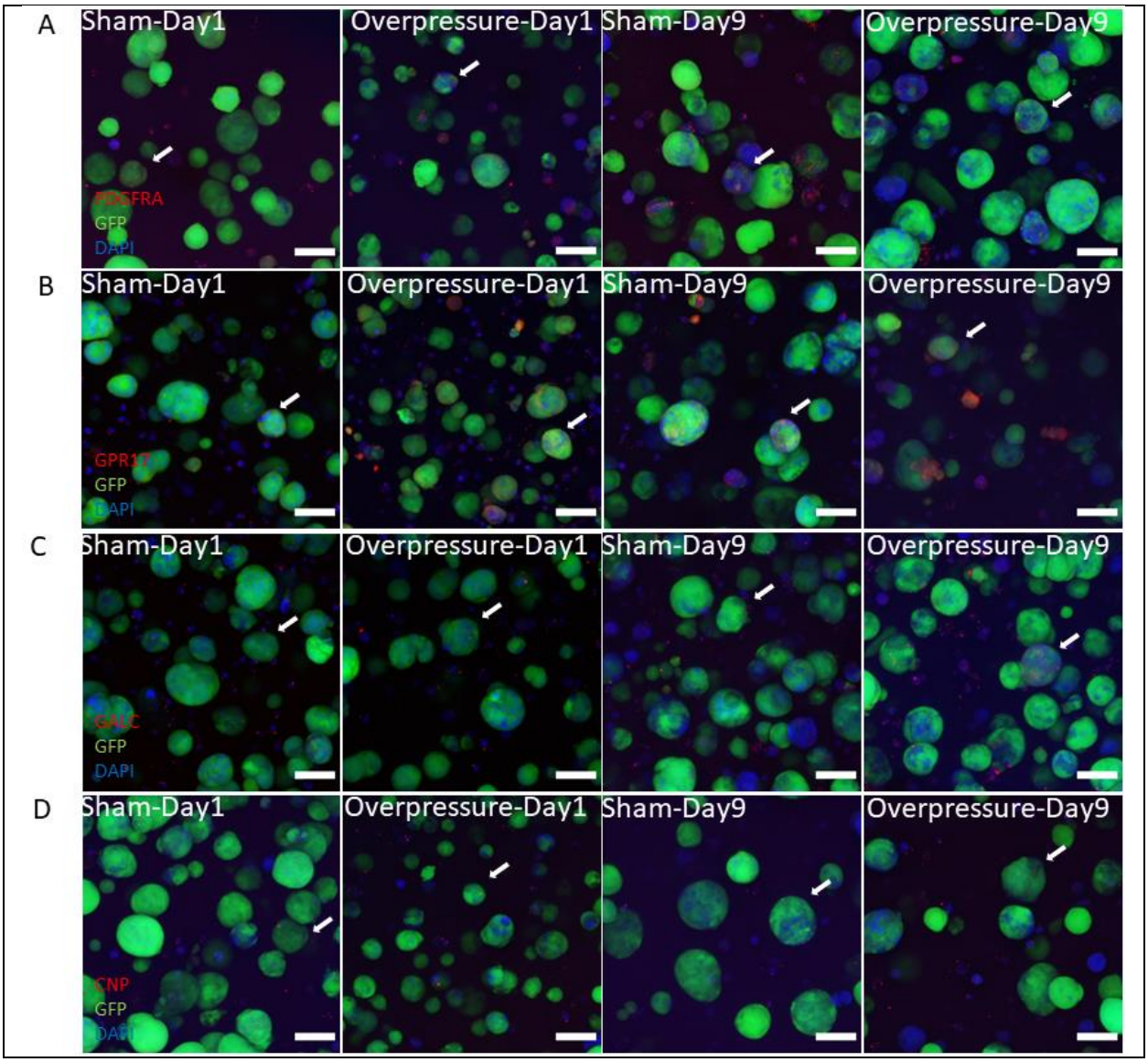
A
Sham-Day1
Overpressure-Day1
Sham-Day9
Overpressure-Day9
PDGFRA
GFP
DAPI
B
Sham-Day1
Overpressure-Day1
Sham-Day9
Overpressure-Day9
GPR17
GFP
DAPI
C
Sham-Day1
Overpressure-Day1
Sham-Day9
Overpressure-Day9
GALC
GFP
DAPI
D
Sham-Day1
Overpressure-Day1
Sham-Day9
Overpressure-Day9
CNP
GFP
DAPI

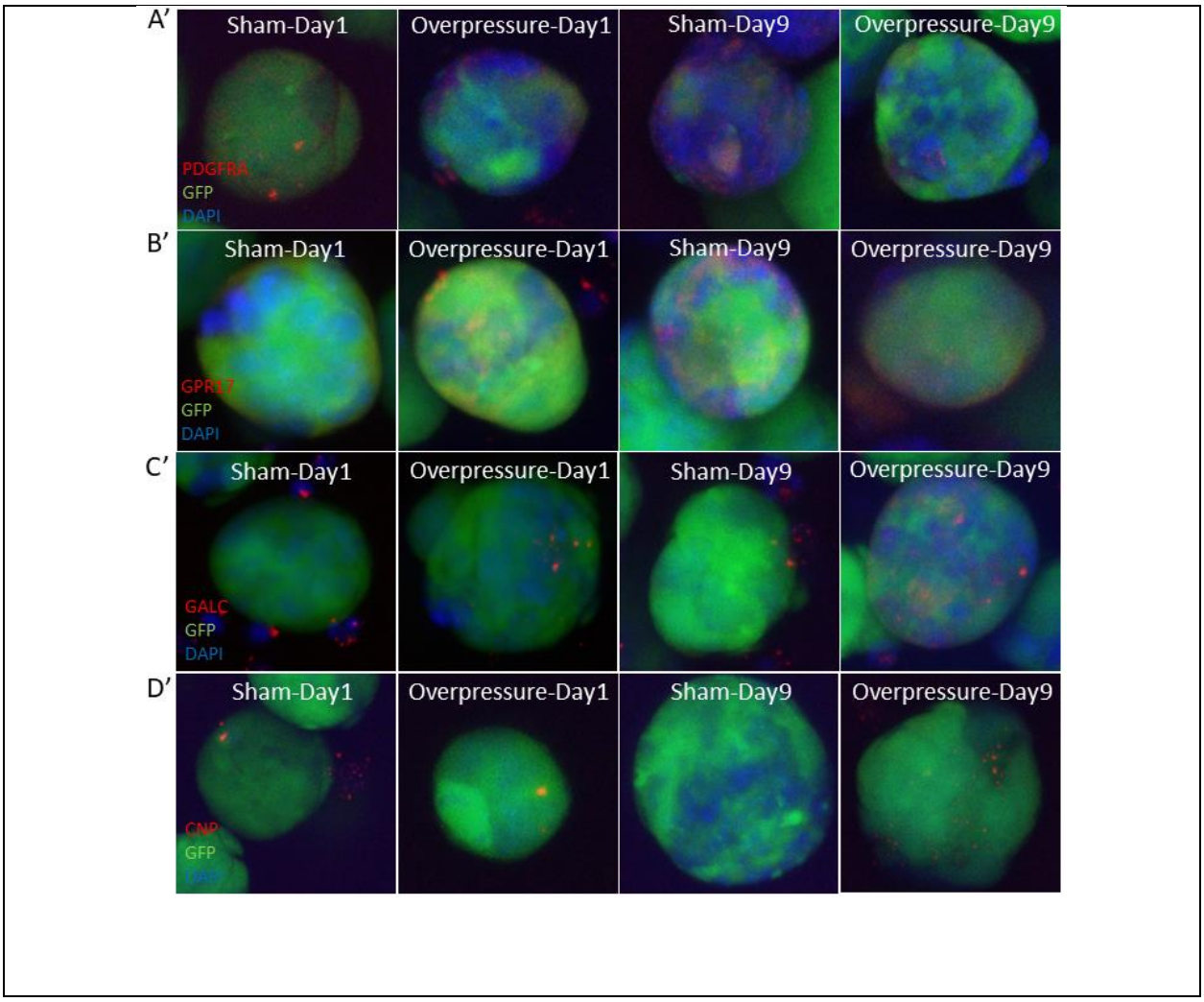
A′
Sham-Day1
Overpressure-Day1
Sham-Day9
Overpressure-Day9
PDGFRA
GFP
DAPI
B′
Sham-Day1
Overpressure-Day1
Sham-Day9
Overpressure-Day9
GPR17
GFP
DAPI
C′
Sham-Day1
Overpressure-Day1
Sham-Day9
Overpressure-Day9
GALC
GFP
DAPI
D′
Sham-Day1
Overpressure-Day1
Sham-Day9
Overpressure-Day9
CNP
GFP

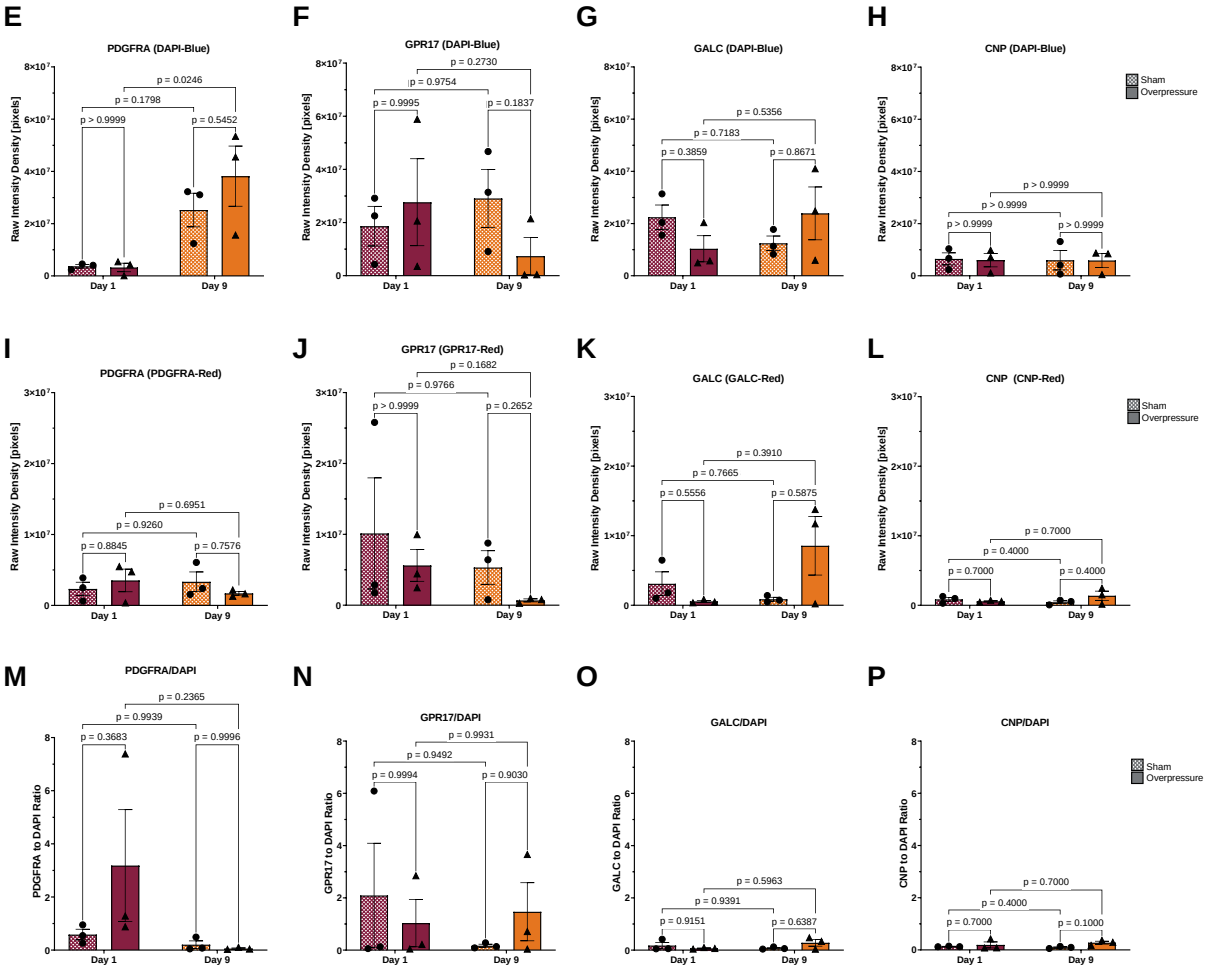

Figure 7.8. Representative immunocytochemistry images: (A) PDGFRA; (B) GPR17; (C) GALC; (D) CNP. Scale bar = 50 µm. (A'-D') Magnified represented spheroid image indicated by white arrows on A through D images. (E-H) Raw intensity density values of DAPI on each molecular target stained in blue. (I-L) Raw intensity density values of each molecular target stained in red . (I-P) Ratio between the molecular target in red and nucleus in blue to determine the expression level per cell nucleus density. Data represented as Mean±SEM.

7.4.7 Protein expression level changes

Normalized protein expression of maturation markers was quantified to investigate its transcription correlation between RNA and protein. PDGFRA expression showed a down regulation over time for both sham (10.47%) and overpressure (14.03%) (Figure 7.9A). GPR17 expression showed a 15.3% decrease on day 1 post-overpressure, and a further downregulation was observed on day 9 in sham and overpressure samples, 66.0% (p=0.0021) and 65.7% (p=0.0109), respectively (Figure 7.9B). GALC expression showed 8.0% downregulation for day 1 post-overpressure, and upregulation was observed for both day 9 sham compared to day 1 sham and day 9 post-overpressure compared to day 9 post-overpressure, 308% (p<0.0001) and

205% ($p<0.0001$), respectively (Figure 7.9C). Upregulation of GALC on day 9 post-overpressure was significantly less than day 9 sham sample ($p=0.0021$).

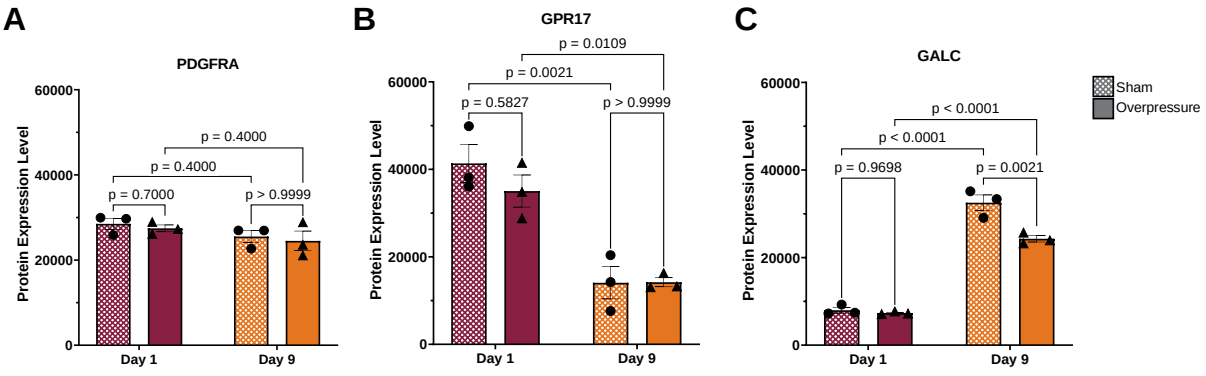

Figure 7.9. Protein concentration of maturation markers. (A) PDGFRA protein expression nonsignificant changes in protein expression. (B) GPR17 protein expression showed not statistically significant between sham and overpressure conditions at all time points, however there was significant decrease with time. (C) GALC protein expression showed significant decrease on day 9 between sham and overpressure. There are also increases over time for both conditions, with sham samples depicting 4 times increases while the overpressure samples showed 3 times increase. Data represented as Mean±SEM.

7.5 Discussion

OPC has been investigated for its abilities of proliferation and differentiation after TBI, however, how OPC responds to the mechanical insult is poorly understood. This study demonstrated a novel application of a NorHA hydrogel system to study the OPC response to an applied mechanical insult using this physiologically relevant *in vitro* platform. Combined with the SWG experimental set-up, the NorHA hydrogel system allowed us to create a novel TBI model to study OPC responses. We demonstrated an applied shockwave as a mechanical insult *in vitro* with average peak pressures of 19.080 ± 6.530 psi and characteristic wave properties similar to that experienced *in vivo* [Bolander 2011].

Hydrogel stiffness is consistent with previous experiments; higher NorHA concentrations result in more crosslinks and a stiffer gel (Figure 7.4). Gels exposed to overpressure insult stiffened relative to sham gels at all three NorHA concentrations, indicating that the gel matrix was slightly compacted by overpressure exposure (Figure 7.4C). When encapsulating OPCs, hydrogel stiffness decreased at all three NorHA concentrations (Figure 7.4B). This result is also consistent with previous findings which show that encapsulating cells reduces the stiffness of elastic hydrogels [Unal 2020]. In cell-containing hydrogels, the 2% NorHA samples exposed to applied overpressure were stiffer than the corresponding sham samples, indicating compaction of the gels following overpressure exposure (Figure 7.4D). However, in more compliant hydrogel formulations (1 and 1.5% NorHA), the overpressure samples were less stiff than the corresponding sham samples. This may indicate that at lower crosslinking densities, exposure to blast overpressure results in crosslink breakage rather than compaction. Notably, these results were specific to cell-containing gels, and were not observed in acellular hydrogel samples. Because cells are present in the precursor solution prior to gelation, crosslinks in the hydrogel system are formed around the cells; cell presence therefore interrupts the crosslinking network. As such, cell-containing samples are more susceptible to mechanical damage resulting from simulated overpressure injury.

Hlavac et al conducted similar experiments on astrocytes and found high viability following high rate overpressure testing suggesting that glia survival following insults of this severity, but the overpressure affected an initiation of mechanotransduction molecules (FAK, integrin, and vinculin) as well as astrocyte reactivity with increased GFAP expression. [Hlavac 2019] Our result showed that OPC microtissues post-overpressure exhibited high viability (Figure 7.5A, 90.00±2.09% on day 1 and 93.00±2.09% on day 9), similar to the viability for sham microtissues that did not receive a mechanical insult (92.08±1.64% on day 1 and 91.44±2.37% on day 9). Similar to other glial cells, our OPC results suggest that the overpressure insult does not cause acute cell death.

The necrotic core of the spheroid is often an issue of spheroid culture [Štampar 2020], however, this study demonstrated that the 2 weeks of cell culture and spheroid formation within a hydrogel did not generate a necrotic core inside the spheroid rather than individual dead cell

attached to a spheroid surface (Figure S6.2). This result indicated that the NorHA hydrogel was an appropriate cell culture platform for this study without causing cell death from lack of diffusion of nutrients.

Spheroid analysis from live/dead imaging showed no significant growth in total spheroid volume and mean spheroid volume within the hydrogel (Figure 7.5C-D). Unal et al also showed the plateaued growth rate by total volume within the NorHA hydrogel after day 3 post-encapsulation with the increased number of live cells on day 7 post-encapsulation [Unal 2020]. This result demonstrated that our experimental timeline on day 6 and day 14 post-encapsulation for sample collection was feasible to conduct the study with consistent spheroid volume and high viability to focus on cell response to the mechanical insult.

In addition to spheroid analysis, cell growth was also quantified by measuring the DNA concentration of cells in a whole hydrogel (Figure 7.6B). The result supported the trend of plateaued cell growth, except for the significant increase of the day 9 sham compared to the day 1 sham ($p=0.0332$). Since the DNA analysis is more comprehensive than the spheroid imaging analysis, there may have been a continuation of cell growth on sham samples and inhibited cell growth on the post-overpressure samples. The drawback of this result is that there may be a possibility of limitation of capacity growing the cells within the hydrogel since there was no significant difference in spheroid to hydrogel ratio (Figure 7.5E). Therefore, future studies targeting a proliferation such as bromodeoxyuridine (BrdU) assay to quantify cells actively synthesizing DNA is needed to confirm the result of changes in DNA concentration.

Previous *in vitro* TBI models have shown that exposure to overpressure influenced astrocytes *in vitro* to become reactive as well as corresponding aberration of metabolic activity within 48 hours after injury. [Hlavac 2019, Hlavac 2020, Guilhaume-Correa 2023] These previous findings are corroborated by our ATP concentration result. Our *in vitro* model showed a significant increase in ATP concentration due to applied overpressure on day 9 ($p=0.0332$) which indicated that the applied overpressure influences cell metabolic activity (Figure 7.6C). Although our results showed a significant change only on day 9, activation of mechanotransduction signaling after applied overpressure may have caused changes in ATP synthesis and consumption [Akay 2021, Hlavac 2019, Chi 2022, Simon 2016, Bauer 2019].

Proliferation of OPC after injury has been reported using TBI models including cell, animal, and human tissue samples [Flygt 2013, Flygt 2016, Lopez-Caraballo 2020]. As we observed that the overpressure potentially inhibited the increase of DNA concentration, the applied overpressure may affect the OPC to stop proliferating and enter the maturation process. PDGFRA molecular expression indicates that the OPC is in a proliferation phase [Huang 2019]. Our study showed that the gene expression of PDGFRA was significantly upregulated at day 1 after applied overpressure ($p=0.0140$) indicating a bias toward OPC self-renewal (Figure 7.7A). This result implies that the applied overpressure affected the promotion of gene regulation of PDGFRA, however, the change was not significant enough to promote DNA synthesis. Protein

expression of PDGFRA demonstrated no significant changes on every experimental condition which implies that the applied overpressure was not significant enough to alter the cell function of proliferation (Figure 7.9A).

Increased GPR17 protein expression was correlated to inhibit OPC from entering a maturation process [Satoh 2017]. Our study showed that a significant decrease in GPR17 protein expression over time ($p=0.0021$, day 9 sham compared to day 1 sham; $p=0.0109$, day 9 post-overpressure compared to day 1 post-overpressure) (Figure 7.9B). This result implies that the OPC inhibited the maturation process at an early time point (day 1 sham and post-overpressure), and then OPC possibly entered the maturation process on day 9.

GALC is a maturation marker that has been used to indicate pre-myelinating OL. Our study quantified the significant increase of GALC protein expression over time ($p<0.0001$, day 9 sham compared to day 1 sham; $p<0.0001$, day 9 post-overpressure compared to day 1 post-overpressure) (Figure 7.9C). This result may correspond to the significant decrease of GPR17 protein expression that may support the cells entering the maturation phase after 8 days of culture regardless of mechanical insult. Although the result suggested the 8 days of culture affected the GALC protein expression, the data also demonstrated that the overpressure exposed samples showed significantly less upregulation on day 9 post-overpressure sample ($p=0.0021$ on day 9 post-overpressure compared to day 9 sham). This result may indicate that the OPC maturation process depends on the cell culture time length regardless of mechanical insult, however, the applied overpressure may affect OPC to mitigate its maturation process.

There was no significant evidence of upregulation in CNP expression in both gene and protein expressions as expected due to the use of the MADM OPC cell line which is an immortalized OPC cell line. Therefore, CNP was excluded from the western blot analysis due to the minimum expression from the ICC analysis (Figure 7.8D, 7.8L, 7.8P).

Gene and protein expressions of PDGFRA and GPR17 showed similar trends of expression level changes, but GALC protein expression showed a drastic increase compared to gene expression. (Supplement Figure 7.3) When gene and protein expressions are compared together, the data showed the correlation of trend for PDGFRA and GPR17, but GALC did not follow the expression change of each other (gene and protein). Thus, the intracellular signaling that caused these trends in PDGFRA and GPR17 or the drastic change of GALC may be an interest of further investigation. Overall, these molecular analyses of maturation markers indicated that the applied overpressure triggers changes in maturation processes, but other factors may be necessary to promote the myelin signaling process such as neurons and microglia [Buchanan 2023, Kalafatakis 2021, Pinezich 2018].

The purpose of this study was the successful implementation of the NorHA hydrogel 3D cell culture system to investigate cellular and molecular responses of OPC after applied mechanical insult. Preliminary cellular responses of metabolism and maturation processes specific to the role of OPC were triggered by the insult. Although there are some limitations

including the use of immortalized cell line and minimal time points to compare, future studies can utilize this cell culture platform to investigate further by co-culturing with neuron or microglia, conducting assays on multiple time points, and quantifying mechanotransduction-related molecules. More studies evaluating the maturation of the OPC are vital to advance the interest in its potential use in regeneration therapy for patients with conditions that develop neurodegeneration.

7.6 References

1. Mahoney SO, Chowdhury NF, Ngo V, Imms P, Irimia A. Mild Traumatic Brain Injury Results in Significant and Lasting Cortical Demyelination. Front Neurol. 2022;13:854396. Published 2022 Jun 23. doi:10.3389/fneur.2022.854396
2. Campos-Pires R, Yonis A, Macdonald W, et al. A Novel *In vitro* Model of Blast Traumatic Brain Injury. J Vis Exp. 2018;(142):10.3791/58400. Published 2018 Dec 21. doi:10.3791/58400
3. Li Y, Li C, Gan C, et al. A Precise, Controllable *in vitro* Model for Diffuse Axonal Injury Through Uniaxial Stretch Injury. Front Neurosci. 2019;13:1063. Published 2019 Oct 17. doi:10.3389/fnins.2019.01063
4. Phipps H, Mondello S, Wilson A, et al. Characteristics and Impact of U.S. Military Blast-Related Mild Traumatic Brain Injury: A Systematic Review. Front Neurol. 2020;11:559318. Published 2020 Nov 2. doi:10.3389/fneur.2020.559318
5. Bryden DW, Tilghman JI, Hinds SR 2nd. Blast-Related Traumatic Brain Injury: Current Concepts and Research Considerations. J Exp Neurosci. 2019;13:1179069519872213. Published 2019 Sep 12. doi:10.1177/1179069519872213
6. Bogdanova Y, Verfaellie M. Cognitive sequelae of blast-induced traumatic brain injury: recovery and rehabilitation. Neuropsychol Rev. 2012;22(1):4-20. doi:10.1007/s11065-012-9192-3
7. Elder GA, Dorr NP, De Gasperi R, et al. Blast exposure induces post-traumatic stress disorder-related traits in a rat model of mild traumatic brain injury. J Neurotrauma. 2012;29(16):2564-2575. doi:10.1089/neu.2012.2510
8. Attilio PJ, Flora M, Kamnaksh A, Bradshaw DJ, Agoston D, Mueller GP. The Effects of Blast Exposure on Protein Deimination in the Brain. Oxid Med Cell Longev. 2017;2017:8398072. doi:10.1155/2017/8398072
9. Borinuoluwa R, Ahmed Z. Does Blast Mild Traumatic Brain Injury Have an Impact on PTSD Severity? A Systematic Review and Meta-Analysis. Trauma Care. 2023; 3(1):9-21. https://doi.org/10.3390/traumacare3010002
10. Przekwas A, Somayaji MR, Gupta RK. Synaptic Mechanisms of Blast-Induced Brain Injury. Front Neurol. 2016;7:2. Published 2016 Jan 21. doi:10.3389/fneur.2016.00002
11. Gefen A, Gefen N, Zhu Q, Raghupathi R, Margulies SS. Age-dependent changes in material properties of the brain and braincase of the rat. J Neurotrauma. 2003;20(11):1163-1177. doi:10.1089/089771503770802853
12. Logsdon AF, Schindler AG, Meabon JS, et al. Nitric oxide synthase mediates cerebellar dysfunction in mice exposed to repetitive blast-induced mild traumatic brain injury. Sci Rep. 2020;10(1):9420. Published 2020 Jun 10. doi:10.1038/s41598-020-66113-7

13. Barateiro A, Fernandes A. Temporal oligodendrocyte lineage progression: *in vitro* models of proliferation, differentiation and myelination. Biochim Biophys Acta. 2014;1843(9):1917-1929. doi:10.1016/j.bbamcr.2014.04.018
14. Dent KA, Christie KJ, Bye N, et al. Oligodendrocyte birth and death following traumatic brain injury in adult mice. PLoS One. 2015;10(3):e0121541. Published 2015 Mar 23. doi:10.1371/journal.pone.0121541
15. Raabe FJ, Slapakova L, Rossner MJ, et al. Oligodendrocytes as A New Therapeutic Target in Schizophrenia: From Histopathological Findings to Neuron-Oligodendrocyte Interaction. Cells. 2019;8(12):1496. Published 2019 Nov 23. doi:10.3390/cells8121496
16. Wolswijk G. Oligodendrocyte survival, loss and birth in lesions of chronic-stage multiple sclerosis. Brain. 2000;123 (Pt 1):105-115. doi:10.1093/brain/123.1.105
17. Bryden DW, Tilghman JI, Hinds SR 2nd. Blast-Related Traumatic Brain Injury: Current Concepts and Research Considerations. J Exp Neurosci. 2019;13:1179069519872213. Published 2019 Sep 12. doi:10.1177/1179069519872213
18. Huntemer-Silveira A, Patil N, Brickner MA, Parr AM. Strategies for Oligodendrocyte and Myelin Repair in Traumatic CNS Injury. Front Cell Neurosci. 2021;14:619707. Published 2021 Jan 11. doi:10.3389/fncel.2020.619707
19. Boda E, Viganò F, Rosa P, et al. The GPR17 receptor in NG2 expressing cells: focus on *in vivo* cell maturation and participation in acute trauma and chronic damage. Glia. 2011;59(12):1958-1973. doi:10.1002/glia.21237
20. Snaidero N, Velte C, Myllykoski M, et al. Antagonistic Functions of MBP and CNP Establish Cytosolic Channels in CNS Myelin. Cell Rep. 2017;18(2):314-323. doi:10.1016/j.celrep.2016.12.053
21. Ehrlich M, Mozafari S, Glatza M, et al. Rapid and efficient generation of oligodendrocytes from human induced pluripotent stem cells using transcription factors. Proc Natl Acad Sci U S A. 2017;114(11):E2243-E2252. doi:10.1073/pnas.1614412114
22. Narine M, Colognato H. Current Insights Into Oligodendrocyte Metabolism and Its Power to Sculpt the Myelin Landscape. Front Cell Neurosci. 2022;16:892968. Published 2022 Apr 28. doi:10.3389/fncel.2022.892968
23. Flygt J, Gumucio A, Ingelsson M, et al. Human Traumatic Brain Injury Results in Oligodendrocyte Death and Increases the Number of Oligodendrocyte Progenitor Cells. J Neuropathol Exp Neurol. 2016;75(6):503-515. doi:10.1093/jnen/nlw025
24. Flygt J, Djupsjö A, Lenne F, Marklund N. Myelin loss and oligodendrocyte pathology in white matter tracts following traumatic brain injury in the rat. Eur J Neurosci. 2013;38(1):2153-2165. doi:10.1111/ejn.12179
25. Li Q, Zhao H, Pan P, et al. Nexilin Regulates Oligodendrocyte Progenitor Cell Migration and Remyelination and Is Negatively Regulated by Protease-Activated Receptor 1/Ras-Proximate-1 Signaling Following Subarachnoid Hemorrhage. Front Neurol. 2018;9:282. Published 2018 Apr 25. doi:10.3389/fneur.2018.00282
26. Marques S, Zeisel A, Codeluppi S, et al. Oligodendrocyte heterogeneity in the mouse juvenile and adult central nervous system. Science. 2016;352(6291):1326-1329. doi:10.1126/science.aaf6463

27. Li P, Li HX, Jiang HY, et al. Expression of NG2 and platelet-derived growth factor receptor alpha in the developing neonatal rat brain. Neural Regen Res. 2017;12(11):1843-1852. doi:10.4103/1673-5374.219045
28. Zhang Y, Chen K, Sloan SA, et al. An RNA-sequencing transcriptome and splicing database of glia, neurons, and vascular cells of the cerebral cortex [published correction appears in J Neurosci. 2015 Jan 14;35(2):846-6]. J Neurosci. 2014;34(36):11929-11947. doi:10.1523/JNEUROSCI.1860-14.2014
29. Sy M, Brandt AU, Lee SU, et al. N-acetylglucosamine drives myelination by triggering oligodendrocyte precursor cell differentiation. J Biol Chem. 2020;295(51):17413-17424. doi:10.1074/jbc.RA120.015595
30. Falcão AM, van Bruggen D, Marques S, et al. Disease-specific oligodendrocyte lineage cells arise in multiple sclerosis. Nat Med. 2018;24(12):1837-1844. doi:10.1038/s41591-018-0236-y
31. Zhang M, Wang J, Zhang K, et al. Ten-eleven translocation 1 mediated-DNA hydroxymethylation is required for myelination and remyelination in the mouse brain. Nat Commun. 2021;12(1):5091. Published 2021 Aug 24. doi:10.1038/s41467-021-25353-5
32. Wang CY, Sun YT, Fang KM, Ho CH, Yang CS, Tzeng SF. Function of B-Cell CLL/Lymphoma 11B in Glial Progenitor Proliferation and Oligodendrocyte Maturation. Front Mol Neurosci. 2018;11:4. Published 2018 Jan 24. doi:10.3389/fnmol.2018.00004
33. Fumagalli M, Daniele S, Lecca D, et al. Phenotypic changes, signaling pathway, and functional correlates of GPR17-expressing neural precursor cells during oligodendrocyte differentiation. J Biol Chem. 2011;286(12):10593-10604. doi:10.1074/jbc.M110.162867
34. Ceruti S, Viganò F, Boda E, et al. Expression of the new P2Y-like receptor GPR17 during oligodendrocyte precursor cell maturation regulates sensitivity to ATP-induced death. Glia. 2011;59(3):363-378. doi:10.1002/glia.21107
35. Satoh JI, Kino Y, Yanaizu M, et al. Expression of GPR17, a regulator of oligodendrocyte differentiation and maturation, in Nasu-Hakola disease brains. Intractable Rare Dis Res. 2017;6(1):50-54. doi:10.5582/irdr.2016.01097
36. Casamassa A, La Rocca C, Sokolow S, et al. Ncx3 gene ablation impairs oligodendrocyte precursor response and increases susceptibility to experimental autoimmune encephalomyelitis. Glia. 2016;64(7):1124-1137. doi:10.1002/glia.22985
37. Marei HE, Shouman Z, Althani A, et al. Differentiation of human olfactory bulb-derived neural stem cells toward oligodendrocyte. J Cell Physiol. 2018;233(2):1321-1329. doi:10.1002/jcp.26008
38. Wang CY, Deneen B, Tzeng SF. BRCA1/BRCA2-containing complex subunit 3 controls oligodendrocyte differentiation by dynamically regulating lysine 63-linked ubiquitination. Glia. 2019;67(9):1775-1792. doi:10.1002/glia.23660
39. Pennati A, Nylen EA, Duncan ID, Galipeau J. Regulatory B Cells Normalize CNS Myeloid Cell Content in a Mouse Model of Multiple Sclerosis and Promote Oligodendrogenesis and Remyelination. J Neurosci. 2020;40(26):5105-5115. doi:10.1523/JNEUROSCI.2840-19.2020

40. Zou Y, Jiang W, Wang J, et al. Oligodendrocyte precursor cell-intrinsic effect of Rheb1 controls differentiation and mediates mTORC1-dependent myelination in brain. J Neurosci. 2014;34(47):15764-15778. doi:10.1523/JNEUROSCI.2267-14.2014
41. Hou X, Zhang R, Wang J, et al. CLC-2 is a positive modulator of oligodendrocyte precursor cell differentiation and myelination. Mol Med Rep. 2018;17(3):4515-4523. doi:10.3892/mmr.2018.8439
42. Egawa N, Hamanaka G, Chung KK, et al. High Mobility Group A1 Regulates Transcription Levels of Oligodendrocyte Marker Genes in Cultured Oligodendrocyte Precursor Cells. Int J Mol Sci. 2022;23(4):2236. Published 2022 Feb 17. doi:10.3390/ijms23042236
43. Huang W, Hu H, Zhang Q, et al. Regulatory networks in mechanotransduction reveal key genes in promoting cancer cell stemness and proliferation. Oncogene. 2019;38(42):6818-6834. doi:10.1038/s41388-019-0925-0
44. Solbu AA, Caballero D, Damigos S, et al. Assessing cell migration in hydrogels: An overview of relevant materials and methods. Mater Today Bio. 2022;18:100537. Published 2022 Dec 29. doi:10.1016/j.mtbio.2022.100537
45. Zhao Z, Vizetto-Duarte C, Moay ZK, et al. Composite Hydrogels in Three-Dimensional *in vitro* Models. Front Bioeng Biotechnol. 2020;8:611. Published 2020 Jun 16. doi:10.3389/fbioe.2020.00611
46. Cho HJ, Verbridge SS, Davalos RV, Lee YW. Development of an *In vitro* 3D Brain Tissue Model Mimicking *In vivo*-Like Pro-inflammatory and Pro-oxidative Responses. Ann Biomed Eng. 2018;46(6):877-887. doi:10.1007/s10439-018-2004-z
47. Pinezich MR, Russell LN, Murphy NP, Lampe KJ. Encapsulated oligodendrocyte precursor cell fate is dependent on PDGF-AA release kinetics in a 3D microparticle-hydrogel drug delivery system. J Biomed Mater Res A. 2018;106(9):2402-2411. doi:10.1002/jbm.a.36432
48. Takase H, Washida K, Hayakawa K, et al. Oligodendrogenesis after traumatic brain injury. Behav Brain Res. 2018;340:205-211. doi:10.1016/j.bbr.2016.10.042
49. Tiane A, Schepers M, Rombaut B, et al. From OPC to Oligodendrocyte: An Epigenetic Journey. Cells. 2019;8(10):1236. Published 2019 Oct 11. doi:10.3390/cells8101236
50. Kuhn S, Gritti L, Crooks D, Dombrowski Y. Oligodendrocytes in Development, Myelin Generation and Beyond. Cells. 2019;8(11):1424. Published 2019 Nov 12. doi:10.3390/cells8111424
51. Fumagalli M, Daniele S, Lecca D, et al. Phenotypic changes, signaling pathway, and functional correlates of GPR17-expressing neural precursor cells during oligodendrocyte differentiation. J Biol Chem. 2011;286(12):10593-10604. doi:10.1074/jbc.M110.162867
52. Hlavac N, Guilhaume-Corrêa F, VandeVord PJ. Mechano-stimulation initiated by extracellular adhesion and cationic conductance pathways influence astrocyte activation. Neurosci Lett. 2020;739:135405. doi:10.1016/j.neulet.2020.135405
53. DeVience SJ, Lu X, Proctor J, et al. Metabolic imaging of energy metabolism in traumatic brain injury using hyperpolarized [1-13C]pyruvate. Sci Rep. 2017;7(1):1907. Published 2017 May 15. doi:10.1038/s41598-017-01736-x

54. Mazur RA, Yokosawa R, VandeVord PJ, Lampe KJ. The need for tissue-engineered models to facilitate the study of oligodendrocyte progenitor cells in traumatic brain injury and repair. Current Opinion in Biomedical Engineering. 2022/06/01/ 2022;22:100378. doi:https://doi.org/10.1016/j.cobme.2022.100378

55. W.M. Gramlich, I.L. Kim, J.A. Burdick, Synthesis and orthogonal photopatterning of hyaluronic acid hydrogels with thiol-norbornene chemistry, Biomaterials 34(38) (2013) 9803-9811.
56. K. Sugitani, D. Egorova, S. Mizumoto, S. Nishio, S. Yamada, H. Kitagawa, K. Oshima, D. Nadano, T. Matsuda, S. Miyata, Hyaluronan degradation and release of a hyaluronan-aggrecan complex from perineuronal nets in the aged mouse brain, Biochimica et Biophysica Acta (BBA)-General Subjects 1865(2) (2021) 129804.
57. Clark LR, Yun S, Acquah NK, et al. Mild Traumatic Brain Injury Induces Transient, Sequential Increases in Proliferation, Neuroblasts/Immature Neurons, and Cell Survival: A Time Course Study in the Male Mouse Dentate Gyrus. Front Neurosci. 2021;14:612749. Published 2021 Jan 7. doi:10.3389/fnins.2020.612749
58. Hernandez A, Tan C, Plattner F, et al. Exposure to mild blast forces induces neuropathological effects, neurophysiological deficits and biochemical changes [published correction appears in Mol Brain. 2021 Nov 10;14(1):164]. Mol Brain. 2018;11(1):64. Published 2018 Nov 9. doi:10.1186/s13041-018-0408-1
59. Dickerson MR, Bailey ZS, Murphy SF, Urban MJ, VandeVord PJ. Glial Activation in the Thalamus Contributes to Vestibulomotor Deficits Following Blast-Induced Neurotrauma. Front Neurol. 2020;11:618. doi:10.3389/fneur.2020.00618
60. Norris C, Weatherbee J, Murphy SF, VandeVord PJ. Quantifying acute changes in neurometabolism following blast-induced traumatic brain injury [published online ahead of print, 2023 Jun 21]. Neurosci Res. 2023;S0168-0102(23)00130-X. doi:10.1016/j.neures.2023.06.008
61. Bolander R, Mathie B, Bir C, Ritzel D, VandeVord P. Skull flexure as a contributing factor in the mechanism of injury in the rat when exposed to a shock wave. Ann Biomed Eng. 2011;39(10):2550-2559. doi:10.1007/s10439-011-0343-0
62. Lopez-Caraballo L, Martorell-Marugan J, Carmona-Sáez P, Gonzalez-Munoz E. iPS-Derived Early Oligodendrocyte Progenitor Cells from SPMS Patients Reveal Deficient *In vitro* Cell Migration Stimulation. Cells. 2020;9(8):1803. Published 2020 Jul 29. doi:10.3390/cells9081803
63. Guilhaume-Correa F, Pickrell AM, VandeVord PJ. The Imbalance of Astrocytic Mitochondrial Dynamics Following Blast-Induced Traumatic Brain Injury. Biomedicines. 2023;11(2):329. Published 2023 Jan 24. doi:10.3390/biomedicines11020329
64. Akay LA, Effenberger AH, Tsai LH. Cell of all trades: oligodendrocyte precursor cells in synaptic, vascular, and immune function. Genes Dev. 2021;35(3-4):180-198. doi:10.1101/gad.344218.120
65. Štampar M, Breznik B, Filipič M, Žegura B. Characterization of In Vitro 3D Cell Model Developed from Human Hepatocellular Carcinoma (HepG2) Cell Line. Cells. 2020; 9(12):2557. https://doi.org/10.3390/cells9122557

66. Bauer MS, Baumann F, Daday C, et al. Structural and mechanistic insights into mechanoactivation of focal adhesion kinase. Proc Natl Acad Sci U S A. 2019;116(14):6766-6774. doi:10.1073/pnas.1820567116
67. Chi S, Cui Y, Wang H, et al. Astrocytic Piezo1-mediated mechanotransduction determines adult neurogenesis and cognitive functions. Neuron. 2022;110(18):2984-2999.e8. doi:10.1016/j.neuron.2022.07.010
68. Simon K, Hennen S, Merten N, et al. The Orphan G Protein-coupled Receptor GPR17 Negatively Regulates Oligodendrocyte Differentiation via Gαi/o and Its Downstream Effector Molecules. J Biol Chem. 2016;291(2):705-718. doi:10.1074/jbc.M115.683953
69. Hlavac N, VandeVord PJ. Astrocyte Mechano-Activation by High-Rate Overpressure Involves Alterations in Structural and Junctional Proteins. Front Neurol. 2019;10:99. Published 2019 Feb 22. doi:10.3389/fneur.2019.00099
70. Buchanan J, da Costa NM, Cheadle L. Emerging roles of oligodendrocyte precursor cells in neural circuit development and remodeling. Trends Neurosci. 2023;46(8):628-639. doi:10.1016/j.tins.2023.05.007
71. Kalafatakis I, Karagogeos D. Oligodendrocytes and Microglia: Key Players in Myelin Development, Damage and Repair. Biomolecules. 2021;11(7):1058. Published 2021 Jul 20. doi:10.3390/biom11071058
72. Kermer P, Klöcker N, Bähr M. Neuronal death after brain injury. Models, mechanisms, and therapeutic strategies in vivo. Cell Tissue Res. 1999;298(3):383-395. doi:10.1007/s004410050061
73. Slemmer JE, Zhu C, Landshamer S, et al. Causal role of apoptosis-inducing factor for neuronal cell death following traumatic brain injury. Am J Pathol. 2008;173(6):1795-1805. doi:10.2353/ajpath.2008.080168

7.7 Supplementary Figures

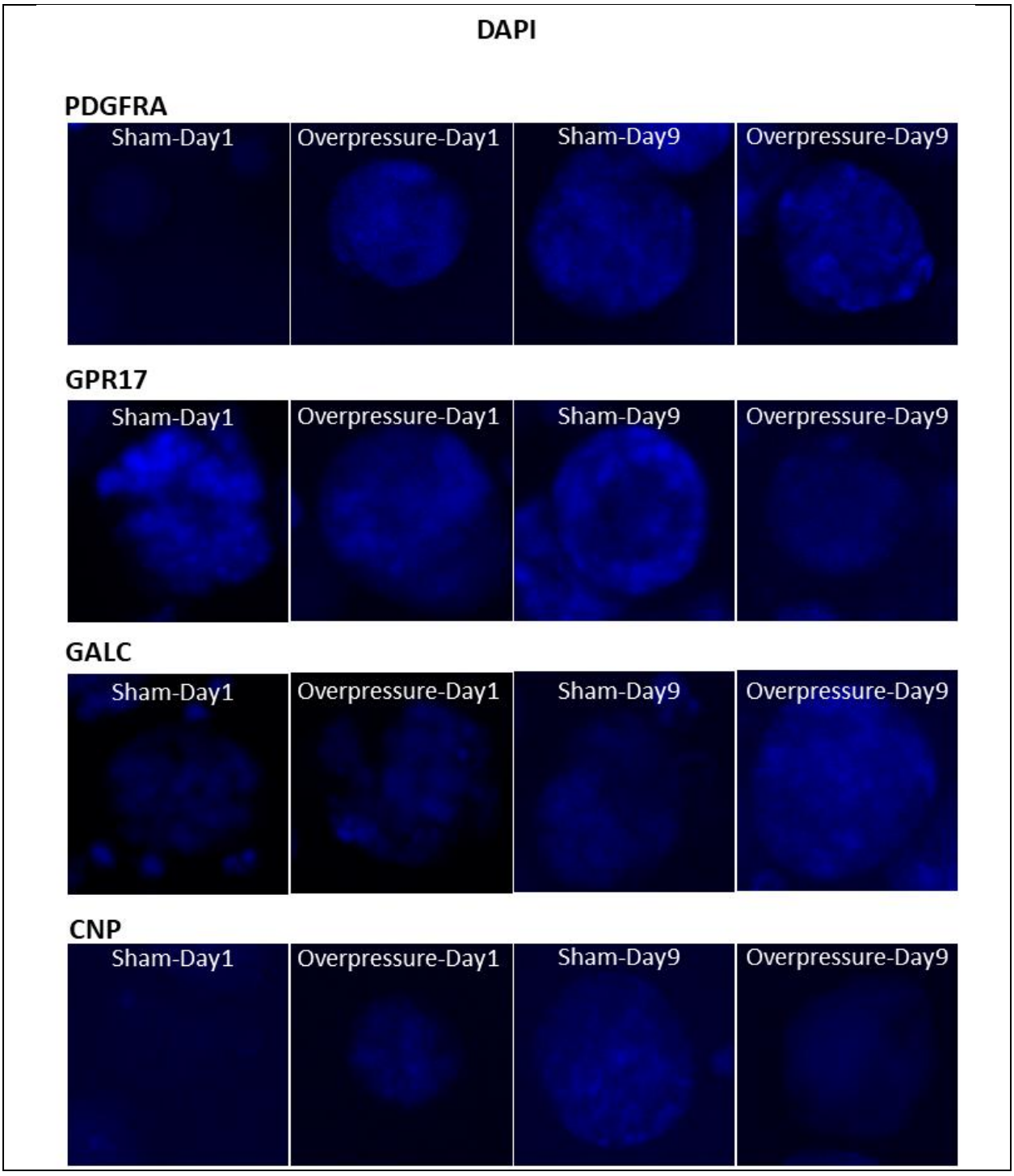
DAPI
PDGFRA
Sham-Day1
Overpressure-Day1
Sham-Day9
Overpressure-Day9
GPR17
Sham-Day1
Overpressure-Day1
Sham-Day9
Overpressure-Day9
GALC
Sham-Day1
Overpressure-Day1
Sham-Day9
Overpressure-Day9
CNP
Sham-Day1
Overpressure-Day1
Sham-Day9
Overpressure-Day9

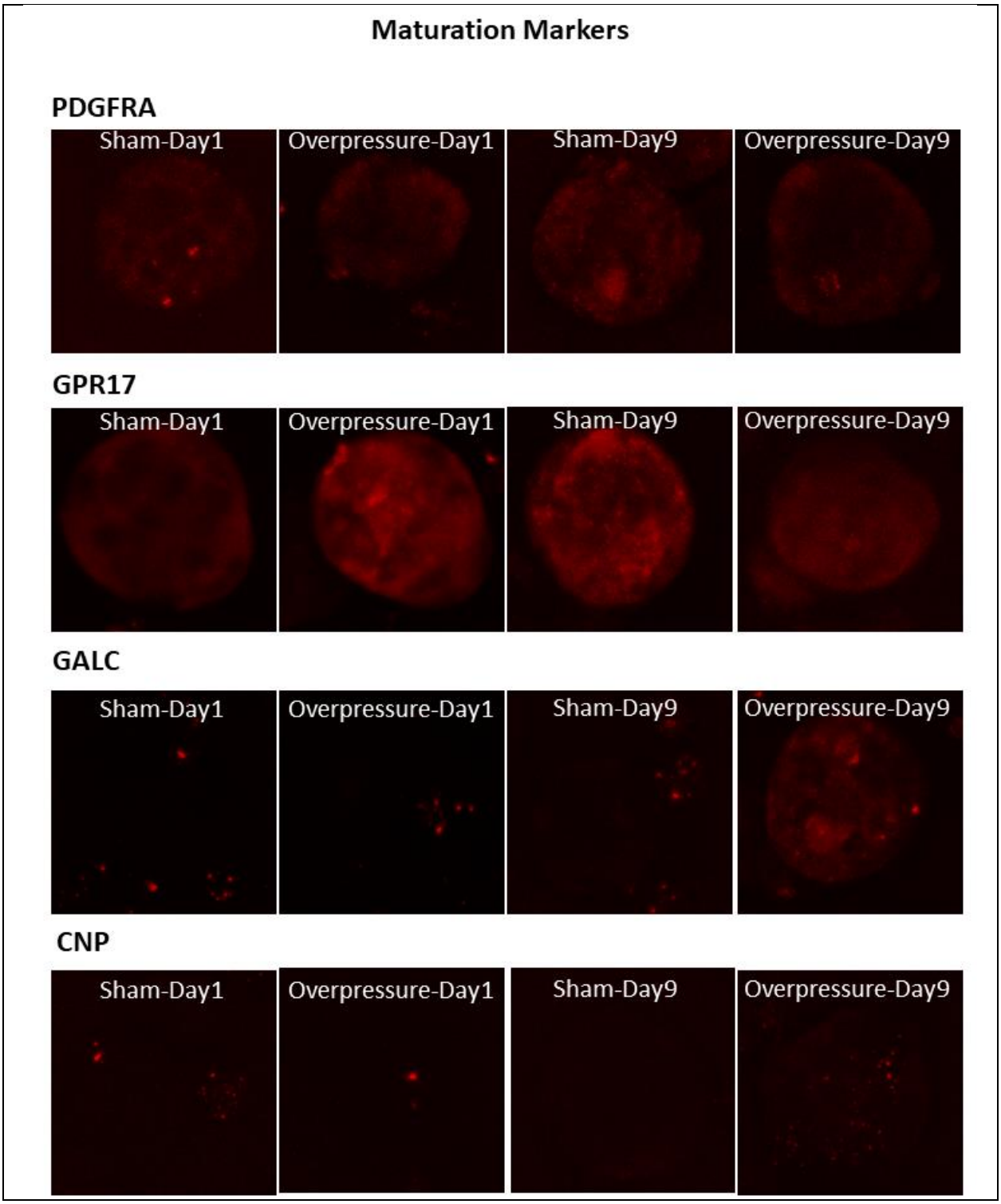
Maturation Markers
PDGFRA
Sham-Day1
Overpressure-Day1
Sham-Day9
Overpressure-Day9
GPR17
Sham-Day1
Overpressure-Day1
Sham-Day9
Overpressure-Day9
GALC
Sham-Day1
Overpressure-Day1
Sham-Day9
Overpressure-Day9
CNP
Sham-Day1
Overpressure-Day1
Sham-Day9
Overpressure-Day9

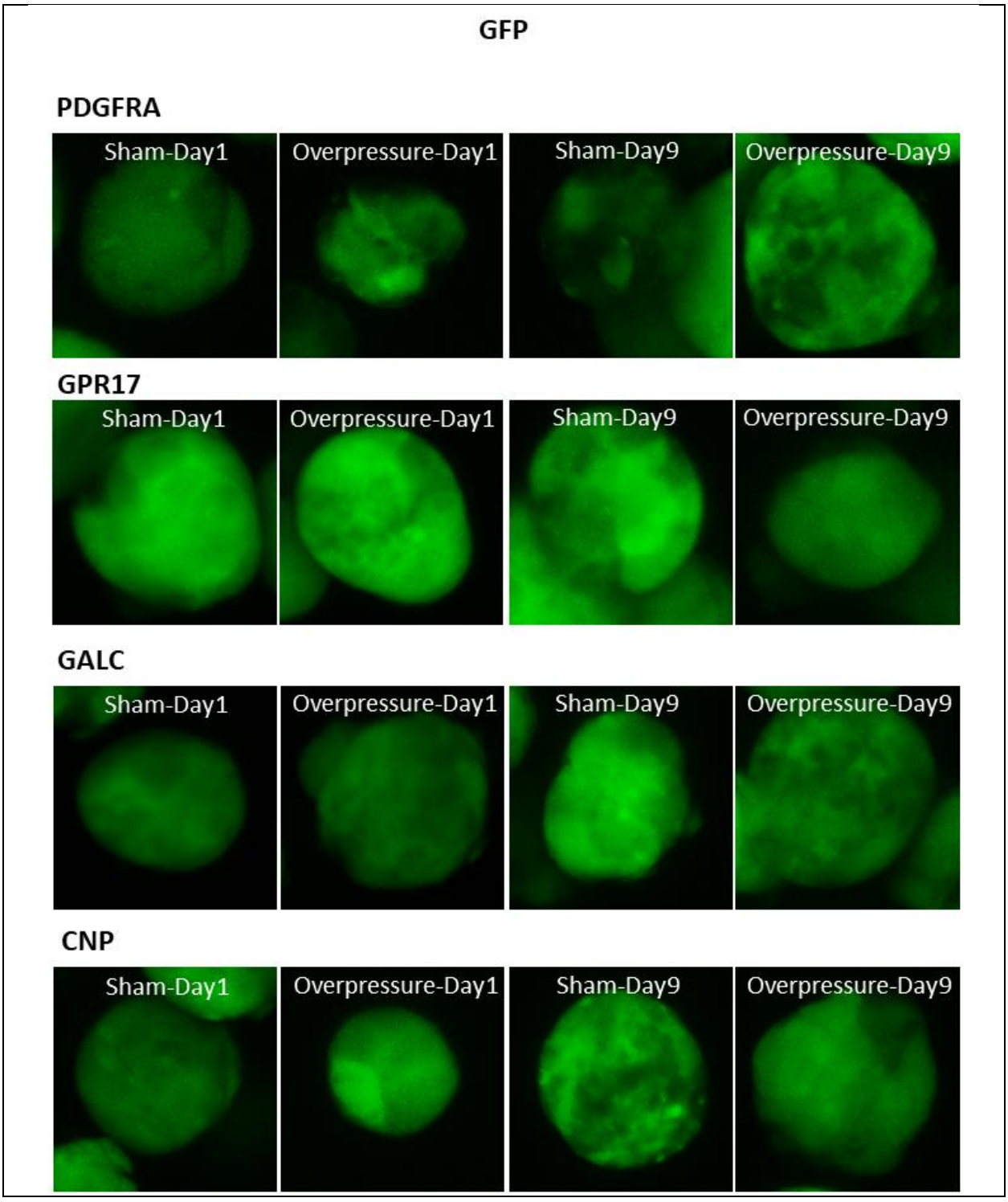
GFP
PDGFRA
Sham-Day1
Overpressure-Day1
Sham-Day9
Overpressure-Day9
GPR17
Sham-Day1
Overpressure-Day1
Sham-Day9
Overpressure-Day9
GALC
Sham-Day1
Overpressure-Day1
Sham-Day9
Overpressure-Day9
CNP
Sham-Day1
Overpressure-Day1
Sham-Day9
Overpressure-Day9

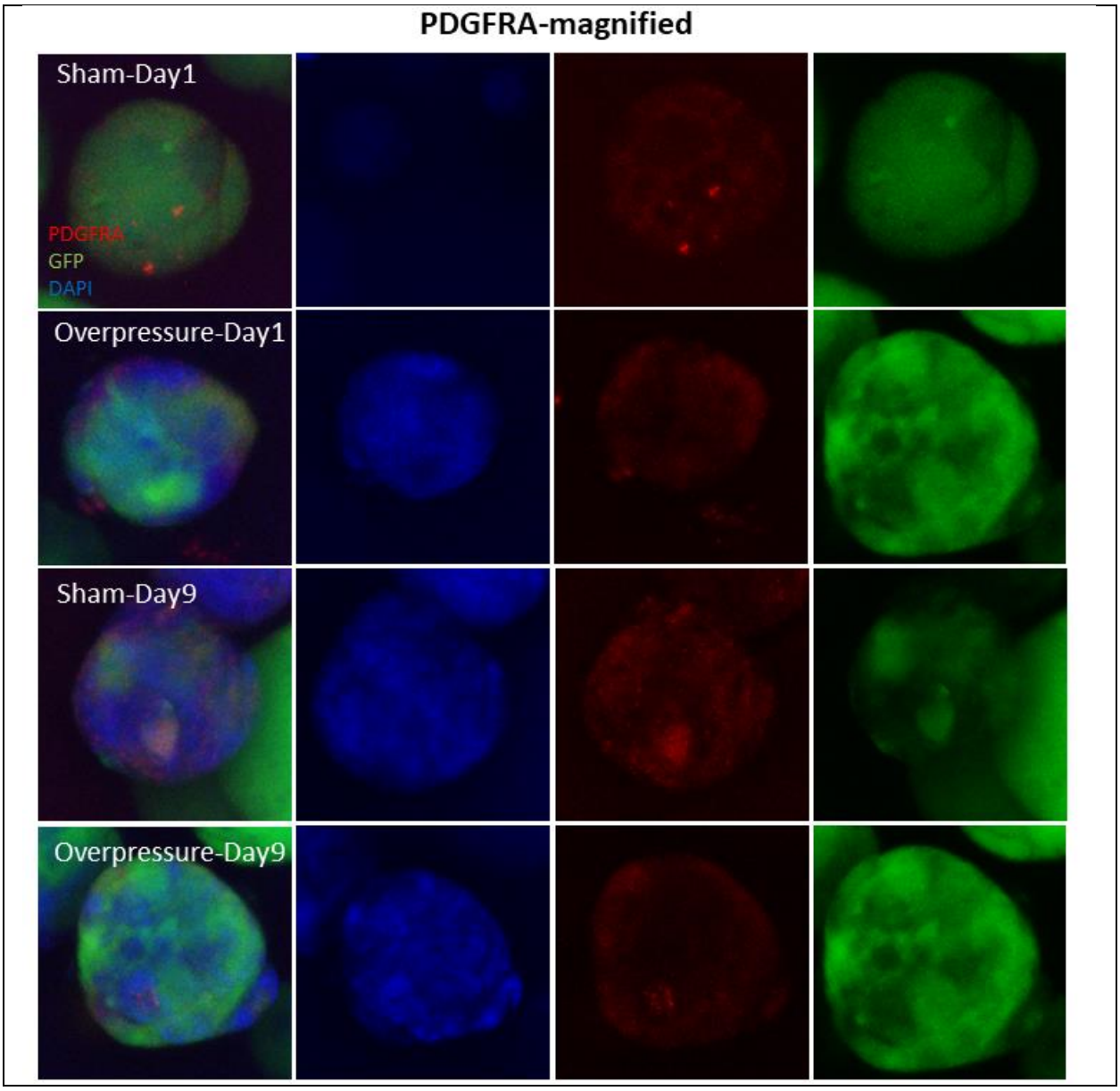
PDGFRA-magnified
Sham-Day1
PDGFRA
GFP
DAPI
Overpressure-Day1
Sham-Day9
Overpressure-Day9

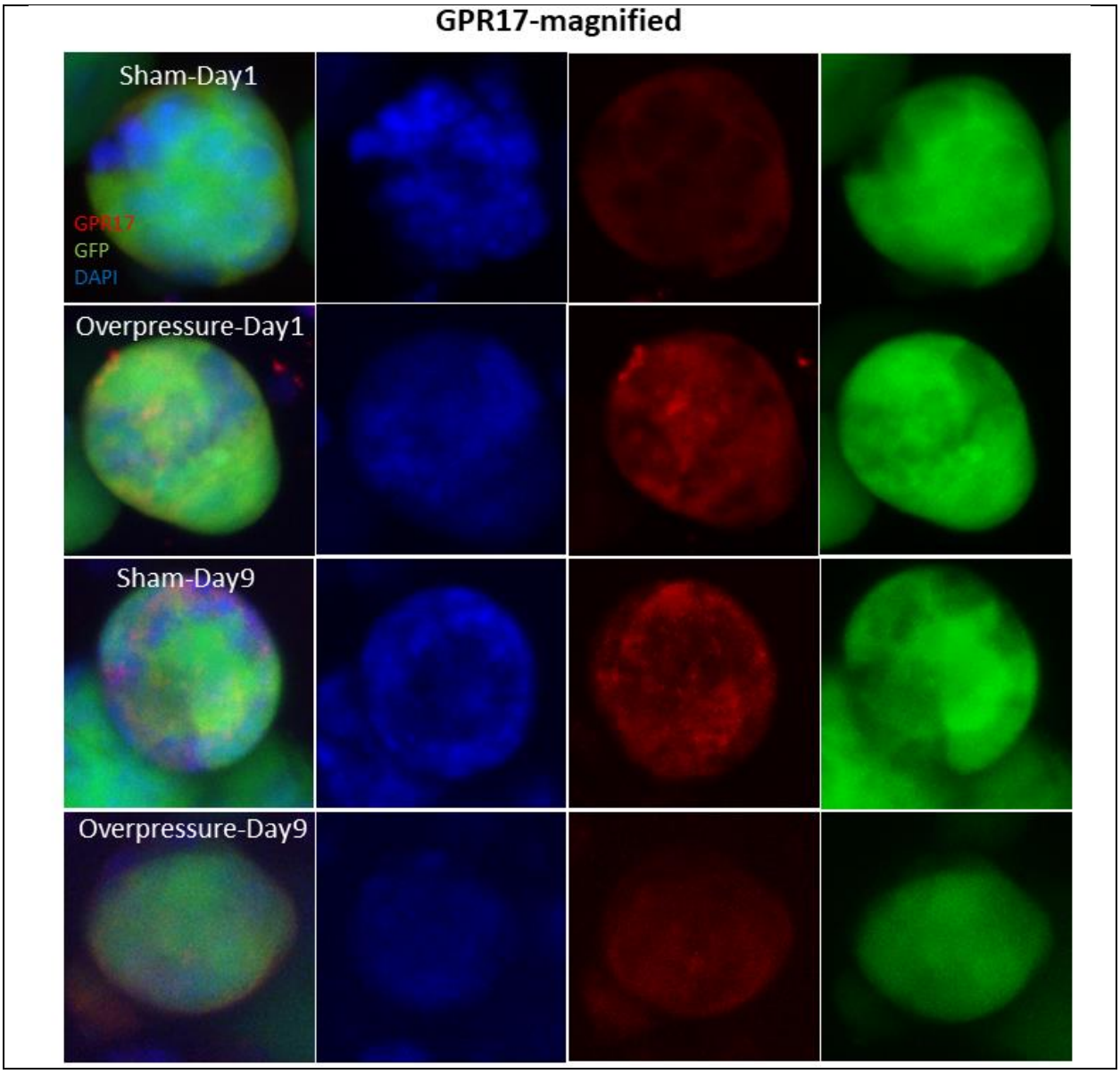
GPR17-magnified
Sham-Day1
GPR17
GFP
DAPI
Overpressure-Day1
Sham-Day9
Overpressure-Day9

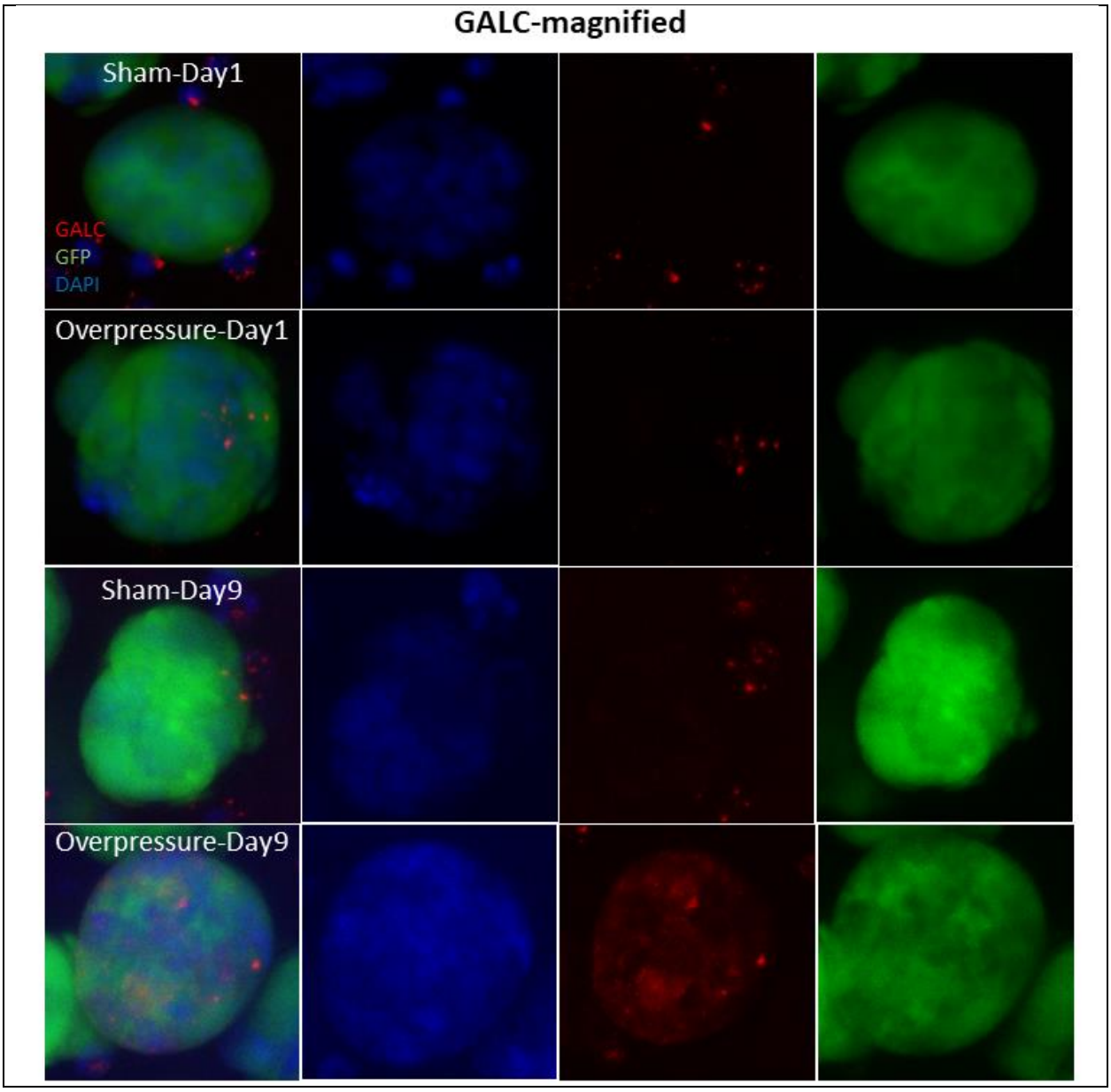
GALC-magnified
Sham-Day1
GALC
GFP
DAPI
Overpressure-Day1
Sham-Day9
Overpressure-Day9

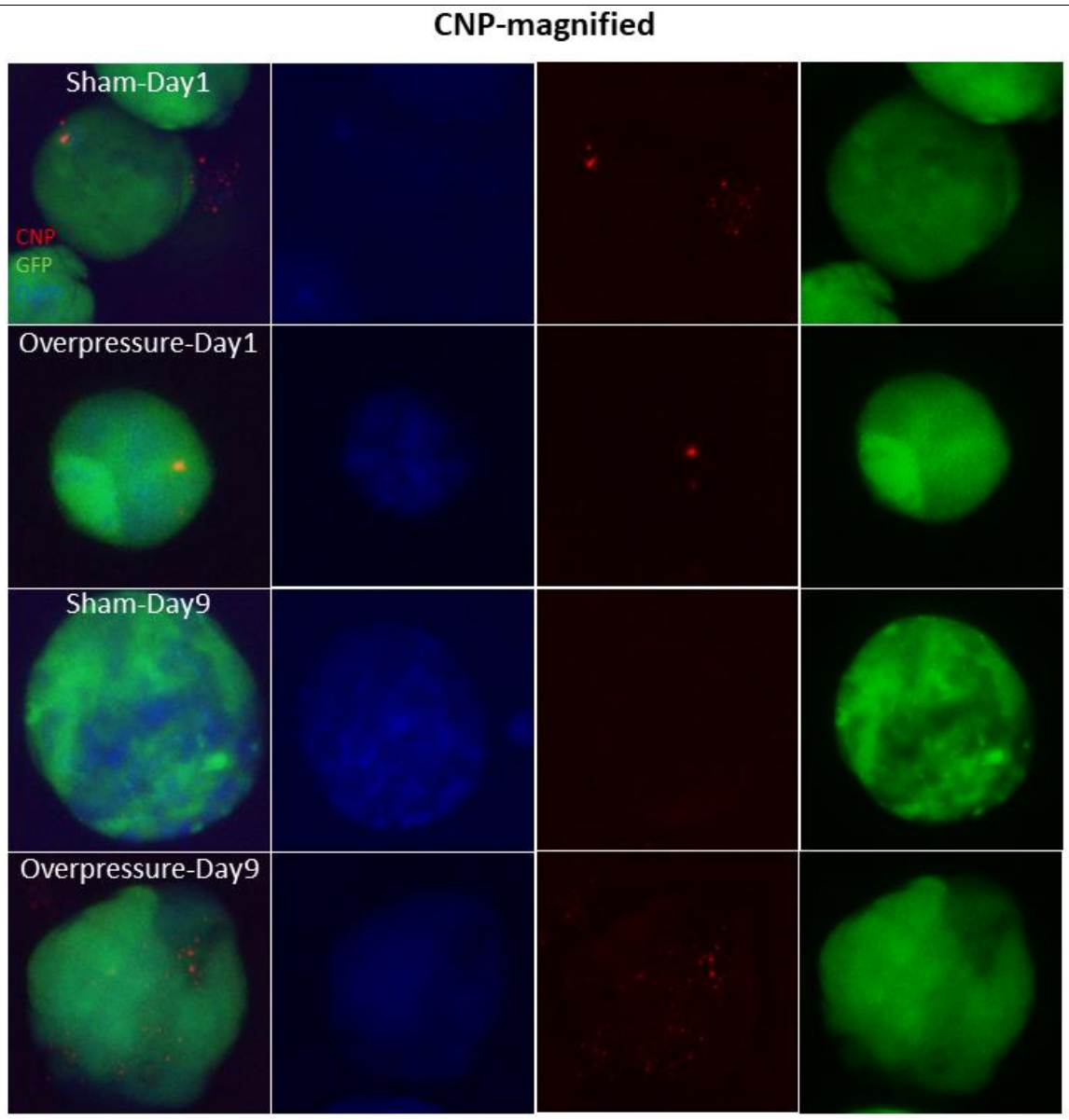
CNP-magnified
Sham-Day1
CNP
GFP
Overpressure-Day1
Sham-Day9
Overpressure-Day9

Figure S7.1.

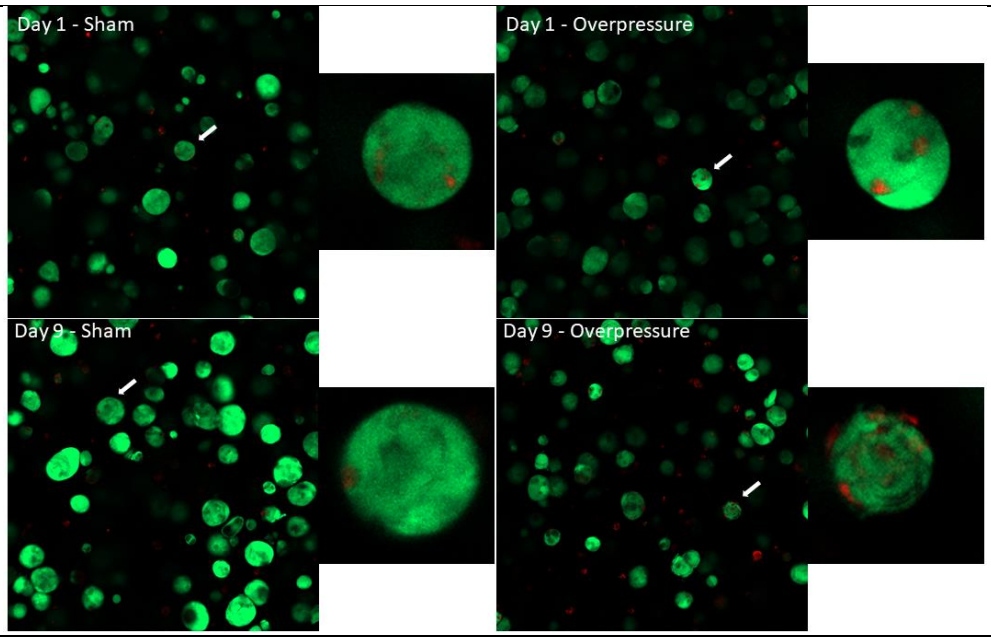

Figure S7.2. Representative images of spheroid middle sliced to show cell condition within a spheroid. These images show no necrotic cores inside the spheroid; rather, individual dead cells are sporadically attached to the spheroid.

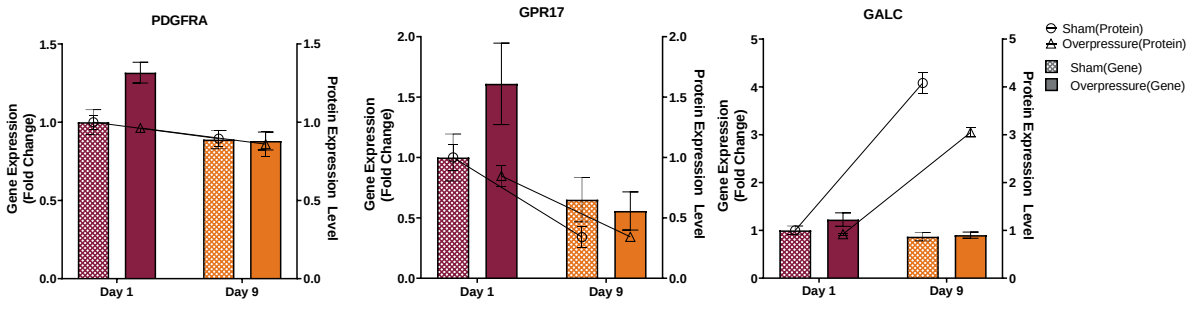

Figure S7.3. Gene expression and protein expression data were combined together to show the regulatory changes and correlation to each other (gene and protein). Both gene expression and protein expression were normalized to the day 1 sham of each marker.

Appendix B: Procedures and Protocols

8.1 OPC culture

8.1.1 OPC culture media

40 mL DMEM (4C refrigerator)

400 uL N2 supplement (aliquots in -20C freezer)

400 uL Pen-Strep (-20C freezer)

800 uL B27 supplement (aliquots in -20C freezer)

Thaw supplements in water bath. Spray everything (including your hands!) with ethanol before placing in the tissue culture hood. Combine all ingredients in sterile 50 mL conical tube in the TC hood. Label with your initials + date. Store in 4C refrigerator.

8.1.2 Coating T75 flasks

Pack of 5 T75 flasks (tissue culture room)

25 mL PBS (tissue culture room)

12.56 uL polyornithine (aliquots in labeled freezer box in -20C freezer)

Combine PBS and polyornithine in sterile 50 mL conical tube in the tissue culture hood. Spray down a pack of T75 flasks with ethanol and open IN THE TC HOOD. Pipette 5 mL of PBS-polyornithine mixture into each flask. Label each with your initials + date. Transfer to incubator (re-spray with ethanol to maintain sterility).

NOTE: coating must be allowed to sit a minimum of 6 hrs. (preferably overnight) before flasks are used!

8.1.3 Seeding OPCs from frozen stock

1) Thaw cell media in water bath.
2) Retrieve a coated T75 flask from the incubator. Aspirate the coating using the vacuum aspirator. Rinse with 10 mL PBS, then aspirate (x3).
3) Retrieve 1 frozen cell vial from liquid nitrogen dewar.
    a. Use cryogloves to protect your hands from liquid nitrogen

b. Allow liquid nitrogen to drain from the dewar insert for a few minutes before removing from dewar
c. Be sure to replace the pin when you put the cells back!
d. Make sure the dewar is sealed!

4) Thaw your cell vial in the water bath
    a. Don't thaw too long as it can affect cell viability
5) While cells are thawing, take your media to the TC hood and transfer 4 mL of media into a 15 mL conical tube.
6) Add your 1 mL of thawed cells to the 4 mL media.
7) Cap the conical tube and transfer your cells to the centrifuge. Centrifuge at 1000 rpm for 5 minutes.
8) Aspirate the media from the conical tube
    a. Be careful not to suck up the cell pellet!
9) Add 8 mL fresh media to cell pellet and mix.
10) Transfer your 8 mL of cells + media to the rinsed T75 flask. Check with microscope that the cells are evenly dispersed.
11) Store cells in 37C incubator.

You should check cells daily to make sure they are living + not contaminated. Cell media should be changed every 2 days (aspirate old media and replace with 8 mL fresh media). Passage cells when ~80-90% confluent.

8.1.4 OPC Expansion (Growth) Protocol

1. Aspirate media off.
2. Add trypsin in DPBS to cell culture (Final concentration of trypsin should be 0.5x).
    A. Trypsin is an esterase that will remove cells adhered to the surface and put them solution.
    B. For OPCs in T-75 plates use 250µL of 2.5% trypsin in 5mL DPBS.
3. Incubate cells for 5 minutes at 37^{o}C.
4. Tap side of petri dish to shake cells off of surface.
5. Gently rinse and agitate cell solution to break up cell clusters.
6. Put cell solution(s) into a LARGE (50 mL) falcon tube.
7. Rinse cell culture T-75 plate with an additional 10mL of DPBS.
8. Centrifuge falcon tube with at 1,000 rpm for 5 minutes.
   Note 1: Do not forget to balance centrifuge.
   Note 2: Bleach used t-75 plate for 10 minutes and throw out.
9. Aspirate off liquid and leave cell pellet.
10. Resuspend cell pellet with pre-warmed cell media (~300 µL per T-75 plate).
11. Extract a 20µL sample for cell counting and place in microtube.
12. Dilute microtube solution with Trypan Blue, and record dilution amount.
    Note 1: Optimal dilution leaves ~50 cells per 4x4 grid when performing cell count on hemocytometer.

Note 2: Perform cell count within 5 minutes of adding Trypan Blue. Over long periods of time the dye starts leaking into live cells.

13. Inject 15 µL of sample into cytometer.
14. Count cells in each of the four 4x4 grids. Cytometer picture shown below.

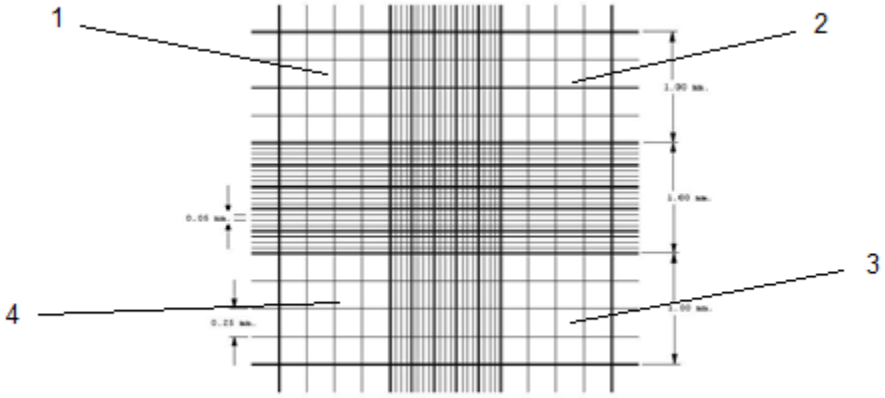

15. Determine cell density from cytometer cell count and dilution amount. Each 4x4 grid is 10^{-4}mL.

    Example Calculation:

    - Cytometer cell counts: 171, 283, 140, 264
    - Dilution: 20 µL cell sample with 80µL Trypan Blue (five-fold dilution)
      Average cell count = (171+283+140+264)/4 = 214.5
      Cell density = 214.5e4*5 = 1.36e7 cells/mL
16. Calculate volume of cell solution needed for each new T-75 plate. The desired cell culture surface area in the new solution is ~1e4 cells/cm^2.

    Example Calculation:

    - T-75 plate surface area is 75 cm^2
      Volume needed = (75 cm^2)*(1e4 cells/cm^2)* (1,000 µL/ml) / (1.36e7 cells/mL) = 55 uL per T-75 plate
17. Immerse cell volume in 8 ml OPC media per T-75 plate.
    A. OPC media mixture:
        i. 40 ml DMEM +G
        ii. 400 µL Pen/Strep (1x)
        iii. 400 µLN2 supplement (1x)
        iv. 800 µLB27 supplement (1x)
18. Add mixture to new T-75 plate.
19. Gently swirl mixture around to get ideal cell monolayer.
20. Inspect cells under microscope to ensure ideal cell surface area.
21. Incubate cell flasks.

    Note 1: Media should be changed every two days.

Note 2: Tissue culture hood and incubator are sterile environments. Take appropriate actions when moving items in and out of them.
Note 3: Clean hemocytometer with water, followed by 70% ethanol and use kim wipes.

8.1.5 OPC cryopreservation

1. Passage cells (follow Cell Expansion Protocol).
2. Mix DMSO with cold OPC media in a 1:9 volumetric ratio, respectively.
   Note1: Make enough solution for 1 ml per 75e4 cells.
   Note2: Make sure to account for sterile filter losses.
3. Sterile filter OPC media and DMSO mixture.
4. Add mixture to cells and pipette into cryopreservation vials in 1 ml aliquots.
5. Fill cell freezing container with isopropanol.
   Note: May not be necessary if container is recently used and isopropanol is still present.
6. Put vials in cell freezing container and store in -80ºC freezer for 2 – 4 hours.
7. Move vials from -80ºC freezer to liquid nitrogen storage container.

8.2 NSC culture

8.2.1 Media

1) Be sure to use DMEM/F12 (1:1) no L-glutamine. DO NOT use the same DMEM as you would for OPC.
2) To the 500 mL DMEM/F12 container, add:
   a) 10 mL B27
   b) 5 mL PenStrep
   c) 5 mL L-glutamine

8.2.2 Flask Coating

1) Dilute poly-L-ornithine (P4957) with sterile water from the stock concentration (20 mg/ml) to yield 20 µg/mL for polystyrene plates (25 µL stock into 25 mL sterile water for batch of 5 T75 flasks).
2) Add enough of the poly-L-ornithine solution to cover the whole surface of the tissue culture-ware. Use 5 mL volume for T75 plates and 15 mL volume for T225 plates. Incubate in a humidified 37 °C incubator for at least one hour.
3) Remove the poly-L-ornithine solution and rinse once with sterile water. Aspirate after the rinse.
4) For the culture, propagation and differentiation of NSCs, dilute laminin (L2020) to final concentration of 5 µg/ml (83.25 µL laminin into 25 mL for batch of 5 T75s). Use 5 mL volume for T75 flasks and 15 mL for T225s. Incubate in a humidified 37C incubator for at least 1 hour. Coated plates and flasks can be stored in the laminin solution at 2-8 °C for 3 weeks or at -20 °C for 6-8 months. Just before use, bring the coated plates or flasks up to room temperature and aspirate the laminin solution. Rinse the plates once with 1X PBS (806552) before use.

8.2.3 Seeding NSC from frozen

1) Remove the vial of Neural Progenitor Cells (SCC007, SCC008, SCR055, SCC035) from liquid nitrogen and incubate in a 37 °C water bath. Closely monitor until the cells are completely thawed. Maximum cell viability is dependent on the rapid and complete thawing of frozen cells.

IMPORTANT: Do not vortex the cells.

2) As soon as the cells are completely thawed, disinfect the outside of the vial with 70% ethanol. In a laminar flow hood, use a 1 or 2 mL pipette to transfer the cells to a sterile 15 mL conical tube. Be careful not to introduce any bubbles during the transfer process.
3) Using a 10 mL pipette, slowly add dropwise 9 mL Neural Expansion Medium (SCM005, SCM004) (pre-warmed to 37 °C) to the 15 mL conical tube.

IMPORTANT: Do not add the whole volume of medium at once to the cells. This may result in decreased cell viability due to osmotic shock.

4) Gently mix the cell suspension by slow pipetting up and down twice. Be careful not to introduce any bubbles.

IMPORTANT: Do not vortex the cells.

5) Centrifuge the tube at room temperature at 200 x g (200* on our centrifuge) for 5 minutes to pellet the cells.
6) Aspirate as much of the supernatant as possible.
7) Resuspend the cells in a total volume of 1 mL of Neural Expansion Medium (prewarmed to 37 °C).
8) Plate the cell mixture onto a poly-L-ornithine and laminin-coated 3.5 cm tissue culture plate containing 12 mL media. Add FGF-2 (20 ng/mL) directly to the flask. To achieve this concentration, add 1 uL FGF-2 for every mL of media (e.g., 26 µL FGF-2 per 13 total mL media)
9) Incubate the cells at 37 °C in a 5% CO2 humidified incubator.
10) The next day, exchange the medium with 13 mL fresh Neural Expansion Medium (prewarmed to 37 °C) containing FGF-2 (20 ng/mL). Exchange with fresh medium every other day thereafter.
11) When the cells are approximately 90 - 100% confluent, they can be dissociated with Accutase™ (A6964) and passaged or alternatively frozen for later use. The cells should be maintained at high cell density at all times and thus the recommended passaging is at 1:2 to 1:6.

8.2.4 Passaging

1) Aspirate media.

2) Add 5 mL accutase to the flask. Allow to sit at room temperature in the hood for 5-8 minutes.
    a) Note: check through the microscope to be sure cells are lifting off the flask!
3) Add cells to a 15 mL conical tube. Rinse flask WELL with additional 5 mL PBS and add to the same conical tube.
4) Centrifuge at 200xg for 5 minutes.
5) Aspirate supernatant and resuspend in media. Count as normal with trypan blue.
    a) Extract a 20µL sample for cell counting and place in microtube.
    b) Dilute microtube solution with Trypan Blue, and record dilution amount.

        Note 1: Optimal dilution leaves ~50 cells per 4x4 grid when performing cell count on hemocytometer.

        Note 2: Perform cell count within 5 minutes of adding Trypan Blue. Over long periods of time the dye starts leaking into live cells.

    c) Inject 15 µL of sample into cytometer.
    d) Count cells in each of the four 4x4 grids. Cytometer picture shown below.

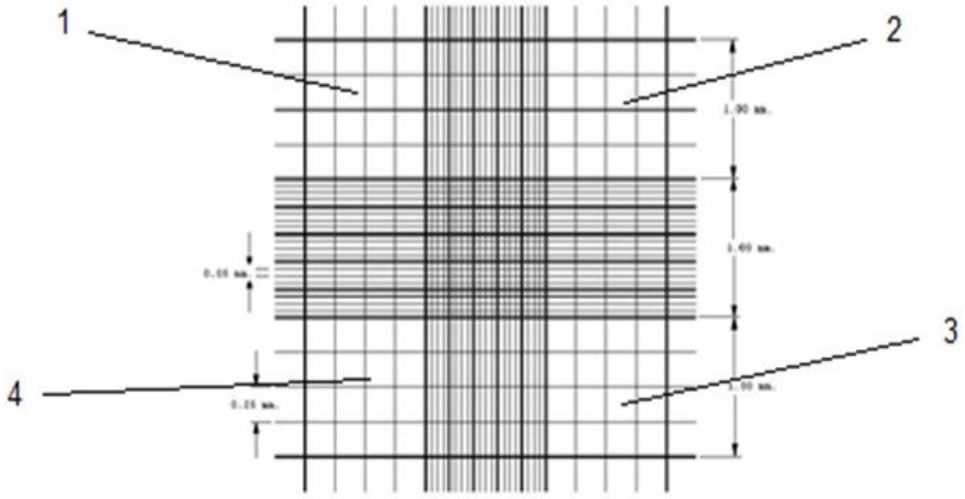

    e) Determine cell density from cytometer cell count and dilution amount. Each 4x4 grid is 10^{-4}mL.

        <u>Example Calculation:</u>

        Cytometer cell counts: 50, 37, 42, 34

        Dilution: 20 µL cell sample with 480 µL Trypan Blue (twenty-five-fold dilution)

Average cell count = (50 + 37 + 42 + 34)/4 = 40.75

Cell density = 40.75e4*25 = 1.02e7 cells/mL

f) Calculate volume of cell solution needed for each new T-75 plate. The desired cell culture surface area in the new solution is ~1e4 cells/cm^2.

Example Calculation:

T-75 plate surface area is 75 cm^2

Volume needed = (75 cm^2)*(1e4 cells/cm^2)* (1,000 µL/ml) / (1.02e7 cells/mL) = 73.5 uL per T-75 plate

6) Rinse desired number of flasks with PBS and distribute cells per above calculations. Each flask should contain 13 mL media, 26 uL FGF-2, and calculated amount of cells.

8.2.5 NSC Cryopreservation

1) Passage cells (follow Cell Expansion Protocol).
2) Mix DMSO with cold NSC media at a ratio of 7% DMSO, 93% media.
   Note1: Make enough solution for 1 ml per 75e4 cells.

   Note2: Make sure to account for sterile filter losses.
3) Sterile filter NSC media and DMSO mixture.
4) Add mixture to cells and pipette into cryopreservation vials in 1 ml aliquots.
5) Fill cell freezing container with isopropanol.
   Note: May not be necessary if container is recently used and isopropanol is still present.
6) Put vials in cell freezing container and store in -80ºC freezer for 2 – 4 hours.
7) Move vials from -80ºC freezer to liquid nitrogen storage container.

8.3 NorHA BOP synthesis

S.R. Caliari; updated 4/22/19 KG

Purpose: To couple norbornene to HA

Materials:

- round bottom flask (RBF), Stir bar, Cannula (cleaned and in oven)
- Stoppers, 21G 1 ½ needles (in drawer in hood room)
- 4 L beaker, large stir bar, stir plate, dialysis tubing (6000-8000 MW cut-off regenerated cellulose)

- 50 mL conical tubes

Reagents Required:

- Hyaluronic Acid Tert-butyl ammonium salt (HA-TBA)
- 5-Norbornene-2-methylamine (Nor-amine)
- Benzotriazole-1-yl-oxy-tris-(dimethylamino)-phosphonium hexafluorophosphate (BOP; in fridge)
- Anhydrous DMSO (in solvent cabinet under synthesis hood)
- Sodium Chloride (NaCl)

Calculations:

See spreadsheet:

Nor-HA synthesis:

HA-TBA:					input
	Nitrogen Methyl Peak Int.	3	*should be 3, at δ=2.1 in NMR		output
	TBA Methyl Peak Int.	15.4945			
	n value	1.291208	*typically ~1.4		
	HA-TBA repeat MW	707.7636	g/mol	CDHA mod	
	Input Mass HA-TBA to use:	2.65	g	NorHA mod	
	Mol. HA-TBA Repeat Units	0.003744		MeHA mod	
				CD mod	
Nor-amine	MW	123.2	g/mol		
	Functionalization desired:	0.4	0.6		
	ul Nor-amine Needed:	287.4043		*assumes ~65% efficiency	
BOP:	Mass BOP Needed:	0.993588	g		

Reaction:

1) Allow HA-TBA and BOP to come to room temperature (30-45 minutes).
2) Rinse 25mL and 500 mL RBF with acetone and place in drying oven.
3) Once dried, remove RBF from the oven. Add a stir bar and put a stopper on immediately.
4) Allow RBF to cool and add small pieces of HA-TBA, followed by Nor-amine, in the hood.
5) Attach RBF to ring stand above stir plate in hood set to ~ 350 rpm.
6) Turn nitrogen on and check airflow.
7) Clear air from RBF. Add nitrogen needle to RBF followed by the purge needle, immediately. Allow to sit and stir for five minutes, then remove in reverse order (first purge needle then nitrogen needle).
8) Clear air from DMSO. Add nitrogen needle to RBF followed by the purge needle, immediately. Allow to sit and stir for two to three minutes, then remove the purge needle.
9) Connect DMSO and RBF with reaction via cannula. Make sure cannula not submerged into DMSO yet. Add the purge needed to reaction RBF after adding the cannula.
10) Once set, submerge the cannula into the anhydrous DMSO and allow DMSO (~

5 mL per 0.1g) to add to the reaction RBF.

11) While HA is dissolving, mass out the required amount of BOP. Remove 25mL RBF from the drying oven and add stopper. After cooling, add BOP.
12) Add ~20 mL anhydrous DMSO to BOP RBF via cannulation.
    a. Clear air from BOP RBF. Add nitrogen needle to RBF followed by the purge needle, immediately. Allow to sit and stir for two to three minutes, then remove the purge and nitrogen needle.
    b. Clear air from DMSO again. Add nitrogen needle to RBF followed by the purge needle, immediately. Allow to sit and stir for two to three minutes, then remove the purge needle.
    c. Add cannula to the anhydrous DMSO and to the BOP RBF. Add purge needle to BOP RBF immediately after.
    d. Lower cannula in anhydrous DMSO.
    e. Remove cannula, purge needle and nitrogen needle once dissolved.
13) Once HA is fully dissolved, cannulate BOP into the reaction.
    a. Add nitrogen needle followed by cannula into BOP RBF.
    b. Add cannula followed by purge into the reaction RBF.
    c. Lower BOP RBF cannula into solution.
14) Rinse cannula with acetone and return to oven.
15) React for at least ~ 2 hrs. at room temperature.
16) Quench the reaction with cold DI water (~10mL) and transfer to pre-soaked
17) dialysis tubing.
18) Perform dialysis 5 days at room temperature (for the first 3 days, include ~ 5 g NaCl in dialysis water). Change the water twice daily.
19) Filter to remove side-products from BOP coupling. If large precipitates have formed, transfer to 50mL tubes, centrifuge, then filter.
20) Return to dialysis for 3-5 days.
21) Transfer to 50 mL tubes, freeze at -80 C, lyophilize.

8.4 NorHA Synthesis via DMTMM Conjugation

Darling *et al*. bioRxiv (2019). https://doi.org/10.1101/765529
Last updated: 08/30/21 JLG

Equipment/glassware needed:

- 1-neck RBF, stir bar
- Dialysis tubing, beakers

Chemicals needed:

- HA (MW: ~60 kDa)
- 4-(4,6-dimethoxy[1.3.5]triazin-2-yl)-4-methylmorpholinium chloride (DMTMM) (MW: 294.74 Da)

- MES buffer (approximately 100 mM)
    - MES (dry) MW: 195.24 g/mol
- 5-norbornene-2-methanamine
- 95% cold ethanol
- 1M brine solution
- 2M brine solution

1. Dissolve 1 g HA and 1.15 g MES hydrate in 40 mL DiH_2O.
2. Adjust pH of solution to 5.5 (approximately 125 uL of 10M NaOH).
3. Add 1.24 g DMTMM to the solution and stir for 10 min to dissolve.
4. Add 0.271 mL 5-norbornene-2-methanamine dropwise into the mixture and stir overnight at room temperature.
5. Precipitate the solution in 250 mL of 95% (190 proof) cold ethanol. Mix precipitate solution thoroughly to improve extraction yield. Collect the precipitate, dissolve in 2M brine solution, and dialyze against DI water for 1 day, then 1M brine solution for 1 day. Repeat the dialysis process 3 times.
    a) Collection via vacuum filtration has worked best for me. Whenever I tried centrifugation, the polymer would turn out weird and even crosslinked.
6. Dialyze against DI water for 24 hours. Freeze product (-80C) and lyophilize. Purge tubes with N_2 and store at -20 C.
7. H^1 NMR with D_2O.

8.5 MeHA Synthesis Protocol

Purpose: To methacrylate hyaluronic acid. Coupling proceeds through methacrylate esterification with the hydroxyl group of HA.

Materials:
- 3-neck 500mL round bottom flask (RBF), stir bar, stoppers
- Stir plate, pH meter
- micropipettes/tips
- 4L beaker, large stir bar, stir plate, dialysis tubing (6000-8000 MW cut-off regenerated cellulose)
- 50 mL conical tubes

Reagents Required:
- Hyaluronic Acid (HA)
- Methacrylic Anhydride (MA)
- 5N Sodium Hydroxide (NaOH; 5N = 40g/200mL)

Reaction:

1. Secure the round bottom flask in a clamp resting on a cork based while sitting on top of a stir plate. Place the football-shaped stir bar in the flask.

2. Weigh out 4g of 65 kDa sodium hyaluronate. Add to the round bottom flask.

3. Add 200 mL of distilled water to the round bottom flask. Stir vigorously until fully dissolved.

4. Calculate the amount of methacrylic anhydride needed for the reaction using the following formula. HA $(C_{14}H_{20}NO_{11}Na)_n$: MW=401.286 g/mol

$$(XgHA)\left(\frac{1mol}{401.286gHA}\right)(0.1)(20)\left(\frac{154.17gMA}{mol}\right)\left(\frac{mL}{1.035gMA}\right)=[Y]mLMA$$

0.1 = 10% modification; change as necessary for desired modification
20 = 20 fold excess of MA

Note: For the reaction performed in the Caliari lab, a 90% methacrylation efficiency was expected. The volume of MA needed was 27.7 mL

5. Place the dissolved HA solution in an ice bath within a crystallization dish and continue to stir.

6. Calibrate the pH probe using the buffer solutions. Then insert the pH probe in the crooked leg of the flask. Make sure that it is anchored properly and away from the stir bar so the stir bar can operate freely.

7. Monitor the pH. It should be around 7 in the dissolved HA solution.

8. Add 1 mL of MA slowly to the stirring solution. Bubbles should form. The pH needs to be adjusted to be 8-9. Add NaOH solution to maintain pH. Only a few drops should be needed.

9. Wait 5 minutes for the pH to stabilize and then add another 1 mL of MA. Again, maintain the pH to be around 8-9.

10. Repeat step 9 until all the MA has been added. By the end of the reaction, the solution should look like a colloidal suspension. This ensures that the organic phase and aqueous phase have mixed and can behave like a stable suspension.

11. The ice bath can be removed. Continue stirring the solution overnight so that excess methacrylic anhydride degrades. Place rubber stoppers over the legs of the flask to prevent evaporation of fluid.

12. After stirring overnight, place the solution in dialysis for several days. Cloudiness should disappear quickly as the MA is replaced by fresh DI water. If there are excess bubbles in the solution for the organic phase, they can be popped by centrifugation. Alternatively, you can wait until lyophilization, and the liquid will be sublimed out.

13. Dialyze against DI water for 5 days; change water 2x per day.

14. Transfer to 50 mL tubes, freeze at -80C, lyophilize.

8.6 Electrospinning

Safety Instructions:

- *Always use gloves when putting together this solution*
- *Glasses or goggles are recommended, especially when removing air from the syringe*
- *Use care when weighing out individual materials as some are very fine and easy to spill/kick up into the air*
- *General lab safety practice should be followed*

Materials:

- MeHA, NorHA, or any functionalized HA
- 1 x Non-sterile PBS

- Poly(ethylene oxide) (PEO, dry chemical 900 kDa)
- Bovine Serum Albumin (BSA) - as desired
- Irgacure D-2959 Photoinitiator (I2959)
- 5 mL plastic syringe with cap
- Small stir bar
- Dithiothreitol (DTT) or dithiol crosslinker of interest (for NorHA only)

	*Lyophilized HA**	*Non-sterile 1x PBS*	*BSA **	*I2959***	*DTT*	*PEO*
2 mL solution	*40 mg*	*1.95 mL (NorHA)* *2 mL (MeHA)*	*20 mg*	*10 mg*	*52 µL*	*50 mg*

** Once allowed to reach room temp*
*** Always protect from the light as best possible - using 0.05% final concentration, with pre-made stock solution at 0.5% concentration (heated at 60C for 1hr) as in literature.*
Grayed items: Use only as needed (i.e., DTT in NorHA systems)

Procedure:
Dissolving contents

1. Warm up HA, BSA, and thaw DTT, I2959 stock, and/or peptide aliquot as needed.
2. Cap syringe and add stir bar.
3. Add DTT (X_{DTT}=0.5, for NorHA only) and DI water to the syringe so that half of the working volume is reached (ex: for a 2 mL solution, add up to 1 mL between the DTT and DI water)
4. Weigh out 1% BSA and add stock 0.5% I2959 solution so that the final I2959 concentration will be 0.05%, and add to syringe
5. Weigh out HA (2%) and add to the syringe.
6. Add PEO (3.5%).
7. Add the remaining volume of DI water needed to reach the final volume
8. Place the plunger back on the syringe to secure all contents inside.
9. Remove cap carefully and move the syringe barrel up until air bubbles have been removed as much as possible.
10. Re-cap and place the syringe on its side to stir (protect from light using the box in lab or a dark room if possible). Make sure the stir bar is spinning lengthwise. Dissolve for at least 24 hr, ideally 48 hrs.

Spinning

1. Keep electrospinning solution covered/protected from light.
2. Clean off mandrel, deflector, etc. with 90% ethanol squirt bottle.
3. Clean out tubing and tips with water or PBS (can also use acetone if there is a large build-up)
4. Tape methacrylated/thiolated coverslips on middle of mandrel with half pieces of scotch tape, zig-zagging arrangement (do max 6 coverslips).
5. Turn on the top, middle, and lowest boxes of the power supply.
6. Remove air bubbles from syringe and place 22G metal needle on syringe.
7. Place syringe in pump and confirm all settings are correct (plastic syringe, volume (enter number higher than actual), 1 mL/h flow rate, etc.) → try a lower flow rate (0.5, 0.65, 0.8)

8. Check all electrodes, clip needle and then cover with generous amount of electric tape.
9. Use liquid nitrogen (mist slightly, don't actually expel) to reduce humidity to ~ 20-25%.
10. Flip on power supply in back to control mandrel.
11. Flip on 3 power supplies underneath (needle power turned up almost all the way, 25-30 kV).
12. Cover coverslips with AL foil for initial collection to determine quality of fibers. Make sure jet is straight and isn't dripping, etc.
13. For 1h spin at 1 mL/h can stop after about 20 min and switch in 2nd set of 6 coverslips

Start pulling voltage first to get a cone at a certain flow rate and then clean up before starting official collection → suggestion from spray base

To reduce humidity, turn the temperature up in the chamber to assist the dehumidifier → another suggestion from spray base

8.7 Encapsulating OPCs in NorHA gels of varying stiffness

NorHA = Norbornene-functionalized hyaluronic acid

1.) Determine the gel types and number of replicates. (Note: it's generally a good idea to round up the number of gels you will need. See troubleshooting section)

Examples of some gel types:

- 1 wt% NorHA (n=12)
- 1.5 wt% NorHA (n=12)
- 2 wt% NorHA (n=12)

2.) Prepare polymer stock solutions in advance. I typically make 40 µL gels using 1 mL syringe top molds. I usually make 1 mL stock solution of 9 wt% NorHA as this provides enough stock solution for 2-4 encapsulation experiments (depending on the number of conditions/replicates).
   a.) Weigh out appropriate amounts of PEG and NorHA into sterile 1.5 mL tubes from the TC hood and incubate (cap open) in TC hood under aseptic UV light for 20 minutes.
   b.) Then add the appropriate volume of sterile PBS to each tube and vortex.
   c.) Unused stock solution may be stored at 4 C for future experiments. Unused dry polymer is stored in the 4C flammables refrigerator.

3.) Prepare other necessary components (23 mM LAP solution, 6 mg/mL DTT solution) in advance by dissolving dry ingredients in sterile PBS.
   a.) Can store these components at 4 C.
   b.) Be sure to make a fresh DTT solution every 2 weeks or so as it degrades over time.

4.) Passage cells and perform cell count to determine how many cells/ml are present in your cell solution.
    a.) Note: make cell stock solution in "simple media" (DMEM and PenStrep only)- this improves cell survival during cell counting/encapsulation process.
    b.) We typically encapsulate OPCs at a final concentration of 0.5e7 cells/ml, but this can be varied depending on the experimental goal.
    c.) Cell stock solution should be concentrated when added to the gels, so that the 0.5e7 cells/ml encapsulation density can be achieved while leaving room in the gel solution for all the other components (LAP, DTT, etc.). I typically resuspend cells in 100-150 µL of simple media per passaged flask (so if passaging 10 flasks, resuspend in 1 to 1.5 mL of simple media).
5.) In the TC hood, combine your gel components in labeled sterile microcentrifuge tubes. Add polymer, then photoinitiator (and DTT in the case of NorHA), then "excess" PBS, and finally cells. Mix by gently pipetting or gentle inversion after each addition. Do NOT vortex or shake once you've added cells.

Example calculations (note: these calculations may require adjustment depending on the functionalization efficiency of the polymer. For example, NorHA gels should contain enough DTT crosslinker to achieve a 0.312 thiol-norbornene ratio)

For 1% NorHA gels:

- Total volume of solution: 40 µL/gel* 12 gels = 480 µL
- Amt 23 mM LAP needed: 12.125 µL per 250 µL solution so = 23.3 µL 23 mM LAP
- Amt cells needed:
    ○ Measure cells from passaged plates: _____
    ○ Dilution factor: _____/0.5e7 cells/mL
    ○ Cell amt: 480 µL/ dilution factor =
- Amt NorHA needed: NorHA is at 9 wt% so dilute to 1/9 of the final solution amount = 53.3 µL
- Amt DTT needed: 21.776 µL DTT (0.312 thiol-norbornene ratio)
- Amt PBS= 480- amt LAP - amt cells - amt NorHA - amt DTT =

For 1.5% NorHA gels:

- Total volume of solution: 40 µL/gel* 12 gels = 480 µL
- Amt 23 mM LAP needed: 12.125 µL per 250 µL solution so = 23.3 µL23 mM LAP
- Amt cells needed:
    ○ Measure cells from passaged plates: _____

    - Dilution factor: _____/0.5e7 cells/ml
    - Cell amt: 480 µL/ dilution factor =
- Amt NorHA needed: NorHA is at 9 wt% so dilute to 1/6 of the final solution amount = 80 µL
- Amt DTT needed: 32.664 µL DTT
- Amt PBS= 480- amt LAP - amt cells - amt NorHA - amt DTT =

For 2% NorHA gels:

- Total volume of solution: 40 µL/gel* 12 gels = 480 µL
- Amt 23 mM LAP needed: 12.125 µL per 250 µL solution so = 23.3 µL 23 mM LAP
- Amt cells needed:
    - Measure cells from passaged plates: _____
    - Dilution factor: _____/0.5e7 cells/ml
    - Cell amt: 480 µL/ dilution factor =
- Amt NorHA needed: NorHA is at 9 wt% so dilute 4.5x = 106.7 µL
- Amt DTT needed: 43.552 µL DTT (0.312 thiol-norbornene ratio)
- Amt PBS= 480- amt LAP - amt cells - amt NorHA - amt DTT =

6.) Aliquot gel solution into your syringe gel molds (you can stand these up in a sterile microtube rack). Each gel has a volume of 40 µL.
7.) Expose gels to UV light from bar lamp (365 nm, ~ 4 mW/cm^2 (intensity will depend on distance from bulb)). NorHA gels have a 2 minute gelation time. Use foil covered reflectors to maximize light exposure and prevent UV light exposure to you and the rest of the hood.
8.) Transfer each gel to a well of a 24 well plate, rinse 3x in PBS to remove any excess, unpolymerized component(s).
9.) Add 1 mL media to each well and place gels in 37C incubator.
10.) Culture gels for desired length of time. Media will need to be changed every other day for the first 4 days of culture, and once per day for each subsequent culture day as cells proliferate.
11.) To conduct ATP/DNA assays, collect individual gels at desired timepoints and freeze in 400 µL lysis buffer at -80C. Conduct assays once you have collected and frozen all gels for that experiment. PCR can be performed on gels collected and frozen in appropriate buffer.

Troubleshooting

My gel solution made fewer gels than I had calculated for!

- This can be due to volume loss when pipetting. It's always a good idea to round up the number of gels or amount of gel solution to ensure you get at least the minimum number of gels you need.
- In the example calculations above, we used replicates of n=12. So, in this example, we may have determined we would need n=9 minimum per condition. Setting up calculations for n=12 ensures that you do get at least 9 gels per condition even with pipetting losses. And if you do end up with a spare gel or two, these are always good to have around in case of accidents.

My gels aren't gelling well…

- Stock solutions may be old. Try making fresh batches. Polymer stock solutions typically should be used within a couple of months. DTT especially needs to be remade frequently (recommend once every 2 weeks)
- Dry polymer should be stored in tightly sealed conical tubes under inert gas to ensure auto-polymerization does not occur.
- Make sure UV light is functioning at correct wavelength, intensity, etc.

My cell solution is too dilute- there is no room in my gel solution for other components!

- Spin cell solution down again and resuspend in a smaller amount of media.

Some of my conditions seem fine, but others have low viability for no clear reason!

- Cells are resuspended in simple media which should keep them healthy over the short-term needed for encapsulation. That said, you should still conduct encapsulations as quickly as possible. Don't leave cell solution sitting for too long!
- If you are encapsulating many conditions and need to encapsulate in multiple batches, your first batch of gels may be sitting in 24 well plates while you encapsulate a second batch. Consider letting the first batch sit in PBS-G (PBS with added glucose equivalent to the amount present in cell media) while they wait, rather than plain PBS.

8.8 DAPI/Phalloidin Staining Protocol

Solutions:

4% Paraformaldehyde (PFA): dilute based on ampoule concentration. There are 16% PFA ampoules (Electron Microscopy Sciences, room temp). Dilute 4x in PBS. Prewarm before use and store long term in -20C fridge.

0.5% Triton X-100: 0.5 mL Triton-X100 into 100 mL PBS (or 25 µL Triton per 5 mL PBS). Make fresh each time. TritonX is on the dry chemicals shelf (and is viscous so be careful when pipetting).

Phalloidin solution: 2 U/ml phalloidin and 1% (10 mg) BSA per mL PBS (scale up based on how many mL you want). BSA is in the bottom of the 4C fridge and phalloidin is in the door of the -20 in a yellow bag.

DAPI solution: 300 nM DAPI in PBS. DAPI is stored in labeled box on the top shelf of the -20. There should be a 300 um aliquot of DAPI which can be diluted 1:1000. MIX WELL BEFORE USE.

1.5% NorHA phalloidin staining (all steps done on an orbital shaker, except PFA fix)

1. Fix cells in 4% pre-warmed PFA for 1 hour at 37C (800 µL per gel). Don't aspirate the PFA afterwards!! Dispose of it in the designated waste container in the cabinet next to the lab whiteboard.

2. Wash 3x in PBS (5 min each) in 4C fridge with shaking (can set up orbital shaker on bottom left of 4C fridge)

3. Permeabilize in PBS-triton (0.1% Triton X-100) for 30 minutes at 4C with shaking (again, enough to cover the gel so ~800 µL)

4. Wash 3x in PBS (5 min each) in 4C fridge with shaking

5. Incubate overnight (with shaking first 60 min) in phalloidin solution (4C, protect from light)

6. Wash 4x in PBS (1hr each) in 4C fridge with shaking (protect from light)
    a.) For first hour, add DAPI to rinse solution to simultaneously rinse out phalloidin and add DAPI stain. Next 3 rinses in PBS alone

7. Store gels at 4C, protected from light until ready to image

8.9 ECM Immunostaining

Culture gels to desired timepoints and fix/permeabilize as per usual.

1. Fixing: 1 hour in 4% PFA
2. Rinse 3x 5 min each with 2% BSA in PBS (800 mg BSA in 40 ml PBS)

DO NOT PERMEABILIZE. We want to see what is secreted NOT what is inside cells

Antibody staining:

1. CUT GELS IN HALF!! We want to image internally to avoid large surface clusters
2. Blocking step- cover with 2% BSA buffer (and incubate 1 hr at RT with shaking)
3. Incubate with primary antibody dissolved at the desired concentration in 2% BSA buffer overnight at 4 °C with shaking
    a. For the fibronectin antibody this was 1:250. Laminin is 1:100
4. Next morning: rinse 2x 5 min each, followed by multi-hour rinse in 2% BSA buffer.
5. Incubate the sample with secondary antibody dissolved at the desired concentration (donkey anti-rabbit 647, 1:200) in 300 µL 2% BSA buffer overnight at RT.
6. Add fresh BSA-PBS and CellMask Orange 1:1000. Leave 35 minutes at room temperature.
7. Wash the samples 3 × 10 min with PBS (RT). Store in PBS overnight (final rinse) and image.

8.10 CellGlo (ATP) Assay

(uses Promega product G7571)

Diet Theory: The CellTiter-Glo Luminescent Cell Viability Assay is a homogeneous

method of determining the number of viable cells in culture based on quantitation of the ATP present, which signals the presence of metabolically active cells. The amount of ATP is directly proportional to the number of cells present in culture. The CellTiter-Glo Assay relies on the properties of a proprietary thermostable luciferase which generates a stable "glow-type" luminescent signal and shows good performance across a wide range of assay conditions. The half-life of the luminescent signal resulting from this reaction is greater than five hours.

This assay is typically done using a white 384-well plate with a maximum well-volume of 70µL. Therefore, all values below reflect that.

1. Bring components for cellglo reagent to room temperature
    a. First check and see if there is some cellglo reagent already prepared in the fridge. If it was prepared within the last 2-3 weeks, it should still be fine to use.
    b. The cellglo reagent as it comes in the kit is two components – a buffer and the reagent, both of which are kept in the freezer. These should only be mixed together when intending to use right away.
    c. It is preferred to bring these to room temp on the bench, however you can add the buffer to the 37^0C water bath to speed up the process.
    d. The reagent is light sensitive so keep it capped in the brown glass vial (which blocks light).
2. Prepare your samples and keep on ice.
    a. For gels, homogenize in lysis buffer and keep on ice.
    b. For monolayers, add lysis buffer and keep on ice.
3. Prepare a standard curve using ATP as below. ATP is stored in the -80^0C freezer. Store ATP standards on ice.
    a. Standard 1: 1 µL stock ATP + 1 mL PBS = 9 µg/mL

b. Standard 2: 500 µL Standard 1 + 500 µL PBS = 4.5 µg/mL
c. Standard 3: 500 µL Standard 2 + 500 µL PBS = 2.25 µg/mL
d. Standard 4: 500 µL Standard 3 + 500 µL PBS = 1.125 µg/mL
e. Standard 5: 500 µL Standard 4 + 500 µL PBS = 0.5625 µg/mL
f. Standard 6: 500 µL Standard 5 + 500 µL PBS = 0.2813 µg/mL
g. Standard 7: 500 µL Standard 6 + 500 µL PBS = 0.1406 µg/mL
h. Standard 8: 500 µL Standard 7 + 500 µL PBS = 0.0703 µg/mL
i. Standard 9: 500 µL Standard 8 + 500 µL PBS = 0.0352 µg/mL
j. Standard 10: 500 µL Standard 9 + 500 µL PBS = 0.0176 µg/mL
k. Standard 11: 500 µL Standard 10 + 500 µL PBS = 0.0088 µg/mL
l. Standard 12: 500 µL PBS = blank
m. If needing to start from lyophilized ATP, dissolve the contents of the vial of ATP (0.9mg) into 100 µL PBS. Store at -80^{0}C in 1.5 µL aliquots.

4. Prepare cellglo reagent if necessary
    a. Add entire contents of the CellTiter-Glo buffer (about 10 mL) to the amber bottle containing the CellTiter-Glo Substrate to reconstitute the lyophilized enzyme mixture. This forms the cellglo reagent.
    b. Mix by gently inverting or swirling. DO NOT shake as you will make a lot of foam. The substrate should go into solution easily within 1 minute
5. Load plate in duplicate or triplicate
    a. You will use a white 384-well plate
    b. Add 25 µL of each standard
    c. Add samples
        i. Skip one row of wells between standards and samples
        ii. For most samples, add 25 µL of your sample to the plate
        iii. For very highly concentrated samples, use the repeater pipettor to add 20 µL of PBS to each well to which you will be adding samples. Then add 5 µL of your gel sample.
6. Pop any bubbles that may interfere with reagent loading
7. Use the repeater pipettor to add 30 µL of cellglo reagent to each well.
    a. Add the reagent quickly and efficiently being careful to avoid transfer between wells.
    b. Add the reagent to the standards going from lowest concentration to highest.
    c. Add reagent in a general left to right fashion going across the plate.
8. Stir and incubate at room temp for 10 minutes to stabilize luminescent signal. Plate may be read up to 1 hour later.
9. Make sure no bubbles exist.
10. Read using the Lumistar plate reader (BMG Labtech) in luminescent mode using Cellglo/ATP protocol.

Notes:

1. This assay is usually very repeatable and has a low error.
2. If you experience high CVs:
    a. Check mixing in your samples. They may not be homogenous
    b. Watch your pipetting. It is easy to make a mistake in such a small well

c. Be careful when using the repeater pipettor to add the reagent. You may be experiencing cross-contamination when moving from a highly concentrated sample to a lower one.

3. If you experience very low raw luminescent values:
   a. Check to make sure that the correct instrument head is installed.
   b. Ensure that all bubbles have been popped.
   c. Did you use the correct buffer in which to lyse your cells?

Example values: note - standard curve below was prepared excluding the two most concentrated standards. A linear trend line was used, and the intercept was set to zero.

Std	ATP (µg/mL)	AVG reading	%CV
1	9	1294667	1.079826
2	4.5	776906	1.008273
3	2.25	403521	0.69616
4	1.125	202258	0.605273
5	0.5625	101923	0.842085
6	0.28125	52079	5.137665
7	0.140625	25780	0.969065
8	0.070313	12765	1.853775
9	0.035156	6549	1.296564
10	0.017578	3255	1.896043
11	0.008789	1713	1.808502
12	0	77	5.126011

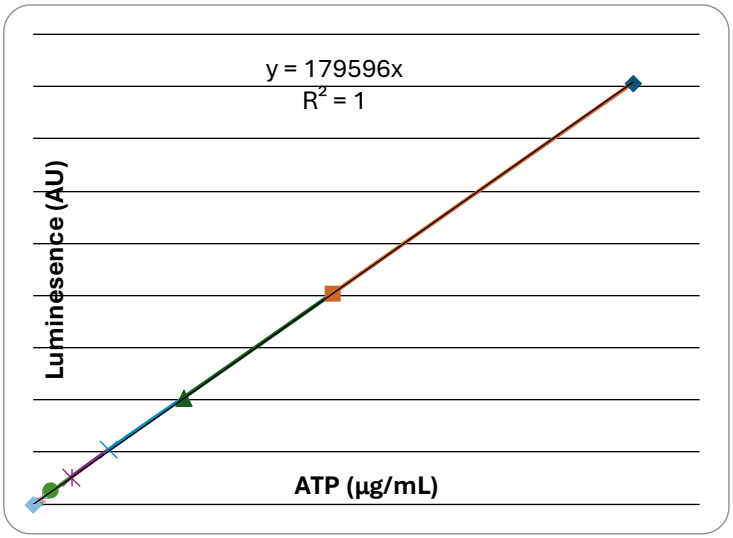

8.11 Pico Green Assay

LIGHT THEORY:

The PicoGreen kit allows you to quantify the amount of DNA you have in a sample. It enables sensitive detection of double stranded DNA in the range of 25 pg – 1 ug with just a single dye concentration. The PicoGreen Reagent is a DNA intercalating agent that is only fluorescent when bound to double stranded DNA due to a conformational change that occurs. It is specific for dsDNA over ssDNA and RNA and is sensitive even in the presence of proteins and other common nucleic acid contaminants.

SAMPLE PREPARATION:

If starting from microparticle-released DNA: no sample preparation needed.

If starting from hydrogels:

1. Collect ice to keep the samples cold to help protect the DNA from degradation
2. Rinse gels off using PBS by placing 1 ml sterile PBS in each well of a 12 well plate that will contain a gel. Label the 12 well plate.
3. Using the open end of a fire-polished glass pipette, transfer the gels to the 12-well plate, on gel per well.
4. Transfer the gels to their own individual 15 ml tube, minimizing the amount of PBS that is transferred with it. (Gels can be frozen at -80C at this step).
5. Add 300ul cold Cell Lysis Buffer (located at 4C) to each 15 ml tube. Once Cell Lysis Buffer is added, the samples need to be stored on ice.
6. Grind gel into small pieces using mortar to break up gel before sonicating.
7. Maintain the samples on ice and sonicate each sample using 3-4 Watts continuously for 15 seconds. Be sure to clean the sonicator's tip between samples using 70% ethanol followed by a water rinse.

If starting from cell pellet:

1. Resuspend pellet in 300ul cold Cell Lysis Buffer (located at 4C) to each 15 ml tube. Once Cell Lysis Buffer is added, the samples need to be stored on ice.
2. Maintain the samples on ice and sonicate each sample using 3-4 Watts continuously for 15 seconds. Be sure to clean the sonicator's tip between samples using 70% ethanol followed by a water rinse.

ASSAY PREPARATION:

Make 1x TE buffer from 20x Stock. This is kept at 4C. It is fine to make 50 mLs at a time and just store left over 1X buffer in the fridge for future assays. 1x TE buffer will be used to make the standards, dye, and dilute samples in well if necessary.

Make Std Curve Samples:

Standards	DNA concentration (ng/ml)	Volume DNA Sample (µl)	Volume 1x TE Buffer (µl)
St 1	**1000**	**5 µl Stock DNA**	**495 µl**
St 2	**500**	**250 µl St 1**	**250µl**
St 3	**250**	**250 µl St 2**	**250 µl**
St 4	**125**	**250 µl St 3**	**250 µl**
St 5	**12.5**	**25 µl St 4**	**225 µl**
St 6	**1.25**	**25 µl St 5**	**225 µl**
St 7	**.125**	**25 µl St 6**	**225 µl**
Blank	**0**	**0**	**250 µl**

Make Diluted Dye: Make enough dye to add 100 µl to each sample and standard in either duplicate or triplicate (plus some extra for pipetting loss). Dilute the dye 200 fold using 1x TE buffer. (**50 µl dye / 10ml 1x TE Buffer).** This dye is photosensitive, so you may want to cover the tube with foil if it is going to take a long time to load the plate.

Running the Assay:

Assembling Plate: obtain a **black** 96 well plate suitable for fluorimetry.

Write down in your notebook where you will put each standard and sample on the plate (in duplicate).

Pipette 100 uL of each standard into the designated wells on the plate.

If diluting samples, add 95 uL of 1x TE to each well destined to contain a sample.

Then, add 5 uL of actual sample to each well. If not diluting samples, just add 100 uL of sample to the designated wells on the plate.

Pipette 100 uL of dye into every well containing either a sample or standard.

Let incubate for 10 minutes before reading.

Read Plate: Read plate on the fluorimeter by exciting at 488nm and collecting the emission at 520 nm.

1. Insert your plate into the FluorStar using the "plate in, plate out" icons.
2. Make sure the FluorStar is set up to measure Fluorescence by choosing "file," then "reader configuration," then "fluorescence." A warning message will pop up asking you to make sure the right measurement heads are installed. Use the cheat sheet posted on the FluoStar to make sure of this.
3. Set up your plate by choosing "test protocols" then "PicoGreen1". Just select what wells have samples in them, then specify that the volume is 200 uL for each sample. Select "Save."
4. Measure the plate by choosing "Measure" then "PicoGreen1". Choose the "Set Gain" tab and measure the gain in a well that contains the most concentrated standard.
5. Select "Run Assay."
6. Select the Graph icon to see the measurements being recorded. This data will be saved automatically, so after the test is complete, this window can simply be closed.
7. To retrieve your data, select the "Xcel" icon. Double-click your particular experiment from the list that comes up. Highlight the raw data, cut, and paste it into a new excel file. Save this new file to your jump-drive.

Trouble Shooting:

1. If samples lye outside the range of the std curve, simply dilute those particular samples and re-run the assay. Take this dilution into account when calculating concentrations of DNA in each sample.
2. If duplicates are not closely matched, more accurate pipetting is needed.
3. You can also perform this assay in a 384 well plate, using 25 uL sample and 25-30 uL dye. (5 uL undiluted sample and 20 uL 1x TE Buffer)

8.12 RT-qPCR

This protocol describes the harvest of RNA from whole cell lysate, cDNA synthesis, and quantitative PCR for gene expression studies.

Materials Needed:

- Cells in culture / encapsulated
- *Quick*-RNA™ Miniprep Kit (Genesee cat. #11-328 or DNA/RNA #R1057)
    - DNase I (ZYMO cat. #E1010)
- 200 Proof Ethanol (Decon Labs cat. #2716)
- 8-tube PCR strips (USA cat. #1402-4700) – cDNA collection

- iScript™ cDNA Synthesis Kit (BIORAD cat. #1708891)
- 1.5mL Eppendorf Tubes – nuclease free
- Multiplate™ 96-Well PCR Plates (BIORAD cat. #MLL9601)
- SsoAdvanced™ Universal SYBR® Green Supermix (BIORAD cat. #1725271)
- UltraPure™ DNase/RNase-Free Distilled Nuclease-Free Water (Invitrogen cat #AM9938)
- Microseal 'B' PCR Plate Sealing Film (BIORAD cat. #MSB1001)
- BIORAD CFX Connect Real-Time Thermal Cycler System (PCR)

Workflow Timeline:

Day 1: Harvest cultured cells into RNA Lysis Buffer

Day 2: Isolate RNA using Zymo Research *Quick*-RNA Miniprep Kit

Day 3: Perform cDNA synthesis on isolated RNA

Day 4: Prepare plate and run qPCR

Day 1: Harvest cultured cells into RNA Lysis Buffer

1. Treat cells in culture with relevant experimental conditions (NB: cells generally cultured in 24-well plates with 30,000 cells per well for neurons or 50,000 cells per well for non-neuronal cells) – For OPCs recommended 50,000 cells/well
2. Aspirate media (carefully)
3. Collect cells in **300 µL** RNA Lysis Buffer; wash cells thoroughly and transfer to labeled Eppendorf tube (nucleases free)
4. ***Freeze lysates at -80 ˚C** or proceed to isolate RNA **[*recommended]**
5. If there are later time-points make sure that there is not any RNA Lysis Buffer left in the wells – wash twice with 1X DPDB.

Day 2: RNA Isolation

Note: Before RNA isolation spray off all surfaces, pipettes, and tips boxes with ZapLock! (RNase inhibitor – increases RNA concentration in sample)

Follow Zymo Quick-RNA Miniprep Kit Protocol; double bind lysate onto green column and include optional DNase I treatment

1. Thaw lysates at room temperature and thoroughly resuspend by pipetting up and down.

2. Transfer the lysate into a Spin-Away Filter (yellow) in a Collection Tube and centrifuge at >10,000 rcf for **1 minute** to remove the majority of gDNA. Save the flow-through for RNA purification!
3. Add 1 volume ethanol [=**300 uL]** (95-100%) to the flow-through from step 2 (1:1). Mix well.
4. Transfer the mixture to a Zymo-Spin IIICG Column (green) in a Collection Tube and centrifuge for 30 seconds.
5. **Re-bind the lysate by transferring flow-through back to Zymo-Spin IIICG Column in a Collection Tube and centrifuge for 1 min. Discard the flow-through.**
6. In-column DNase I Treatment
    a. Prewash the column with 400 µL RNA Wash Buffer. Centrifuge for 30 seconds. Discard the flow-through
    b. For each sample to be treated, prepare DNase I Reaction Mix in an RNase-free tube. Mix well by gentle inversion (NB: Prepare enough for 2 extra RNA samples to ensure enough material):

Reagent	Volume
DNase I	5 µL
DNA Digestion Buffer	75 µL

    c. Add 80 µL DNase I Reaction Mix directly to the column matrix. Incubate at room temperature (20-30 ˚C) for 15 minutes. Then centrifuge for 30 seconds.
7. Add 400 µL RNA Prep Buffer to the column and centrifuge for 30 seconds. Discard the flow-through.
8. Add 700 µL RNA Wash Buffer to the column and centrifuge for 30 seconds. Discard the flow-through.
9. Add 400 µL RNA Wash Buffer to the column and centrifuge for 30 seconds. Discard the flow-through.
10. Centrifuge the column for **2 minutes** to ensure complete removal of the wash buffer. Transfer the column carefully into a labeled Eppendorf tube.
11. Add 30-50 µL DNase/RNase-Free Water directly to the column matrix. Incubate for 2-3 minutes at room temperature. Centrifuge for 30 seconds.
12. **Re-transfer eluent directly onto column matrix. Centrifuge for 1 minute**.
13. **Measure RNA concentration using Epoch microplate reader with microspot adapter**
14. Proceed to cDNA synthesis or freeze RNA samples at -80 ˚C.

RNA quantification

Measure absorbance at 260, 280, 230 and 340 nm using BMG LABTECH CLARIOstar monochromatic microplate reader. Use **(2uL/sample)**.

Confirm RNA purity with two parameters:

260/280 nm absorbance ratio > 1.7
260/230 nm absorbance ratio > 1

Note: Ideal Abs 260/230 > 1.8

Calculate RNA concentration

$$RNA_{Conc}(ug/ml) = Abs260mm * 40 * dilution\ factor$$

15. Normalize RNA concentration in all samples to 30 ug/ml by diluting further with RNase- free water. (This concentration will give you 0.45 ug of RNA for each reaction of cDNA synthesis).

Note: This is a stopping point. Samples can be stored at -20°C. However, it is better to make and store cDNA because it is more stable than RNA.
Note 2: For next mixing steps use plates, tubes and pipettes designed for PCR machine.
iScript cDNA Synthesis Kit (BIO-RAD catalog # 170-8891)

Day 3: cDNA Synthesis

1. Prepare iScript cDNA Synthesis Mix by adding **5X iScript Reaction Mix** (Containing - random hexamers and oligo(dT)), **iScript Reverse Transcriptase** (including RNase inhibitor) and **nuclease-free H_2O** for each sample according to the table below (NB: Prepare enough for 2 extra RNA samples to ensure enough material):

Reagent	Volume
5X iScript Reaction Mix	**4 µL**
iScript Reverse Transcriptase	**1 µL**
RNA Sample	10-15 µL (or 100 fg - 1ug)
dH_2O	Up to final volume (up to 20 **µL**)

2. Combine RNA Reaction Master Mix and RNA samples in **8-tube PCR strip**, mix gently by flicking the tubes, and then centrifuge briefly (1,000 rpm for 2 min – to ensure the liquid is at the bottom)

3. Run the samples using following protocol on the thermocycler:

In "**Startup Wizard" window → User-defined**

In "**Run Setup**" window → in **Protocol** section→ **Select Existing → Patryk→ cDNA synthesis → Next** →In **Plate** Section → you should be able to pick all necessary wells you use or by clicking **Express Load→ Quick Plate_96wells_SYBR Only.pltd** you can upload it. → **Start Run** (Choose and save in your folder)

** You will be getting warnings that this protocol doesn't contain SYBR QUANTIFICATION – click OK (Approve**). It is just making cDNA not quant.**

Protocol details:

- 5 minutes at 25°C (Priming)
- 20 minutes at 46°C (Reverse transcription)
- 1 minute at 95°C (Reverse transcription inactivation)
- Hold samples at 4°C

Note: This is a stopping point. Samples can be stored at -20°C.

4. Proceed to qPCR or freeze cDNA samples at -20 ˚C. Vortex really briefly and spin down cDNA before use.

Day 4: RT-qPCR

SsoAdvanced Universal SYBR Green Supermix (BIO-RAD catalog # 172-5271)

1. **Thaw SsoAdvanced Universal SYBR Green Supermix (BIO-RAD catalog # 172-5271) and allow it to reach RT. Leave other solutions on ice.**
2. Prepare the qPCR Master Mix for each primer pair working stock by combining **SsoAdvanced Universal SYBR Green Supermix**, **F+R Primer Working Stock**, and **DNase/RNase-free water** according to the table below:
   (Note1: Prepare enough for 2/3 extra cDNA samples to ensure enough material. Note2: Prepare enough for duplicates of each sample):

Reagent	Volume
SsoAdvanced Universal SYBR Green Supermix	10 µL
F+R Primer Stock (5uM)*	1 µL
RNase-free water (dH_2O)	7 µL
	Total: 18 µL/well

3. Add **2 µL cDNA sample** per well in a 96-well
4. Mix Master Mix by flicking tube gently and add 18 µL to appropriate wells in the qPCR plate
5. Cover the top of the plate with the PCR Plate Sealing Film and plate sealer to ensure a tight seal around all wells

6. Place the plate in the TC tabletop centrifuge in appropriate rotor adapter and balanced. Pulse spin to make sure all material is at the bottom of the wells and no air bubbles are present (1000 rpm/ 3 min)

7. Load the plate into the CFX Connect Real-Time PCR Detection System with the following thermal cycling protocol:

In "**Startup Wizard" window → User-defined**

In "**Run Setup**" window → in **Protocol** section→ **Select Existing → Patryk→ qPCR → Next**

In **Plate** Section → you should be able to pick all necessary wells you use or by clicking **Express Load→ Quick Plate_96wells_SYBR Only.pltd** you can upload it. → **Start Run** (Choose and save in your folder)

Protocol details:

1. Polymerase activation: 30 seconds at 95°C
2. Denaturation: 15 seconds at 95°C
3. Annealing/Extension: 30 seconds at 60°C
4. Cycles: 50
5. 10 seconds at 95°C.
6. Melt curve analysis: 65 - 95°C range with 0.5°C increments at 5 seconds per step.

8. Start experiment by clicking close lid and start procedure button (PCR procedure takes about ~1.5h)

OPC protein expression by stage.

	Early OPC	Late OPC	Immature OL	Mature OL
PDGFRa	+	+	-	-
NG2	+	+	-	-
O4	-	+	+	+
GalC (O1)	-	-	+	+
MBP	-	-	-	+

MOG	-	-	-	+
MAG	-	-	-	+
PLP	-	-	-	+